New Jersey Institute of Technology
Digital Commons @ NJIT

Dissertations | Electronic Theses and Dissertations

Summer 8-31-2006

Automatic modulation classification of communication signals

Zaihe Yu
New Jersey Institute of Technology

Follow this and additional works at: https://digitalcommons.njit.edu/dissertations

Part of the Electrical and Electronics Commons

Recommended Citation

Yu, Zaihe, "Automatic modulation classification of communication signals" (2006). *Dissertations*. 793.
https://digitalcommons.njit.edu/dissertations/793

This Dissertation is brought to you for free and open access by the Electronic Theses and Dissertations at Digital Commons @ NJIT. It has been accepted for inclusion in Dissertations by an authorized administrator of Digital Commons @ NJIT. For more information, please contact digitalcommons@njit.edu.

Copyright Warning & Restrictions

The copyright law of the United States (Title 17, United States Code) governs the making of photocopies or other reproductions of copyrighted material.

Under certain conditions specified in the law, libraries and archives are authorized to furnish a photocopy or other reproduction. One of these specified conditions is that the photocopy or reproduction is not to be "used for any purpose other than private study, scholarship, or research." If a, user makes a request for, or later uses, a photocopy or reproduction for purposes in excess of "fair use" that user may be liable for copyright infringement,

This institution reserves the right to refuse to accept a copying order if, in its judgment, fulfillment of the order would involve violation of copyright law.

Please Note: The author retains the copyright while the New Jersey Institute of Technology reserves the right to distribute this thesis or dissertation

Printing note: If you do not wish to print this page, then select "Pages from: first page # to: last page #" on the print dialog screen

NJIT
New Jersey's Science & Technology University

The Van Houten library has removed some of the personal information and all signatures from the approval page and biographical sketches of theses and dissertations in order to protect the identity of NJIT graduates and faculty.

ABSTRACT

AUTOMATIC MODULATION CLASSIFICATION OF COMMUNICATION SIGNALS

by
Zaihe Yu

The automatic modulation recognition (AMR) plays an important role in various civilian and military applications. Most of the existing AMR algorithms assume that the input signal is only of analog modulation or is only of digital modulation. In blind environments, however, it is impossible to know in advance if the received communication signal is analogue modulated or digitally modulated. Furthermore, it is noted that the applications of the currently existing AMR algorithms designed for handling both analog and digital communication signals are rather restricted in practice. Motivated by this, an AMR algorithm that is able to discriminate between analog communication signals and digital communication signals is developed in this dissertation. The proposed algorithm is able to recognize the concrete modulation type if the input is an analog communication signal and to estimate the number of modulation levels and the frequency deviation if the input is an exponentially modulated digital communication signal. For linearly modulated digital communication signals, the proposed classifier will classify them into one of several nonoverlapping sets of modulation types. In addition, in M-ary FSK (MFSK) signal classification, two classifiers have also been developed. These two classifiers are also capable of providing good estimate of the frequency deviation of a received MFSK signal.

For further classification of linearly modulated digital communication signals, it is often necessary to blindly equalize the received signal before performing modulation

recognition. This doing generally requires knowing the carrier frequency and symbol rate of the input signal. For this purpose, a blind carrier frequency estimation algorithm and a blind symbol rate estimation algorithm have been developed. The carrier frequency estimator is based on the phases of the autocorrelation functions of the received signal. Unlike the cyclic correlation based estimators, it does not require the transmitted symbols being non-circularly distributed. The symbol rate estimator is based on digital communication signals' cyclostationarity related to the symbol rate. In order to adapt to the unknown symbol rate as well as the unknown excess bandwidth, the received signal is first filtered by using a bank of filters. Symbol rate candidates and their associated confident measurements are extracted from the fourth order cyclic moments of the filtered outputs, and the final estimate of symbol rate is made based on weighted majority voting.

A thorough evaluation of some well-known feature based AMR algorithms is also presented in this dissertation.

AUTOMATIC MODULATION CLASSIFICATION OF COMMUNICATION SIGNALS

by
Zaihe Yu

A Dissertation
Submitted to the Faculty of
New Jersey Institute of Technology
in Partial Fulfillment of the Requirements for the Degree of
Doctor of Philosophy in Electrical Engineering

Department of Electrical and Computer Engineering

August 2006

Copyright © 2006 by Zaihe Yu

ALL RIGHTS RESERVED

APPROVAL PAGE

AUTOMATIC MODULATION CLASSIFICATION OF COMMUNICATION SIGNALS

Zaihe Yu

Dr. Yun Q. Shi, Dissertation Advisor — Date
Professor of Electrical and Computer Engineering, NJIT

Dr. Ali Abdi, Committee Member — Date
Assistant Professor of Electrical and Computer Engineering, NJIT

Dr. Nirwan Ansari, Committee Member — Date
Professor of Electrical and Computer Engineering, NJIT

Dr. Roy R. You, Committee Member — Date
RBS Greenwich Capital, New York, NY

Dr. Wei Su, Committee Member — Date
US Army RDECOM CERDEC I2WD, Fort Monmouth, NJ

BIOGRAPHICAL SKETCH

Author: Zaihe Yu

Degree: Doctor of Philosophy

Date: June 2006

Undergraduate and Graduate Education:

- Doctor of Philosophy in Electrical Engineering,
  New Jersey Institute of Technology, Newark, NJ, 2006

- Master of Engineering in Electrical Engineering,
  Tsinghua University, Beijing, P. R. China, 1989

- Bachelor of Engineering in Electrical Engineering,
  Tsinghua University, Beijing, P. R. China, 1987

Major: Electrical Engineering

Presentations and Publications:

Z. Yu, Y. Q. Shi, and W. Su, "Symbol-rate estimation based on filter bank," Proceedings of the 2005 International Symposium on Circuits and Systems, Kobe, Japan, Vol. 2, pp. 1437-1440, May 2005.

Z. Yu, Y. Q. Shi, and W. Su, "A blind carrier frequency estimation algorithm for digitally modulated signals," Proceedings of the 2004 Military Communications Conference, Monterey, CA, Vol. 1, pp. 48-53, Nov. 2004.

Z. Yu, Y. Q. Shi, and W. Su, "A practical classification algorithm for *M*-ary frequency shift keying signals," Proceedings of the 2004 Military Communications Conference, Monterey, CA, Vol. 2, pp. 1123-1128, Nov. 2004.

Z. Yu, Y. Q. Shi, and W. Su, "Carrier frequency estimation of single-tone digital communication signals," Proceedings of the 2004 Global Signal Processing Conferences & Expos for the Industry, Santa Clara, CA, Sept. 2004.

Z. Yu, Y. Q. Shi, and W. Su, "Automatic classification of *M*-ary frequency shift keying signals," Proceedings of the 2004 Global Signal Processing Conferences & Expos for the Industry, Santa Clara, CA, Sept. 2004.

Z. Yu, Y. Q. Shi, and W. Su, "M-ary frequency shift keying signal classification based-on discrete Fourier transform," Proceedings of the 2003 Military Communications Conference, Boston, MA, Vol. 2, pp. 1167-1172, Oct. 2003.

献 给 我 的 家 人

To my beloved family

ACKNOWLEDGMENT

I would like to express my sincere gratitude to my advisor, Dr. Yun Q. Shi. He not only serves as my research supervisor, provides valuable and countless resources, insight and intuition, but also constantly gives me support, encouragement and reassurance. His constant support, detailed guidance and encouragement cover every aspect during my student life from problem solving to technical writing. My study is always inspired by his enthusiasm and hard work in the research on communication and signal processing areas.

I would also like to express my appreciation to the distinguished members of the dissertation committee: Drs. Ali Abdi, Nirwan Ansari, Roy R. You, and Wei Su, for their active participation and valuable comments. Special thanks are given to Dr. Wei Su for his constant support, remarkable comments on my research, and careful revising of my final version of the dissertation. Without his supports, my dissertation will not be in its current shape.

Many of my present and former colleagues in the Electrical and Computer Engineering Department at NJIT are deserving of recognition for their help during my graduate study life.

Thanks are given to my dear friends and former colleagues at Tsinghua University: Ms. Zhengfang Chen, Ms. Jian Lin, Ms. Hong Xia, Ms. Ping Gao, Mr. Shen Liu, and Mr. Junfeng Pan, for their help and encouragement during the past years.

My gratitude goes to my friends Ms. Lingming Sun and Dr. Chuanchao Pang. Without their efforts of taking care of my parents and my personal affairs in China, I would have not been able to concentrate on my Ph.D. program during these years.

Finally, I am and will always be grateful to my parents, my parents-in-law and my wife for their endless support and encouragement in my life.

TABLE OF CONTENTS

Chapter	Page
1 INTRODUCTION	1
1.1 Motivations and Objectives	1
1.2 The Existing AMR Algorithms	3
1.2.1 Algorithms for Analog Communication Signals Only	4
1.2.2 Algorithms for Digital Communication Signals Only	9
1.2.3 Algorithms for Both Analog and Digital Communication Signals	30
1.3 Outline of this Dissertation	40
2 EVALUATION OF AZZOUZ AND NANDI'S AMR ALGORITHMS	42
2.1 Introduction	42
2.2 Signal Models and Feature Definitions	43
2.3 Evaluation of the Key Features	46
2.3.1 Comments on the Segment Size N_s	46
2.3.2 Comments on the Feature σ_{dp}	49
2.3.3 Comments on the Feature $\gamma_{\max}$	51
2.3.4 Comments on the Feature μ_{42}^{a}	52
2.3.5 Comments on the Feature μ_{42}^{f}	54
2.3.6 Comments on the Feature σ_{a}	55
2.3.7 Comments on the Feature σ_{aa}	55
2.3.8 Comment on the Feature σ_{ap}	57
2.3.9 Comments on the Feature σ_{af}	59

TABLE OF CONTENTS
(Continued)

Chapter **Page**

2.3.10 Comments on the Feature P 61

2.3.11 Comments on Classification of Other Modulation Types..... 63

2.4 Conclusions..... 65

3 BLIND CARRIER FREQUENCY ESTIMATION OF DIGITAL COMMUNICATION SIGNALS..... 69

3.1 Introduction..... 69

3.2 Problem Statement and Assumptions..... 71

3.3 Carrier Frequency Estimation Based on Phases of Autocorrelation Functions.. 73

3.4 Simulation Results and Discussions..... 79

3.5 Conclusions..... 85

4 BLIND SYMBOL RATE ESTIMATION OF DIGITAL COMMUNICATION SIGNALS..... 87

4.1 Introduction..... 87

4.2 Problem Statement and Assumptions..... 90

4.3 Symbol Rate Estimation Based on Filter Bank and cyclic Moments..... 92

4.3.1 Estimation of Coarse Symbol Rate Range..... 95

4.3.2 Design of the Lowpass Filter Bank..... 97

4.3.3 Extraction of the Symbol Rate Candidates Corresponding to the $l-th$ LPF..... 98

4.3.4 Determination of the Symbol Rate and Some Discussions..... 101

4.4 Simulation Results and Conclusions..... 105

5 AUTOMATIC CLASSIFICATION OF M-ARY FREQUENCY SHIFT KEYING SIGNALS..... 113

5.1 Introduction..... 113

TABLE OF CONTENTS
(Continued)

Chapter **Page**

5.2 Problem Statement and Assumptions..... 115

5.3 A simple FFT Based Classifier (FFTC) for MFSK Signals..... 117

5.4 Extra Classification Rules and the Enhanced FFTC..... 122

5.5 Results and Discussions..... 130

5.6 Conclusions..... 138

6 AUTOMATIC MODULATION CLASSIFICATION OF JOINT ANALOG AND DIGITAL COMMUNICATION SIGNALS..... 139

6.1 Introduction..... 139

6.2 Problem Statement and Assumptions..... 140

6.3 Cyclostationarities of Communication Signals..... 145

6.4 Examination of the Presence of Cyclostationarity..... 170

6.4.1 Cycle Frequency Detection and Signal Classification Based on M_{1y}^{α}.... 173

6.4.2 Cycle Frequency Detection and Signal Classification Based on $M_{2,0y}^{\alpha}$... 178

6.4.3 Cycle Frequency Detection and Signal Classification Based on $M_{2,1y}^{\alpha}$... 180

6.5 Other Features for Signal Classification..... 184

6.6 The Proposed Classification Algorithm..... 189

6.7 Test Results and Discussions..... 196

6.8 Conclusions..... 202

7 SUMMARY AND FURTURE WORKS..... 204

7.1 Evaluation of Azzouz and Nandi's Approach to AMR..... 204

7.2 Estimation of Carrier Frequency and Symbol Rate..... 204

TABLE OF CONTENTS
(Continued)

Chapter **Page**

7.3 Classification of MFSK..... 206

7.4 AMR Involving both Analog and Digital Modulations..... 207

7.5 Future Research..... 208

APPENDIX A DERIVATION OF THE POWER SPECTRAL DENSITY OF AN MFSK SIGNAL..... 209

APPENDIX B THE RELATIONSHIP BETWEEN THE NORMALIZED PSD OF AN AM SIGNAL AND THAT OF ITS SQUARED SIGNAL..... 214

REFERENCES 219

LIST OF TABLES

Table		Page
2.1	Models of Some Signals in Reference [12].....	43
2.2	Success Rates of Discrimination between AM Signals and ASK Signals Based on the Feature μ_{42}^{α} (β is the Roll-off Factor of Raised-cosine Function).....	53
5.1	A Simple FFT Based Classifier for MFSK Signals.....	120
5.2	The Enhanced FFT based Classifier for MFSK Signals.....	129
5.3	Classification Results by the Original FFTC when SNR=0 dB.....	131
5.4	Classification Results of MFSK Data Available on [135].....	135
6.1	Cycle frequencies of Communication Signals.....	169
6.2	Test of the Presence of Cyclostationarity.....	173
6.3	Cycle Frequency Detection and Signal Classification Based on M_{1y}^{α}	177
6.4	Cycle Frequency Detection and Signal Classification Based on $M_{2,0y}^{\alpha}$	179
6.5	Symbol Rate Detection and Signal Classification Based on $M_{2,1y}^{\alpha}$	182
6.6	The Testing Modulation Formats.....	197
6.7	Definitions of Correct Classifications.....	198
6.8	Data Record Size in Different Experiments.....	198

LIST OF FIGURES

Figure **Page**

2.1 Measured values of σ_{aa} under SNR = 20 dB (Left column: N_s=2048, Right column: N_s=65536)..... 47

2.2 Measured values of σ_{ap} under SNR = 20 dB (Left column: N_s=2048, Right column: N_s=65536)..... 47

2.3 Measured values of σ_{af} under SNR = 20 dB (Left column: N_s=2048, Right column: N_s=65536)..... 48

2.4 Measured values of σ_{dp} : SNR = 20 dB, N_s = 65536 (Left column: f_c is exactly known, Right column: f_c is estimated from the received data)..... 50

2.5 Measured values of σ_{dp} : SNR = 15 dB, N_s = 65536 (Left column: f_c is exactly known, Right column: f_c is estimated from the received data)..... 50

2.6 Measured values of $\gamma_{\max}$: N_s=65536; SNR is 10 dB for the left subfigure and 20 dB for the right one (up-triangle: AM-0.6, down-triangle: AM-0.8, six-point star: FM-5.0, square: FM-0.5, circle: FSK2, asterisk: FSK4)..... 51

2.7 Measured values of μ_{42}^{f} : N_s=65536 (Left subfigure: SNR=10 dB, Right subfigure: SNR=20 dB)..... 54

2.8 Measured values of σ_{aa} : N_s=65536 (Left subfigure: SNR=10 dB, Right subfigure: SNR=20 dB)..... 56

2.9 Measured values of σ_{ap} : N_s=65536, and f_c is exactly known (Left subfigure: SNR=10 dB, Right subfigure: SNR=20 dB)..... 57

2.10 Measured values of σ_{ap} : N_s=65536, SNR=20 dB, and f_c is estimated from the received signal (circle sign: DSB; diamond sign: PSK2; asterisk sign: FM-0.5, FM-5.0, FM-10.0, FSK2, FSK4, and PSK4)..... 57

2.11 Measured values of σ_{af} : N_s=65536 (Left subfigure: SNR=10 dB, Right subfigure: SNR=20 dB)..... 61

LIST OF FIGURES
(Continued)

Figure		Page
2.12	Measured values of $P:N_s$=65536, and f_c is estimated from the instantaneous phase (Left subfigure: SNR=10 dB, Right subfigure: SNR=20 dB).....	62
3.1	Symbol constellations (Left: Cross-32 QAM, Right: HF-64 QAM).....	80
3.2	Simulation results on PSK2 (Left subfigure: ENMSE vs. SNR, Right subfigure: RMEE vs. SNR).....	81
3.3	Simulation results on PSK8 (Left subfigure: ENMSE vs. SNR, Right subfigure: RMEE vs. SNR).....	81
3.4	Simulation results on Cross-32 QAM (Left subfigure: ENMSE vs. SNR, Right subfigure: RMEE vs. SNR).....	82
3.5	Simulation results on HF-64 QAM (Left subfigure: ENMSE vs. SNR, Right subfigure: RMEE vs. SNR).....	82
4.1	Structure of the proposed symbol rate estimator.....	101
4.2	Symbol rate estimation results by the proposed method: β=0.0.....	107
4.3	Success rate of symbol rate estimation: β=0.2 (Solid curves: results by the proposed method, Dotted-dished curves: results by the reference method).....	107
4.4	Success rate of symbol rate estimation: β=0.4 (Solid curves: results by the proposed method, Dotted-dished curves: results by the reference method).....	108
4.5	Success rate of symbol rate estimation: β=0.6 (Solid curves: results by the proposed method, Dotted-dished curves: results by the reference method).....	108
4.6	Success rate of symbol rate estimation: β=0.8 (Solid curves: results by the proposed method, Dotted-dished curves: results by the reference method).....	109
4.7	Success rate of symbol rate estimation: β=1.0 (Solid curves: results by the proposed method, Dotted-dished curves: results by the reference method).....	109
4.8	Symbol rate estimation results when there is channel distortion: β=0.2 (Solid curves: results by the proposed method, Dotted-dished curves: results by the reference method).....	110
5.1	The normalized PSD amplitude vs. frequency of an FSK8 signal.....	126

LIST OF FIGURES
(Continued)

Figure		Page
5.2	P_c versus SNR when the input data contains 300 symbols	132
5.3	P_{FA} versus SNR when the input data contains 300 symbols	132
5.4	P_c versus SNR when the input data contains 500 symbols	133
5.5	P_{FA} versus SNR when the input data contains 500 symbols	133
5.6	Normalized PSD of An FSK2 data	136
6.1	Decision Tree of the Proposed Classifier (CF stands for *cycle frequency*)	195
6.2	The overall correct classification rate vs. SNR	199
6.3	The overall false alarm rate vs. SNR	199

CHAPTER 1

INTRODUCTION

1.1 Motivations and Objectives

In a conventional communications system, the receiver works cooperatively with the transmitter. That is, the receiver has *a priori* knowledge of the *modulation format* of the transmitted signal. For an analog communication system, the modulation format includes *modulation type*, *nominal carrier frequency*, *modulation index*, etc. For a digital communication system, the modulation format includes *modulation type*, *symbol constellation*, *alphabet size*, *nominal carrier frequency*, *symbol rate*, *pulse-shaping function*, *frequency deviation* (for frequency modulated signals only), and so on. Since both the transmitter and the receiver are under the control of the system designers, the conventional communication studies generally focus on making communications systems more reliable, higher power and/or bandwidth efficient, and more secure.

As mentioned above, one of the fundamental requirements for a communication system is the security. The two parties in communication do not want their communications being known by a third party. In contrast to this, the communication management authority might wish to monitor communications for some purposes such as detection of non-licensed transmitters. The essential step of doing so is to recognize or classify the modulation format of the intercepted signal, which is the signature of a transmitter. Such demands also arise in many other civilian and military applications such as surveillance, signal confirmation, verification, interference identification, selection of proper demodulation methods in software defined radio, electronic warfare, threat analysis, and so on.

Originally, the analysis of modulation formats was performed manually. As the number of modulation types in use is continuously growing and the modern communications systems become more and more complex, however, it becomes more and more difficult to apply manual analysis. In addition, manual modulation classification requires experienced analyzers and cannot guarantee reliable classification results. To solve this problem, the researchers in the signal processing community have conducted deep research in the automatic modulation recognition (AMR) in the past decades (e.g., [1]-[13], [18]-[77] and [79]-[106]).

In many cases, the AMR problems are blind in nature. That is, the signals captured by an AMR receiver may be either digital communication signals or analog communication signals. Then those AMR algorithms, which are designed to handle only analog communication signals or only digital communication signals, will fail in practice. For instance, even though the intercepted signal is an analog communication signal, an AMR algorithm designed only for digital communication signals will eventually report it as a digital communication signal of a certain type, resulting in a misclassification. Therefore, AMR algorithms capable of handling both analog communication signals and digital communication signals are required in blind environments.

The objective of this dissertation is to present an AMR algorithm that is able to separate between analog communication signals and digital communication signals and is able to recognize the concrete type of an analog communication signal. In addition, two algorithms for classifying M-ary frequency shift keying (MFSK) signals, one algorithm for estimating the carrier frequency of digital communication signals, and one algorithm for estimating the symbol rate of digital communication signals are also presented.

1.2 The Existing AMR Algorithms

Automatic modulation recognition is an intermediate step between signal detection and demodulation, and plays a key role in various civilian and military applications. In the past decades, many AMR algorithms have been developed for various applications. The earliest work in this area may be that by Weaver et al. [1]. However, it was not until late 1980's when more researchers paid their attention to the AMR of communication signals.

According to the signal types that an AMR algorithm is able to handle, the existing AMR algorithms can be categorized into three families. The algorithms of the first family are designed to classify analog communication signals only (e.g., [2]-[11]). Those in the second family are only concerned with the classification of digital modulations (e.g., [21]-[77] and [79]-[86]). The classifiers in the third family are able to classify some analog modulations as well as some digital modulations (e.g., [87]-[106]).

The classification methods can also be categorized into two general classes: decision theory based approaches (DTBAs), and feature matching based approaches (FMBAs). In AMR problems, it is generally assumed that each possible modulation format happens with a same probability. Owing to this, the maximum likelihood (ML) criterion is employed in the DTBAs. In a DTBA algorithm, the ML criterion is applied to either the received signal directly or to a certain transform of it (e.g., the instantaneous phase or the instantaneous amplitude of the received signal), resulting in a likelihood ratio or a set of likelihood functions. The classification decision is made by comparing the likelihood functions or comparing the likelihood ratio with a threshold. The solution offered by a DTBA algorithm is optimal in the sense that it minimizes the probability of misclassifications. However, such optimal solutions generally suffer from heavy

computational complexity. On the other hand, an FMBA algorithm employs one or several features extracted from the received signal to make decisions. These employed features are generally chosen in an ad-hoc way. Even though the FMBAs may not be optimal, they are generally simple to implement, with near-optimal performance, when designed properly.

In Subsection 1.2.1 through Subsection 1.2.3, most AMR algorithms developed after the year of 1984 and available in the public literature will be briefly reviewed and commented on. It should be noted that different AMR algorithms are developed for different applications and evaluated under different conditions. Therefore, it is meaningless to simply compare the reported performance of different AMR algorithms. Owing to this consideration and the space limitation, the achieved performance of most of these algorithms will not be introduced.

1.2.1 Algorithms for Analog Communication Signals Only

Since it is difficult to assume a proper probability distribution function (PDF) for the modulating signal (i.e., the information-bearing signal), the classification of analog communication signals is generally based on some selected features derived from the received signals. Only a few researchers paid their attention to the classification of analog communication signals.

Y. T. Chan et al. [2] derived the analytic expressions of the ratio of the variance of the instantaneous amplitude (IA) to the square of the mean value of IA for the following signal groups: amplitude modulation (AM), double-sideband (DSB) modulation, single-sideband (SSB) modulation, and frequency modulation (FM), where the term *FM* in [2] actually stands for analog FM, analog phase modulation (PM) and

digital frequency-shift-keying (FSK) modulation. It is found in [2] that the above ratio will fall in different ranges for different groups if the signal-to-noise ratio (SNR) is not very low. Accordingly, three thresholds are chosen to separate the four groups. It was claimed that a correct classification rate of 97% was achieved for SNR≥7 dB. However, the nominal feature values (NFVs) are obtained by assuming the modulating signal is lowpass-filtered Gaussian sequence. If the modulating signal does not comply with this assumption, the measured feature values may be greatly different from the NFVs, and thus the preset thresholds may not work.

Fabrizi et al. [3] suggested a modulation recognizer for carrier wave (CW), AM, FM and SSB signals. The key features are the mean of the absolute value of the centralized instantaneous frequency and the ratio of the envelope peak to its mean. The first feature is used to discriminate between the following subsets: {FM, SSB} and {CW, AM}. The further classification in each of the above subsets is based on the second feature. This method has the following limitations: (1) the threshold selection of the first feature heavily depends on the lowest peak frequency deviation of all possible FM signals; (2) it requires a very high SNR to separate CW and AM from FM and SSB — the SNR lower bound for achieving reasonably good results is 35 dB under their simulation conditions.

Nagy [4] proposed a modulation recognizer for AM, DSB, SSB, FM, CW and noise signals. In addition to the feature of [2], the variance of the instantaneous frequency normalized to the squared sample time and the mean value of the instantaneous frequency are also used as key features for discriminating among the modulation types of interest. It is reported that the modulation classification could be achieved for SNR≥15 dB.

In discriminating between a low modulation-depth AM signal and a CW signal, Jovanovic et al. [5] employed the ratio of the variance of the in-phase component to that of the quadrature component of the complex envelope of the input signal as the classification feature. The only thing mentioned about the performance is that the proposed key feature is highly reliable even if the SNR is poor.

Al-Jalili [6] studied the centralized instantaneous frequency (CIF) of SSB signals, and found that the CIF of a lower-sideband (LSB) modulated signal contains more positive spikes than negative spikes and that of an upper-sideband (USB) modulated signal has more negative spikes than positive spikes. Thus the ratio of the number of the positive spikes to that of the negative spikes was used as the classification feature. A universal threshold is set at one. It was claimed that the classifier performed well for SNR≥0 dB.

Nandi and Azzouz [7] developed four features for classification of AM, DSB, LSB, USB, FM, vestigial-sideband (VSB) and combined AM-FM modulation signals. The first feature, $\gamma_{\max}$, is the maximum value of the estimated power spectral density (PSD) of the normalized centralized instantaneous amplitude of the input. The second one, denoted by σ_{ap}, is the standard deviation of the absolute centralized instantaneous phase. The third feature, σ_{dp}, is the standard deviation of the centralized instantaneous phase. In calculating both σ_{ap} and σ_{dp}, the instantaneous phase items whose corresponding instantaneous amplitudes are less than a certain threshold are excluded. The fourth feature is $P = |P_L - P_U| / (P_L + P_U)$, where P_L is the received signal's power in the frequency range from zero Hz to carrier frequency, f_c, and P_U is that for the frequency

range from f_c to $2f_c$. The signals of interest are hierarchically classified by using the above features. These features are meaningful but not reliable as expected. Detailed discussions on them can be found in Chapter 2.

Druckmann et al. [8] introduced four key features that are extracted from the instantaneous amplitude of the received signal. Five schemes for classifying AM, DSB, SSB and FM signals are proposed, where each of the first four schemes is based on a single feature, and the last scheme is based on two selected features. The proposed AMR schemes as well as that of [2] were tested via simulations in [8]. It is reported that the schemes based on single feature (including the one of [2]) do not perform well, while the one based on two features performs well for SNR≥10 dB.

Seaman and Braun [9] analyzed the cyclostationarities of AM, DSB, SSB, CW and noise signals. The estimated cyclic spectral density (CSD) of the received signal is used in signal classification. Several figures of the estimated CSDs have been used to show the validity of their proposed approach in [9]. It should be noted that, however, it might be very difficult for machine to automatically recognize a CSD pattern even though it will be very simple for human eye inspection. Unfortunately, how to implement the approach has not been revealed in [9].

In discriminating between FM and PM signals, Waller and Brushe [10] proposed first demodulating the received signal by using FM and PM demodulators, respectively. Both FM and PM demodulated signals are then re-modulated by using FM and PM modulators, respectively. Finally, the four re-modulated signals are correlated with the received signal. Modulation classification is based on the detection of the pattern of the correlation peaks. One limitation of this method is that the carrier frequency is assumed

accurately known in advance. Moreover, no performance evaluation result has been reported in [10].

Taira and Murakami [11] employed a statistics of the instantaneous amplitude of the received signal as the feature to separate the following two groups: exponentially modulated signals (i.e., FM, PM and FSK), and linearly modulated signals (i.e., AM, DSB and SSB). For signals recognized as exponential modulation, the instantaneous frequency compactness feature μ_{42}^{f} of [12] is employed to further separate between analog (i.e., FM or PM) and digital (i.e., FSK) signals. For linear modulations, the feature of [2] is used to further discriminate among AM, DSB and SSB signals. It should be noted that the instantaneous amplitudes are not normalized by their mean value in the above step. This means the feature value curves will not be as clear as reported in [11].

Some of the above introduced classification schemes employ multiple features in modulation classification, where the features are examined either hierarchically (e.g., [7] and [11]) or all at once (e.g., [8]). In the former, each feature is compared with a preset threshold associated with the feature. This implies each decision boundary in the multidimensional feature space is assumed to be perpendicular to some feature axes and be parallel to the other feature axes. In reality, however, the decision regions are generally multidimensional-cubes with irregular shapes. Therefore, the all-at-once method is expected to be able to provide better performance even though it is more difficult to implement. A simple implementation of the all-at-once method is to represent the decision regions by using their centers, which can be found by using clustering techniques (see, e.g., [13]-[17]) in advance. When classifying an unknown signal, the classifier makes decisions simply based on the weighted/non-weighted distances between

the observed feature vector and the decision region centers. The above discussion is also applicable to the FMBAs introduced in Subsections 1.2.2 and 1.2.3.

A common problem with the above AMR algorithms is that the modulation types they are able to handle are limited. Another common problem with most of them is that the feature thresholds and/or decision regions are determined experimentally even though this doing has not been mentioned explicitly. However, the key feature values will vary as the SNR condition, modulation parameters and parameters of the information-bearing signal change. Other classification conditions such as the data record size may also affect the feature values (see e.g., Figure 1 and Figure 2 of [8]). Therefore, the predetermined feature thresholds and/or decision regions may not be feasible if the algorithms work in blind environments. Key features like the one of [6] are preferred since they are relatively robust to the SNR condition, modulation parameters, and so on.

1.2.2 Algorithms for Digital Communication Signals Only

Due to the current trend to use digital communications instead of analog communications, most publications in the area of AMR are concerned with digital communication signals. A general assumption with digital communication signals is that the PDF of the symbols of each modulation type is known in advance. In fact, it is often assumed that the transmitted symbols are independent identically distributed (i.i.d.) with equal probability. This makes not only FMBAs but also DTBAs are applicable to the modulation classification.

The FMBAs and DTBAs for digital communication signals will be overviewed in Subsections 1.2.2.1 and 1.2.2.2, respectively. Some partial surveys and comparisons of algorithms for identifying digitally modulated signals can also be found in [18]-[20]. For

the simplicity of the description of these algorithms, four working conditions are defined as follows: (1) **WC1:** the impulse response of the transmission filter (also referred to as *pulse-shaping function*) is the standard unit pulse of duration T, where T is the symbol period and its reciprocal is the symbol rate; (2) **WC2:** the symbol rate of the received signal is known in advance; (3) **WC3:** the communication channel does not introduce amplitude distortion except the additive white Gaussian noise (AWGN) and a fixed phase shift; (4) **WC4:** the carrier frequency is known in advance.

1.2.2.1 Feature Matching Based Approaches. Similar to the classification of analog signals, the features for classification of digital signals are generally chosen in ad-hoc ways. The FMBAs for digital communication signals vary greatly in their employed features, their working conditions, etc. The existing FMBAs for classifying digital communication signals are empirically categorized into the following groups.

Phase based approaches: Liedtke [21] built up a scheme to recognize two-ary amplitude-shift-keying (ASK2), two-ary FSK (FSK2), two-ary phase-shift-keying (PSK2), four-ary PSK (PSK4), eight-ary PSK (PSK8) and CW signals, which only assumes to roughly know the carrier frequency and symbol rate. The received signal is first filtered by a bank of bandpass filters (BPFs) centered at the estimated carrier frequency but have different bandwidths, where each of the bandwidths is an approximate estimate of the symbol rate. A demodulator following each BPF then extracts the symbol amplitudes, frequencies and the delta-phase (i.e., the phase difference between two adjacent phase samples). In each demodulator, a timing recovery circuit is employed to extract a sinusoidal waveform that is used to retrieve the significant points of time for the signal. A classification decision will be made based on each demodulator

output as follows. The amplitude variance is used to discriminate between ASK2 signal and signals of other types. The frequency variance is used as the feature to separate FSK2 from PSK. For each possible PSK type, Liedtke established a phase PDF template that can be represented as $\left(R_{j,i}, W_{j,i}\right)$, where the whole delta-phase range for the $j-th$ PSK type is divided into L_j subdivisions, $R_{j,i}$ represents the delta-phase range of the $i-th$ subdivision for the $j-th$ PSK type, $W_{j,i}$ is the weighting factor associated with $R_{j,i}$ and is assigned a value of either $+1$ or -1, and $i = 1, 2, \cdots L_j$. For a signal classified as PSK, its delta-phase histogram is weighted with the delta-phase template of each possible PSK type, and the concrete PSK type is determined as the one giving rise to the largest weighted sum. The advantage of Liedtke's method is to use the delta-phase instead of the direct phase itself, so that the carrier frequency offset (CFO) will be eliminated in PSK recognition. Furthermore, with the timing recovery circuit, all feature parameters are observed at the Nyquist sampling rate, and pulse shaping will no longer significantly affect the recognition result. However, Liedtke did not reveal how to make the final decision based on the classification decisions from the outputs of all demodulators, but only claimed "the best classification result will be automatically obtained behind the filter which matches the signal bandwidth best." Moreover, this method assumes the sampling rate is an integer multiple of the symbol rate, and needs a manual tuning of the time-recovery BPF.

Mammone et al. [22] classified CW, PSK2 and PSK4 based on the instantaneous phases. At first, the instantaneous phases are extracted from the analytic signal, and then the delta-phases (i.e., the first-difference of the instantaneous phase) are calculated — this step includes phase unwrapping operations even though it has not been explicitly

mentioned in [22]. Secondly, the mean value of the delta phases is removed, and then the modified delta-phases are integrated, resulting in another phase sequence. Thirdly, the phase sequence obtained in the previous step is processed by using a filter that computes the absolute difference of samples separated by L samples, where L is a design factor. Finally, the classification decision is made by comparing the histogram of the filter outputs with two thresholds. The implied working conditions of [22] are WC1 and WC3, and the received signal should be over-sampled with respect to the symbol rate as well as the carrier frequency.

Based on the observation that the phase PDF of an M-ary PSK (MPSK) signal consists of a series of sinusoidal functions of the phase itself and that the fundamental frequency is proportional to the number of the modulation levels, M, Sapiano et al. developed an MPSK classifier in [23]. The classifier first forms the instantaneous phase's histogram with N bins as the estimate of the phase PDF. Then the N-point discrete Fourier transform (DFT) of the histogram is calculated. The classification is carried out by finding the maximum DFT magnitude among the DFT bins that are of interest. For example, when CW (its M is one), PSK2, PSK4, and PSK8 are to be classified, DFT bins 1, 2, 3, and 4 are examined. If the DFT magnitude of bin 4 is the maximum, the signal is classified as PSK4. The required working conditions of [23] are WC1, WC3, and WC4.

<u>*M-th order power law (MOPL) based approaches*</u>: The idea of MOPL is that the $M'-th$ order power of an MPSK signal will contain a sinusoidal component at frequency $M'f_c$ if M' is an integer multiple of M, where f_c is the carrier frequency. Based on MOPL and other features, DeSimio and Prescott [24] developed a scheme to classify ASK2, PSK2, PSK4 and FSK2 signals. The first two features are the mean value $\bar{m}_{env}$

and variance σ_{env} of the instantaneous envelope, respectively. The separation of ASK2 from the others is based on the observation that the ASK2 signal has smaller $\bar{m}_{env}$ and larger σ_{env} since its envelope is non-constant. The frequencies and magnitudes of the two largest correlation peaks of the received signal's spectrum with a $\sin c^2(x)$ function are used as key features to discriminate between FSK2 and PSK signals. The correlations of a $\sin c^2(x)$ function with the spectra of the squared and quadrupled signal are also calculated, respectively, and the largest correlation values for frequencies near $2f_c$ and $4f_c$ are used as features to discriminate between PSK2 and PSK4. Instead of comparing features with thresholds, DeSimio and Prescott proposed to derive a weighting vector for each assumed modulation type via training. The inner product of the extracted feature vector and the weighting vector for each type is then calculated, and the modulation type is determined as the one giving rise to the largest inner product. The implied working conditions are WC1 and WC3 in [24]. However, if it is used to classify MPSK signals only, these constraints can be removed.

Reichert [25] proposed to classify ASK2, PSK2, PSK4, FSK2 and minimum-shift-keying (MSK) signals by detecting the existence of dominant spectral lines and their locations in the spectra of the received signal, the squared received signal, and the quadrupled received signal, respectively. If the estimated PSD and its continuous component at frequency f are respectively denoted by $S(f)$ and $S_c(f)$, then this frequency corresponds to a spectral line if $S(f) > \lambda$, where λ satisfies $P_{FA} = e^{-\frac{\lambda}{S_c(f)}}$, P_{FA} is the false alarm rate, and $S_c(f)$ is estimated from $S(f)$ via median filtering. This classifier is very simple to implement. In deriving the expression of the decision

threshold λ, however, they imposed very weak assumptions on the distributions of the detection statistics. Therefore, the performance is not reliable as expected. Nevertheless, the employed feature is insensitive to the pulse shaping function and modulation parameters.

The MOPL approach can also be used for ASK or quadrature-amplitude-modulation (QAM) signals (see e.g., [62] for details).

Zero-crossing (ZC) based approaches: Hsue and Soliman [26]-[27] introduced a ZC-based scheme to classify CW, MPSK and MFSK signals. The variance of ZC intervals is shown to increase as the number of the sub-carrier frequencies increases. The distribution of the variance of ZC intervals is analyzed, and then an ML criterion is employed to discriminate between multi-tone signals (i.e., MFSK) and single-tone signals (i.e., CW and MPSK). For a signal classified as MFSK, the number of hills in the ZC interval histogram is taken as the estimate of M (generally rounded to its nearest power of two). For a signal recognized as MPSK, the estimation of its alphabet size is accomplished in a way similar to [21], but the weighting factors of the delta-phase templates are modified. This approach will encounter the following problems in practice. At first, in separating MFSK from the other types, the threshold of ZC interval variance is a function of SNR, carrier frequency f_c, and frequency deviation f_d of MFSK signals. Hsue and Soliman only proposed methods to estimate the former two parameters, but did not mention how to handle f_d that is unknown in blind applications. Secondly, when the SNR is low, they proposed to use the average ZC intervals and average delta-phases in classification. This doing requires detecting the inter-symbol transition instants, which in turn requires priori knowledge of (M, f_c) for MPSK signals and (M, f_c, f_d) for MFSK

signals, resulting in deadlocks in implementation. How these deadlocks are solved cannot be found in [26]-[27]. Thirdly, it is not trivial to recognize the hills of histogram by machine. Moreover, the performance will be poor if the received signal does not satisfy WC1 and WC3. Finally, ZC-based methods generally require a very high sampling rate in order to detect the ZC instants.

Grimaldi et al. [28] proposed a scheme to classify ASK2, ASK4, PSK2, PSK4, PSK8, FSK2, FSK4, FSK8, QAM16, QAM64 and some orthogonal frequency division multiplexing (OFDM) signals. The fourth-order cumulants with specific delay parameters as proposed in [29] are adopted as the feature for discriminating between OFDM and non-OFDM signals. The feature $\gamma_{\max}$ of [7] is employed to discriminate between amplitude modulations (i.e., M-ary ASK (MASK) and QAM) and phase modulations (i.e., MPSK and MFSK). The mean value of the normalized-centralized magnitudes is compared with a threshold to discriminate between MASK and QAM. The discrimination between MPSK and MFSK is ZC-based and carried out in the same way of [26] and [27]. The alphabet size of MPSK is determined in a similar way of [21], that of MFSK is estimated by counting the hills in the ZC interval histogram, and that of MASK and QAM are estimated by counting the hills in the histogram of normalized-centralized magnitudes. For OFDM signals, the concrete modulation type is recognized by comparing the estimated symbol rate and PSD with that of existing standards. The working conditions of [28] are WC1 and WC3. It should be noted that counting the histogram hills is not a trivial task for machine. Moreover, the signal filtering in preprocessing may make MPSK lose the constant envelope property although the signal

satisfies WC1. Then the feature value of γ_{max} for MPSK will increase, and thus MPSK may be classified into the group of MASK and QAM, resulting in misclassifications.

Statistical moments/cumulants based approaches: The general idea here is to seek some statistics of the received signal or its transforms as the classification features such that different modulation formats will correspond to different feature value ranges. When the features are used hierarchically, each feature is compared with its associated threshold. The features can also be checked all at once.

In classifying some commercial PSK, FSK and QAM signals, Benvenuto and Daumor [30] examined experimentally the behavior of a set of second-order moments of the complex envelope of the received signal. Three moments are selected for classification. Since the feature selection and the partition of feature value ranges for different modulation types rely on experiments, their designed recognizer only works for the dedicated modulation types. The recognizer of [31] is a modified version of [30], where a rectifier is used instead of the complex demodulator of [30], and the classifier works with the second-order moments of the real value output of the rectifier.

Soliman and Hsue [32] derived the exact expressions of the moments of the instantaneous phase of MPSK signals and found that the even order moments are monotonic functions of M. Therefore, any even order moment could be chosen as the feature for classifying MPSK signals. By applying central limit theorem, the estimated moment is shown to be asymptotically normal under all hypotheses. Then the decision thresholds are determined accordingly. Similar approach is employed in [33]. The limitation with this approach is that WC1 through WC3 should be satisfied.

Assaleh et al. [34] introduced a technique to classify PSK2, PSK4, FSK2, FSK4 and CW signals. The received data are divided into several segments, and the frequency and bandwidth of each segment are estimated by using second-order autoregressive (AR) model. The standard deviation of the frequencies estimated from all segments is used to discriminate between FSK and non-FSK signals. If a signal is recognized as non-FSK, the standard deviation of the bandwidths will be used to further discriminate between CW and PSK. The feature for classifying PSK2 and PSK4 is the average magnitude of the peaks of the estimated bandwidths. The discrimination between FSK2 and FSK4 is performed in a similar way, but it works on the first-difference of the instantaneous frequencies. The assumed signal models of [34] satisfy WC1 and WC3, and the thresholds are chosen empirically.

Spooner [35] considered the case where the signal of interest is mixed with co-channel signals and cannot be separated by filtering or processed sequentially. The classifier of [35] employs a set of cyclic cumulants of the received signal's complex envelope at the pure cycle frequencies of all possible modulation formats as the features for classifying PSK and QAM signals. The orders and lags of the cumulants are optimized off-line. The classifier decides the modulation format of the input signal as the one giving rise to the minimum Euclidean distance between the theoretical cumulants and the measured cumulants. Instead of using multiple cumulants, Marchand et al. [36] used the linear combination of the magnitude of a fourth-order cyclic cumulant and the squared magnitude of a second-order cyclic cumulant as the classification feature to discriminate between two QAM constellations. The key work of [36] is to optimize the parameters of the defined feature off-line, and the classification is also made by

comparing the measured feature value with the theoretical feature values for different modulation types. The approach of [36] is further applied to classification of multiple signals in [37]. The limitation of the above approaches is that they require knowing the cycle frequencies of each possible modulation formats, which may be unavailable in blind environments.

Azzouz and Nandi [12] developed several schemes to classify ASK2, ASK4, PSK2, PSK4, FSK2 and FSK4 signals. In addition to the features $\gamma_{\max}$, σ_{ap} and σ_{dp} of [7], two new features are introduced: the standard deviation of the absolute normalized-centralized instantaneous amplitude (denoted by σ_{aa}), and the standard deviation of the absolute normalized-centralized instantaneous frequency (denoted by σ_{af}). In ideal cases, $\gamma_{\max}$ will be very small for FSK and large for other types; σ_{dp} will be zero for ASK and nonzero for the other modulation types. Therefore, by using $\gamma_{\max}$ and σ_{dp}, the received signal can be classified to three subsets: ASK, PSK, FSK. The value of σ_{aa} is expected to be smaller for ASK2 and larger for ASK4, thus it is used to discriminate between ASK2 and ASK4. Similarly, σ_{ap} is used to discriminate between PSK2 and PSK4, and σ_{af} is used to discriminate between FSK2 and FSK4. These features as well as other features defined in [12] or their modified versions are quite often cited and adopted by other researchers (e.g., [38]-[42]). For this reason, they will be evaluated in Chapter 2.

Swami and Sadler [43] employed $|C_{40}|$ and C_{42} as the features to classify some PSK, PAM and QAM signals, where the pth-order cumulant $C_{p,q}$ of the received signal $x(n)$ is defined as $C_{p,q} = cum\left(x^*(n): q \text{ entries}, x(n): p-q \text{ entries}\right)$. In deriving the theoretical feature values for the signals of interest, it is assumed the symbol constellation

of each type has been normalized to have unit energy. This is equivalent to normalize the fourth-order cumulants by the squared signal power in blind environments. The classification is performed in a hierarchical way. The received signal is first classified into four subsets based on C_{42}: {PSK2}, {MPSK with $M \geq 4$}, {PAM}, and {QAM}. $|C_{40}|$ is used to further discriminate among the signals classified as QAM. For signals recognized as MPSK, $|C_{40}|$ is used to separate PSK4 from the others. An extensive study on using these features in modulation classification can be found in [44]. It is noted that these features are invariant with respect to an unknown fixed phase rotation. However, this approach may suffer from carrier frequency offsets, residual channel effects (or equivalently, the unknown pulse shaping function) and synchronization errors. To combat the channel distortion and/or unknown pulse shaping function, Swami et al. [45] proposed to apply alphabet matching algorithm (AMA) to equalize the received signal before signal classification. To combat the constellation rotation due to frequency offsets, Han et al. [46] developed an algorithm to classify differential PSK (DPSK) signals by using fourth-order cumulants of the delta-phase sequence of the received signal. The constraints of [46] are WC1-WC3, and the received signal is sampled at symbol rate.

Dai [47] developed a moment-based algorithm to classify ASK4, PSK2, PSK4, PSK8 and some QAM signals. Denote the pth-order moment of the received signal y by $M_{p,q} = E\left[y^{p-q} (y^*)^q \right]$, they have shown $M_{2,1} = S + N$, $M_{4,2} = k_2 S^2 + 4S \times N + 2N^2$ and $M_{6,3} = k_3 S^3 + 9kS^2 N + 18SN^2 + 6N^3$, where S and N are the powers of the transmitted signal and noise, respectively. The theoretical values of k_2 and k_3 for each concerned modulation type are calculated off-line. In classification, they first assumed the input

signal is of a particular modulation type, and then estimated the signal power S by using the theoretical value of k_2, the estimated value of $M_{2,1}$ and the estimated value of $M_{4,2}$. After that, the value of k_3 is estimated and compared with its theoretical value. The algorithm decides the modulation type as the one giving rise to the minimum error in estimating k_3. Due to the special forms of the used moments, the phase offset as well as frequency offset will not affect the performance. The implied constraints of [47] are WC1 and WC3.

Rosti and Koivunen [48] found that the mean of the complex envelope of an MFSK signal is A/M in ideal case and thus used it as the classification feature, where A is the signal amplitude. It is noted that the feature distance decreases as the value of M increases. For large M values and lower SNR, the measured features for different types will mix with each other. Therefore, this algorithm may only work when M is not too large (e.g., $M \leq 8$) and the SNR is relatively high. Moreover, the value of A is implied known in their study. In practice, it should be estimated from the received data. Then the feature performance will be worse than that reported in [48].

Wavelet transform based approaches: Based on the observation that the amplitude of Haar wavelet transform (HWT) is a staircase function with M distinct DC levels (may have spikes around symbol transition instants) for an MFSK signal and will be DC with spikes at the instants of symbol transitions for an MPSK signal, Ho et al. [49] developed a scheme to classify MPSK and MFSK signals. The variance of the median filtered HWT magnitudes is used to discriminate between MFSK and MPSK, where the classification threshold is determined based on decision theory so as to achieve constant false alarm rate (CFAR). The number of modulation levels, M, of an MPSK signal is determined by

matching the histogram of HWT magnitude peaks with the theoretical PDFs of the HWT peaks for different values of M. For an MFSK signal, the number of peaks in the histogram of HWT magnitudes is taken as the estimate of M. The signal models of [49] satisfy C1 and C3. It should be noted that the recognition of the histogram peaks is not trivial for machine, especially when the SNR is not high. Furthermore, no systematic method has been reported on how to select the wavelet scale factors in blind applications. Some modifications have been made to adapt to the lower carrier-to-noise ratio (CNR) cases in [50]. Hong and Ho [51] further extended this approach to classify PSK, QAM and FSK, where the HWT magnitudes of the received signal and that of the amplitude-normalized received signal are employed in signal classification. It should be noted that the wavelet based methods generally require a high sampling rate. Otherwise, the extracted HWT magnitudes may not be staircase-like.

Cho et al. [52] developed a scheme to classify PSK2, PSK4, FSK2 and jammer signals. They stated that, for any particular wavelet scale factor, a wavelet transform coefficient (WTC) can be predicted from the previous WTCs. Thus the WTC's for a particular scale factor can be characterized by using a vector of linear predictive coefficients (LPCs). The vectors of LPCs for several different scale factors are extracted from the received signal based on the minimum mean-square-error (MSE) criterion, and are used to form a feature matrix. The classification decision is made by comparing the Itakura's LPC distances between the measured feature matrix and those of the reference signals. This classifier may fail even though the received signal's modulation type is in the pre-assumed set of modulation types but its modulation parameters are not.

Classifiers based on other features, such as histogram correlation based classifier [53], PDF matching based classifier [54] and characteristic function based classifier [55], can also be found in the public literature. For the simplicity, they will not be introduced.

Summary In general, the feature matching based approaches (FMBAs) for digital communication signals have the following advantages and limitations.

FMBAs are generally simpler than DTBAs in term of computational burden, and they are easy to implement. Although not being optimal, the feature-based approaches usually need less or even no prior knowledge of the received signal models if well designed.

However, FMBAs often require that a received sequence contains more symbols in order to meet the i.i.d. assumption. Secondly, for most FMBAs, it is difficult to find universal thresholds or decision regions that will automatically adapt to SNR conditions and modulation parameters — in fact, many classifiers employ empirically or experimentally determined thresholds or decision regions. Thirdly, most of the existing FMBAs assume the pulse-shaping function satisfies WC1 or is known in advance — however, such condition or priori knowledge cannot be guaranteed in blind applications. Fourthly, most FMBAs assume the communication channel satisfies WC3, which may not be met well in practice. Fifthly, some FMBAs also depend on accurate estimations of the modulation parameters — an example is the features σ_{ap} and σ_{dp} of [12], which require an accurate estimate of the carrier frequency.

It is noted that some researchers also employed the neural network (NN) techniques to realize modulation classifiers based on certain features (see e.g., [56]-[59]). This doing avoids selecting feature thresholds or determining the decision regions

explicitly. However, the NN cannot be applied until it has been trained by using data of the known modulation formats. When the target modulation types' parameters change, it is generally necessary to train the NN again. This implies the NN-based classifiers will not perform well in blind applications.

Fuzzy logic realizations can also be found in the public literature (see e.g., [60]-[61]). In general, it is not easy to comment on their performance. However, the fuzzy logic architecture and its parameters are generally designed empirically. Then their abilities to adapt to blind environments are doubtable.

1.2.2.2 Decision Theory Based Approaches. As mentioned before, the DTBAs suffer from high computational complexity. To overcome this problem, a lot of efforts have been made on simplifying the likelihood functions or the likelihood ratio, resulting in some sub-optimal solutions. Another issue in designing a DTBA is how to deal with the unknown parameters of the received signal, such as carrier phase and timing offset. One way is to treat the unknown parameter as deterministic and estimate them from the received data, resulting in the so-called generalized likelihood ratio test (GLRT). A second way is to treat such parameters as random variables and average the likelihood functions with respect to them, resulting in the average likelihood ratio test (ALRT) based classifiers. If ALRT is applied to some unknown parameters and GLRT is applied to the other unknown parameters, hybrid likelihood ratio test (HLRT) based classifiers are derived.

Classifiers for PSK signals: Kim and Polydoros studied the classification of PSK2 and PSK4 signals [62]. In deriving the classifier, the likelihood function of the received signal for each hypothesis is decomposed into Taylor series and only the dominant term

is used in classification, resulting in the so-called quasi log-likelihood ratio (qLLR) rule based classifier. In addition, the ALRT technique has been applied to handle the unknown carrier phase offset. An extensive study can be found in [63]. In the qLLR classifiers of [62] and [63], the received signal's model should satisfy WC1-WC4, and the signal power and noise power (or equivalently, the SNR) are assumed known.

Hong and Ho studied the classification of PSK2 and PSK4 signals with unknown power levels [64]-[67]. The unknown power level is treated as deterministic in [64], resulting in an HLRT classifier (ALRT for unknown symbols plus GLRT for unknown power). In [65], the ALRT technique is employed to handle the unknown power level. An antenna array is employed to improve the performance by space diversity in [66] and [67], where both the unknown power level and the delay between antennas are handled by GLRT technique. In addition to WC1-WC4, the noise power and the carrier phase are also assumed known in [64] through [67].

Yang and Soliman proposed to classify CW and MPSK signals based on the PDF of the received signal's phase [68]. Again, the likelihood function for each hypothesis is deployed to a series and some dominant terms are used in classification. The classifier requires WC1-WC4, and the carrier phase and CNR are also assumed known in advance. Similar work can be found in [69] and [70].

Huang and Polydoros [71] developed a scheme to classify CW and multiple MPSK signals based on the real-valued received data. It is assumed that WC2, WC3, and WC4 are satisfied. The pulse shaping function may not satisfy WC1, but it is implied to be known in advance. In addition, the signal power and SNR are assumed known. If the carrier phase and/or timing offset are unknown, they will be handled by ALRT technique.

Some simplifications have been conducted on the LFs, resulting in a set of suboptimal classifiers. Denote the decision statistics and its associated threshold for M-ary PSK as q_m and Th_m, respectively, where m satisfies $M = 2^m$ for MPSK, and $M = 1$ corresponds to CW. For classification multiple modulation types, the classifier performs sequential tests: (1) it first compares q_0 with Th_0 to assess if the hypothesis $M = 1$ is more likely than that of $M = 2$; (2) if it is, it will also more likely than any other $M > 2$, and then a final decision is made as $M = 1$ (i.e., CW); otherwise, it will repeat the examination on (q_2, Th_2) for $M = 2$ vs. $M = 4$, etc. This method is very interesting since it has the ability to report not-of-the-above although it is only limited to MPSK classification.

The classifier by Sapiano and Martin [72] is also designed to classify CW and multiple MPSK signals. It is based on the joint PDF of in-phase and quadrature components of the received signal. Some simplifications have been made, but no approximation is performed on the LFs. In addition to C1-C4, the classifier requires knowing signal power, SNR, and carrier phase.

Classifiers for QAM signals: Also based on the received signal's PDF, Hwang and Polydoros [73] developed a technique to classify some PSK and QAM signals. In order to reduce the computational burden, approximate versions of the LFs for the signals of interest have been derived. In addition to WC1-WC4, this approach requires knowing signal power, noise power, and synchronization timing. The carrier phase is treated as random and handled by ALRT technique.

Long et al. [74] discussed the criteria to choose the decision threshold for classify a pair of linear modulation types. They found the suboptimal threshold formula will be very simple if the symbol energy, the input SNR and the symbol rate are known in

advance. In [75], the symbol energy and noise power are automatically estimated from the received data, then the decision threshold is set up according to the results of [74]. Even though the technique is only applied to some PSK signals, it should be able to be extended to QAM signals as well.

The classifier of Benvenuto and Goeddel [76] only assumes knowing the symbol rate. The received signal is blindly equalized by using constant modulus algorithm (CMA), and the magnitudes of the equalizer outputs are used to classify modulation types based on the *maximum a posterior probability* (MAP) rule. Since the channel response and pulse-shaping function are unknown, it is impossible to derive mathematical expressions for the conditional PDF $p(x \mid C_j)$, where x represents the amplitude of the equalizer output, and C_j stands for the $j-th$ hypothesis. The authors of [76] proposed to use the experimentally measured PDF, i.e., the histogram of the equalizer output magnitudes. This implies a training procedure for each possible modulation type is necessary before the proposed classifier is able to work. Moreover, for large symbol constellations, the performance of the CMA equalizer cannot be guaranteed.

Lay and Polydoros [77] developed techniques to classify a pair of linear modulations. The received signal is assumed having been shifted to baseband and sampled at symbol rate. This implies WC1 and WC2 should be satisfied. Moreover, it is implied the carrier phase and the timing offset are both zero. The sampled data may contain intersymbol interference (ISI), which is due to combined response of channel and the pulse shaping filter. In the cases of known combined response, the classification is based on either ALRT or GLRT. In the former case, the noise variance should be known in advance. For the latter case, the symbols are estimated by using Viterbi algorithm

(VA), and the noise variance is no longer necessary. When applying GLRT, however, the classification decision threshold is empirically determined by analyzing the histograms of the decision variables. In a case of not knowing the combined response, the unknown response is estimated by pre-survivor processing (PSP) [78], and the above mentioned GLRT technique is used to classify modulation types. It should be noted that the PSP will fail if the received signal's modulation type is beyond the pre-assumed ones.

Wei [79] applied ML criterion to the baseband data to classify linear modulations. It is assumed that the symbol rate, carrier frequency and combined channel-filter response are exactly known, and the additive noise is AWGN. It is claimed that the noise power can be estimated when *signal* is not present, and thus the noise power is assumed known. The transmitted signal power is estimated by subtracting the noise power from the received signal's power. The most interesting work of [79] may be the estimation of the unknown carrier phase, which is accomplished by matching the received data with some virtual constellations associated with the assumed modulation types. The details are not introduced for simplicity. The classifier of [80] could be thought of as a simplified version of [79]. However, the signal power, noise power and carrier phase are all assumed known in [80].

Sills [81] introduced a different way to handle the unknown carrier phase by establishing the approximate joint PDF of the magnitude and the first-difference of the phase of the demodulated data. Based on this joint PDF, a conventional ML classifier was derived. The implied priori knowledge includes the symbol rate, carrier frequency, timing offset, pulse-shaping function, and SNR.

Taira [82] classified the symbols of a QAM constellation into several subsets, where the symbols in each subset have the same magnitude. It is stated that the number of subsets increases with the QAM constellation size. For each possible modulation type, the joint PDF of the magnitudes in different sets is derived. Then the ML criterion is employed to accomplish modulation classification. The implied working conditions of [29] include: (1) the pulse shaping function is known; (2) the symbol rate is known; (3) the channel affects the signal only via additive Gaussian noise, or the channel may also attenuate the magnitude of the transmitted signal but the attenuation factor is known; (4) the noise power is known.

Classifiers for FSK signals: Very few DTBAs are concerned with FSK classification. For a complex MFSK signal, its LF is the integration of a zero-order modified Bessel function of first class, whose independent variable is the Fourier transform of the received complex signal. To bypass the estimation of the received complex signal's spectrum at any frequency and thus simply the calculation of LFs, Beidas and Weber decomposed the LFs into series expression, and then established a connection between the LFs and their defined higher-order correlations (HOCs) of the received signal [83]-[84]. That is, the LFs can be represented by the defined HOCs. Some truncated versions of the LFs are derived and studied via simulations. References [83]-[84] are concerned with the synchronous cases. Beidas and Weber [85]-[86] further extended their approach to the asynchronous cases, where the unknown timing epoch was handled by ALRT technique. In [83]-[86], symbol rate, frequency deviation, carrier frequency, signal power and noise power are assumed known, whereas the carrier phase is assumed to be uniformly distributed on $[-\pi, \pi)$ and is averaged out of the LFs.

Summary In general, the decision theory based approaches (DTBAs) for digital communication signals have the following advantages and limitations.

As aforementioned, DTBAs are optimal in the sense that they are able to minimize the probability of misclassification. In ideal conditions, the DTBAs are able to achieve a high probability of correct classification with a relatively short received data. A DTBA under ideal conditions can be used as a benchmark to evaluate the performance of other classifiers.

However, DTBAs are restricted in practice. At first, DTBAs are designed to classify a finite many pre-assumed modulation formats and generally only work for the pre-assumed modulation formats — that is, the DTBAs are generally not feasible to blind applications. Secondly, in order to reduce the computational complexity, approximate realizations of DTBAs are often employed, resulting in suboptimal solutions — even though having been simplified, many DTBAs are still intensive in computational complexity. Thirdly, SNR is usually an irreducible variable in the LFs of a DTBA — such DTBAs certainly can estimate the SNR as done in [79], but the performance would be worse than reported. Fourthly, most DTBAs impose strong assumptions on the data model, e.g., assuming knowing the symbol rate, carrier frequency, pulse shaping function, channel response, signal power, and noise power in advance — this greatly limits the applications of the DTBAs.

Certainly, modulation parameters such as carrier frequency and symbol rate can be estimated from the received data if they are not available. However, perfect recovery of carrier frequency and symbol rate is almost impossible in practice. The errors in estimating these parameters, especially the residual carrier frequency offset (CFO), may

degrade the performance greatly. To the author's best knowledge, no DTBA has been evaluated when there is symbol rate error.

As to the pulse shaping function and channel response, most DTBAs assume that the channel satisfies C3 and that the pulse-shaping function either satisfies C1 or is known *a priori*. In reality, however, pulse-shaping function may not satisfy C1 in practical communications systems and is unknown in some applications, and the channel may not be AWGN. In the DTBAs introduced above, only [76] and [77] are concerned with the unknown combined channel response. However, the techniques of [76] and [77] are still inadequate for blind applications as discussed above.

In a word, there is still a long way to go in making DTBAs feasible to blind environments. The key is to develop advanced techniques for estimating the modulation parameters and channel parameters, rather than the ML criterion itself.

1.2.3 Algorithms for Both Analog and Digital Communication Signals

In a blind environment, the communication signal intercepted by an AMR system may be of either analog modulation or digital modulation, but unknown in advance. Therefore, AMR algorithms able to handle both analog and digital signals are preferred in practice. However, only a few such algorithms can be found in the public literature.

Jondral [87] proposed two schemes to classify AM, SSB, ASK2, PSK2, FSK2, FSK4 and noise signals. The key features are the histograms of the instantaneous amplitude normalized to its maximum value, the instantaneous direct phase (i.e., the instantaneous phase after removing the phase portion due to the carrier frequency), and the instantaneous frequency, respectively. In the first scheme, the measured feature vector is projected onto a 7-dimensional vector (7-D) via linear transform, and the decision is

made by comparing the distances from the resultant 7-D vector to S_k for $k = 1, 2, \cdots, 7$, where S_k is a 7-D vector whose entries are all zeros except that the $k-th$ is equal to one, and each S_k corresponds to a distinct modulation type. In the second scheme, the feature vector is projected onto the 7-D space via a quadratic transform instead of linear transform. In an effort to reduce the computational complexity, the quadratic transform is not directly applied to the raw feature vector. Instead, the dimensions of the raw features are lowered by using Karhunen-Loève transform. It seems that no assumption is imposed on the received data models. However, the coefficients of the linear transform, the quadratic transform and Karhunen-Loève transform are all determined via training. Then the schemes may not work well if the modulation parameters and/or the SNR condition differ from those of the training data to some extent. In fact, algorithms such as [88] and [89] whose classifier parameters are determined via training will suffer from the same problem. It is also noted that the modulation types these schemes can handle are still not adequate.

The same features and similar processing strategy of [87] are adopted by Adams et al. [88]. They discussed more on enhancing the processing of the raw feature vector, including the data reduction and the determination of the modulation type based on the reduced feature vector. Even though it was claimed that their investigation was concerned with a range of analog and digitally modulated signals, Adams et al. have not reported any performance evaluation results in [88].

With some modifications, Domínguez et al. [89] applied the approach of [87] to classify AM, DSB, SSB, FM, ASK2, ASK4, FSK2, FSK4, PSK2, PSK4, CW and noise signals. It is noticed that this work attempts to identify most of the well-known analog

and digital modulation types. However, its performance is not adequate — at an SNR of 10 dB the probability of correct modulation recognition is 0% for all digital modulation types except for PSK4 (7%) and at SNR = 15 dB the performance is still wanting, especially for FSK4 (56%), FSK2 (84%) and ASK4 (87%).

Callaghan et al. [90] proposed a modulation recognizer for CW, AM, FM, SSB, OOK, FSK2 and noise signals, where the features are the mean and standard deviation of the instantaneous envelope and the mean and standard deviation of ZC intervals. Noting that the carrier frequency may be severely suppressed or absent for some modulation types such as AM with high modulation depth, Callaghan et al. used a hardware phase-locked loop (PLL) for carrier recovery in [90]. This solution overcomes the problem of needing high SNR for accurate instantaneous frequency estimation from the zero-crossings. It is claimed that this recognizer requires SNR≥20 dB for the correct recognition of the different modulation types of interest. However, this recognizer cannot discriminate between the MPSK and the DSB signals when the carrier frequency is not correctly estimated. This often happens in the weak intervals of a signal segment. Also, the accuracy of this recognizer deteriorated rapidly if the receiver is not perfectly tuned to the center frequency. Finally, although not explicitly claimed, the features are treated as joint Gaussian and independent of each other, where the mean values and variances for each modulation type of interest are obtained via training. Thus it will suffer the same problem with [87].

Hipp [91] developed a classifier for CW, intermittent CW, AM, DSB, SSB, FM, PSK2, FSK and noise signals. Six statistical moments of the received signal's phase, frequency and spectrum are chosen as the key features for classification in [91]. The

distribution of the features is modeled as multivariate joint Gaussian, where the mean and the covariance matrix are determined from training data for each signal type of interest. Then the classification is accomplished based on ML criterion. Some simulation results are reported in [91]. However, it seems that the reported performance in [91] is the average for four SNR conditions: 10 dB, 20 dB, 40 dB, and 100 dB. Furthermore, the performance is still wanting even though the reported performance is for SNR=10 dB — the correct classification rate for SSB is only 78.5%.

Aisbett [92] pointed out that AMR classifiers (e.g., [87]), which are based on time-average behavior of instantaneous amplitude, instantaneous direct phase and instantaneous frequency, are less successful at low SNR due to the followings: (1) the extracted time-domain signal parameters such as instantaneous amplitude are biased estimations of their true values when band-limited Gaussian noise presents; (2) the standard approach to modulation recognition does not explicitly deal with SNR, and so ignores the fact that noisy signals are more similar to each other, regardless of modulation type, than they are to strong signals of the same modulation type. To overcome the above problem, Aisbett [92] proposed several features that are functions of the signal envelope, the first-difference of the signal envelope, and the instantaneous frequency. It has been shown that these features are unbiased and thus are noise resistant. This classifier is able to classify AM, DSB, FM, ASK2, PSK2, FSK2 and CW signals. In [92], it is claimed that the success rate of the discrimination among the modulation types appears to be at least good on strong signals. However, the classifier also has to resort to training data since it is difficult to assume a proper PDF for the modulating signal of an unknown analog communication signal.

Krsmanovic et al. [93] developed a classifier for CW, AM, SSB, FM, ASK2, FSK2, multichannel FSK and noise signals. The first two features are the activity factors, where an activity factor represents the percentage of time the detected signal envelope exceeds a predetermined threshold. The first activity factor serves to distinguish noise from the other types, whereas the second distinguishes discontinuous signals such as ASK or SSB voice and other continuous forms. The third feature, which is the mean value of the full-wave rectified AC signal envelope component, serves to separate CW and angle modulated carrier from the remaining signal types. The fourth feature is the frequency mean value of the impulses generated each time the AC signal envelope component crosses zero level. It is used to discriminate between ASK2 and SSB. The further discrimination between FSK2 and multichannel FM is achieved based on the last two features which are extracted from the instantaneous frequency — their definitions are omitted for simplicity. It is mentioned that the results of the preliminary tests with real signals show the success of this recognizer. However, only some results on classification of ASK2 and FSK2 can be found in [93]. The same work is also reported in [94]-[95].

McMillan et al. [96] proposed to use the feature of [2] as well as two novel features to classify AM, DSB, SSB, FM, PM, on-off-keying (OOK), FSK2 and PSK2 signals. The first new feature is the weighted instantaneous frequency's PDF variance divided by the bandwidth of the information embedded in the frequency. The second one is defined in the same way, but the underlying is the direct phase instead of the instantaneous frequency. The features' empirical value ranges for signals of interests are given in [96], but no performance evaluation is reported. In fact, the classifier's structure

and implementation have not been mentioned in [96]. Instead, its performance test part is focused on the estimation of amplitude, phase and frequency.

Martin [97] proposed a recognizer for CW, AM, SSB, FM, OOK and FSK signals based on the features derived from the histogram of instantaneous amplitude, PSD, and short-time Fourier transform (STFT) of the received signal. It is claimed that the correct classification rate are higher than 92% for all the modulation types of interest except the FM (= 80%). However, the SNR condition for the above result is not mentioned in [97]. Moreover, this classifier requires training before it can be used.

Azzouz and Nandi developed several algorithms for classification of some analog and digital communication signals in [12], [98] and [99]. These algorithms are slightly different in implementations but are the same in essence since they employ the same set of features. In addition to the features of [7] and [12] introduced in Subsection 1.2.2.1, i.e., $\gamma_{\max}$, σ_{ap}, σ_{dp}, σ_{aa}, σ_{af} and P, three novel features σ_a, μ_{42}^a and μ_{42}^f have been employed, where σ_a is the standard deviation of the normalized-centralized instantaneous amplitude in the non-weak segment of a signal, μ_{42}^a is the kurtosis of the normalized instantaneous amplitude, μ_{42}^f is the kurtosis of the normalized instantaneous frequency. It is worth noting that there are slight modifications in the definitions of $\gamma_{\max}$ and P in [12], [98] and [99] compared to those in [7]. Their new definitions can be found in Chapter 2. The classification is realized by hierarchically comparing the features with their associated thresholds along a decision tree. These classifiers are able to classify AM, DSB, LSB, USB, FM, VSB, combined AM-FM, ASK2, ASK4, PSK2, PSK4, FSK2 and FSK4 signals. Some of Azzouz and Nandi's features or their modifications are frequently

adopted by other researchers in their work (e.g., [38] and [41]). For this reason, these features will be analyzed in Chapter 2.

Based on the features $\gamma_{\max}$, σ_{ap}, σ_{dp}, σ_a and μ_{42}^f of [99], Dubuc et al. [38] developed a scheme to classify CW, AM, DSB, SSB, FM, PSK2, PSK4 and OTHER signals, where OTHER represents QAM or MPSK signal with $M \geq 4$ (i.e., PSK4 may also be classified as OTHER). In testing the performance, the pulse shaping function for PSK and QAM is chosen as either raised function or square-root raised cosine function, and FSK signals are continuous phase signals generated by using filtered M-ary symbols to modulate the carrier. However, only the simulation results for SNR=5 dB are reported in [38], and they are not good — the classification success rates for AM (voice) and DSB (voice) are less than 50%.

The classifier of [41] is also an extension of [99]. It is able to classify CW, AM, DSB, PSK2, PSK4, $\pi/4$-QPSK, FM, low-modulated commercial FM, AMPS FM, FSK, MPSK with $M \geq 8$ (but the value of M is unrecognized), noise and OTHER signals, where commercial FM and AMPS FM contains a pilot tone along with the modulated signal, and OTHER stands for other non-constant envelope signals such as QAM. It is worth noting that fourth-order power law has been applied to the discrimination among PSK types. That is, for a signal recognized as M-ary PSK with $M \geq 4$, its fourth-order power's fast Fourier transform (FFT) spectrum will be examined — the signal will be classified as PSK4 if one peak presents in the spectrum, as $\pi/4$-QPSK if two peak present, and as M-ary PSK with $M \geq 8$ if no peak presents, respectively. For MFSK, the value of M is estimated by counting the number of peaks in the FFT spectrum of the squared received signal. However, how the spectral peak counting is implemented has not been reported.

Kim et al. [100] developed a classifier for CW, AM, SSB, FM, OOK, PSK2, PSK4, FSK2, FSK4, QAM16, QAM32 and noise signals. This classifier employs 29 features, among which some are the features of [99]. The features are used in a hierarchical way. Unlike other hierarchical classifiers, however, each level of this classifier uses several features which are selected by Genetic Algorithm (GA). It is claimed that the misclassification rate is less than 0.3% for SNR in the range from 7 dB to 12 dB.

In addition to classification of analog communication signals, Taira and Murakami [11] also mentioned discriminating between analog communication signals and digital communication signals by using the estimated symbol rate. The symbol rate is estimated from the PSD of the squared instantaneous amplitude of the received signal. They stated that analog signals do not have symbol rate and its symbol rate estimation results will become an arbitrary value. However, their method will eventually lead to an estimate of the symbol rate no matter if the received signal is digitally modulated or not. That is, it is impossible to separate between analog and digital signals by using their approach. This is because they confused the problem of the detection of the presence of symbol rate and the problem of symbol rate the estimation — the two problems are different in essence.

Dobre1 et al. [101] presented a technique for classifying some analog and digital communication signals that have been shifted to baseband. The employed features include: (1) γ_1 — the integral of the Fourier transform magnitude of the cross-spectrum between in-phase component and quadrature component of the received signal normalized to the received signal's power; (2) γ_2 — the integral of the above-mentioned

cross-spectrum divided by the integral of the in-phase component's spectrum, where both integrals are for frequency greater than or equal to zero; (3) γ_3 — the ratio of the power of quadrature component to that of in-phase comment; (4) γ_4 — the mean value of the received signal normalized to the square root of its power; (5) the presence of symbol rate. In the hierarchical decision tree, γ_1, γ_2, γ_3 and γ_4 are compared with their preset thresholds whenever necessary — γ_1 for discriminating between SSB and other types of interest, γ_2 for distinguishing between LSB and USB, γ_3 for discriminating between complex (PSK4, PSK8, QAM16 and QAM64) and real (AM, DSB and PSK2) signals, and γ_4 for separating AM from DSB and PSK2, respectively. Further discrimination among complex signals is suggested using the existing AMR algorithms such as [44]. The discrimination between DSB and PSK2 is accomplished by *detecting* the presence of symbol rate, rather than *estimating* the symbol rate as suggested in [11]. It is claimed that the lowest SNR required to achieve a probability of correct classification of almost one is 2 dB. An extremely strict assumption in developing this classifier is that carrier frequency offset and carrier phase have been compensated without any residual effect. This is almost impossible in practice, thus limits the applications of this classifier. Moreover, it is not clear if the value of the symbol rate has been known in advance when detecting the presence of the symbol rate in [101].

Kitchen [102] proposed to classify signal types via matching the measured PSD with the PSD templates of known modulation types based on ML criterion. This classifier is designed to classify analog as well as digital communication signals. Some examples have been used to show its validity. Even for the same modulation method (e.g., PSK2), however, the theoretical PSD will be different if the modulation parameters (e.g., symbol

rate, pulse shaping function and excess bandwidth factor) are different. Then when matching the estimated PSD of the received signal with the PSD template for each concerned modulation type in a blind environment, the classifier may have to exhaustively try each combination of the modulation parameters for the same modulation type. This will make the computational burden extremely heavy even though the search grids are not very fine. Moreover, the PSD templates for analog modulations are obtained via training in [102]. Therefore, the applications of this approach are restricted in blind environments.

Some other publications such as [103]-[106] are also on the classification of analog and digital communication signals. For the simplicity of presentation, they are not introduced here.

Summary Due to the difficulty in seeking a universal PDF for an analogue modulated signal, the classifiers of this category generally employ feature matching based approaches. Therefore, the classifiers also have the advantages and limitations as mentioned in Subsection 1.2.1 and Subsection 1.2.2.1. It is noted that some algorithms such as [38] are designed to handle digital communication signals with non-rectangular pulse shaping. However, they are still inherently training-based algorithms, and thus may be only feasible to modulation types with modulation parameters very close to that of training data. Since much more have been talked on individual classifiers for both analog and digital communication signals, no further discussion will be conducted here.

1.3 Outline of this Dissertation

As aforementioned, some of the key features proposed by Azzouz and Nandi in [7], [12], [98] and [99] are quite often employed by other researchers. These features are straightforward and very simple to implement. In order to examine their robustness and their capability of handling other modulation formats, a thorough evaluation of these features has been carried out and the results are presented in Chapter 2.

For signals recognized as linearly modulated digital communication signals, it is often necessary to blindly equalize the received signal before the recognition of the concrete modulation type can be done. This generally requires knowing the carrier frequency and symbol rate of the received signal. A blind carrier frequency estimation algorithm and a blind symbol rate estimation algorithm for digital communication signals are developed in Chapter 3 and Chapter 4, respectively. The carrier frequency estimator is based on the phases of the autocorrelation functions of the received signal. Unlike the cyclic correlation based estimators, it does not require the transmitted symbols being non-circularly distributed. The symbol rate estimator is based on the cyclostationarity of digital communication signals. In order to adapt to the unknown symbol rate as well as the unknown excess bandwidth, the received signal is first filtered by using a bank of lowpass filters (LPFs). Symbol rate candidates and their associated measurements of confidence are extracted from the fourth-order cyclic moments of the complex envelopes of the LPF outputs, and the final estimate is made based on majority voting.

By exploring the properties of the PSDs of MFSK signals, two fast Fourier transform (FFT) based algorithms have been developed for classifying MFSK signals. In addition to recognizing the number of modulation levels, these two classifiers also

provide very good estimate of the frequency deviation of the received MFSK signal. This work is reported in Chapter 5.

In the past decades, hundreds of publications have been awarded to the AMR of communication signals. However, most of them assume that the received signal is only of analog modulation or is only of digital modulation. In blind environments, an analogue modulated communication signal fed to an AMR algorithm designed only for digital communication signals will eventually be recognized as a certain digital modulation, and vice versa. That is, AMR algorithms that are able to handle both analog and digital communication signals are required in practice. On the other hand, it is noted that the currently existing algorithms designed for both analog and digital communication signals are restricted in real world cases. Motivated by this, an AMR algorithm that is able to discriminate between analog communication signals and digital communication signals is developed in Chapter 6. In addition to the discrimination between analog and digital modulations, this classifier is able to recognize the concrete modulation type of an input analog communication signal, to estimate the symbol rate of linear digital modulations, and to estimate the frequency deviation and the number of modulation levels of MFSK signals.

Chapter 7 concludes this dissertation and outlines the future works.

CHAPTER 2

EVALUATION OF AZZOUZ AND NANDI'S AMR ALGORITHMS

2.1 Introduction

Azzouz and Nandi developed several feature-based AMR algorithms in [7], [12], [98] and [99]. Their developed features are quite often employed by other researchers (see e.g., [38], [41] and [100]). Thus it is worth thoroughly evaluating the performance of these algorithms.

The concerned modulation types by Azzouz and Nandi include AM, DSB, LSB, USB, FM, VSB, ASK2, ASK4, PSK2, PSK4, FSK2, FSK4 and combined AM-FM modulations. The algorithms of [7], [12], [98] and [99] are designed to discriminate among the above modulation types or among a subset of them. Azzouz and Nandi [98] have also considered the classification of digital communication signals with higher alphabet sizes. The algorithm of [98] does not recognize the concrete modulation type of the input signal. Instead, it classifies the input into one of the following three groups: amplitude modulations (including ASK2, ASK4, ASK8 and PSK2), combined amplitude-phase modulations (including PSK4 and PSK8), and angle modulations (including FSK2, FSK4, and FSK8). Due to the band-limited characteristic of communication channels, PSK signals will have amplitude variations. This is the reason why PSK signals are recognized either as amplitude modulation or as combined amplitude-phase modulation in [98]. The algorithms of [7], [12], [98] and [99] have some differences in the concerned modulation types and the implementations. However, they are all based on part or all of the same set of features extracted from the received signal. Therefore, the evaluation will be performed on these features, rather than on the details of each algorithm. In next

section, the signal models and the feature definitions of [12] will be introduced. Simulation results, analysis and discussions on these features will be presented in Section 2.3. Conclusions are drawn in Section 2.4.

2.2 Signal Models and Feature Definitions

The AM, DSB, LSB, USB, FM, PM, VSB, PSK2 and PSK4 signals in [12] are defined in the same way as in [107], while the definitions of MASK and MFSK signals are slightly different. To be concrete, the definitions of MASK, MFSK and combined AM-FM modulations defined in [12] are listed in Table 2.1. It should also be noted that the pulse shaping function for digital modulations defined in [12] is assumed to be the standard unit pulse of duration T with T standing for the symbol period.

Table 2.1 Models of Some Signals in Reference [12]

Type	Transmitted Signal	Remarks
ASK2	$x(t) = s_n \cos(2\pi f_c t)$ for $nT \le t < (n+1)T$	f_c is carrier frequency, T is symbol duration, and s_n takes discrete values of 0.2 or 1.0.
ASK4	$x(t) = s_n \cos(2\pi f_c t)$ for $nT \le t < (n+1)T$	Values of s_n: 0.25, 0.5, 0.75 and 1.0.
FSK2	$x(t) = \cos(2\pi(f_c + f_n)t)$ for $nT \le t < (n+1)T$	f_n takes discrete values of $-2R_s$ or $2R_s$, where $R_s = \frac{1}{T}$ is the symbol rate.
FSK4	$x(t) = \cos(2\pi(f_c + f_n)t)$ for $nT \le t < (n+1)T$	f_n takes discrete values of $-2R_s$, $-R_s$, R_s or $2R_s$.
AM-FM	$x(t) = \left(1 + K_a s_1(t)\right)\cos\left[2\pi f_c t + 2\pi f_\Delta \int_{-\infty}^{t} s_2(\tau)d\tau\right]$	$s_1(t)$ and $s_2(t)$ are the modulating signals, K_a is the amplitude modulation index, f_Δ is the peak frequency deviation.

Azzouz and Nandi [12] considered the transmitted signal is blurred by zero mean additive Gaussian noise (AWGN), and both the transmitted signal and the noise are band-limited. The received signal, which is sampled at sampling rate f_s Hz, is expressed in

complex form by applying Hilbert transform. The complex data sequence is divided into several nonoverlapping segments, where each segment contains N_s samples. For each segment, the instantaneous amplitudes $\{a(i):\ i=1,2,\cdots,N_s\}$ and instantaneous phases $\{\phi(i):\ i=1,2,\cdots,N_s\}$ are then extracted, where the index i represents that $a(i)$ and $\phi(i)$ are for the $i-th$ complex sample. A simple scheme is employed to unwrap the instantaneous phases, resulting in an unwrapped phase sequence $\{\phi_{uw}(i):\ i=1,2,\cdots,N_s\}$. The nonlinear phases $\{\phi_{NL}(i):\ i=1,2,\cdots,N_s\}$ are then obtained by removing the linear phase owing to the carrier frequency from the unwrapped phases. The instantaneous frequencies $\{f(i):\ i=1,2,\cdots,N_s-1\}$ are also derived by differentiating the sequence of $\{\phi_{uw}(i)\}$. Based on the above sequences, some other sequences are defined as follows:

Normalized instantaneous amplitude $a_n(i)$

$$a_n(i) \overset{\Delta}{=} a(i) \Big/ \left(\tfrac{1}{N_s} \sum_{i=1}^{N_s} a(i) \right) \tag{2.1}$$

Centralized-normalized instantaneous amplitude $a_{cn}(i)$

$$a_{cn}(i) \overset{\Delta}{=} a_n(i) - 1 \tag{2.2}$$

Centralized-nonlinear instantaneous phase $\phi_{NLC}(i)$

$$\phi_{CNL}(i) \overset{\Delta}{=} \phi_{NL}(i) - \tfrac{1}{N_s} \sum_{i=1}^{N_s} \phi_{NL}(i) \tag{2.3}$$

Centralized-normalized instantaneous frequency $f_{cn}(i)$

$$f_{cn}(i) \overset{\Delta}{=} \left(f(i) - \tfrac{1}{N_s} \sum_{i=1}^{N_s} f(i) \right) \Big/ R_s \tag{2.4}$$

where R_s stands for the symbol rate of the input signal. Then nine key features are defined as:

$$\gamma_{\max} \overset{\Delta}{=} \max \left| DFT\left(a_{cn}(i)\right) \right|^2 / N_s \tag{2.5}$$

$$\sigma_a \overset{\Delta}{=} \sqrt{\frac{1}{L}\left[\sum_{a_{cn}(i)>a_t} a_{cn}^2(i)\right] - \left[\frac{1}{L}\sum_{a_{cn}(i)>a_t} a_{cn}(i)\right]^2} \tag{2.6}$$

$$\sigma_{aa} \overset{\Delta}{=} \sqrt{\frac{1}{N_s}\left[\sum_{i=1}^{N_s} \left|a_{cn}^2(i)\right|\right] - \left[\frac{1}{N_s}\sum_{i=1}^{N_s} \left|a_{cn}(i)\right|\right]^2} \tag{2.7}$$

$$\mu_{42}^a \overset{\Delta}{=} E\left[a_{cn}^4(i)\right] \Big/ \left(E\left[a_{cn}^2(i)\right]\right)^2 \tag{2.8}$$

$$\sigma_{ap} \overset{\Delta}{=} \sqrt{\frac{1}{L}\left[\sum_{a_{cn}(i)>a_t} \phi_{CNL}^2(i)\right] - \left[\frac{1}{L}\sum_{a_{cn}(i)>a_t} \left|\phi_{CNL}(i)\right|\right]^2} \tag{2.9}$$

$$\sigma_{dp} \overset{\Delta}{=} \sqrt{\frac{1}{L}\left[\sum_{a_{cn}(i)>a_t} \phi_{CNL}^2(i)\right] - \left[\frac{1}{L}\sum_{a_{cn}(i)>a_t} \phi_{CNL}(i)\right]^2} \tag{2.10}$$

$$\sigma_{af} \overset{\Delta}{=} \sqrt{\frac{1}{L}\left[\sum_{a_{cn}(i)>a_t} f_{cn}^2(i)\right] - \left[\frac{1}{L}\sum_{a_{cn}(i)>a_t} \left|f_{cn}(i)\right|\right]^2} \tag{2.11}$$

$$\mu_{42}^f \overset{\Delta}{=} E\left[f_{cn}^4(i)\right] \Big/ \left(E\left[f_{cn}^2(i)\right]\right)^2 \tag{2.12}$$

$$P \overset{\Delta}{=} \frac{P_L - P_U}{P_L + P_U} \tag{2.13}$$

where $DFT\left(a_{cn}(i)\right)$ stands for the N_s-point DFT of $\{a_{cn}(i)\}$, L is the number of non-weak samples in a segment, a_t is a preset threshold for detecting non-weak samples, and

$$P_L \overset{\Delta}{=} \sum_{i=1}^{f_{cn}} \left|S_x(i)\right|^2 \tag{2.14}$$

$$P_U \overset{\Delta}{=} \sum_{i=1}^{f_{cn}} \left|S_x(i+f_{cn}+1)\right|^2 \tag{2.15}$$

where $S_x(i)$ stands for the DFT of the received complex signal, and $(f_{cn}+1)$ is the index of the DFT bin corresponding to the carrier frequency f_c.

2.3 Evaluation of the Key Features

Azzouz and Nandi [12] claimed that their algorithms are able to operate on real-time and succeed under relatively high SNR (i.e., SNR≥10 dB for analog modulations only or digital modulations only, and SNR≥15 dB for joint analog and digital modulations). To check their features' feasibility and extendibility, this dissertation will also assess the performance of their features under lower SNRs and for modulation types not considered by Azzouz and Nandi. Some modifications are also suggested to make these features more practical.

2.3.1 Comments on the Segment Size N_s

The performance evaluation in [12] is performed under the following conditions: (1) the carrier frequency f_c is 150×10^3 Hz; (2) the symbol rate R_s is 12.5×10^3 symbols per second for digital modulations; (3) the bandwidth of modulating signal is 8×10^3 Hz for analogue modulations; (4) before adjusting the SNR, both the modulated signal and the AWGN are filtered using a BPF, which is centered at f_c and whose bandwidth is 1.2 times of the theoretical bandwidth of the modulated signal; (5) the sampling rate f_s is 1200×10^3 Hz; (6) the number of data samples in a segment is N_s=2048.

Azzouz and Nandi claimed that their algorithms are able to operate on real-time since a segment only corresponds to about 17 milliseconds in time and the feature calculations are very fast. However, the above settings imply a segment only contains

about 21 symbols for digital communication signals. Such a few symbols are generally not adequate to reveal the statistical characteristics of a digital communication signal. To verify this, some simulation results on the features σ_{aa} , σ_{ap} and σ_{af} are shown respectively in Figure 2.1, Figure 2.2 and Figure 2.3, where the simulation settings except N_s are exactly the same as mentioned above, the SNR is 20 dB, and the carrier frequency is assumed known when extracting the values of σ_{ap} and σ_{af} .

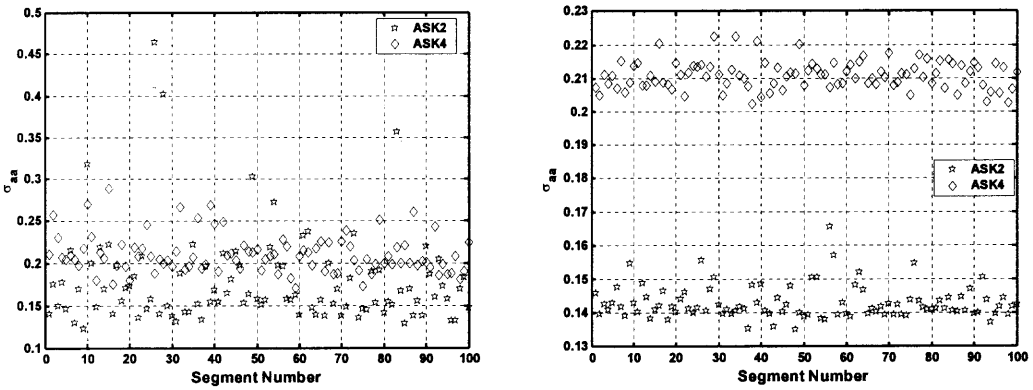

Figure 2.1 Measured values of σ_{aa} under SNR = 20 dB (Left column: N_s=2048, Right column: N_s=65536).

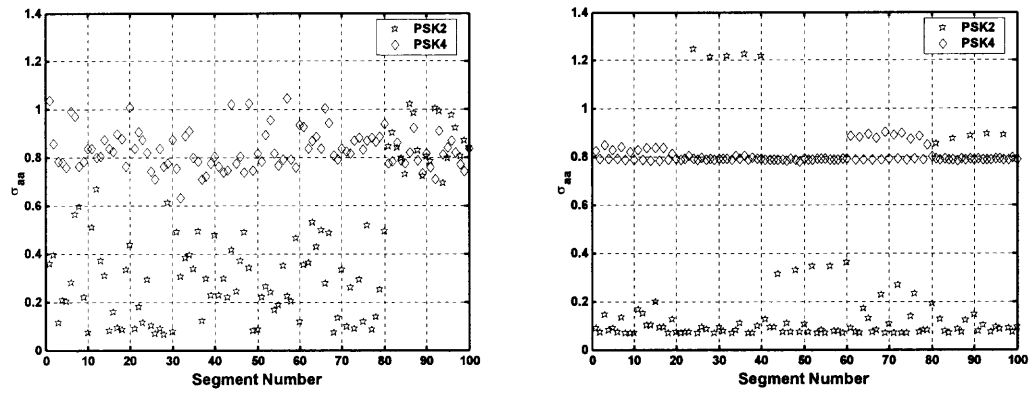

Figure 2.2 Measured values of σ_{ap} under SNR = 20 dB (Left column: N_s=2048, Right column: N_s=65536).

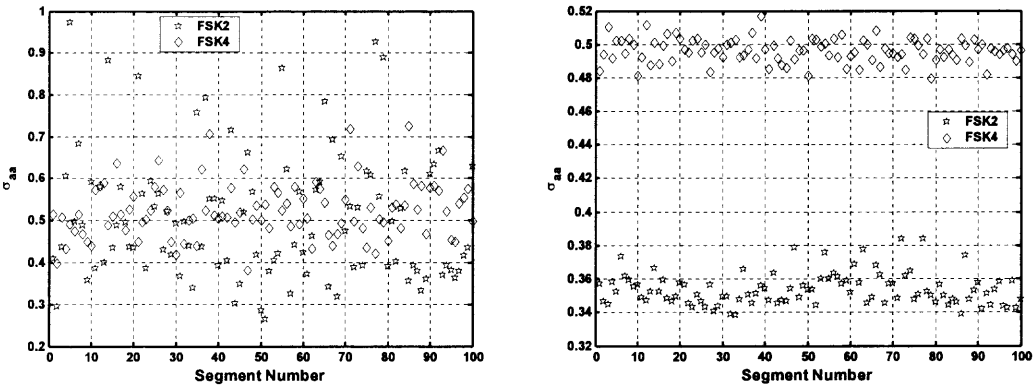

Figure 2.3 Measured values of σ_{af} under SNR = 20 dB (Left column: N_s=2048, Right column: N_s=65536).

The feature σ_{aa} is designed to classify ASK2 and ASK4, the feature σ_{ap} is designed to classify PSK2 and PSK4, and the feature σ_{af} is for classification of FSK2 and FSK4. In Figure 2.1 through Figure 2.3, the left columns represent the measured feature values when N_s is chosen as 2048, whereas the right columns correspond to N_s=65536. It is evident that the measured feature values for different modulation types will mix with each other if the segment size is N_s=2048, and thus it will be difficult to discriminate the modulation types. If the segment size is increased, however, the gap between the measured feature values for different modulation types will increase, and the modulation classification would become more reliable. This can be observed from the right columns of Figures 2.1 through 2.3.

Based on the above analysis and observation, it is suggested that the segment size should be increased. In the reset of this chapter, the reported simulation results are all obtained with N_s = 65536, except explicitly pointed out.

2.3.2 Comments on the Feature σ_{dp}

The feature σ_{dp} is designed to discriminate signals without direct phase information (e.g., AM and ASK) and signals with direct phase information (e.g., DSB, LSB, USB, FM, FSK, PSK). It is expected to be smaller for the former and larger for the latter.

In extracting this feature, it requires to unwrap the instantaneous phases and estimate the carrier frequency. If errors happen in either of the above two steps, the measured values of σ_{dp} may differ greatly from their theoretical values, resulting in misclassifications. To verify this claim, the simulation results on some AM, FM and ASK signals are shown in Figure 2.4 and Figure 2.5, where the decimal following the notation of AM or FM stands for the modulation depth (e.g., AM-0.6 stands for an AM signal with modulation depth being 0.6), and ASK8 stands for an ASK signal with its eight amplitude levels being $0.125 \times m$ for $m = 1, 2 \cdots, 8$. The SNR is 20 dB for Figure 2.4 and 15 dB for Figure 2.5, the segment size is N_s =65536, the threshold for detection of non-weak samples is chosen as $a_t = 0.95$, and the other simulation settings are the same as mentioned in Subsection 2.3.1.

The results in the left columns of Figure 2.4 and Figure 2.5 are obtained when the carrier frequency is exactly known, while those in the right columns are obtained when the carrier frequency is estimated from the unwrapped instantaneous phases. It can be observed that the performance of modulation classification based on σ_{dp} is still wanting even though the segment size has been enlarged to N_s = 65536 and the carrier frequency is exactly known, and that the performance will be worse if the carrier frequency is not exactly known.

In a word, due to errors happening during phase unwrapping and carrier frequency estimation, the discrimination based on the feature σ_{dp} is not reliable although the SNR is high. To improve the performance, advanced phase unwrapping technique and carrier frequency estimation technique are required.

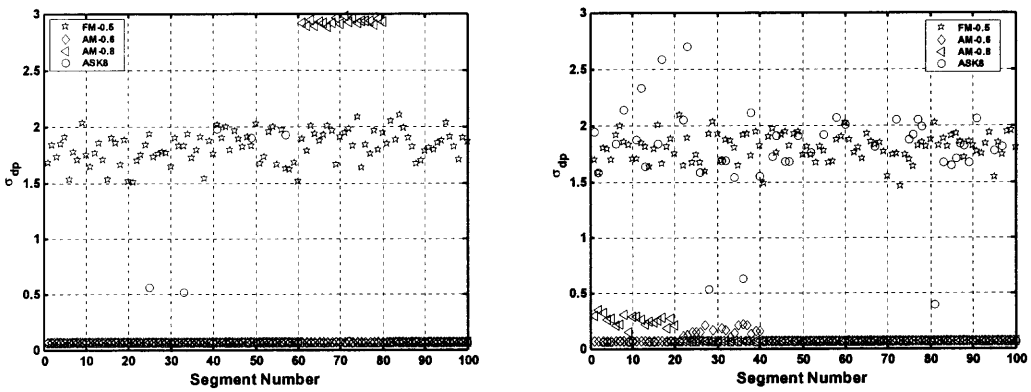

Figure 2.4 Measured values of σ_{dp} : SNR = 20 dB, N_s = 65536 (Left column: f_c is exactly known, Right column: f_c is estimated from the received data).

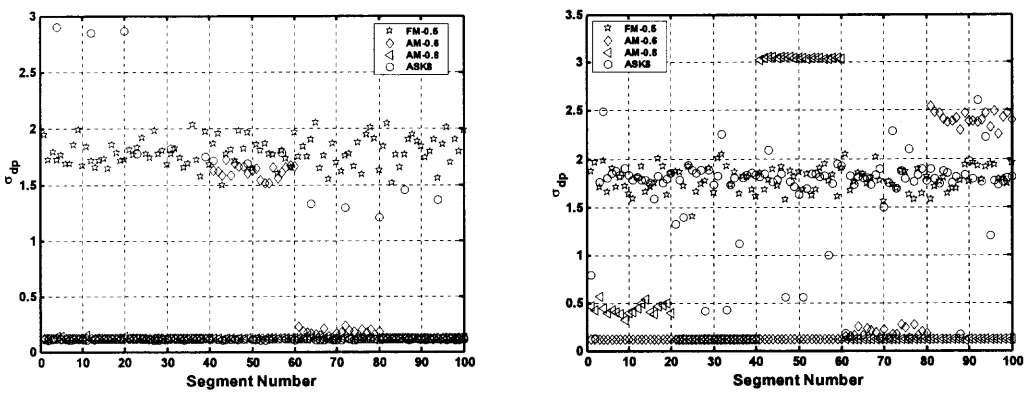

Figure 2.5 Measured values of σ_{dp} : SNR = 15 dB, N_s = 65536 (Left column: f_c is exactly known, Right column: f_c is estimated from the received data).

2.3.3 Comments on the Feature γ_{max}

The feature γ_{max} is designed to discriminate between constant envelope (CE) signals (e.g., FM and FSK) and non-CE signals (e.g., AM, DSB, SSB, ASK, band-limited PSK). It is expected to be smaller for the former and larger for the latter.

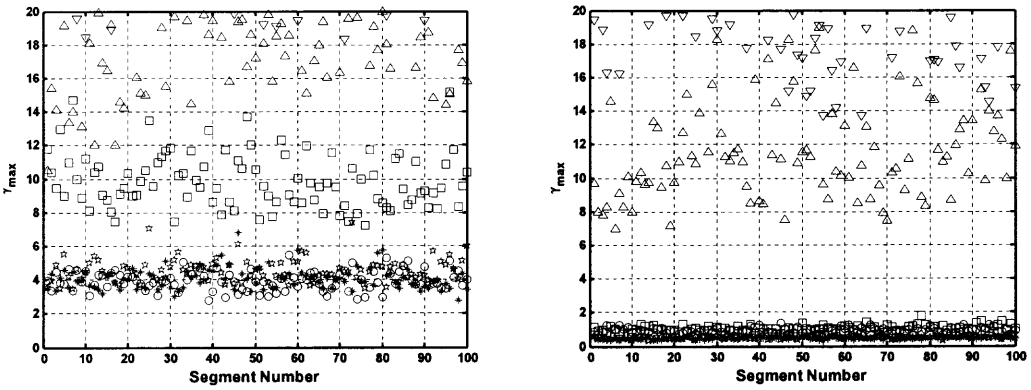

Figure 2.6 Measured values of γ_{max} : N_s=65536; SNR is 10 dB for the left subfigure and 20 dB for the right one (up-triangle: AM-0.6, down-triangle: AM-0.8, six-point star: FM-5.0, square: FM-0.5, circle: FSK2, asterisk: FSK4).

It is found through simulations that this feature is reliable for higher SNR (e.g., SNR≥15 dB). However, the measured feature values are heavily dependent on the SNR. If the SNR is lower (e.g., 10 dB), the range of the measured feature values for a modulation format may greatly change. In a worse case, it is even impossible to find a threshold workable for both lower and higher SNRs. To explain this point, the simulation results on AM-0.6, AM-0.8, FM-0.5, FM-5.0, FSK2 and FSK4 are shown in Figure 2.6. In order to reveal the details, the measured feature values that are greater than 20 (corresponding to non-CE signals) are not shown in Figure 2.6. It is clear that the workable threshold can be chosen in a relatively wide range and the highest workable

threshold is about 6.5 if the SNR is 20 dB. However, when the SNR is 10 dB, the threshold can only be chosen in a very narrow range and the lowest workable threshold is about 13.0. Then it is impossible to choose a threshold workable for both SNR=10 dB and SNR=20 dB.

The above discussed SNR dependency will limit the applications of the feature $\gamma_{\max}$ since it is very likely that the SNR of the received signal is lower than 15 dB in practice. This suggests estimating the SNR and then adjusting the decision threshold accordingly if one still wants to discriminate CE signals and non-CE signals by using the feature $\gamma_{\max}$.

2.3.4 Comments on the Feature μ_{42}^{a}

This feature evaluates the amplitude compactness of a received signal, thus is used to discriminate between AM signals and ASK signals. It is expected to be larger for AM signals and smaller for ASK signals.

This feature is found not reliable if the segment size is N_s = 2048. Simulations on some AM and ASK signals with segment size N_s=65536 have been carried out, and the resultant success rates of discrimination between AM signals and ASK signals based on μ_{42}^{a} are reported in Table 2.2, where the decision threshold for μ_{42}^{a} is selected as 2.75. It is evident that the discrimination is very reliable if a larger segment size (e.g., N_s=65536) is used and the SNR is not too low (e.g., SNR≥10 dB). In fact, if the SNR is greater than or equal to 10 dB, the decision threshold can be selected in the range from 2.5 to 2.7 and the success rate is 100% for all testing modulation formats. For SNR=5 dB, however, the measured feature values for different modulation formats are near to each other. In this

case, the decision threshold can only be selected in a very narrow range, and the best decision threshold is 2.75. It can be seen from Table 2.2 that the performance of discrimination based on μ_{42}^{a} is not good for SNR=5 dB. It should be noted that some ASK signals with raised-cosine pulse shaping functions have also been tested.

Table 2.2 Success Rates of Discrimination between AM Signals and ASK Signals Based on the Feature μ_{42}^{a} (β is the Roll-off Factor of Raised-cosine Function)

Signal Type	SNR=5 dB	SNR=10 dB	SNR=15 dB	SNR=20 dB
AM-0.2	96%	100%	100%	100%
AM-0.3	98%	100%	100%	100%
AM-0.4	92%	100%	100%	100%
AM-0.6	95%	100%	100%	99%
AM-0.8	86%	100%	98%	98%
AM-1.0	83%	95%	98%	98%
ASK2: rectangular pulse of duration T	100%	100%	100%	100%
ASK4: rectangular pulse of duration T	100%	100%	100%	100%
ASK8: rectangular pulse of duration T	99%	100%	100%	100%
ASK2: raised cosine function, β=0.35	87%	100%	100%	100%
ASK4: raised cosine function, β=0.35	91%	100%	100%	100%
ASK8: raised cosine function, β=0.35	92%	100%	100%	100%

In summary, the feature μ_{42}^{a} is very reliable for SNR≥10 dB if the segment size is larger (e.g., N_s=65536). However, it may become unreliable if the SNR is lower (e.g., SNR=5 dB).

2.3.5 Comments on the Feature μ_{42}^{f}

This feature describes the frequency compactness of the received signal, and thus is used to discriminate between FM signals and FSK signals. It is expected to be larger for the former and smaller for the latter.

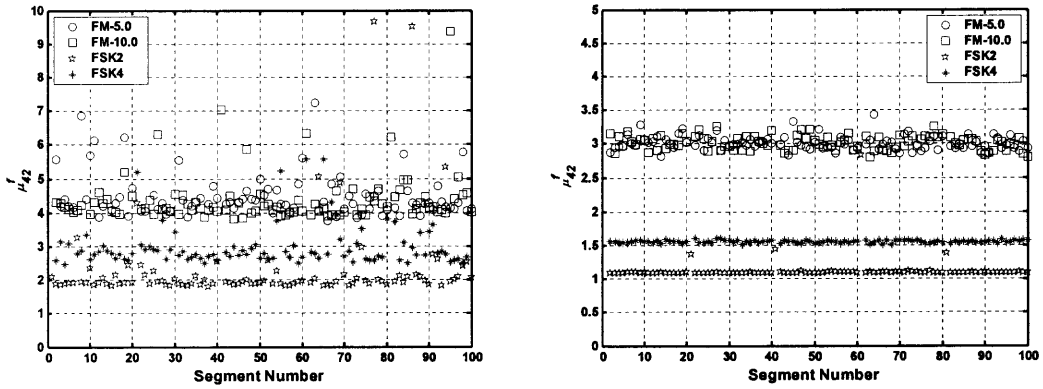

Figure 2.7 Measured values of μ_{42}^{f}: N_s=65536 (Left subfigure: SNR=10 dB, Right subfigure: SNR=20 dB).

To demonstrate the characteristics of this feature, some simulations results with N_s=65536 are reported in Figure 2.7. It is observed from Figure 2.7 that the decision threshold for SNR=20 dB should be less than 2.8, while the decision threshold for SNR=10 dB should be at least greater than 3.0. That is, no common threshold can be found workable for both SNR=10 dB and SNR=20 dB. On the other hand, it is found through extensive simulations that a common decision threshold does exist for the above signals if the SNR is greater than or equal to 15 dB.

From the above, it can be concluded that this feature is highly SNR-dependent. It is able to work well for higher SNR (e.g., SNR≥15 dB), but is not feasible for a wider SNR range (e.g., SNR≥10 dB). Moreover, it is found through simulations that this feature is not reliable if the segment size is N_s=2048.

2.3.6 Comments on the Feature σ_a

This feature is designed to discriminate between PSK2 signals and DSB signals and to discriminate between PSK4 signals and combined AM-FM signals. It is expected to be smaller for PSK2 and PSK4 and larger for DSB and combined AM-FM.

In addition to DSB and combined AM-FM signals, extensive simulations have also been carried out on PSK2, PSK4 and PSK8 signals with rectangular pulse shaping function, raised-cosine pulse shaping function and square-root raised-cosine pulse shaping function. The simulation results show that this feature is very reliable for SNR≥5 dB even when the segment size is chosen as N_s=4096. Certainly, the gap between the measured feature values for PSK signals and those for DSB and combined AM-FM signals will decrease as the SNR decreases.

2.3.7 Comments on the Feature σ_{aa}

If the modulation type of a received signal is recognized as MASK, the feature σ_{aa} will be employed to further recognize its alphabet size, i.e., M. This feature is originally designed to discriminate between ASK2 and ASK4 signals. It is expected to be smaller for ASK2 and larger for ASK4.

Since the feature σ_{aa} is the only means to recognize the value of M of an MASK signal in the algorithms proposed by Azzouz and Nandi, it is necessary to check its capability of recognizing ASK signals with higher alphabet size. By following the ASK definitions of Azzouz and Nandi, the symbols of an MASK signal can be defined as $s_m = m/M$, $m = 1, 2, \cdots, M$. If the transmitted symbols are i.i.d., the received signal is noise free and the sampling rate is an integer multiple of the symbol rate, then the values

of σ_{aa} for ASK2, ASK4, ASK8, ASK16 and ASK32 will be 0.0, 0.2, ≈0.2485, ≈0.2696 and ≈0.2794, respectively. It can be observed that the minimum feature distance decreases as the value of M increases. Then it can be predicted that the recognition of the value of M will become more difficult if the received signal is noisy and the possibly highest value of M is greater than four.

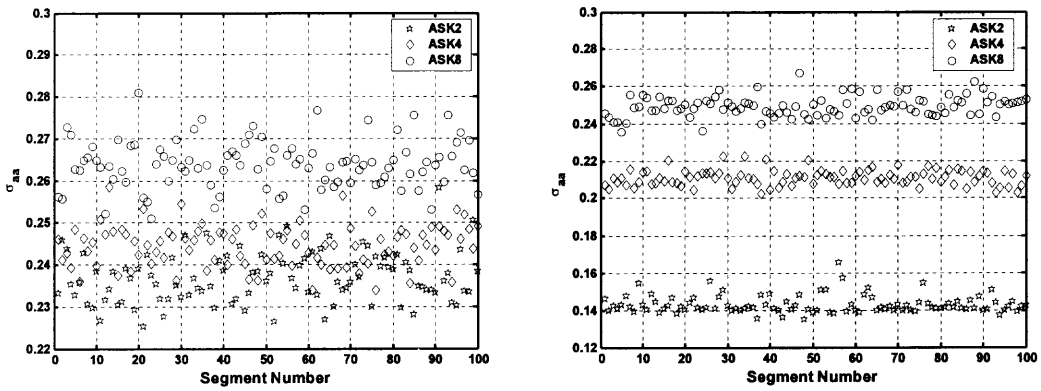

Figure 2.8 Measured values of σ_{aa} : N_s =65536 (Left subfigure: SNR=10 dB, Right subfigure: SNR=20 dB).

It is found through simulations that the segment size for calculating the feature σ_{aa} should be increased with respect to that proposed by Azzouz and Nandi. With the segment size enlarged to N_s =65536, this feature is found to be able to discriminate among ASK2, ASK4 and ASK8 signals for SNR≥15 dB. However, the discrimination based on this feature becomes difficult if the SNR is lower (e.g., SNR=10 dB). Moreover, it is impossible to find decision thresholds that are workable for both lower SNR (e.g., 10 dB) and higher SNR (e.g., 20 dB). This is evident by inspecting the simulation results reported in Figure 2.8. Therefore, this feature can only work when the SNR is high (e.g., SNR≥15 dB).

2.3.8 Comment on the Feature σ_{ap}

This feature serves to check if the received signal contains indirect phase information or not. It is expected to be smaller for modulation types in the set {PSK2, DSB} and be larger for the modulation types in the set {combined AM-FM, FM, FSK, MPSK with $M \geq 4$}.

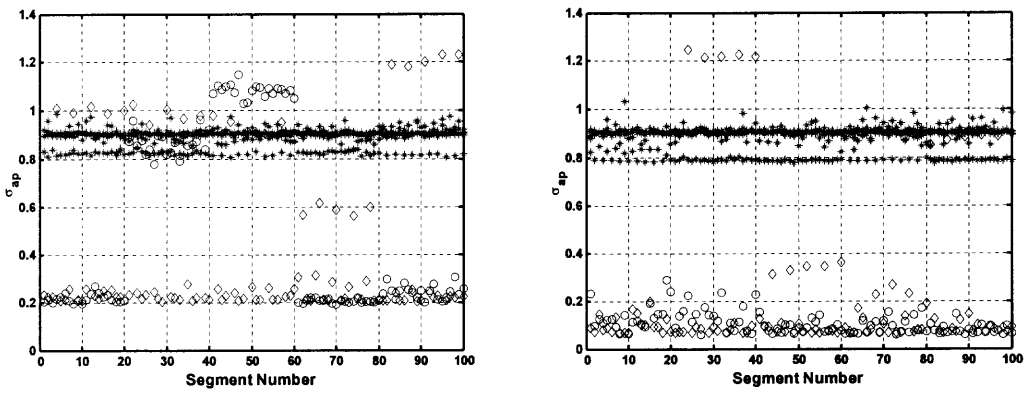

Figure 2.9 Measured values of σ_{ap} : N_s=65536 , and f_c is exactly known (Left subfigure: SNR=10 dB, Right subfigure: SNR=20 dB).

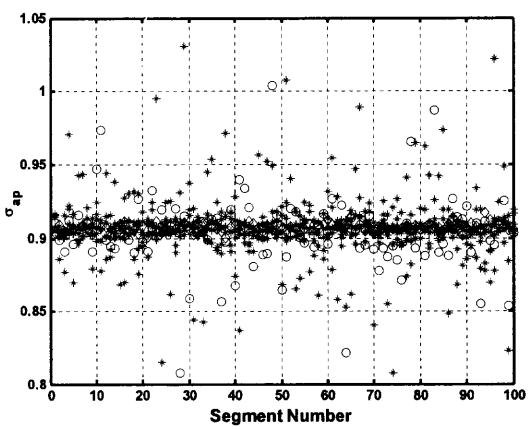

Figure 2.10 Measured values of σ_{ap} : N_s=65536 , SNR=20 dB, and f_c is estimated from the received signal (circle sign: DSB; diamond sign: PSK2; asterisk sign: FM-0.5, FM-5.0, FM-10.0, FSK2, FSK4, and PSK4).

Some simulation results on this feature are reported in Figure 2.9, where the measured feature values for DSB signal is denoted by circle signs, those for PSK2 are denoted by diamond signs, and those for FM-0.5, FM-5.0, FM-10.0, FSK2, FSK4 and PSK4 signals are all denoted by asterisk signs. It can be observed that this feature is able to successfully discriminate between the modulation-type set of {DSB, PSK2} and the modulation-type set of {FM, FSK, PSK4} when the SNR is SNR=20 dB. However, the success rate will dramatically decrease if the SNR is 10 dB. It should be noted that the results of Figure 2.9 are obtained when the carrier frequency is exactly known. It is found through extensive simulations that the performance of modulation classification based on σ_{ap} will be much worse or the classification may even totally fail if the carrier frequency is estimated from the received signal rather than exactly known. This is evident in the partial simulation results reported in Figure 2.10.

The feature σ_{ap} is also the only means to recognize the alphabet size of an MPSK in the algorithms proposed by Azzouz and Nandi. Extensive simulations on PSK2, PSK4 and PSK8 signals have shown that the performance of recognizing the value of M of an MPSK signal based on σ_{ap} is poor even though the carrier frequency is exactly known and the SNR is 20 dB, and that the discrimination among PSK2, PSK4 and PSK8 is impossible if the carrier frequency is estimated from the instantaneous phase although the SNR is 20 dB. Such results can be imagined via inspecting Figure 2.9 and Figure 2.10. For the simplicity, the detailed results are not reported here. In fact, the theoretical values of σ_{ap} for PSK2, PSK4, PSK8, PSK16 and PSK32 are 0, ≈0.7875, ≈0.8781, ≈0.8998 and ≈0.9051, respectively. That is, the minimum feature distance decreases as the possibly highest value of M increases. Then the above results are not surprising.

In a word, the feature σ_{ap} may be the most unreliable one among the features proposed by Azzouz and Nandi. Due to its sensitivity to the carrier frequency estimation error and the SNR condition, this feature may even fail when the SNR is high (e.g., 20 dB). Moreover, this feature is not capable of recognizing the value of M when the possible value of M of the input MPSK signal is higher than four.

2.3.9 Comments on the Feature σ_{af}

This feature is designed to discriminate between FSK2 signals and FSK4 signals. It is expected to be smaller for FSK2 and larger for FSK4.

It is noted that this feature is actually the standard deviation of the absolute normalized-centralized instantaneous frequency, where the frequency normalization is performed by dividing the centralized instantaneous frequency by the symbol rate R_s. The modulating frequencies of a general MFSK will take the following discrete values

$$f_d \times (2m-1-M)/2 \text{ for } m = 1, 2, \cdots, M \tag{2.16}$$

where f_d is the frequency deviation between immediately neighboring modulating frequencies. In an ideal case (i.e., the received signal is noise free, the transmitted symbols are i.i.d., the sampling rate is an integer multiple of the symbol rate, and the instantaneous frequency has been perfectly extracted), the value of σ_{af} for an MFSK signal will be $\sigma_{af} = \frac{f_d}{R_s}\sqrt{\frac{M^2-4}{48}}$ for an even M and $\sigma_{af} = \frac{f_d}{R_s}\sqrt{\frac{(M^2-1)\times(M^2+3)}{48M^2}}$ for an odd M. It is clear that σ_{af} will be zero for $M = 2$ no matter what value the frequency deviation ratio f_d / R_s will be. However, the frequency deviation ratio does affect the value of σ_{af} if M is not equal to two. In practice, the frequency deviation ratio may be any

positive real value as long as it is greater than or equal to 0.5 [108]. Then it is easy to find frequency deviation ratios that make the value of σ_{af} for an FSK4 signal is greater than that for an FSK8 signal, and vice versa. That is, the definition of this feature makes it inherently not suitable for classifying MFSK signals with higher alphabet sizes.

In fact, the feature σ_{af} will encounter problems even when used to discriminate between FSK2 and FSK4. This is explained as follows. As mentioned above, the theoretical value of σ_{af} for an FSK2 signal is zero. The FSK4 signal defined in [12] can be thought of as a 5-ary FSK with f_d / R_s being one. Then the theoretical value of σ_{af} for the FSK4 defined in [12] will be $\sigma_{af} \approx 0.7483$. Therefore, a decision threshold can be selected around 0.374 to discriminate between FSK2 and FSK4 — Azzouz and Nandi [12] set the threshold for σ_{af} as 0.4. In practice, however, the frequency deviation ratio may be as low as 0.5. In this case, the theoretical value of σ_{af} for an FSK4 signal defined according to (2.16) will be $\sigma_{af} = 0.25$. Then this FSK signal will be recognized as an FSK2 signal if the threshold of Azzouz and Nandi is used.

The above ambiguity with σ_{af} can be removed if the instantaneous frequency is normalized by using the frequency deviation f_d. However, the blind estimation of the frequency deviation remains open.

In addition to the above limitations, this feature is also heavily SNR-dependent. To be intuitive, some simulation results on FSK2, FSK4 and FSK8 signals are shown in Figure 2.11, where FSK2 and FSK4 signals are as defined in Section 2.2, the eight modulating frequencies of FSK8 are $\pm R_s$, $\pm 2R_s$, $\pm 3R_s$ and $\pm 4R_s$, respectively, and

$R_s = 12.5k$ Hz is the symbol rate. It is evident that no common decision threshold can be found for discriminating between FSK2 and FSK4 or discriminating between FSK4 and FSK8 for SNR=10 dB and SNR=20 dB. That is, this feature may only work for a high SNR, but does not work for a wider SNR range (e.g., SNR≥10 dB).

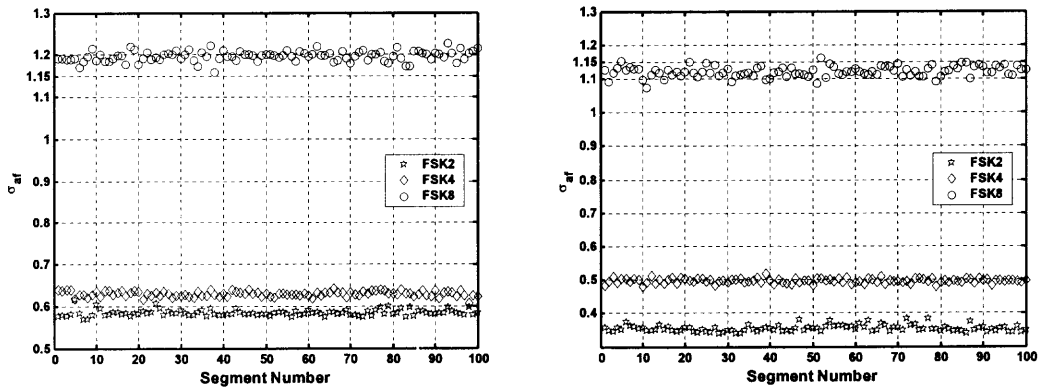

Figure 2.11 Measured values of σ_{af} : N_s=65536 (Left subfigure: SNR=10 dB, Right subfigure: SNR=20 dB).

2.3.10 Comments on the Feature P

This feature evaluates the spectral symmetry of the received signal. If its absolute value is greater than a preset threshold, the received signal will be recognized as a SSB signal; otherwise, the received signal is classified as non-SSB signal. If a received signal is classified as SSB, it will be further recognized as LSB when the value of P is positive and as USB when the value of P is negative.

It is found through simulations that this feature is able to successfully discriminate among LSB, USB and non-SSB if the carrier frequency is exactly known. If the carrier frequency can only be estimated from the received data, however, the classification performance will be worse, especially when the SNR is poor. To be intuitive, some

simulation results on LSB, USB and DSB signals are reported in Figure 2.12. It is evident that this feature is able to work for SNR=20 dB. However, it performs much worse if the SNR is 10 dB.

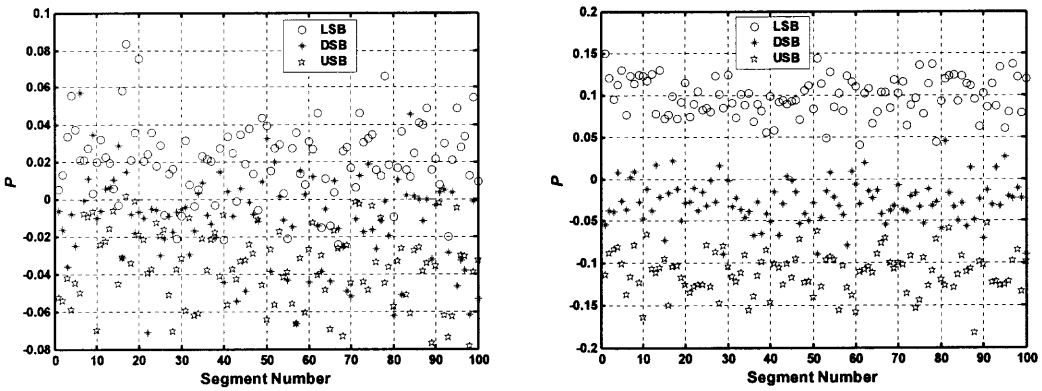

Figure 2.12 Measured values of P: N_s=65536, and f_c is estimated from the instantaneous phase (Left subfigure: SNR=10 dB, Right subfigure: SNR=20 dB).

The above problem is mainly due to the phase errors introduced by noise and the errors introduced during phase unwrapping, which in turn causes errors in estimating the carrier frequency. Azzouz and Nandi [12] proposed two carrier frequency estimation methods that are able to avoid the work of phase unwrapping. One is the frequency-centered method [109] as

$$\hat{f}_c = \frac{\sum_{k=1}^{N/2}\left\{k\left|Z(k)\right|^2\right\}}{\sum_{k=1}^{N/2}\left|Z(k)\right|^2} \tag{2.17}$$

where $Z(k)$ is the $k-th$ bin of the N-point DFT of the received complex signal. This method is a good estimator for signals with symmetric spectra and is poor for signals with asymmetric spectra. That is, the carrier frequency estimation error will be larger for SSB signals, and thus it is very likely that the measured value of the feature $|P|$ for a SSB

signal is less the preset threshold, resulting in misclassifications. The second method is to take the reciprocal of the average zero-crossing intervals as the estimate of the carrier frequency. Since this method is very sensitive to the noise, Azzouz and Nandi [12] proposed only using zero-crossings in the non-weak intervals of the received signal. However, the zero-crossing based estimator generally requires a very high sampling rate, which is prohibited in some circumstances. That is, these two carrier frequency estimators are either low accuracy for SSB signals or restricted in practice. Therefore, advanced blind carrier frequency techniques that are universal for SSB, FM, PSK and FSK signals should be developed and employed if one wants to adopt the feature P in his/her AMR algorithm.

In addition, the measured values of the feature P are not reliable even for SNR=20 dB if the segment size is N_s=2048. Therefore, the segment size should be enlarged in extracting P.

2.3.11 Comments on Classification of Other Modulation Types

In digital communications, pulse-amplitude-modulation (PAM) and QAM are often employed in addition to ASK, PSK and FSK. Both PAM and QAM signals can be expressed in complex form [108] as

$$x(t) = \sum_n I_n g(t - nT) e^{j2\pi f_c t} \tag{2.18}$$

where I_n represents the $n-th$ transmitted symbol, f_c is the carrier frequency, and $g(t)$ is the pulse-shaping function. For a QAM signal, the symbols $\{I_n\}$ take discrete complex values which are drawn from a constellation in the two-dimensional complex plane. For an MPAM signal, the symbols $\{I_n\}$ takes the following discrete values

$$(2m-1-M)/2, \quad \text{for } m=1,2,\cdots,M \tag{2.19}$$

It should be noted that a 2-ary PAM signal is equivalent to PSK2. In the following, it is implied that M is greater than two when mentioning MPAM signals.

The features introduced in Section 2.2 can be used to separate MPAM and QAM from the other modulation types. At first, both MPAM and QAM signals vary in amplitude no matter what kind of pulse shaping function is used. Then the feature $\gamma_{\max}$ can be employed to discriminate between the modulation types in the set {MPAM, QAM, ASK, PSK, AM, DSB, SSB, VSB, combined AM-FM} and the modulation types in the set {FM, FSK}. Secondly, both MPAM and QAM signals have direct phase information. Thus the feature σ_{dp} can be used to discriminate between the following subsets: {MPAM, QAM, PSK, DSB, SSB} and {AM, ASK, VSB}. The feature P can be employed to separate SSB from MPAM, QAM, PSK and DSB. It is noted that MPAM does not have indirect phase information and QAM does have. Therefore, the feature σ_{ap} can be used to discriminate between the modulation types in the set {PSK2, MPAM, DSB} and the modulation types in the set {QAM, MPSK with $M \geq 4$}. The feature σ_a can be used to separate PSK2 from DSB and MPAM. The discrimination between MPAM and DSB can be done by using the feature μ_{42}^a, which is expected to be smaller for MPAM and larger for DSB. That is, the features of Azzouz and Nandi may be able to separate MPAM from the other modulations and classify QAM into the set of {PSK4, QAM}. However, these features are not capable of recognizing the concrete value of M for a PAM signal or recognizing the concrete symbol constellation of a QAM signal.

It should be noted that, owing to the limitations of the features as discussed in Subsection 2.3.2 through Subsection 2.3.10, the separation of MPAM and QAM from the other modulations can only be done well for relatively high SNR. This has been verified via simulations.

2.4 Conclusions

The works by Azzouz and Nandi in [7], [12], [98] and [99] have made great progress to the automatic modulation classification of communication signals. Their defined features are meaningful and easy to implement. Simulations have shown the validity of the features when the SNR is high (e.g., SNR≥15 dB). However, these features may encounter some problems in practice.

At first, the number of samples in a segment, as proposed by Azzouz and Nandi, is not adequate to represent the statistical characteristics of a communication signal. The result is that the features are unreliable if the SNR is lower. In fact, only the feature σ_a is found able to work well with a short data record. Azzouz and Nandi might have noticed the problem caused by a small segment size, and proposed to generate a decision for each short segment and then make the final decision by voting over multiple segments. If the rate of misclassification is high for each segment, however, the confidence of majority voting cannot be expected to be high enough. Moreover, Azzouz and Nandi did not mention how many segments are used in the majority voting in [7], [12], [98] and [99]. To make the features reliable, the author suggests increasing the segment size. This is especially important for digital communication signals. It should be noted that a larger segment size may make the algorithms not hold the property of real-time operation.

The second problem with the features of Azzouz and Nandi is their heavy SNR-dependency. That is, the feature distance between two different groups of modulation types generally decreases as the SNR decreases. This means that the decision threshold can only be selected in a narrower range if the SNR is lower. For the features $\gamma_{\max}$, μ_{42}^{f}, σ_{aa}, σ_{af} and P, it has been found through simulations that the thresholds workable for higher SNR (e.g., 20 dB) are not able to work when the SNR is lower (e.g., 10 dB), and vice versa. That is, no common thresholds can be found for both lower SNR and higher SNR. This makes the algorithms only able to work for higher SNR. To increase the workable SNR range, the author suggests estimating the SNR and adjusting the decision thresholds adaptively whenever possible.

It is also found via analysis and simulations that the features of Azzouz and Nandi may be able to recognize an *M*-ary ASK signal as MASK, an *M*-ary FSK signal as MFSK and an *M*-ary PSK signal as MPSK, respectively. However, these features are generally not capable of recognizing the concrete value of *M* if the possibly highest value of *M* is greater than four.

In extracting the features P, σ_{ap} and σ_{dp}, it requires knowing the carrier frequency. There are some discussions and simulations on the carrier frequency estimation in [12]. However, it seems that Azzouz and Nandi simply used the accurate carrier frequency in [7], [12], [98] and [99] since no discussion can be found on the influence of carrier frequency offset (CFO) to the classification performance. The author has carried out some simulations on the features P, σ_{ap} and σ_{dp} with carrier frequency estimated from the received data. The results show that the CFO does degrade the performance.

The pulse-shaping functions for digital communications are assumed to be the standard unit pulse of duration T (i.e., rectangular pulse shaping) in the works of Azzouz and Nandi. In reality, however, many practical communications systems do employ some kind of non-rectangular pulse-shaping function such as raised-cosine function in the transmitter to adapt to the band-limited channels. No discussions on non-rectangular pulse shaping functions can be found in [12]. The author has carried out a limited number of simulations on communication signals with raised-cosine pulse shaping or square-root raised-cosine pulse shaping and found that the classification performance is not affected greatly. Extensive study should be conducted in order to thoroughly evaluate the affection of the pulse-shaping function to these features.

The separation of MPAM and QAM from the other modulation types based on the features of Azzouz and Nandi has also been discussed. A limited number of simulations have been carried out and the results support the author's suggested scheme. Certainly, such a scheme can only work for higher SNR (e.g., SNR$\geq$15 dB).

In addition to the above, the author suggests using these features all at once, rather than using them hierarchically. In the algorithms proposed by Azzouz and Nandi (not including those implemented by using artificial neural network), it is noted that only one feature is used in each node of the decision tree. This implies that the classification algorithms assume the boundaries of the decision regions are perpendicular to some feature axes and parallel to the other feature axes in the multidimensional feature space. This is generally not true. Thus the classification performance may be improved if all the features are used at once.

In summary, the main merit of Azzouz and Nandi's works in [7], [12], [98] and [99] is a set of simple but meaningful features. However, their algorithms may only be capable of recognizing some simple modulation patterns in some ideal cases and are restricted in practice. Some modifications have been suggested to make the classification based on these features more practical.

CHAPTER 3

BLIND CARRIER FREQUENCY ESTIMATION OF DIGITAL COMMUNICATION SIGNALS

3.1 Introduction

The problem of estimating carrier frequency or carrier frequency offset of communication signals originally arises when there exists a relative motion between the transmitter and the receiver in a communication system. Due to the influence of the pulse-shaping filter, the channel response and the transmitted symbols, it is more appropriate to model the received signal as a sinusoidal signal corrupted by both multiplicative and additive noise. This makes the classical frequency estimation approaches such as [110] and [111] not applicable.

In cooperative communications systems, data-aided (DA) methods (e.g., [112]-[113]) are often employed to estimate the carrier frequency, where a known training or pilot symbol sequence is required being periodically transmitted in addition to the effective information-bearing dada. The training sequence does simplify the estimation of carrier frequency. However, it will reduce the effective transmission rate. The carrier frequency estimation can also benefit from a certain kind of precoders in the transmitter (e.g., [114]), or the known pulse-shaping function (e.g., [115]-[116]), etc. It should be noted that such schemes are not feasible to non-cooperative applications although they are claimed to be blind.

Some non-data-aided (NDA) methods have been developed to overcome the problems with DA methods. A widely applied NDA method is the conjugate cyclic correlation based (CCB) approach (e.g., [117]). The CCB estimators assume that the

transmitted symbols $\{s_n\}$ be *noncircularly* distributed (i.e., $E[(s_n)^2] \neq 0$). Based on the observation that the unique nonzero conjugate cycle frequency of the received signal is twice of the carrier frequency, the CCB estimators retrieve the carrier frequency by searching the peak of the discrete Fourier transform (DFT) of the conjugate time-varying correlations. If the transmitted symbols are circularly distributed (i.e., $E[(s_n)^2] = 0$), however, higher-order (denoting the order by K) cyclic moments should be used as proposed in [118], where K satisfies $K \geq \min\{k: E[(s_n)^k] \neq 0\}$. The nonlinear least-square (NLLS) estimators (e.g., [119] are also popular in carrier frequency estimation. Giannakis and Zhou [120] studied the relationship between the cyclic estimators and the NLLS estimators and found they are equivalent. The problems with CCB estimators and NLLS estimators are as follows. First, the workable frequency range of an estimator is proportional to the sampling rate and inverse-proportional to the value of K. For some modulation types, the minimum value of K is very large (e.g., K=16 for PSK16). This implies that the workable frequency range will be very narrow for a fixed sampling rate, or a very high sampling rate should be used for a fixed carrier frequency. Secondly, for a fixed data record size, a larger K also means the variances of the estimated statistics are higher, resulting in a worse performance.

In the AMR applications, it is often necessary to blindly equalize the received signal before modulation recognition can be done. This in turn requires estimating the carrier frequency blindly. This issue is quite different from that in the cooperative communications systems since the AMR receiver does not have *a priori* knowledge of the transmitted signal such as modulation type, pulse shaping function, symbol constellation and symbol rate. Certainly, a known training symbol sequence is

unavailable in AMR problems. Moreover, due to the asynchronous nature of the sampling, the sampled data may be neither stationary nor cyclostationary. It is straightforward to observe that most existing carrier frequency estimation schemes are inapplicable.

It is noted that some AMR related publications have been concerned with the estimation of carrier frequency. For example, Hsue and Soliman [27] took the reciprocal of the average zero-crossing interval as the estimate of the carrier frequency; Assaleh et al. [34] estimated the carrier frequency by averaging the instantaneous frequency of the received signal, and etc. The implied pulse-shaping function is rectangular in time domain and only limited to one symbol duration in these schemes. When a non-rectangular pulse shaping function is employed in the transmitted signal, the performance of these schemes may degrade greatly. Furthermore, these schemes are generally of low accuracy.

Motivated by the above, a carrier frequency estimator is developed and reported in this chapter. The rest of this chapter is organized as follows. Section 3.2 formulates the problem. Section 3.3 derives the proposed algorithm. Section 3.4 reports the simulation results and briefly compares the proposed algorithm's performance with that of cyclic moment based estimators. A brief conclusion is drawn in Section 3.5.

3.2 Problem Statement and Assumptions

The received communication signal $y(t)$ can be expressed in complex form as

$$y(t) = x(t-\varepsilon) + w(t) \tag{3.1}$$

$$x(t) = \sum_l s_l g(t-lT) e^{j(2\pi f_c t + \theta_c)} \tag{3.2}$$

where $x(t)$ is the transmitted signal, $w(t)$ is zero-mean white Gaussian noise that is independent of $x(t)$, s_l is the $l-th$ transmitted symbol, f_c is carrier frequency, θ_c is the deterministic carrier phase, T is symbol duration, ε is the timing offset between the transmitter and the AMR receiver, and $g(t)$ is the pulse-shaping function.

In developing the carrier frequency estimation algorithm, the following assumptions are made without loss of generality: (1) $\{s_l\}$ is a set of i.i.d. discrete random variables, the elements of which are uniformly distributed on the symbol constellation of the modulation type employed by the transmitter; (2) the modulation type of the received signal may be ASK, PSK or QAM, but unknown in advance; (3) $g(t)$ is an unknown real function that will decrease to zero as time t increases to infinity; (4) the signal sampling may be asynchronous, i.e., the sampling rate f_s may be neither an integer multiple of symbol rate R_s nor that of carrier frequency f_c, where $R_s = 1/T$.

It should be noted that the term *ASK* stands for both the ASK modulation of [107] and the PAM modulation of [108], where the former only modulates the signal's magnitude, and the latter consists of amplitude modulation and phase modulation — the two possible symbol phases are zero or π radians.

The task of carrier frequency estimation will be carried out based on a finite number of samples $\{y(n) \overset{\Delta}{=} y(nT_s) : n = 0, 1, \cdots, N-1\}$, where T_s is the sampling period that is the reciprocal of the sampling rate f_s.

3.3 Carrier Frequency Estimation Based on Phases of Autocorrelation Functions

To be concise, the proposed algorithm is introduced by using the MPSK signal. For an MPSK signal, the transmitted symbols $\{ s_l \}$ will take the following discrete values

$$I_m = \sqrt{\tfrac{E_s}{T}} e^{j\frac{2\pi}{M}m}, \; m = 0,1,\cdots,M-1 \tag{3.3}$$

where E_s is the symbol energy, and M is alphabet size. The MPSK symbol constellation used in practical communications systems may be a rotated version of that in (3.3), but this phase rotation can be absorbed into the carrier phase, i.e., θ_c. Therefore, the model of (3.3) can be used to represent an MPSK symbol constellation without loss of generality.

The autocorrelation function (ACF) of the received data $\{ y(n) \}$ is defined as

$$\hat{r}_{yy}(k) \overset{\Delta}{=} \frac{1}{N-k} \sum_{n=0}^{N-k-1} y(n+k) y^*(n) \tag{3.4}$$

where * stands for the complex conjugate operation, and k is the lag of the ACF. By the definition of (3.3) and the assumptions in Section 3.2, it is straightforward to show that the expectation value of $\hat{r}_{yy}(k)$ with lag k not equal to zero has the following form:

$$r_{yy}(k) = E[\hat{r}_{yy}(k)] = \frac{\sigma_s^2}{N-k} \sum_{n=0}^{N-k-1} \Gamma(n,k) \times e^{j2\pi T_s f_c k} \tag{3.5}$$

$$\Gamma(n,k) = \sum_l g(nT_s + kT_s - lT - \varepsilon) \times g(nT_s - lT - \varepsilon) \tag{3.6}$$

where σ_s^2 represents the variance of the MPSK symbols.

Equation (3.5) suggests a way to estimate the carrier frequency based on the phases of $\{ r_{yy}(k) \}$ if the phase ambiguity introduced by the sign of $\Gamma(n,k)$ can be removed. Since the pulse shaping function $g(t)$ is assumed to be real-valued, the phase of $\Gamma(n,k)$ will be either zero or π radians. Then the phase of $\left[r_{yy}(k) \right]^2$ will be

$$\angle\left[r_{yy}(k)\right]^2 = 4\pi T_s f_c k \text{, for } k = 1, 2, \cdots, N-1 \tag{3.7}$$

where $\angle$ stands for the phase extracting operation. Thus f_c can be estimated by using

$$\bar{f}_c = \frac{f_s}{4\pi(N-2)} \sum_{k=1}^{N-2} \psi(k) \tag{3.8}$$

where

$$\psi(k) \overset{\Delta}{=} \angle\left(\hat{r}_{yy}(k+1)\hat{r}^*_{yy}(k)\right)^2 \tag{3.9}$$

where the expectation value of $\psi(k)$ is $4\pi T_s f_c$ for $k = 1, 2, \cdots, N-2$.

To avoid aliasing in frequency domain, the sampling rate f_s should be greater than $4f_c$. This also means that the expectation value of $\psi(k)$ will be in the range of $(0, \pi)$. Before continuing, it is worth exploring the distribution of random variable $\psi(k)$ more carefully. For this purpose, the three lemmas are introduced as follows.

Lemma 1 If complex random variables V_1 and V_2 are independent of each other and are symmetrically distributed with respect to (w.r.t.) the horizontal axis of the complex plane, i.e., $p_1(V_1 = v_1) = p_1(V_1 = v_1^*)$ and $p_2(V_2 = v_2) = p_2(V_2 = v_2^*)$, then the phase of $Y = l_1 V_1 + l_2 V_2$ is symmetrically distributed w.r.t. zero, where l_1 and l_2 are deterministic real values, and $p_1(\bullet)$ and $p_2(\bullet)$ stand for the probabilities of the events in curves.

Proof If at least one of l_1 and l_2 is zero, then the above statement certainly holds. Therefore, both l_1 and l_2 are assumed to be nonzero in the following. Since V_1 and V_2 are independent of each other, their joint PDF $p_{\underline{V}}(v_1, v_2)$ can be represented as

$p_{\underline{V}}(v_1, v_2) = p_1(V_1 = v_1) \times p_2(V_2 = v_2)$. By following the procedure in [108], it can be shown that the PDF of Y is

$$p_Y(Y = y) = \frac{1}{|l_1|} \int_C p_1\left(V_1 = \tfrac{y - l_2 v_2}{l_1}\right) \times p_2(V_2 = v_2)\, dv_2 \tag{3.10}$$

where $y = l_1 v_1 + l_2 v_2$, and C denotes the complex plane. If V_1 and V_2 take values of v_1^* and v_2^*, respectively, then the value of Y will be $Y = l_1 v_1^* + l_2 v_2^* = y^*$, and its probability is

$$p_Y(Y = y^*) = \frac{1}{|l_1|} \int_C p_1\left(V_1 = \tfrac{y^* - l_2 v_2}{l_1}\right) \times p_2(V_2 = v_2)\, dv_2 \tag{3.11}$$

By changing the integration variables, equation (3.11) can be rewritten as

$$p_Y(Y = y^*) = \frac{1}{|l_1|} \int_C p_1\left(V_1 = \tfrac{y^* - l_2 v_2^*}{l_1}\right) \times p_2(V_2 = v_2^*)\, dv_2 \tag{3.12}$$

It can be derived from the given conditions that $p_1\left(V_1 = \frac{y^* - l_2 v_2^*}{l_1}\right) = p_1\left(V_1 = \frac{y - l_2 v_2}{l_1}\right)$ and $p_2(V_2 = v_2^*) = p_2(V_2 = v_2)$. Applying these to (3.12), it is straightforward to show that $p_Y(Y = y^*)$ is equal to $p_Y(Y = y)$. It is noted that $\angle y^* = -\angle y$. Then the above result implies the probability of $\angle Y = \theta$ is equal to that of $\angle Y = -\theta$. This ends the proof.

Lemma 2 Complex random variables V_1 and V_2 are independent of each other, and V_i is symmetrically distributed w.r.t. a straight line starting from the origin with an angle θ_i w.r.t. the positive horizontal axis of the complex plane, where $i = 1, 2$. Then the phases of $V_1 V_2$, $V_1 V_z^*$ and $V_1^* V_2$ are symmetrically distributed with respect to $\theta_1 + \theta_2$, $\theta_1 - \theta_2$ and $\theta_2 - \theta_1$, respectively.

Proof If denoting V_1 and V_2 by $V_1 = |V_1| e^{j(\theta_1+\phi_1)}$ and $V_2 = |V_2| e^{j(\theta_1+\phi_1)}$, respectively, the phase of their product will be $\angle(V_1 V_2) = \theta_1 + \theta_2 + \phi_1 + \phi_2$. The given conditions imply that ϕ_1 and ϕ_2 are independent of each other, and they are both zero mean random variables symmetrically distributed w.r.t. zero. Then by applying the method for proving Lemma 1, it is straightforward to show that the random variable $\phi_1 + \phi_2$ is also symmetrically distributed w.r.t. zero. This proves that the random variable $\angle(V_1 V_2)$ is symmetrically distributed w.r.t. $\theta_1 + \theta_2$. Similarly, one can show that $\angle(V_1 V_z^*)$ and $\angle(V_1^* V_2)$ are symmetrically distributed w.r.t. $\theta_1 - \theta_2$ and $\theta_2 - \theta_1$, respectively.

Lemma 3 Complex random variables V_1 and V_2 are independent of each other, and both of them are symmetrically distributed w.r.t. a straight line starting from the origin with an angle θ_0 w.r.t. the positive horizontal axis of the complex plane. Then the phase of $Y = l_1 V_1 + l_2 V_2$ is symmetrically distributed w.r.t. θ_0, where l_1 and l_2 are deterministic real values.

Proof According to the given conditions, V_i can be written as $V_i = V_{is} e^{j\theta_0}$, where V_{is} is a complex random variable symmetrically distributed w.r.t. the horizontal axis of the complex plane, and $i = 1, 2$. Then Y can be represented as $Y = e^{j\theta_0} \sum_{i=1}^{2} l_i V_{is}$. By using Lemma 1, it can be shown that the phase of $\sum_{i=1}^{2} l_i V_{is}$ is symmetrically distributed w.r.t. zero. Therefore, the phase of Y is symmetrically distributed with respect to θ_0.

Now go back to discuss the distribution of $\psi(k)$. Assuming the SNR is high, the received data sample $y(n)$ be approximated [121] by using

$$y(n) = x(nT_s) + w(nT_s) \approx x(nT_s)e^{j\phi(n)} \tag{3.13}$$

where $\phi(n)$ is a zero-mean Gaussian random variable. Then by applying the above lemmas repeatedly, $\psi(k)$ has been shown to be symmetrically distributed w.r.t. $4\pi T_s f_c$. That is, $\psi(k)$ can be represented as

$$\psi(k) = 4\pi T_s f_c + \varphi(k) \tag{3.14}$$

where $\varphi(k)$ is a real-valued random variable symmetrically distributed w.r.t. zero.

Note that the above conclusion is obtained based on the following assumption: the phase extracted from a complex value may take any real value. In reality, however, the phase extracted from a complex value will be in the range of $(-\pi, +\pi]$ due to modulo-2π operation. The modulo-2π operation will cause phase-wrapping phenomena. This can explained as follows. Since the sampling rate is greater than $4f_c$, the value of $4\pi T_s f_c$ will be in the range $(0,\ \pi)$. If $\varphi(k)$ is within the range $(-\pi,\ \pi - 4\pi T_s f_c)$, no phase wrapping will happen even though the resultant $\psi(k)$ may be a negative value. If $\varphi(k)$ is in $(\pi - 4\pi T_s f_c,\ \pi)$, however, the resultant $\psi(k)$ will be greater than π, and then it will be wrapped as a negative value of $\psi(k) - \pi$ which is in the range of $(-\pi,\ 0)$.

From the above, it can be concluded that a $\psi(k)$ may be a wrapped phase if it is in the range of $(-\pi,\ 0)$; otherwise, it must be a non-wrapped phase. In order to achieve better performance, the wrapped phase items of $\{\psi(k)\}$ should be excluded in the carrier

frequency estimation. Therefore, the following modified carrier frequency estimator is suggested:

$$\hat{f}_c = \frac{f_s}{4\pi K_0} \sum_{0<\psi(k)<\pi} \psi(k) \tag{3.15}$$

where K_0 is the number of $\psi(k)$ that are in the range of $(0,\ \pi)$.

By excluding the wrapped phase items, the modified estimator in (3.15) is expected to provide better estimate of the carrier frequency. However, it should be noted that the non-wrapped phase items of $\{\psi(k)\}$, i.e., those $\psi(k)$ that are in the range of $(0,\ \pi)$, may not be symmetrically distributed w.r.t. $4\pi T_s f_c$ if f_s is not equal to $8f_c$. This may make the estimator of (3.15) a biased estimator. On the other hand, it is expected that those $\{\psi(k)\}$, which are in the range of $(4\pi T_s f_c - \lambda,\ 4\pi T_s f_c + \lambda)$, would be symmetrically distributed w.r.t. $4\pi T_s f_c$, where λ is the smaller one of $4\pi T_s f_c$ and $(\pi - 4\pi T_s f_c)$. Therefore, a better estimator can be formed as

$$\hat{\lambda} = \min\left(4\pi T_s \hat{f}_c,\ \pi - 4\pi T_s \hat{f}\right) \tag{3.16}$$

$$\psi_{\min} = 4\pi T_s \hat{f}_c - \hat{\lambda} \tag{3.17}$$

$$\psi_{\max} = 4\pi T_s \hat{f}_c + \hat{\lambda} \tag{3.18}$$

$$\tilde{f}_c = \frac{f_s}{4\pi K_1} \sum_{\psi_{\min}<\psi(k)<\psi_{\max}} \psi(k) \tag{3.19}$$

where $\hat{f}_c$ is the coarse estimate obtained by using (3.15), $\hat{\lambda}$ is the estimate of λ based on $\hat{f}_c$, K_1 is the number of $\psi(k)$ that are in the range of $(\psi_{\min}, \psi_{\max})$, and $\tilde{f}_c$ is the refined estimate of carrier frequency.

The above refining operation is inherently to estimate the symmetrically distributed region of $\psi(k)$. It can be performed iteratively to reduce the estimation bias. Thus, the proposed carrier frequency estimation algorithm is formed as (1) calculate $\psi(k)$ according to (3.4) and (3.9) for $k = 1, 2, \cdots, N-2$; (2) Obtain a rough estimate of carrier frequency by using (3.15) and store the result in the variable $\hat{f}_c$; (3) Calculate $\hat{\lambda}$, $\psi_{\min}$ and $\psi_{\max}$ according to (3.16) through (3.18); (4) Estimate $\tilde{f}_c$ by using (3.19); (5) if $\left|\tilde{f}_c - \hat{f}_c\right|$ is greater than a preset small value ξ and the maximum iteration number has not been achieved, update $\hat{f}_c$ with $\tilde{f}_c$, and then repeat from Step 3; otherwise take $\tilde{f}_c$ as the final estimate of carrier frequency f_c.

For ASK and QAM signals, it has been shown that the phases $\{\psi(k)\}$, defined by (3.4) and (3.9), are also symmetrically distributed w.r.t. $4\pi T_s f_c$ if the SNR is not too low. Then the above analysis about the phases $\{\psi(k)\}$ of MPSK signals holds for ASK and QAM signals as well. That is, the proposed algorithm is universally valid for the concerned digital communication signals.

3.4 Simulation Results and Discussions

In all simulations, the impulse response of the pulse-shaping filter is square-root raised cosine function with roll-off factor $\beta = 0.35$, the sampling rate is $f_s = 1.0$, the symbol rate is $R_s = 0.05$, the carrier frequency is $f_c = 0.1$, and each set of the received data contains 4096 symbols. The simulated data's SNR in dB is defined as

$$SNR = 10\log_{10}\frac{P_{x,BW}}{P_{w,BW}} \tag{3.20}$$

where BW is the effective bandwidth of the transmitted signal $x(n)$, $P_{x,BW}$ and $P_{w,BW}$ are respectively the power of $x(n)$ and the power of $w(n)$, and both $P_{x,BW}$ and $P_{w,BW}$ are evaluated in the frequency range $\left(f_c - BW/2, f_c + BW/2\right)$.

The carrier frequency of the received signal is estimated by using the proposed method, the second-order cyclic statistics based method (referred to as *C-2 method* here) [118], the fourth-order cyclic statistics based method (referred to as *C-4 method* here) [118], and the eighth-order cyclic statistics based method (referred to as *C-8 method* here) that is an extension of [118], respectively. The cyclic estimators are used as references in performance comparison.

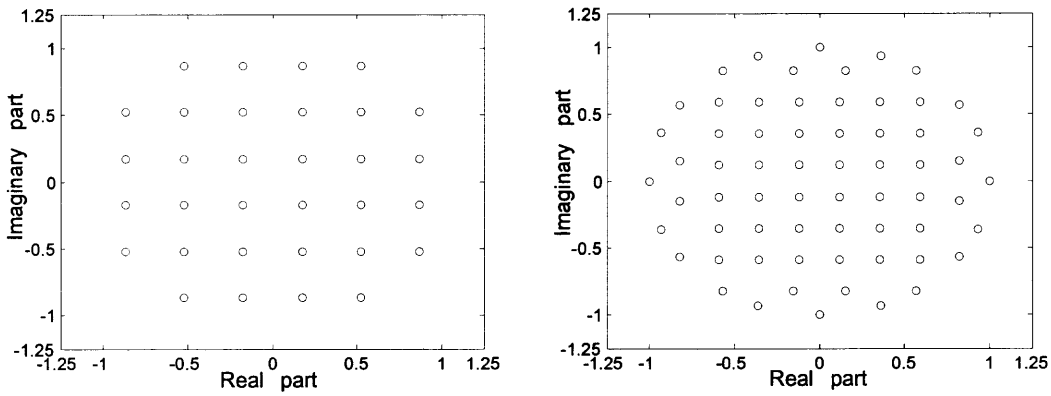

Figure 3.1 Symbol constellations (Left: Cross-32 QAM, Right: HF-64 QAM).

The performance of an estimator is evaluated by means of the empirical normalized mean square error (*ENMSE*) and the relative mean estimation error (*RMEE*), which are respectively defined as

$$ENMSE = \frac{1}{N_{simu}} \sum_{n=1}^{N_{simu}} \left(\tilde{f}_{c,n} / f_c - 1\right)^2 \tag{3.21}$$

$$RMEE = \frac{1}{N_{simu}} \sum_{n=1}^{N_{simu}} \left(\tilde{f}_{c,n} / f_c - 1\right) \times 100 \tag{3.22}$$

where N_{simu} is the number of available data sets for the testing modulation type under the given SNR, $\tilde{f}_{c,n}$ is the carrier frequency estimated from the $n-th$ data set, and f_c is the true value of the carrier frequency.

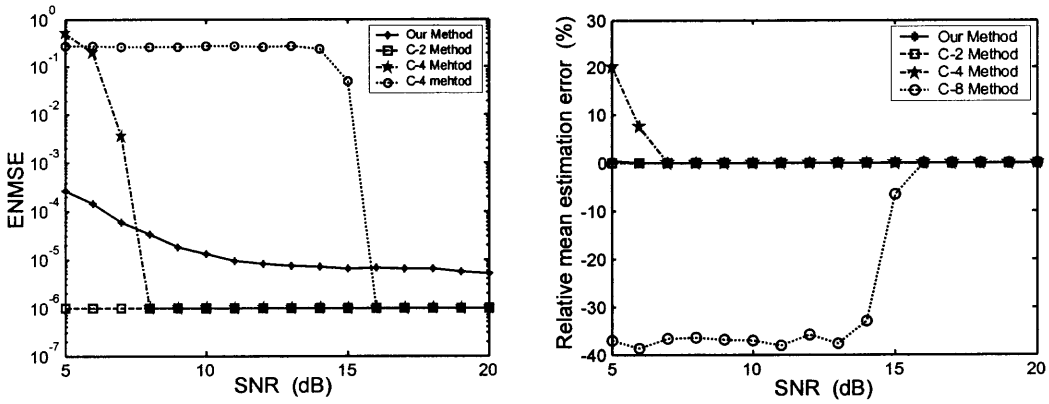

Figure 3.2 Simulation results on PSK2 (Left subfigure: ENMSE vs. SNR, Right subfigure: RMEE vs. SNR).

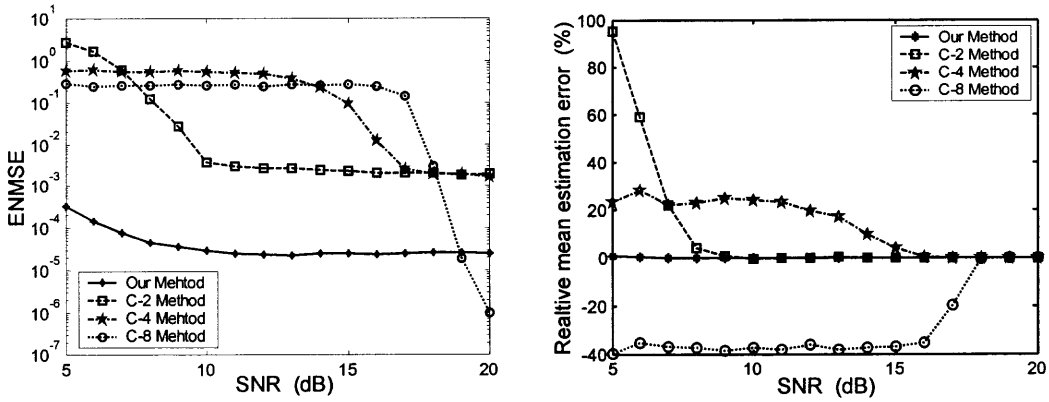

Figure 3.3 Simulation results on PSK8 (Left subfigure: ENMSE vs. SNR, Right subfigure: RMEE vs. SNR).

The testing modulation types include PSK2, PSK8, Cross-32 QAM and HF-64 QAM signals, where the symbol constellations of Cross-32 QAM and HF-64 QAM are shown in Figure 3.1. For each of the above modulation types, one thousand data sets are

generated and the carrier frequency is estimated by using the aforementioned methods under each SNR, i.e., N_{simu}=1000. The performance is reported in Figure 3.2 through Figure 3.5. Since zeros can not be represented in the logarithmic coordinate system, the value of 10^{-6} in Figure 3.2 is used to denote a zero *ENMSE*.

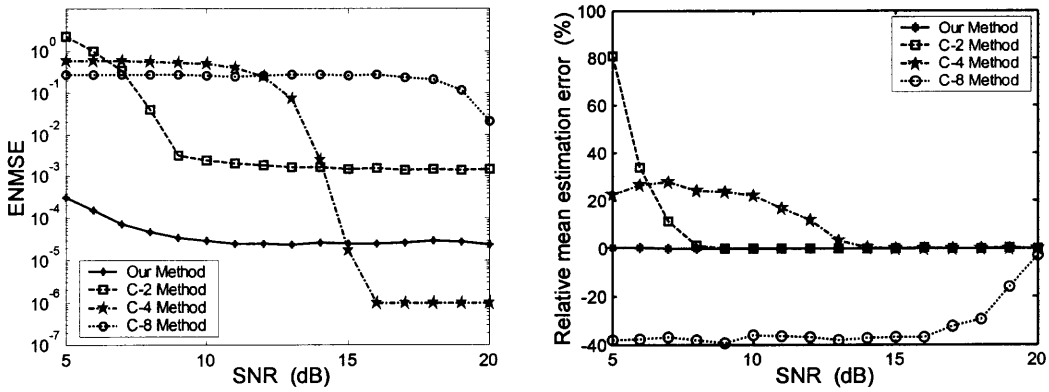

Figure 3.4 Simulation results on Cross-32 QAM (Left subfigure: ENMSE vs. SNR, Right subfigure: RMEE vs. SNR).

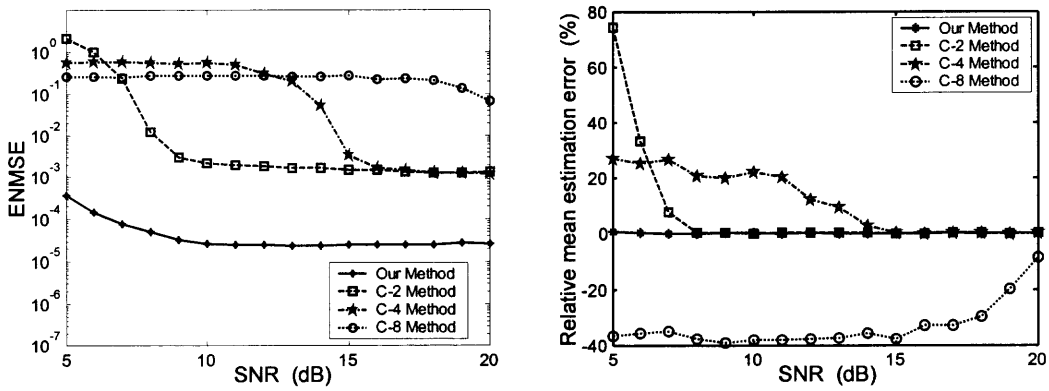

Figure 3.5 Simulation results on HF-64 QAM (Left subfigure: ENMSE vs. SNR, Right subfigure: RMEE vs. SNR).

For the simplicity of discussion on the results reported in Figure 3.2 through Figure 3.5, a measure for describing to what extent a symbol constellation is circularly distributed is defined and named as *Minimum Necessary Order* (*MNO*). For a specific symbol constellation with symbol set $\{I_m\}$, the MNO is defined as

$$MNO = \min_k \left\{ E\left[(I_m)^k \right] \neq 0 \right\} \tag{3.23}$$

If the *MNO* is two for a constellation, then this constellation is non-circularly distributed; otherwise, it is circularly distributed. It is clear that the order of a cyclic statistics based carrier frequency estimator should be higher than or at least equal to the *MNO* of the symbol constellation of the target signal.

For the testing modulation types, the values of *MNO* are 2, 8, 4 and 4 for PSK2, PSK8, Cross-32 QAM and HF-64 QAM, respectively. That is, only the symbols of PSK2 are noncircularly distributed. Then it is not surprising that C-2 method and C-4 method do not work well for PSK8, and that C-2 method does not work well for Cross-32 QAM and HF-64 QAM.

It is noted that the order of cyclic statistics greatly affects the performance of the cyclic estimators. Higher order generally leads to worse performance. For example, under the simulation conditions described at the beginning of this section, the C-2 method is able to exactly retrieve the carrier frequency from PSK2 signals for SNR≥5 dB, while the C-8 method can only achieve the same performance for SNR≥16 dB. It is observed via extensive simulations (not reported here) that the performance of the cyclic estimators would be much worse than that shown in Figure 3.2 through Figure 3.5 if the order of the cyclic statistics is further increased.

Among the tested carrier frequency estimation methods, the proposed algorithm is not the best one in some circumstances. For example, the C-2 method works better for PSK2 signals than the proposed algorithm does. However, the AMR problem is inherently blind. The modulation type of a received signal is unknown at the stage of carrier frequency estimation. If a cyclic statistics based approach is applied in this situation, one should employ cyclic statistics of sufficiently higher order to adapt to all possible modulation types. For the testing modulation types, the minimum order satisfying the above requirement is eight. It is observed that the overall performance of the proposed algorithm is better than that of C-8 method in terms of *ENMSE* and *RMEE*. The proposed algorithm is robust in the sense that its ENMSE under the same SNR value is almost the same for different modulation types.

For the proposed algorithm, if the sampling rate f_s is eight times of the true carrier frequency f_c, the expectation value of $\psi(k)$ will be equal to the center of $(0,\ \pi)$. Then all the phases $\{\ \psi(k)\ \}$ in the range of $(0,\ \pi)$ would be non-wrapped and are expected to be symmetric w.r.t. the expectation value of $\psi(k)$. In this case, the proposed algorithm would achieve the best performance. This has been verified by extensive simulations and can be used as a clue to choose the sampling rate if a rough range of the carrier frequency has been obtained in the preprocessing.

When calculating $\hat{r}_{yy}(k)$ by using (3.4), it requires $4\times(N-k)$ real-valued multiplication operations for $k=1,2,\cdots,N-1$, resulting in $2\times(N^2-N)$ real-valued multiplication operations. The amplitude normalization in (3.4) is unnecessary and thus its computation burden has not been counted. In calculating each $\psi(k)$ by using (3.9),

the calculation of $\left(\hat{r}_{yy}(k+1)\hat{r}_{yy}^{*}(k)\right)^{2}$ requires seven real-valued multiplication operations, and the operation of extracting the phase of $\left(\hat{r}_{yy}(k+1)\hat{r}_{yy}^{*}(k)\right)^{2}$ requires P real-valued multiplication operations, where the value of P depends on the concrete algorithm used to extract the phase of a complex value. Then for calculating $\psi(k)$ for $k=1,2,\cdots,N-2$, it requires $(7N+PN)$ real-valued multiplication operations. The other calculations are trivial and thus their computation burden can be ignored. It follows the proposed carrier frequency estimator has a computational complexity (evaluated by the number of real-valued multiplications) of $O\left(2N^{2}+5N+PN\right)$, where N is the number of available data samples, and P stands for the equivalent number of real-valued multiplications in extracting the phase of a complex value.

3.5 Conclusions

The autocorrelation functions (ACFs) of digital communication signals contain the information of carrier frequency in their phases. In this chapter, the phase distribution of the ACFs of a received signal has been analyzed. It has been shown that only the symmetrically distributed phases in the range of $(0,\ \pi)$ should be utilized in carrier frequency estimation. The proposed carrier frequency estimation algorithm is able to iteratively estimate the range of the symmetrically distributed phases so as to achieve better performance.

The convergence of the iterative processing in the proposed algorithm has not been proved yet. Nevertheless, simulations show that the proposed algorithm converges to the true carrier frequency with small error after only a few iterations.

The proposed algorithm is able to estimate a carrier frequency that is less than a quarter of the sampling rate. It is noted that this algorithm achieves the best performance if the sampling rate is eight times of carrier frequency. That is, if the rough range of carrier frequency is available, the sampling rate should be chosen to be about eight times of the central frequency of that range.

The proposed algorithm is a universal carrier frequency estimator for ASK, PSK and QAM signals. In developing this algorithm, only reasonable assumptions are made on the models of the transmitted signals. Therefore, it is feasible to the blind carrier frequency estimation for single-tone digitally modulated signals with unknown modulation formats.

Some simulation results have been presented to demonstrate the validity of the proposed algorithm. Compared to the cyclic moment based estimators, the proposed algorithm is shown to be able to achieve a better overall performance in the AMR environment.

CHAPTER 4

BLIND SYMBOL RATE ESTIMATION OF DIGITAL COMMUNICATION SIGNALS

4.1 Introduction

In the AMR of communication signals, it often requires to estimate some modulation parameters before the signal classification can be done [12]. In fact, the final goal of AMR is not only to recognize the modulation type but also to decode the transmitted symbols. This in turn requires estimating the modulation parameters such as carrier frequency and symbol rate. The symbol rate estimation is emphasized in this paper.

Intuitively, the time intervals among pairs of intersymbol transition (IST) instants contain the information of symbol period. Several symbol rate estimators are based on detection of IST instants. For example, Hsue and Soliman [27] estimated the symbol rate of PSK signals based on the zero-crossings of the received signal. In detecting the IST samples, however, the method of [27] requires knowing the value of M (i.e., the alphabet size) of an MPSK signal. Assaleh et al. [34] first estimated the instantaneous frequency (IF) and instantaneous bandwidth (IB) by using autoregressive (AR) model, and then took the reciprocal of the time difference between the two closest pulses in the IB for PSK or that in the differentiated IF for FSK as the estimate of the symbol rate. This method requires knowing whether the modulation type is FSK or PSK in advance. However, the knowledge of the input signal's modulation type is generally not available at the stage of symbol rate estimation. Moreover, the IST-detection based symbol rate estimators generally require a very high sampling rate to achieve an acceptable frequency resolution. All these make them impractical in AMR applications.

Wavelet transform is an alternative method to investigate a digital communication signal's inherent periodicity. An example is the one proposed by Chan et al. for PSK [122]. The method first calculates the Haar wavelet transform coefficients (HWTCs) of the received at different scale factors, and then adds together the squared magnitudes of HWTCs with the same shift. The symbol rate is estimated as the frequency corresponding to the first significant peak in the magnitude spectrum of the above mentioned summed HWTC magnitudes. The so-called *first significant peak* may be easily determined by human eye inspection if it does exist. However, it is not an easy work for machine even though the SNR is high. The symbol rate estimator for PSK and FSK in [50] only employs HWTCs at one scale factor. The HWTC magnitudes at different shifts are first centralized by removing their mean value, and then the autocorrelation functions (ACFs) of the centralized HWTC magnitudes are estimated. The symbol rate estimator of [50] detects the peaks of the above ACFs by comparing them with a threshold function that decreases as the ACF lag increases. Once the ACF peaks have been identified, a histogram of the width between two successive peaks is generated. The mode of the histogram is taken as the estimate of the symbol period. However, the formulation of the adaptive threshold contains a design parameter. Moreover, the selection of the scale factors greatly influences the performance. Unfortunately, no discussion on how to choose the above mentioned parameters for unknown modulation formats can be found in [50] or [122].

The most popular approaches for symbol rate estimation may be the ones based on cyclic correlations (e.g., [123]). These approaches rely on the observation that the over-sampled received signal is cyclostationary and its nonzero cycle frequencies are

integer multiples of the symbol rate. In the case where the excess bandwidth factor β satisfies $0 < \beta \leq 1$, the only positive cycle frequency of the cyclic correlations will be the symbol rate. That is, the symbol rate corresponds to a peak in the amplitude plot of the cyclic correlation functions — such a peak is referred to as *symbol-rate line* in this chapter. Then the symbol rate estimation is equivalent to searching the symbol-rate line in the amplitude of cyclic correlations. If the excess bandwidth is zero, however, the cyclic correlation based estimators such as [123] will fail since the symbol-rate line vanishes [124]. In this case, higher-order cyclic statistics should be used. Further, even though the excess bandwidth is not zero, the magnitude of the symbol-rate line is not guaranteed to be the global maximum of the cyclic correlation magnitudes if the SNR is low and/or β is small. Thus it is not trivial to recognize the symbol-rate line even though it does exist. Trying to solve this problem, Mazet and Loubaton have proposed a scheme to enhance the symbol-rate line and deemphasize the cyclic correlations for frequency not equal to the symbol rate [125]. It is claimed that a considerable performance improvement has been achieved. However, only simulation results at SNR=60 dB are reported in [125]. The major drawback of the method in [125] is that it requires estimating a weighting matrix and then computing the inverse of this matrix for each discrete frequency in the search range, resulting in a very heavy computational burden. To make the symbol rate line stronger, Kueckenwaitz et al. [126] proposed to remove the continuous component from the estimated cyclic correlations, where the continuous component is estimated from the estimated cyclic correlations by median filtering. The resultant cyclic correlation vector is further weighted with a decreasing ramp which prefers cyclic correlations at lower frequencies. A simple maximum search over the

weighted vector is used to find a coarse estimate of the symbol rate. For the simplicity, the fine estimate will not be introduced here. It is noted that the parameters of median filtering as well as the design of the decreasing weighting ramp may greatly affect the symbol rate estimation. However, Kueckenwaitz et al. have not introduced the details of these in [126].

The approach of [127] is able to jointly perform the equalization and symbol rate estimation by minimizing a contrast function of the equalized outputs. In essence, it is a grid-searching method. The computational burden to achieve high estimation accuracy may be not affordable in practice. Moreover, it is not easy to find a universal contrast function that works well when the modulation type is unknown in advance.

In this chapter, a fourth-order cyclic moment based symbol rate estimation algorithm is developed. The rest of this paper is organized as follows. Section 4.2 formulates the signal model and establishes the working conditions. Section 4.3 presents the proposed symbol rate estimation algorithm. Section 4.4 reports some simulation results and briefly compares the performance of the proposed algorithm with that of the cyclic correlation based approach in [123]. A brief conclusion is drawn in Section 4.5.

4.2 Problem Statement and Assumptions

It is assumed that the received signal has been shifted to baseband by preprocessing. The complex-valued signal can be mathematically expressed as

$$y(t) = \sum_{l} s_l g(t - lT - \varepsilon) + w(t) \tag{4.1}$$

where the first term on the RHS represents the transmitted communication signal, s_l is the $l-th$ transmitted symbol, T is the symbol period, ε denotes the timing offset between

the transmitter and the AMR receiver, $g(t)$ is the pulse-shaping function, and $w(t)$ is the complex additive noise. The symbol rate R_s is the reciprocal of T.

In developing the proposed symbol rate estimator, the following working conditions are assumed without loss of generality: (1) $\{s_l\}$ is a set of i.i.d. discrete random variables with zero mean and variance σ_s^2, the elements of which are uniformly distributed on the symbol constellation of the modulation type employed by the transmitter; (2) the modulation method may be MPAM, MPSK or QAM, but is unknown in advance; (3) $w(t)$ is zero mean white Gaussian noise with variance σ_w^2, and $w(t)$ is independent of the transmitted signal; (4) $g(t)$ may be the standard unit pulse of duration T, raised-cosine function, or square-root raised-cosine function, but is unknown in advance; (5) the sampling rate f_s satisfies $f_s \geq 4R_s$, but is not guaranteed to be an integer multiple of the symbol rate R_s.

The signal model in (4.1) implies the carrier frequency offset is zero. This constraint can be removed in practice as explained later. Moreover, as discussed in Subsection 4.3.4, the proposed symbol rate estimator can also handle MASK signals.

It should also be noted that the task here is to *estimate* the symbol rate rather than to *detect* the presence of the symbol rate as discussed in [128]. This implies the input signal has been classified as a linearly modulated digital communication signal in preprocessing. In the following, the available data are denoted by $y(n) \stackrel{\Delta}{=} y(nT_s)$ for $n = 0, 1, \cdots N-1$, where N is the number of available data samples.

4.3 Symbol Rate Estimation Based on Filter Bank and Cyclic Moments

To accommodate signals with zero excess bandwidth, the proposed symbol rate estimator is based on fourth-order cyclic moments instead of cyclic correlations. The fourth-order time-varying moments of the received data $y(n)$ is defined as

$$m_{4y}(n;\boldsymbol{\tau}) \overset{\Delta}{=} E\left[y^*(n)y^*(n+\tau_1)y(n+\tau_2)y(n+\tau_3)\right] \tag{4.2}$$

where $\boldsymbol{\tau}=[\tau_1,\ \tau_2,\ \tau_3]$, and τ_1, τ_2 and τ_3 are lags of the cyclic moment. If $m_{4y}(n;\boldsymbol{\tau})$ is a periodic or almost periodic function of n, it will accepts a Fourier series expansion with respect to (w.r.t.) n [129] as

$$m_{4y}(n;\boldsymbol{\tau}) = \sum_{\alpha\in\Omega_{m,4}} M_{4y}^{\alpha}(\boldsymbol{\tau})e^{j2\pi\alpha n} \tag{4.3}$$

$$M_{4y}^{\alpha}(\boldsymbol{\tau}) = \lim_{N\to\infty}\frac{1}{N}\sum_{n=0}^{N-1} m_{4y}(n;\boldsymbol{\tau})e^{-j2\pi\alpha n} \tag{4.4}$$

$$\Omega_{m,4} = \left\{\alpha:\ M_{4y}^{\alpha}(\boldsymbol{\tau})\neq 0,\ 0\le\alpha\le 1\right\} \tag{4.5}$$

where $M_{4y}^{\alpha}(\boldsymbol{\tau})$ is called the *fourth-order cyclic moment* of $y(n)$ at frequency α, the value of α is called the *cycle frequency* if for which $M_{4y}^{\alpha}(\boldsymbol{\tau})\neq 0$, and $\Omega_{m,4}$ is the set of cycle frequencies. In the context of this dissertation, however, the zero frequency will never be called a cycle frequency even though its corresponding cyclic statistics (including $M_{4y}^{\alpha}(\boldsymbol{\tau})$ as defined above) is nonzero. The above defined fourth-order cyclic moment, $M_{4y}^{\alpha}(\boldsymbol{\tau})$, can be estimated [138] by

$$\hat{M}_{4y}^{\alpha}(\boldsymbol{\tau}) = \frac{1}{N-\lambda}\sum_{n=0}^{N-\lambda-1} y^*(n)y^*(n+\tau_1)y(n+\tau_2)y(n+\tau_3)e^{-j2\pi\alpha n} \tag{4.6}$$

where $\lambda \overset{\Delta}{=} \max(\tau_1,\tau_2,\tau_3)$.

According to the above definitions, it is straightforward to show that the cycle frequencies of $M_{4y}^{\alpha}(\boldsymbol{\tau})$ for the concerned digital modulations will be $\alpha = k \times (R_s / f_s)$, where k is a positive integer. The value set of k (equivalently, the value set of cycle frequencies and the number of cycle frequencies) depends on the bandwidth of the pulse shaping function $g(t)$. Denoting the bandwidth of $g(t)$ by B, then the value of k should satisfy

$$0 < k \times (R_s / f_s) \leq \min(0.5,\ 4B/f_s) \tag{4.7}$$

The first design task in using cyclic moments to estimate the symbol rate is to select the lag vector $\boldsymbol{\tau}$ that makes the symbol-rate line as strong as possible. It is found through simulations that the optimal lags of fourth-order cyclic moments are dependent on the pulse shaping function. This is similar to the case of using second-order cyclic moments as discussed in [130]. However, the pulse shaping function is unknown in advance. For this reason, all the lags are simply set as zeros in the proposed algorithm, i.e., $\tau_1 = \tau_2 = \tau_3 = 0$.

As mentioned above, the cycle frequencies of the fourth-order cyclic moments will be $\alpha_k = k \times (R_s / f_s)$ with the positive integer k satisfying (4.7). This implies that, in addition to the frequency R_s / f_s that corresponds to the symbol rate, the frequency $2R_s / f_s$ (or even $3R_s / f_s$, and etc) will also be the cycle frequency of $M_{4y}^{\alpha}(\boldsymbol{\tau})$ if the bandwidth B is greater than $0.5R_s$. Unfortunately, this is generally true in practical communication systems. The extra cycle frequencies may make the symbol rate estimation very complicated. To make the work of searching symbol-rate line simpler, it is expected that the fourth-order cyclic moment has and only has one cycle frequency that

corresponds to the symbol rate. This can be achieved by using a lowpass filter (LPF) to filter the received signal before estimating the fourth-order cyclic moments, where the bandwidth of this LPF, denoted by B_{LPF}, should satisfy

$$0.25R_s < B_{LPF} < 0.5R_s \tag{4.8}$$

However, the symbol rate is the very parameter one wants to estimate. Moreover, it is found through simulations that the value of bandwidth B_{LPF} will affect the performance of the symbol rate estimator and its optimal value is related to the symbol rate. Then a deadlock is formed.

Actually, the above deadlock can be broken by using a bank of LPFs instead of a single LPF. This is achieved as follows. Firstly, a rough range of symbol rate is estimated from the received signal. Secondly, the estimated symbol rate range is divided into L subdivisions. Thirdly, the center of each subdivision is temporarily taken as the true symbol rate, and a proper LPF bandwidth is determined accordingly. In this way, L LPFs can be designed. Fourthly, the received signal is filtered by these LPFs in parallel. Finally, the fourth-order cyclic moments of each LPF's outputs are calculated.

By the above doing, it is expected that the cyclic moments corresponding to one or more LPFs will contain symbol-rate line. Similar to the case of using cyclic correlations to estimate the symbol rate, however, the symbol-rate line may only be a local peak of the cyclic moments. To overcome this problem, the proposed algorithm employs a confidence measurement to assess to what extent a peak of cyclic moments would be the symbol-rate line. The proposed algorithm is designed to extract symbol rate candidates (SRCs) from the cyclic moments corresponding to each LPF and assign a confidence measurement to each obtained SRC. Based on these SRCs and their

associated confidence measurements, a majority voting scheme is then used to determine the final estimate of the symbol rate.

In the rest of this section, the realization details of the above ideas will be presented step by step. In the rest of this chapter, an over-caret is used to denote the estimate of the corresponding parameter.

4.3.1 Estimation of Coarse Symbol Rate Range

At first, a kind of bandwidth of the pulse shaping function $g(t)$ is defined as

$$B_g = \arg\{f:\ |G(f)|/|G(0)| = 0.5\} \tag{4.9}$$

where $G(f)$ is the Fourier transform of $g(t)$.

For the pulse-shaping functions assumed in Section 4.2, it is straightforward to verify the following relationship

$$0.5R_s \le B_g \le 0.6667R_s \tag{4.10}$$

or equivalently,

$$1.5B_g \le R_s \le 2B_g \tag{4.11}$$

This implies that the symbol rate range can be determined if the value of B_g is known.

On the other hand, it is well-known that the PSDs of the communication signals with modulation types as assumed in Section 4.2 have the following common form [108]

$$S_y(f) = \frac{\sigma_s^2}{T}|G(f)|^2 + \sigma_w^2 \tag{4.12}$$

Then a simple method to estimate the value of B_g can be formed as follows. The first step is to estimate the PSD of the received signal by using Welch's average periodogram method [131] and then further smoothen it by median filtering. The resultant estimated

PSD is denoted by $\hat{S}_y(f)$. The second step is to estimate the noise floor, i.e., σ_w^2. This can be done by averaging the estimated PSD $\hat{S}_y(f)$ for the frequencies that are beyond the received signal's effective bandwidth. In the third step, the estimated value of σ_w^2 is subtracted from $\hat{S}_y(f)$, and the square root of the absolute value of the resultant PSD is taken as the estimate of a scaled version of $|G(f)|$ and denoted by $|\hat{G}(f)|$. Finally, the bandwidth B_g is estimated by

$$\hat{B}_g = (f_s - f_H + f_L)/2 \tag{4.13}$$

$$f_L \overset{\Delta}{=} \arg\left\{\max_f \left\{|\hat{G}(f)| \geq 0.5\rho,\ 0 < f < 0.5 f_s\right\}\right\} \tag{4.14}$$

$$f_H \overset{\Delta}{=} \arg\left\{\min_f \left\{|\hat{G}(f)| \geq 0.5\rho,\ 0.5 f_s < f < f_s\right\}\right\} \tag{4.15}$$

where ρ is the global maximum of $|\hat{G}(f)|$. Then the symbol rate range can be estimate by substituting $\hat{B}_g$ into (4.11).

The above method is very simple, but its accuracy may be low, especially when the SNR is low. To make the determined symbol rate range do include the true value of the symbol rate, the estimated symbol rate range is enlarged with respect to (4.11) as

$$f_A \leq \hat{R}_s \leq f_B \tag{4.16}$$

$$f_A \overset{\Delta}{=} 1.2\hat{B}_g \tag{4.17}$$

$$f_B \overset{\Delta}{=} \min\left(2.4\hat{B}_g, f_s/4\right) \tag{4.18}$$

where the minimizing operation in (4.18) is owing to the assumption of $f_s \geq 4R_s$.

4.3.2 Design of the Lowpass Filter Bank

The duty of each LPF is to make its corresponding fourth-order cyclic moments have and only have one cycle frequency at the location corresponding to the symbol rate. As aforementioned, this requires the bandwidth of the LPF being in the range $(0.25R_s,\ 0.5R_s)$. It is noted that the bandwidth of the LPF will greatly influence the relative strength of the symbol-rate line, and the optimal bandwidth is related to both the symbol rate and the pulse shaping function. That is, it will be very difficult to determine an optimal or near optimal bandwidth for the LPF if not having the knowledge of the symbol rate or the pulse shaping function. Unfortunately, this is the case of this study.

To overcome the problem, the estimated coarse symbol rate range is divided into L subdivisions, and the center frequency of each subdivision will be taken as a guess of the true symbol rate in designing the LPFs. The bandwidth $B_{LPF,l}$ of the $l-th$ LPF is designed as

$$B_{LPF,l} = 0.375 \times R_{s,l}, \text{ for } l = 1, 2, \cdots, L \tag{4.19}$$

$$R_{s,l} \overset{\Delta}{=} f_A + (l - 0.5) \times (f_B - f_A) / L \tag{4.20}$$

where f_A and f_B are defined in (4.17) and (4.18), respectively. In (4.19), $R_{s,l}$ is the center of the $l-th$ subdivision (i.e., the $l-th$ coarse guess of the symbol rate), and the factor of 0.375 makes $B_{LPF,l}$ fall in the middle of the range $(0.25R_{s,l},\ 0.5R_{s,l})$.

The above arrangement ensures that several LPFs' bandwidths will be in the workable range $(0.25R_s,\ 0.5R_s)$, and one or two of them may be near to the optimum bandwidth. To let the proposed algorithm not too complicated, the filtering by the $l-th$ LPF is realized as (1) calculating the FFT of the received data $\{y(n)\}$; (2) setting

the FFT bins corresponding to the range $\left(B_{LPF,l}, f_s - B_{LPF,l}\right)$ to be zeros; (3) performing inverse FFT operation on the modified FFT sequence. Then the resultant data are the lowpass filtered data by using the $l-th$ LPF.

4.3.3 Extraction of the Symbol Rate Candidates Corresponding to the $l-th$ LPF

At first, the fourth-order cyclic moments of the outputs of the $l-th$ LPF are estimated by using (4.6) with $\tau_1 = \tau_2 = \tau_3 = 0$ — this procedure can be realized by using FFT algorithm. Then one or several symbol rate candidates (SRCs) will be extracted from the estimated cyclic moments, and each SRC will be assigned a confidence measurement. For the convenience of further discussion, the magnitudes of the estimated fourth-order cyclic moment at frequency f will be denoted by $\left|\hat{M}_{4y,l}(f)\right|$, where the subscript l represents that the cyclic moments corresponds to the outputs of the $l-th$ LPF.

If the $l-th$ LPF's bandwidth (i.e., $B_{LPF,l}$) is greater than $0.25R_s$, $\left|\hat{M}_{4y,l}(f)\right|$ may contain the symbol-rate line. However, the symbol-rate line is generally neither the global maximum of $\left|\hat{M}_{4y,l}(f)\right|$ nor the maximum in the range of (4.16), especially when the SNR is low and/or the excess bandwidth of the received signal is small. Therefore, a simple maximum search method is not feasible.

By carefully study, it is found that the symbol-rate line satisfies the following properties with very high probability if it does exist in $\left|\hat{M}_{4y,l}(f)\right|$:

P1. It is a local peak, i.e., $\left|\hat{M}_{4y,l}(R_s)\right|$ is greater than that of the two FFT frequencies immediately neighboring to the frequency R_s.

P2. Owing to the effect of the LPF, its magnitude is greater than that of higher FFT frequencies, i.e., $\left|\hat{M}_{4y,l}(R_s)\right| > \left|\hat{M}_{4y,l}(f)\right|$ for $R_s < f < 0.5f_s$.

P3. It is a *clear peak* of $\left|\hat{M}_{4y,l}(R_s)\right|$. That is, it not only satisfies P1 and P2 but is also associated with a relatively large value $D_l(R_s)$, where $D_l(f)$ is defined as

$$D_l(f) = f - \max\left\{ \lambda : \left|\hat{M}_{4y,l}(\lambda)\right| \geq \left|\hat{M}_{4y,l}(f)\right|,\ 0 \leq \lambda < f \right\} \tag{4.21}$$

According to the above properties, the confidence measurement for a SRC is defined as

$$C_{l,k} = D_l(f_{l,k}) \times \frac{\left|\hat{M}_{4y,l}(f_{l,k})\right| - \left|\hat{M}_{4y,l}(f_{l,k-1})\right|}{\left|\hat{M}_{4y,l}(f_{l,k})\right|} \tag{4.22}$$

where $f_{l,k}$ stands for the $k-th$ SRC extracted from the cyclic moments corresponding to the $l-th$ LPF, $C_{l,k}$ is the confidence measurement for $f_{l,k}$, and $f_{l,k} < f_{l,k-1}$.

Based on the above, the proposed algorithm searches the SRCs from high frequency towards low frequency — it starts from the frequency f_B and ends at frequency f_{A*}, where $f_{A*} = 0.8\hat{B}_g$, and f_B is defined in Subsection 4.3.2. The SRC search over the cyclic moments corresponding to the $l-th$ LPF will perform as: (1) find the first FFT frequency which is less than f_B and whose corresponding cyclic moment is a local peak of $\left|\hat{M}_{4y,l}(f)\right|$, and then assign this frequency and the magnitude of its associated cyclic moment to the variable f_{cur} and the variable $\left|\hat{M}_{4y,l}\right|_{last}$, respectively; (2) let the variable k equal to zero; (3) decrease the value of f_{cur} by one FFT frequency unit (i.e., moving to the next FFT bin to the left of the current value of f_{cur}); (4) stop the SRC

search if $f_{cur} < f_{A*}$; (5) repeat from Step-3 if $\left|\hat{M}_{4y,l}(f_{cur})\right|$ is less than $\left|\hat{M}_{4y,l}\right|_{last}$ or if $\left|\hat{M}_{4y,l}(f_{cur})\right|$ is not a local peak of $\left|\hat{M}_{4y,l}(f)\right|$; else, increase the variable k by one; (6) find the frequency $f_{new} \overset{\Delta}{=} \max\left\{f:\ \left|\hat{M}_{4y,l}(f)\right| \geq \left|\hat{M}_{4y,l}(f_{cur})\right|,\ 0 \leq f < f_{cur}\right\}$ — if such a frequency cannot be found, f_{new} will be assigned a value of zero; (8) store the value of f_{cur} in the variable $f_{l,k}$, and assign the value of $(f_{cur} - f_{new}) \times \dfrac{\left|\hat{M}_{4y,l}(f_{cur})\right| - \left|\hat{M}_{4y,l}\right|_{last}}{\left|\hat{M}_{4y,l}\right|_{last}}$ to the variable $C_{l,k}$; (9) update $\left|\hat{M}_{4y,l}\right|_{last}$ with $\left|\hat{M}_{4y,l}(f_{cur})\right|$, and then update f_{cur} with f_{new}; (10) repeat from Step-4.

At the end of SRC search, a set of SRCs are obtained from the cyclic moments corresponding to the outputs of the $l-th$ LPF, an these SRCs are represented as

$$SRC_{l,k} = \left(f_{l,k},\ C_{l,k}\right),\ \text{ for } k = 1, 2, \cdots K_l \tag{4.23}$$

where K_l is the number of the obtained SRCs.

It should be noted that the SRC searching range is a little different from that used to design LPFs as described in (4.16). This is owing to the following consideration. Since the proposed method for estimating B_g is very simple, the estimation accuracy is not high. For a signal with large excess bandwidth, the true value of the symbol rate occasionally may be less than the lower bound of (4.16), i.e., f_A. To accommodate such cases, the frequency lower bound in searching SRCs is empirically decreased to f_{A*}.

4.3.4 Determination of the Symbol Rate and Some Discussions

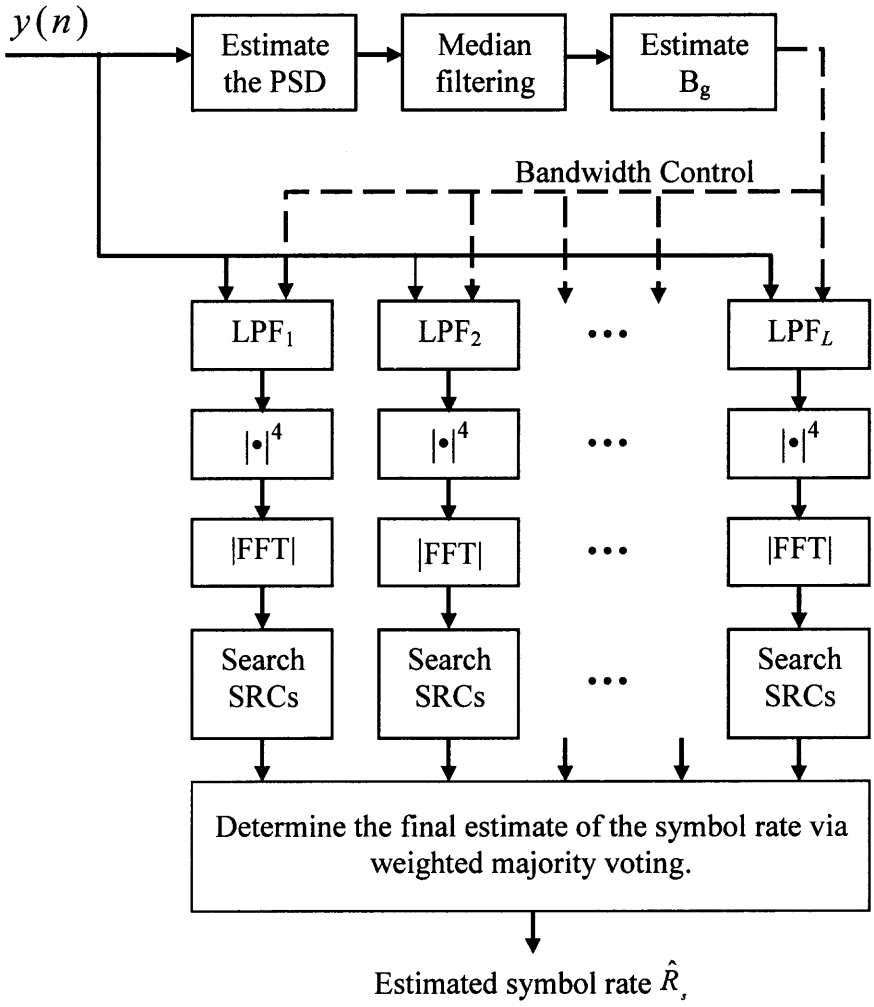

Figure 4.1 Structure of the proposed symbol rate estimator.

Several SRCs extracted from the cyclic moments corresponding to different LPFs as described in (4.23) may have a same frequency — such SRCs will be merged as one final SRC with its confidence measurement equal to the sum of the confidence measurements of the merged SRCs. The resultant final SRCs can be expressed as

$$SRC_k = (f_k,\ C_k),\ \text{ for } k = 1, 2, \cdots K \tag{4.24}$$

where K is the number of the final SRCs, f_k is the frequency of the $k-th$ final SRC, C_k is the confidence measurement of the $k-th$ final SRC, and $K \geq \max\{K_l : l = 1, 2, \cdots, L\}$. Then the final estimate of the symbol rate will be determined as

$$\tilde{R}_s = \arg\left\{ f_k : \max_k (C_k),\ k = 1, 2, \cdots K \right\} \tag{4.25}$$

The overall structure of the proposed symbol rate estimator can be described by using Figure 4.1.

Remarks: In the signal model of (4.1), it is implied that the carrier frequency offset (CFO) has been perfectly removed. However, this generally cannot be satisfied in practice. Nevertheless, it is reasonable to assume that the CFO is much less than the symbol rate. Owing to the special form of the time-varying moments as shown in (4.2), the influence of CFO has been completely removed from the cyclic moments. The CFO may only influence the proposed algorithm through the stage of estimating B_g. The estimation error in $\hat{B}_g$ can be digested by the LPF bank if it is not too large. That is, the proposed algorithm has the ability to tolerate small CFO in the received signal.

The proposed algorithm can also be implemented in passband provided that the carrier frequency is higher than $0.5R_s \times (1+\beta)$, where β is the excess bandwidth factor of the received signal. In this case, a bank of BPFs should be used instead of the LPFs, and the estimation of B_g should also be slightly modified. The modifications are straightforward. For the simplicity, the details are omitted.

In the above investigation, the influence of the channel response has not been taken into account. The symbol-rate line in the fourth-order cyclic moments will vanish if the cutoff frequency of the equivalent lowpass channel response is less than $0.25R_s$.

Then the proposed algorithm will fail. Certainly, the cyclic correlation based approaches such as [123], [125] and [126] will fail too. In fact, the cooperative communications may even be impossible in such cases. Therefore, only the cases where the cutoff frequency of the equivalent lowpass channel response is greater than $0.5R_s$ will be discussed. In such cases, the channel response mainly influences the proposed algorithm through the stage of estimating the value of B_g. As long as the estimated symbol rate range derived from $\hat{B}_g$ includes the true symbol rate and is not too rough, however, the proposed symbol rate estimator will be able to work even though the performance may degrade. This robustness is provided by the filter bank, which ensures one or several branch will generate the symbol-rate line.

As mentioned in Subsection 4.3.1, the estimated PSD of the received signal is filtered by using a median filter during estimating the value of B_g. This median filter serves to smooth the estimated PSD and thus improves the accuracy of the estimated B_g. It also makes the proposed algorithm workable for MASK signals. Theoretically, the PSD of the equivalent lowpass signal of an MASK signal will have an impulse at zero frequency since its symbol mean value is nonzero. That is, the PSD of an MASK signal does not comply with (4.12), which is the basis of the proposed method for estimating B_g. After median filtering, however, the peak in the PSD owing to the nonzero mean value of symbols will be removed. Then the value of B_g for an MASK signal can also be estimated by using the method proposed in Subsection 4.3.1. Accordingly, the proposed symbol rate estimator is able to estimate the symbol rate of MASK signals.

The algorithm and parameters of the used median filter can only influence the proposed symbol rate estimator through $\hat{B}_g$. Also owing to the LPF bank, the proposed symbol rate estimator is not sensitive to the selection of median filter. Nevertheless, it still remains open to develop a scheme to adaptively adjust the parameters of the median filter according to characteristics of the received signal.

The proposed symbol rate estimator can be implemented by using FFT technique. In estimating the PSD of the received signal, the N available samples are divided into Q nonoverlapping segments, leading to $\left(4N\log_2\frac{N}{Q}+2N\right)$ real-valued multiplication operations, where both N and Q are integer powers of two (if necessary, the received data will be padded with zeros). In filtering the received data by using a LPF, it requires $8N\log_2 N$ real-valued multiplication operations. The calculation of the fourth-order cyclic moments corresponding to each LPF requires $(3N+4N\log_2 N)$ real-valued multiplication operations. For searching symbol rate candidates, it only requires knowing the amplitudes of the cyclic moments in the frequency range from zero to $f_s/4$, resulting in N real-valued multiplication operations in each branch. Then the number of real-valued multiplication operations required in each branch will be $(4N+12N\log_2 N)$. The computational burden of the other calculations is trivial and thus can be ignored. It follows the proposed symbol rate estimator has a computational complexity in the order of $\left(N\times(4L+2)+N\times(12L+4)\times\log_2 N-4N\log_2 Q\right)$, where L is the number of LPFs, and the computational complexity is evaluated by the number of real-valued multiplication operations.

4.4 Simulation Results and Conclusions

In all simulations, the impulse response of the pulse-shaping filter is square-root raised-cosine function, the sampling rate is $f_s = 1.0$, the symbol rate is $R_s = 0.25$, the carrier frequency is uniformly distributed in the range $(-0.004Rs,\ 0.004Rs)$ but is fixed for each data set, and each set of the received data contains 4096 symbols. The number of LPFs in the simulations is set as $L = 10$. The SNR is defined in the same way as in Section 3.4.

The cyclic correlation based approach analyzed in [123] is used as a reference method in performance comparison. It employs multiple cyclic correlations with different lags in symbol rate estimation and searches the symbol rate by

$$\hat{R}_s = \arg\max_{f \in \Psi} \left(\hat{M}_{2y}^{(f)H} \mathbf{W} \hat{M}_{2y}^{(f)} \right) \tag{4.26}$$

$$\hat{M}_{2y}^{(f)} = \left[\hat{M}_{2y}^{(f)}(-\Upsilon), \hat{M}_{2y}^{(f)}(-\Upsilon+1) \cdots, \hat{M}_{2y}^{(f)}(\Upsilon-1), \hat{M}_{2y}^{(f)}(\Upsilon) \right]^T \tag{4.27}$$

where the superscript H stands for Hermitian transposition, the superscript T stands for transposition, $\hat{M}_{2y}^{(f)}(\tau)$ represents the estimated cyclic correlation at frequency f under lag τ for the received signal $y(n)$, $\mathbf{W}$ is a weighting matrix which is Hermitian and positive-definite, Ψ is the frequency range to search symbol rate, Υ is a positive integer, and the number of different lags is $2\Upsilon + 1$.

Ciblat et al. [123] claimed that the performance of the coarse search of the symbol rate can be dramatically improved if the matrix $\mathbf{W}$ is chosen as the pseudo inverse of the asymptotic covariance matrix of the estimation error in $\hat{M}_{2y}^{(f)}$. This implies the asymptotic covariance matrix and its inverse should be calculated at each frequency in the search range Ψ. When the search range Ψ is large, the computational burden will be

very heavy and may not be affordable. For this reason, $\mathbf{W}$ is chosen as the identity matrix in the simulations reported in this section. The value of Υ is set as 49 in the simulations. As to the symbol rate search range Ψ, Ciblat et al. [123] only mentioned that it is a closed subinterval included in $(0, f_s/4)$ since the sampling rate is assumed greater than $4R_s$. In fact, the public literature has rarely introduced how to derive this subinterval in practice. Mazet and Loubaton [125] mentioned that an examination of the bandwidth of the received signal makes it possible to limit the search interval to $f > R_s/2$, but they have not revealed the details. To make the performance comparison fair, the search range Ψ is set as (f_{A*}, f_B). That is, both the reference method and the proposed method use the same search range in the simulations.

For a modulation type under a given SNR condition, the performance of a symbol rate estimator is evaluated by using success rate, which is defined as

$$\text{Success-Rate} = \frac{1}{N_{simu}} \sum_{n=1}^{N_{simu}} q\left(\hat{R}_{s,n} - R_s, RES_{\text{FFT}}\right) \tag{4.28}$$

$$q(x,y) = \begin{cases} 1 & \text{if } |x| \le |y| \\ 0 & \text{if } |x| > |y| \end{cases} \tag{4.29}$$

where N_{simu} is the number of simulations for that modulation type under the given SNR, $\hat{R}_{s,n}$ is the estimated symbol rate in the n-th simulation, R_s is the true value of the symbol rate, and RES_{FFT} is the FFT resolution in estimating the cyclic moments (i.e., the FFT resolution in searching the SRCs). That is, a successful estimation means the absolute value of the symbol rate estimation error is less than or equal to the FFT resolution.

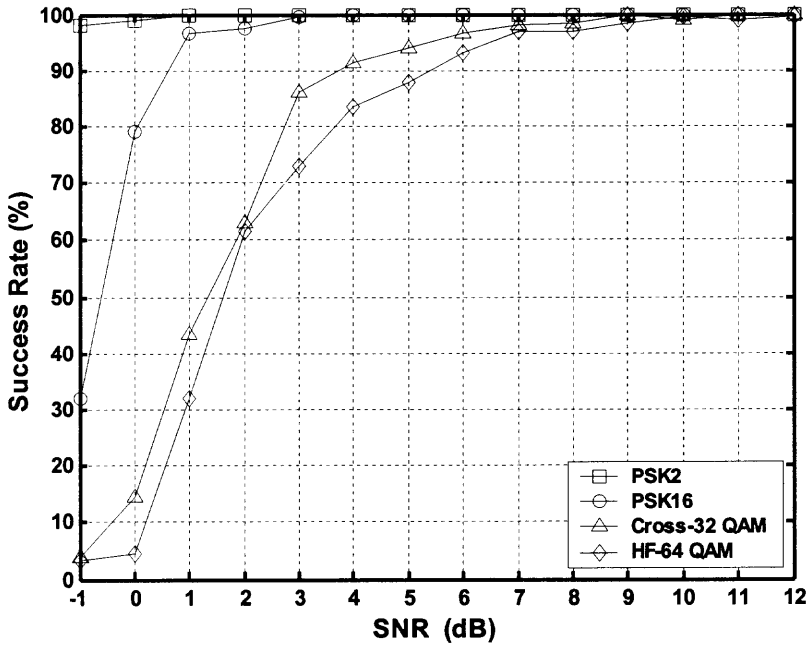

Figure 4.2 Symbol rate estimation results by the proposed method: β=0.0.

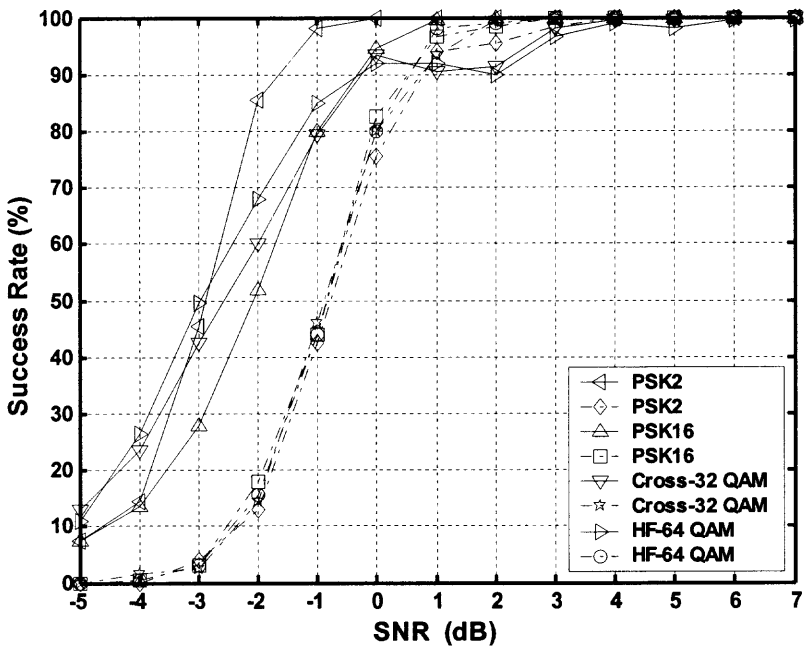

Figure 4.3 Success rate of symbol rate estimation: β=0.2 (Solid curves: results by the proposed method, Dotted-dished curves: results by the reference method).

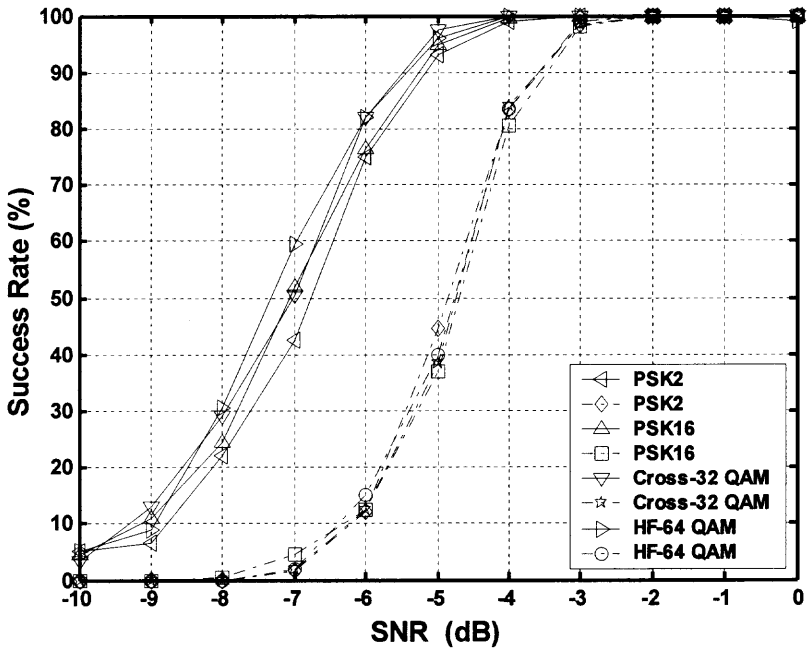

Figure 4.4 Success rate of symbol rate estimation: β=0.4 (Solid curves: results by the proposed method, Dotted-dished curves: results by the reference method).

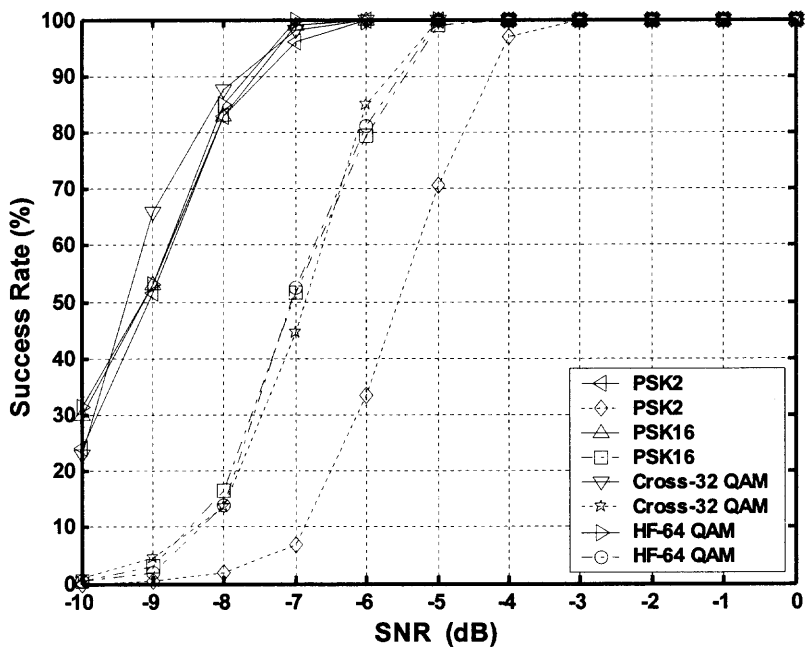

Figure 4.5 Success rate of symbol rate estimation: β=0.6 (Solid curves: results by the proposed method, Dotted-dished curves: results by the reference method).

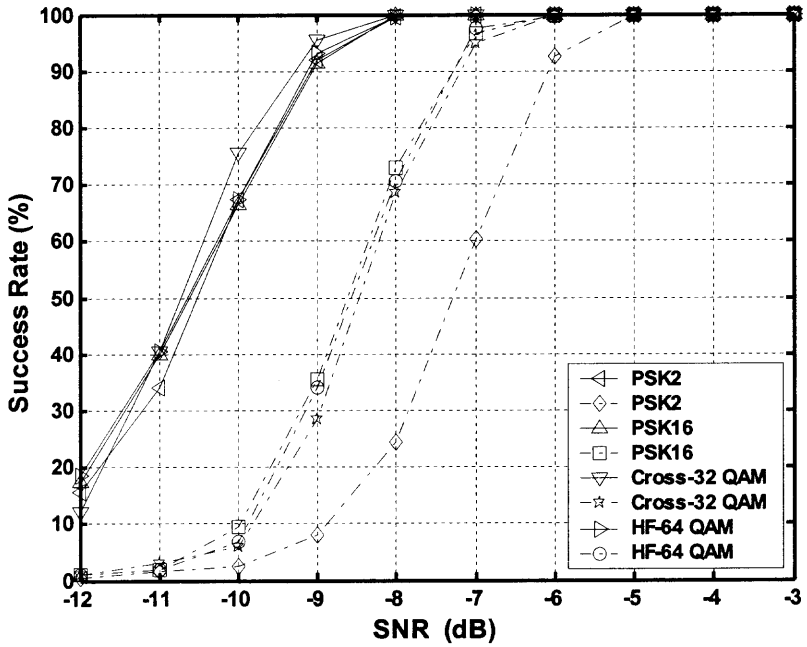

Figure 4.6 Success rate of symbol rate estimation: β=0.8 (Solid curves: results by the proposed method, Dotted-dished curves: results by the reference method).

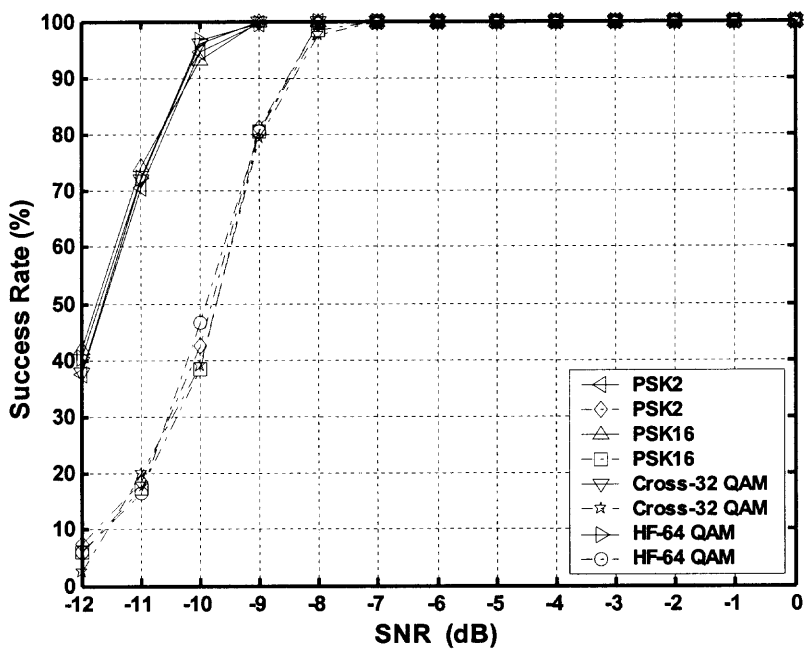

Figure 4.7 Success rate of symbol rate estimation: β=1.0 (Solid curves: results by the proposed method, Dotted-dished curves: results by the reference method).

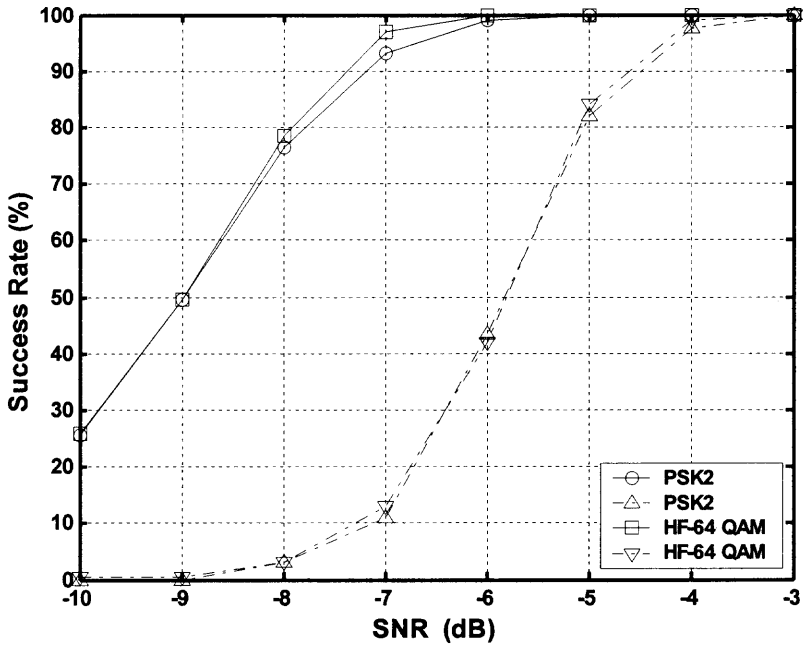

Figure 4.8 Symbol rate estimation results when there is channel distortion: β=0.2 (Solid curves: results by the proposed method, Dotted-dished curves: results by the reference method).

In the first experiment, the communication channel is assumed to be ideal except the AWGN. The testing modulation types include PSK2, PSK16, Cross-32 QAM and HF-64 QAM, where the symbol constellations of Cross-32 QAM and HF-64 QAM can be found in Figure 3.1. The roll-off factor of the pulse shaping function takes values of 0.0, 0.2, 0.4, 0.6, 0.8 and 1.0. Under each SNR, one thousand simulations are carried out for each modulation format. That is, the value of N_{simu} is 1000.

In the case where the roll-off factor is $\beta = 0.0$, only the proposed method is tested. The results in Figure 4.2 show the validity of the proposed method in accommodating signals with zero excess bandwidth. For signals with nonzero excess bandwidth, the symbol rate is also estimated by using the reference method, and the results are shown in Figure 4.3 through Figure 4.7. It can be observed that a considerable performance

improvement has been achieved by the proposed symbol rate estimator, except that there is some performance loss for PSK2 and Cross-32 QAM with $\beta = 0.2$ when the SNR is greater than 1 dB and less than 6 dB.

In the second experiment, only PSK2 and HF-64 QAM signals are tested. The roll-off factor of the pulse shaping function is set as $\beta = 0.2$, and the channel response sampled at $\frac{T}{4}$-spaced is $\mathbf{h} = [1.0,\ -0.075,\ -0.5,\ -0.1719,\ 0.2,\ 0.2719,\ 0.3]$.The number of simulations for a modulation type under each SNR is still $N_{simu} = 1000$. The simulation results are shown in Figure 4.8. It is evident that the proposed method does work and still outperforms the reference method when the channel distortion exists.

In summary, a blind and universal algorithm has been developed for estimating the symbol rate of PAM, PSK and QAM signals with unknown modulation formats. In the proposed symbol rate estimator, fourth-order cyclic moments are employed to accommodate signals with very small or even zero excess bandwidth, and a bank of lowpass filters are used to adapt to the unknown range of the symbol rate. Along each branch of the filter bank, one or more symbol-rate candidates will be extracted, and each symbol-rate candidate is assigned a confidence measurement that is designed based on the study of the properties of the symbol-rate line. Finally, the symbol rate is estimated by voting among the symbol-rate candidates, where the weight of each symbol-rate candidate is its confidence measurement.

The proposed algorithm only imposes reasonable assumptions on the model of the received signal. In implementation, all the unknown parameters are automatically extracted from the received data. Therefore, the proposed symbol-rate estimator is practical in many cases.

A great number of simulations have been carried out for different modulation formats. The simulation results show that the proposed algorithm has achieved a considerable improvement in performance, compared to the cyclic correlation based symbol rate estimator.

CHAPTER 5

AUTOMATIC CLASSIFICATION OF *M*-ARY FREQUENCY SHIFT KEYING SIGNALS

5.1 Introduction

This chapter is concerned with the classification of *M*-ary frequency shift keying (MFSK) signals. An MFSK signal can be described by a modulation format with four parameters: carrier frequency f_c, symbol rate R_s, frequency deviation f_d, and the number of distinct modulating frequencies (i.e., *M*). In this work, the major task is to estimate the value of *M*. However, it is not assumed having *a priori* knowledge of f_c, R_s and f_d. Furthermore, the possible values of *M* are not assumed known in advance. Then it is straightforward that the hypothesis-test based approaches such as [83]-[86] are not feasible, since they assume the received signal belongs to a set of pre-assumed modulation formats.

Many existing AMR algorithms classify MFSK signals based on some features extracted from the received data. For example, Jondral [87] employed a 192-dimensional feature vector, whose entries are the histograms of instantaneous amplitude, instantaneous phase and instantaneous frequency of the received signal, to classify FSK2, FSK4 and some other modulation types. The dimension of the extracted feature vector is reduced by linear or quadratic transform, and then the modulation type is determined by comparing the distances between the reduced-dimension feature vector extracted from the received signal and those extracted from the reference signals. The major drawback with this approach is that the transform coefficients as well as the feature vectors of the reference signals are obtained via off-line training. This implies the classifier will not perform well or may even fail if the modulation format of the received signal is not

within the set of the modulation formats of the reference signals. The classifier of [89] will suffer from the same drawback since it employs the approach of [87]. Hatzichristos and Fargues [57] employ some statistical moments and cumulants of the received signal as the key features to hierarchically classify FSK2, FSK4, FSK8 and some other digital modulations, where the nominal feature values for FSK signals are derived experimentally. Kim et al. [100] employ 29 statistics of the received signal as the key features to classify some analog and digital communication signals including FSK2 and FSK4. This method also classifies the modulation type hierarchically, but each node of the decision tree uses multiple features. The way to use the features in [100] is determined via off-line learning. Therefore, the approaches of [57] and [100] will suffer from the same drawback with [87] since they are also dependent on off-line training.

In classifying FSK2 and FSK4, Assaleh et al. [34] divide the received data into several segments and then estimate the instantaneous frequency of each segment based on the second-order autoregressive (AR) model. Then the average value of the peaks of the first-difference of the instantaneous frequencies is compared with a preset threshold to discriminate between FSK2 and FSK4. This method relies on that the FSK2 signal and FSK4 signal have the same bandwidth. Thus it is impractical in blind environments.

In [12], [98] and [99], Azzouz and Nandi used the standard deviation of the absolute normalized-centralized instantaneous frequency of the received signal as the key feature to discriminate between FSK2 and FSK4. As analyzed in Subsection 2.3.9, the theoretical feature value for an MFSK signal is a function of both frequency deviation ratio and M. Thus it is not capable of recognizing the value of M if the frequency deviation ratio of the input signal is unknown in advance.

The most intuitive and reasonable way to estimate the value of M may be to directly count the number of the modulated frequencies. In [26], [27] and [28], the number of the hills in the histogram of the zero-crossing (ZC) intervals of an MFSK signal is taken as the estimate of M. The classifiers of [49] and [50] take the number of hills in the histogram of the Haar wavelet transform (HWT) magnitudes as the estimate of M. It should be noted that it is not trivial for machine to recognize the hills of a histogram, especially when the SNR is low. Unfortunately, the methods to recognize the histogram hills have not been introduced in [26]-[28] and [49]-[50]. Boudreau et al. [41] mentioned to estimate the value of M by counting the number of the spectral peaks of the squared MFSK signal, but did not introduce the details either.

Based on the analysis of the PSDs of MFSK signals, two AMR algorithms are developed for estimating the value of M of the input MFSK signal. The proposed algorithms also provide a good estimate of the frequency deviation. The rest of this chapter is organized as follows. Section 5.2 formulates the problem. A simple MFSK classifier is developed in Section 5.3, and it is further enhanced in Section 5.4. The performance evaluation results and some discussions are presented in Section 5.5. Conclusions are drawn in Section 5.6.

5.2 Problem Statement and Assumptions

A received MFSK signal $y(t)$ can be modeled as

$$y(t) = x(t) + w(t) \tag{5.1}$$

$$x(t) \overset{\Delta}{=} \sqrt{\frac{2E_s}{T}} \sum_l \cos\left(2\pi\left(f_c + f_l\right)t\right) p(t - lT) \tag{5.2}$$

$$p(t) \overset{\Delta}{=} \begin{cases} 1 & \text{for } 0 \le t < T \\ 0 & \text{otherwise} \end{cases} \tag{5.3}$$

where $x(t)$ is the transmitted MFSK signal, E_s is the symbol energy, T is the symbol period and its reciprocal is the symbol rate R_s, f_c is the carrier frequency, f_l is the modulating frequency in the $l-th$ symbol duration, $w(t)$ is zero-mean white Gaussian noise with a single-sided spectral density level of N_0 (W/Hz) , $w(t)$ and $x(t)$ are independent of each other.

$\{f_l\}$ is a set of i.i.d. discrete random variables, the elements of which uniformly distributed on the following M values

$$f^{(m)} = \frac{2m-1-M}{2} f_d, \quad m = 1, 2, \cdots, M \tag{5.4}$$

where f_d is the frequency deviation.

In this study, it is assumed that the received signal has been classified as MFSK by preprocessing. Further, the sampling rate f_s is high enough such that the aliasing in frequency domain can be avoided. However, all the modulation parameters of the received signal are unknown in advance. In addition, the signal sampling may be asynchronous and non-coherent. That is, the sampling may start at arbitrary instant, and the sampling rate may be neither integer multiples of the modulated frequencies nor an integer multiple of the symbol rate.

It should also be noted that the initial carrier phase and the timing offset between the transmitter and the AMR receiver have not been taken into account in the above signal model. Both of them are assumed to be deterministic but unknown for a data record. As shown later, the proposed method is based on the PSD of the received signal.

Then these two unknown parameters are not relevant and thus are assumed to be zero without loss of generality.

The proposed algorithms work with a sample sequence of $y(t)$, i.e., $\{y(n):\ n=0,1,\cdots,N-1\}$, where $y(n)\overset{\Delta}{=}y(n/f_s)$ is the $n-th$ sample of $y(t)$, and N is the number of the available samples.

5.3 A Simple FFT Based Classifier (FFTC) for MFSK Signals

Since the signal component $x(t)$ and noise component $w(t)$ of the received signal are independent of each other, the PSD $S_y(f)$ of $y(t)$ can be expressed as

$$S_y(f)=\frac{1}{2}\left(S_{lp,x}(f-f_c)+S_{lp,x}(f+f_c)+N_0\right) \tag{5.5}$$

where $S_{lp,x}(f)$ is the PSD of the equivalent lowpass signal of $x(t)$. In Appendix A, it has been shown that $S_{lp,x}(f)$ can be mathematically expressed as

$$\begin{aligned} S_{lp,x}(f)=\frac{2E_s}{M^2T}\Bigg\{&\sum_{m=1}^{M}\delta\left(f-f^{(m)}\right)+(M-1)T\sum_{m=1}^{M}\mathrm{sinc}^2\left(Tf-Tf^{(m)}\right)\\ &-2T\sum_{m=1}^{M-1}\sum_{l>m}^{M}\mathrm{sinc}\left(Tf-Tf^{(m)}\right)\mathrm{sinc}\left(Tf-Tf^{(l)}\right)\cos\left(\pi T\left(f^{(m)}-f^{(l)}\right)\right)\Bigg\} \end{aligned} \tag{5.6}$$

where $\delta(f)$ is the Dirac delta function.

It is evident that the PSD of $y(t)$ consists of a continuous component and M impulses for frequency $f>0$, where each spectral impulse corresponds to a modulated frequency of the input MFSK signal. Then in ideal case, it can expected that the PSD estimated from $\{y(n):\ n=0,1,\cdots,N-1\}$ will have and only have M peaks for frequency less than one half of the sampling rate, and these peaks correspond to the modulated

frequencies of the received MFSK signal. Since the received data contains noise and is only of finite length, however, these peaks generally cannot be easily recognized by simply comparing the estimated PSD amplitude with a preset threshold.

By careful study, several rules have been established to classify MFSK signals based on the estimated PSD of the received signal. The idea is to choose the frequencies corresponding to some peaks of the estimated PSD as the candidates of the modulated frequencies, then estimate the frequency deviation f_d based on these candidates, and finally refine the modulated frequency candidates based on the estimated frequency deviation. The number of the refined candidates of the modulated frequencies will be taken as the estimate of M.

The PSD can be estimated by using the periodogram method or the average periodogram method [132], which can be implemented by using DFT technique. In order to obtain a good estimate of the frequency deviation f_d, the frequency resolution in estimating the PSD should be sufficiently high. Therefore, $S_y(f)$ is estimated by using the periodogram method without averaging. That is, the estimate of $S_y(f)$, denoted by $\hat{S}_y(f)$, is evaluated as

$$\hat{S}_y(f) = \frac{1}{N}\left|\sum_{n=0}^{N-1} y(n) e^{-j\frac{2\pi}{N}nf}\right|^2, \quad \text{for } f = 0,1,\cdots,N-1 \tag{5.7}$$

where the estimation is based on N-point DFT of $y(n)$, and the DFT frequency resolution is f_s / N. It should be noted that the DFT frequency f in (5.7) is actually the index of the $(f+1)-th$ DFT bin. That is, it is a normalized frequency and represents a

true frequency value of $\left(\frac{f-1}{N}f_s\right)$ Hz. In the rest of this chapter, if not explicitly mentioned, the term *frequency* and the notation f will represent a normalized frequency.

Since $S_y(f)$ contains an impulse at the frequency corresponding to a modulated frequency, then the magnitudes of $\hat{S}_y(f)$ at such frequency locations will be greater than that at other frequency locations. Moreover, the impulses in $S_y(f)$ are equally spaced in frequency. These lead to the following classification rules.

Magnitude Rule: If a DFT frequency f^* corresponds to a modulated frequency of the input MFSK signal, then the parameter $\mu(f^*)$ will be greater than a certain threshold, where $\mu(f^*)$ is defined as

$$\mu(f^*) = \hat{S}_y(f^*) \Big/ \max_f\left(\hat{S}_y(f)\right) \tag{5.8}$$

Local-peak Rule: If a DFT frequency f^* corresponds to a modulated frequency of the input MFSK signal, then $\hat{S}_y(f^*)$ would be a local peak of $\hat{S}_y(f)$, i.e., $\hat{S}_y(f^*) > \hat{S}_y(f^*+1)$ and $\hat{S}_y(f^*) > \hat{S}_y(f^*-1)$.

Equal-distance Rule: The modulated frequencies are equally spaced, and the frequency separation is f_d.

The maximum value of $\hat{S}_y(f)$ is expected corresponding to a modulated frequency. Furthermore, if not considering the influence of the noise and the continuous component of $S_y(f)$, the estimated PSD is expected having equal magnitudes at DFT

frequencies corresponding to all modulated frequencies. Then a natural selection of the threshold for $\mu(f)$, denoted by μ_{TH}, would be 0.5.

Table 5.1 A Simple FFT Based Classifier for MFSK Signals

Step 1	Calculate the estimated PSD $\hat{S}_y(f)$ by using (5.7), and let $\mu_{TH} = 0.5$.
Step 2	Find the global maximum of $\hat{S}_y(f)$, and denote it and its corresponding DFT frequency by $\hat{S}_{y,\max}$ and f_{start}, respectively.
Step 3	Apply Magnitude Rule and Local-peak Rule: for each DFT frequency f, calculate the value of $\mu(f)$ as defined in (5.8) — if $\mu(f)$ is greater than μ_{TH} and $\hat{S}_y(f)$ is a local peak, this DFT frequency will be taken as a candidate of the modulated frequencies. At the end of this step, a set of candidates of the modulated frequencies will be obtained, and they are denoted by $f^0_{ca,k}$, $k = 1, 2, \cdots, K^0$.
Step 4	Form the histogram of the first-difference of $\{ f^0_{ca,k} \}$, then take the most frequently occurring one as the estimate of the frequency deviation f_d and denote it by $\hat{f}_d$.
Step 5	Apply Equal-distance Rule: for $k = 1, 2, \cdots, K^0$, if an integer n cannot be found to satisfy $\left| f_{start} + n\hat{f}_d - f^0_{ca,k} \right| < \varepsilon$, then $f^0_{ca,k}$ will be excluded from the set of candidates of the modulated frequencies, where ε is a tolerance that is much less than $\hat{f}_d$. At the end of this step, a subset of $\{ f^0_{ca,k} : k = 1, 2, \cdots, K^0 \}$ will be kept as the refined candidates of the modulated frequencies, and the remaining candidates are denoted by $f^1_{ca,k}$, $k = 1, 2, \cdots, K^1$, where $K^1 \le K^0$.
Step 6	Apply Equal-distance Rule to interpolate possibly missing candidates and increasing the total number of candidates accordingly: calculate $\hat{M} = K^1 + \sum_{k=1}^{K^1-1} round\left(\frac{f^1_{ca,k+1} - f^1_{ca,k}}{\hat{f}_d} - 1 \right)$, where the operator $round(\bullet)$ will round its operand to its nearest integer.
Step 7	Take $\hat{M}$ as the estimate of M, and the estimate of f_d will be $\left(\frac{f_d - 1}{N} f_s \right)$ Hz.

Based on the above rules, a simple classifier for MFSK signals can be formed as shown in Table 5.1, where the tolerance ε in Step-5 is chosen as $1\% \times \hat{f}_d$ in all the simulations reported in this section and Section 5.5.

The DFT of the received signal requires $4N^2$ real-valued multiplication operations, where N is the DFT length. Since the sampling rate is at least higher than twice of the highest modulated frequency, the proposed classifier only needs to check the lower half of the estimated PSD. Moreover, the normalization by N in (5.7) can be removed since the proposed algorithm extracts candidates of the modulated frequencies by comparing the PSD magnitude of a DFT frequency against the global maximum of the estimated PSD. Then it only requires N real-valued multiplication operations to calculate the lower half of $\hat{S}_y(f)$ from the DFT of the received signal. When determining the initial candidates, only those DFT frequencies whose PSD magnitudes are local peaks will be examined. This requires at most $N/4$ real-valued multiplication operations. The computational burden of the other calculations is trivial and thus can be ignored. Therefore, the main computational complexity of this classifier is in the order of $O\left(4N^2 + 1.25N\right)$. If the data sequence $\{ y(n) \}$ is properly padded with zeros, the classifier can be implemented by using FFT algorithm. For this reason, the proposed algorithm is referred to as FFT-based classifier (FFTC). Similar to the above, it can be shown that the computational complexity of the FFTC will be $O\left(4N_{opt} \log_2 N_{opt} + 1.25N_{opt}\right)$, where the FFT length is N_{opt}, and N_{opt} is the smallest integer power of two that satisfies $N_{opt} \geq N$.

Simulation results have shown that the FFTC developed in this section is able to successfully classify 2-FSK, 4-FSK, 8-FSK, 16-FSK and 32-FSK signals for SNR≥0 dB, and it provides very good estimation of the frequency deviation f_d as well [133].

5.4 Extra Classification Rules and the Enhanced FFTC

Based on some practical considerations, three extra classification rules have been developed in this section. The way to estimate the frequency deviation is also modified. Based on these new rules as well as the rules developed in Section 5.3, an enhanced FFT based classifier (EFFTC) for MFSK signals is then developed.

As mentioned above, the FFTC requires the DFT resolution to be as high as possible. The purpose is to let each modulated frequency correspond to a distinct peak in the estimated PSD. However, this doing may result in many false candidates surrounding a DFT frequency that corresponds to a true modulated frequency, where a *false candidate* is a DFT frequency which does not correspond to any modulated frequency but the estimated PSD magnitude of which satisfies Local-peak Rule and Magnitude Rule. When the number of initial candidates of the modulated frequencies is very large, the computational burden in estimating the frequency deviation as discussed later will be extremely heavy and cannot be afforded. Via further investigation, it is found that most of the false candidates can be rejected according to the following rule, thus the computational burden can be reduced dramatically.

Group Rule: The initial candidates of the modulated frequencies (obtained by applying Local-peak Rule and Magnitude Rule) may be classified into several nonoverlapping groups. The frequency difference between any two immediately

neighboring candidate frequencies in a same group is less than a certain small value ζ, while the frequency difference between any two candidate frequencies from different groups is larger than ζ. Each of such groups should be merged as one candidate modulated frequency.

A natural selection of the resultant candidate-modulated-frequency of an above mentioned group is the one with the largest PSD magnitude among that group. The only design parameter of Group Rule is the value of ζ. According to the communication theory, the frequency deviation f_d of an MFSK signal should be greater than or at least equal to one half of symbol rate R_s. Therefore, ζ can be chosen as $\zeta = \hat{R}_s / Q$, where $\hat{R}_s$ is an estimate of R_s and can be obtained by using the existing symbol-rate estimation method such as [134], and Q is a positive parameter that is greater than or equal to eight. It should be noted that the frequency gap between neighboring groups of candidates of the modulated frequencies is not very strict. Therefore, a rough estimate of the symbol rate is sufficient for determining the parameter ζ. If one does not want to estimate the symbol rate, the parameter ζ can also be chosen as $\zeta = BW_y / M_{\max} / Q$, where BW_y is a rough estimate of the received signal's bandwidth obtained by preprocessing, $M_{\max}$ is the possibly maximum value of M of the received MFSK signal, and Q is a positive parameter that is greater than or equal to four. The implementation of Group Rule is straightforward after the parameter ζ is determined.

After applying Local-peak Rule, Magnitude Rule and Group Rule, a set of refined candidates of the modulated frequencies will be obtained. Then the frequency deviation f_d will be estimated based on the refined candidate frequencies. Instead of only

generating one estimate of f_d, however, several different estimates of the frequency deviation may be extracted in the enhanced algorithm. This modification is motivated by the observation that some refined candidates are still false candidates. Then the estimation error in $\hat{f}_d$ will be large if $\hat{f}_d$ is estimated by using the method employed in the original FFTC. The modified estimator of f_d is formed as (1) calculate the frequency differences among all possible pairs of the refined candidates of the modulated frequencies, resulting in $N^{(0)}$ distinct frequency differences $\{\Delta f_i : i = 1, 2, \cdots, N^{(0)}\}$, where $\Delta f_i < \Delta f_{i+1}$, and the occurring- times of Δf_i is υ_i; (2) calculate the first-difference of $\{\Delta f_i : i = 1, 2, \cdots, N^0\}$, resulting in $N^{(1)}$ distinct values that are denoted by $\Delta^{(2)} f_i$ for $i = 1, 2, \cdots, N^{(1)}$; (3) find the largest one among $\{\Delta^{(2)} f_i : i = 1, 2, \cdots, N^{(1)}\}$ that is not greater than the mean value of $\{\Delta^{(2)} f_i\}$, and denote it by $\Delta^{(2)} f_{TH}$; (4) classify the pairs of $\{(\Delta f_i, \upsilon_i) : i = 1, 2, \cdots, N^{(0)}\}$ into several nonoverlapping subsets such that the range of Δf_i in each set is less than the minimum value among $\min\{\Delta f_1 / 8, \Delta^{(2)} f_{TH}, \zeta / 4\}$, where ζ is defined in Group Rule; (5) generate one frequency deviation candidate (FDC) from each subset of $(\Delta f_i, \upsilon_i)$ obtained in last step, and assign the FDC extracted from the $k-th$ subset three parameters $(\bar{f}_{d,k}, \upsilon_{sum,k}, \rho_k)$, where $\bar{f}_{d,k}$ is the value of the $k-th$ FDC and equals to the mean value of Δf_i in the $k-th$ subset, $\upsilon_{sum,k}$ represents the occurring-times of $\bar{f}_{d,k}$ and equals to the sum of υ_l in $k-th$ subset, ρ_k equals to the value range of Δf_i in the $k-th$ subset, and $k = 1, 2, \cdots, N_{fdc}$ with N_{fdc} being the number of FDCs (i.e., the subsets obtained in Step 4).

Due to the discrete nature of DFT, the PSD peaks corresponding to the modulated frequencies may be not equally spaced even though the received MFSK signal is noise free. This requires that the algorithm should allow a certain tolerance in estimating the frequency deviation based on the refined candidates of the modulated frequencies. The fifth step in deriving the FDCs is just to take the frequency differences that only have *small deviation* with each other as the same one, while the second through the fourth steps serves to determine the *small deviation* adaptively.

Up to now, a set of frequency deviation candidates (FDCs) has been extracted, where the $k-th$ FDC is described by ($\overline{f}_{d,k}, \upsilon_{sum,k}, \rho_k$), $k = 1, 2, \cdots, N_{fdc}$. It should be noted that different FDCs will result different estimates of M. Then it is necessary to establish a rule to examine if an FDC is acceptable or not (equivalently, if an estimate of M is acceptable or not). This can be done by checking if the following rule meets.

Confidence Rule: Some of the candidates of the modulated frequencies obtained by applying Group Rule will be rejected by Equal-distance Rule. Then based on the remaining candidates (RCs) of the modulated frequencies, some possibly missing candidates of the modulated frequencies will be interpolated by applying Equal-distance Rule again. In the above steps, an FDC is temporarily taken as the true value of the frequency deviation. If this FDC does correspond to the frequency deviation, then the number of RCs should be greater than that of the interpolated candidates.

Confidence Rule is self-explained. It makes the classification result robust. In realization, the enhanced classifier will sort the FDCs described by ($\overline{f}_{d,k}, \upsilon_{sum,k}, \rho_k$) in the descending order of occurring-times $\upsilon_{sum,k}$, and then sort those FDCs with the same value of $\upsilon_{sum,k}$ in the ascending order of $\overline{f}_{d,k}$. The enhanced classifier then examines each FDC

staring from the one with the highest occurring-times towards the one with the lowest occurring-times. If the currently examined FDC satisfies the Confidence Rule, the examination will stop. Then this FDC is taken as the final estimate of the frequency deviation, and the number of its associated candidates of the modulated frequencies (including the remaining ones and the interpolated ones by applying Equal-distance Rule) will be taken as the estimate of M.

The above examination order of FDCs ensures that a possibly small frequency deviation will not be skipped. The frequency deviation estimated in this way is found better and more reliable. However, it should be pointed out that the so-called final estimate of the frequency deviation is only associated with the current threshold μ_{TH} for Magnitude Rule. As shown next, the threshold μ_{TH} will be dynamically adjusted. For a different value of μ_{TH}, the final estimated frequency deviation as well as that of M may be different.

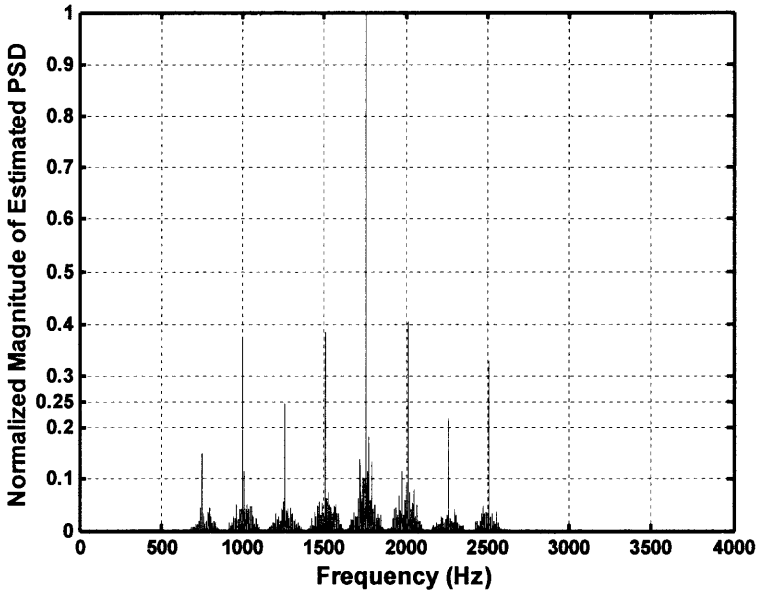

Figure 5.1 The normalized PSD amplitude vs. frequency of an FSK8 signal.

The basis of Magnitude Rule is that the transmitted symbols should be i.i.d. and uniformly distributed over the true modulated frequencies. This makes the PSD magnitudes corresponding to different modulated frequencies be roughly equal. Then a fixed threshold would work. In reality, however, the above requirement may not be met well, especially when the number of symbols contained in the received data is small. In fact, the contributions of the continuous spectral component of the transmitted signal to the PSD magnitudes of different modulated frequencies are inherently unequal. This can be observed from (5.5) and (5.6). Moreover, the transmission filter and the AMR receiving filter as well as the channel response may also introduce unequal attenuation onto different modulated frequencies. The above implies that the PSD magnitudes of the modulated frequencies may be greatly different from each other, and thus the classification may fail if the threshold μ_{TH} is a fixed value. To be intuitive, the estimated PSD of an FSK8 data available on [135] is shown in Figure 5.1, where the FSK8 data are collected from a real-world communication channel. It is evident that the selection of $\mu_{TH} = 0.5$ does not work anymore. Instead, the value of μ_{TH} should be chosen as a smaller value, e.g., chosen within the range (0.1, 0.15). To accommodate such cases, the following classification rule is introduced.

Adaptive-threshold Rule: The threshold μ_{TH} for Magnitude Rule should be adaptively adjusted until certain conditions meet.

In implementation, the initial threshold is still chosen as $\mu_{TH} = 0.5$. If the value of $\hat{M}$ determined by other classification rules based on the current value of μ_{TH} is equal to one, the value of μ_{TH} will be decreased as $\mu_{TH} \Leftarrow \gamma \times \mu_{TH}$, and then the classifier will

repeat from the beginning, where γ is a preset positive constant that is less than one, and the operator $\Leftarrow$ will assign its RHS value to the variable on its left-hand side; otherwise, the classifier will store the current estimate of M in variable $\hat{M}_{old}$, store the estimate of f_d in variable $\hat{f}_{d,old}$, and store the remaining candidates (RCs) of the modulated frequencies — obtained by applying Equal-distance Rule — into the set Ω_{RC}.

After the above doing, the classifier will perform as the following: (1) further decrease μ_{TH} by $\mu_{TH} \Leftarrow \gamma \times \mu_{TH}$; (2) apply other rules as usual to derive new RCs, and estimate the values of M and f_d under the new threshold; (3) if the stop conditions have not been met, update variables $\hat{M}_{old}$ and $\hat{f}_{d,old}$ with their corresponding new values obtained in Step-2, remove all elements from Ω_{RC} and then put the new RCs into the set Ω_{RC}, and then repeat from Step-1; otherwise, take $\hat{M}_{old}$ and $\hat{f}_{d,old}$ as the final estimates of M and f_d, respectively, and then the classification stops.

The stop conditions for the above procedure include: (a) the estimate of M associated with the new threshold is less than $\hat{M}_{old}$; (b) the estimate of M associated with the new threshold is equal to $\hat{M}_{old}$, but the estimate of f_d associated with the new threshold is less than $\hat{f}_{d,old}$; (c) the estimate of M associated with the new threshold is larger than $\hat{M}_{old}$, but some elements in the set Ω_{RC} are not included in the new set of RCs. When any of the above events happens, the Adaptive-threshold Rule will stop. It should be noted that it does not make sense to decrease the threshold endlessly. Therefore, a lower bound should be set for μ_{TH}. If the new value of μ_{TH} is less than this lower bound, the classifier will also stop. In the simulations reported in Section 5.5, this lower bound

for μ_{TH} is empirically set as 1‰, i.e., -30 dB w.r.t. the global maximum of the estimated PSD.

Table 5.2 The Enhanced FFT Based Classifier for MFSK Signals

Step 1	Estimate the received signal's PSD by using FFT algorithm.
Step 2	Apply Local-peak Rule: set those bins of the estimated PSD, whose magnitudes are not local peaks, as zeros. The estimated PSD's global maximum and its corresponding FFT frequency will also be found in this procedure — they are denoted by $PSD_{\max}$ and f_{start}, respectively.
Step 3	Normalized the above modified PSD by dividing $PSD_{\max}$ — only the bins with nonzero magnitudes need to be normalized.
Step 4	Based on the estimated symbol rate or bandwidth of the received signal, set the value of ζ as discussed in the part of Group Rule; set the threshold factor as $\gamma = 0.5$.
Step 5	Initialize other variables: $\gamma = 0.5$, $Flag \Leftarrow 0$, $\mu_{TH} \Leftarrow 0.5$, $\hat{M}_{old} \Leftarrow 1$, $\hat{f}_{d,old} \Leftarrow 0.0$, and let the set Ω_{RC} only contain the value of f_{start}.
Step 6	Apply Magnitude Rule to extract initial candidates (ICs) of the modulated frequencies.
Step 7	Apply Group Rule to merge those ICs, which are very near to each other, as one refined candidate (RC) for the modulated frequencies.
Step 8	If the number of RCs obtained in last step is equal to one and *Flag* is equal to zero, let $\mu_{TH} \Leftarrow \gamma \times \mu_{TH}$ and then repeat from Step-6; if the number of RCs is one and *Flag* is nonzero, let $\mu_{TH} \Leftarrow \gamma \times \mu_{TH}$ and then go to Step-13; otherwise, let $Flag \Leftarrow 1$, and then go to next step.
Step 9	Generate the frequency deviation candidates (FDCs) based on the RCs obtained in last step, and sort them as described in the part of Confidence Rule.
Step 10	Apply Equal-distance Rule based on each of the sorted FDCs until the Confidence Rule is met, and take the FDC satisfying Confidence Rule as the final estimate of f_d associated with the current threshold μ_{TH}. This step also derives new RCs and new estimate of *M*.
Step 11	Compare $\hat{M}_{old}$, $\hat{f}_{d,old}$ and Ω_{RC} with their corresponding values associated with the current value of μ_{TH} to determine if any stop condition has been met.
Step 12	If a stop condition meets, go to Step-14; otherwise, update $\hat{M}_{old}$, $\hat{f}_{d,old}$ and Ω_{RC}, let $\mu_{TH} \Leftarrow \gamma \times \mu_{TH}$, and then go to Step-13.
Step 13	Go to Step-14 if the current value of μ_{TH} is less than the preset lower bound; otherwise repeat from Step-6.
Step 14	Take $\hat{M}_{old}$ and $\hat{f}_{d,old}$ respectively as the final estimates of *M* and f_d, then the chaffier stops.

Based on the classification rules introduced in both this section and Section 5.3, the enhanced FFT based classifier (EFFTC) for MFSK signals is finally formed as shown in Table 5.2.

5.5 Results and Discussions

In generating simulation data by using software, the SNR is defined in the same way as done in [12]. For the simplicity, the details are omitted.

The first measure used to evaluate the performance of the proposed classifiers is the correct classification rate P_c. For an M-ary FSK signal with frequency deviation f_d, P_c under a given test condition is defined as

$$P_c(M) \stackrel{\Delta}{=} \frac{1}{N_{simu}} \sum_{n=1}^{N_{simu}} q\left(M, \hat{M}_n, f_d, \hat{f}_{d,n}, f_s, N\right) \tag{5.9}$$

$$q\left(M, \hat{M}_n, f_d, \hat{f}_{d,n}, f_s, N\right) \stackrel{\Delta}{=} \begin{cases} 1, & \text{if } \hat{M}_n = M \text{ and } \left|f_d - \hat{f}_{d,n}\right| < f_s / N \\ 0, & \text{otherwise} \end{cases} \tag{5.10}$$

where N_{simu} is the number of experiments for this modulation format under the given test condition, $\hat{M}_n$ is the estimate of M obtained from the $n-th$ experiment, $\hat{f}_{d,n}$ is the estimate of f_d obtained from the $n-th$ experiment, f_s is the sampling rate, and N is the FFT length in estimating the PSD of $\{ y(n) \}$.

It is also necessary to evaluate the performance by using the false alarm rate P_{FA}. For an M^*- ary FSK format, the false alarm rate P_{FA} under a given test condition is defined as

$$P_{FA}\left(M^*\right) \overset{\Delta}{=} \frac{1}{N_{simu} \times C} \sum_{c=1}^{C} \sum_{n=1}^{N_{simu}} u\left(M_c, \hat{M}_{c,n}, M^*\right) \tag{5.11}$$

$$u\left(M_c, \hat{M}_{c,n}, M^*\right) \overset{\Delta}{=} \begin{cases} 1, & \text{if } M^* \neq M_c \text{ and } M^* = \hat{M}_{c,n} \\ 0, & \text{otherwise} \end{cases} \tag{5.12}$$

where C is the number of different modulation formats under test, M_c is the true value of M of the $c-th$ modulation format, N_{simu} is the number of experiments for each modulation format under the given test conditions, and the $n-th$ estimate of M_c is $\hat{M}_{c,n}$ for $n = 1, 2, \cdots, N_{simu}$.

When evaluating the performance under an SNR condition, both $P_c\left(M_c\right)$ and $P_{FA}\left(M_c\right)$ will be calculated for $c = 1, 2, \cdots, C$. It should be noted that the value of $\hat{M}_{c,n}$ may be not within the set $\{M_c : c = 1, 2, \cdots, C\}$. In such cases, the input signal will be classified into a class named $OTHER$. Then an extra false alarm rate, i.e., $P_{FA}\left(M^* = OTHER\right)$ will also be calculated in performance evaluation.

Table 5.3 Classification Results by the Original FFTC when SNR=0 dB

Recognized as / True type	FSK2	FSK4	FSK8	FSK16	FSK32	FSK64
FSK2	100%					
FSK4		100%				
FSK8		1%	99%			
FSK16				100%		
FSK32				4%	95%	1%

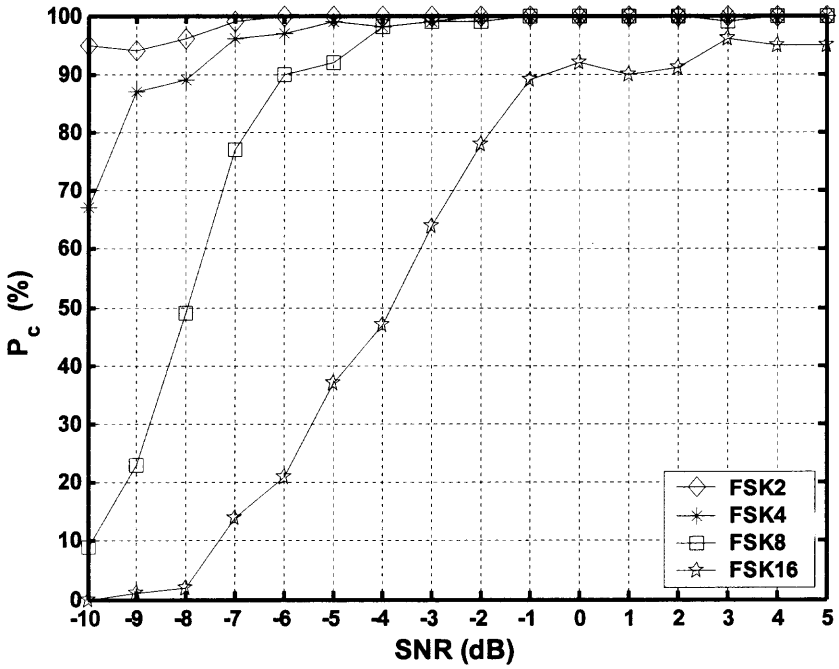

Figure 5.2 P_c versus SNR when the input data contain 300 symbols.

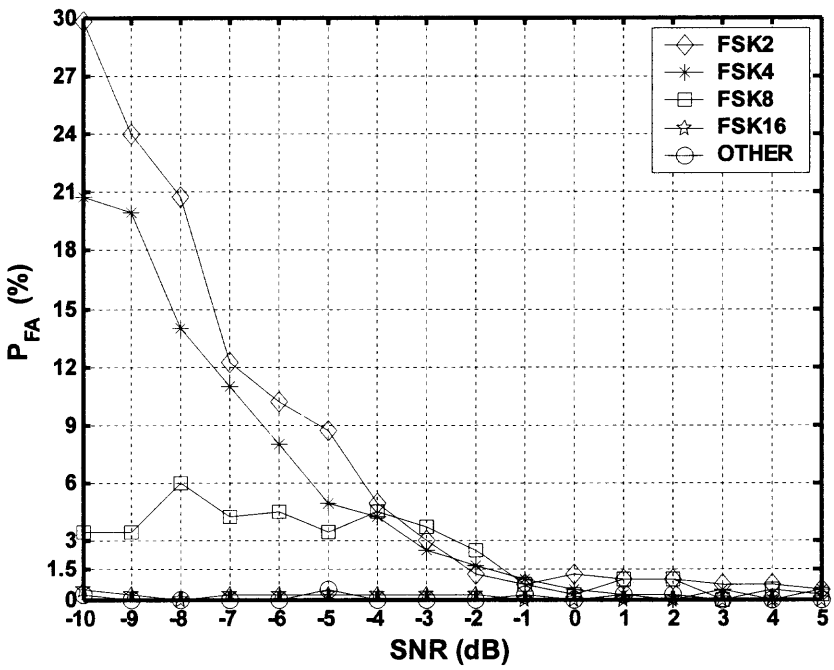

Figure 5.3 P_{FA} versus SNR when the input data contain 300 symbols.

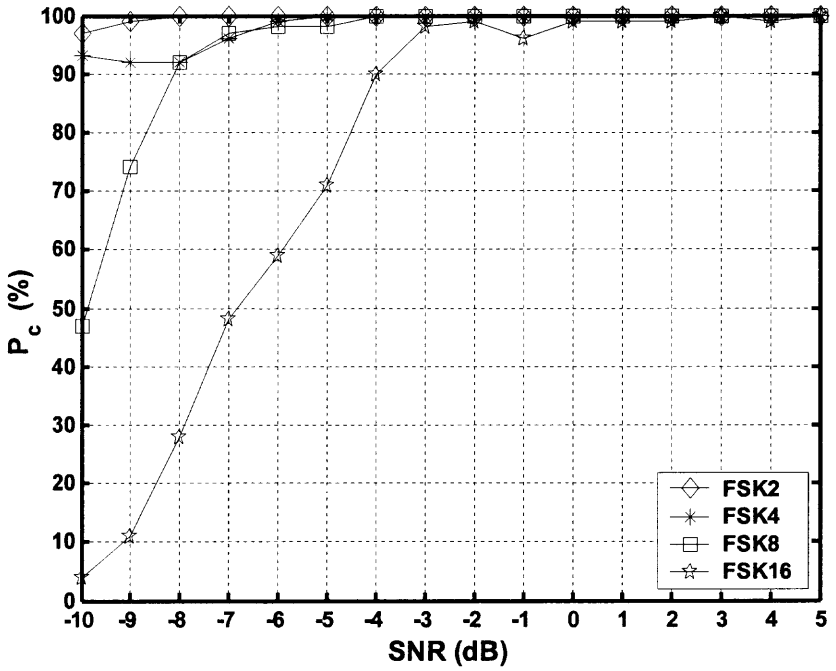

Figure 5.4 P_c versus SNR when the input data contain 500 symbols.

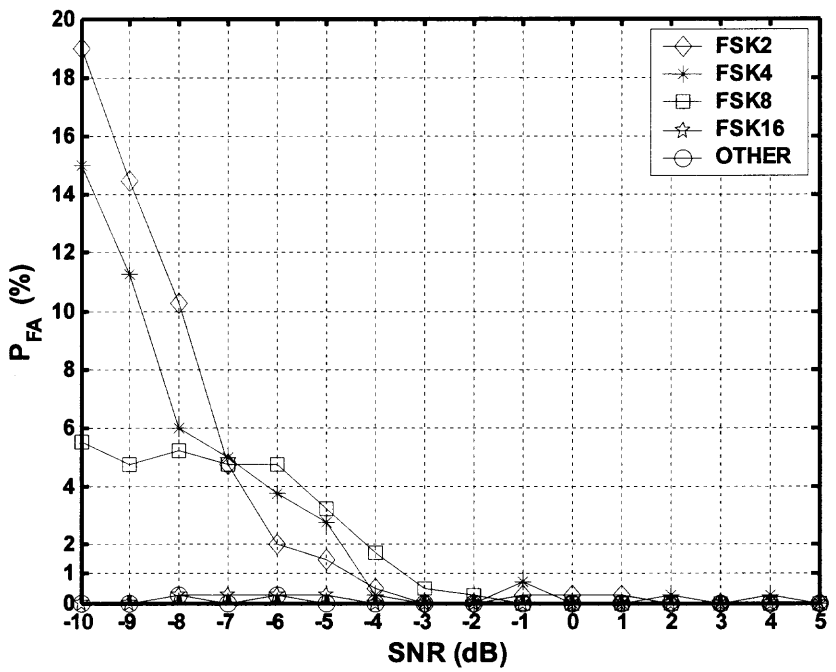

Figure 5.5 P_{FA} versus SNR when the input data contain 500 symbols.

As mentioned in Section 5.3, the original FFTC has been tested with simulated data generated by software. When each data set contains 1200 symbols, the original FFTC has been shown to be able to successfully classify FSK2, FSK4, FSK8, FSK16 and FSK32 signals and to provide good estimates of the frequency deviation. For SNR≥0 dB, the value of P_c for each of the above modulations is higher than 95% [133]. For the simplicity, only the confusion matrix for SNR=0 dB is listed in Table 5.3.

The enhanced FFTC is first tested with FSK2, FSK4, FSK8 and FSK16 data simulated by software generator, and then tested with some MFSK data collected from real-world communication channels. For the simulated data, the carrier frequency f_c is 150×10^3 Hz, the sampling rate f_s is 600×10^3 Hz, the frequency deviation ratio f_d / R_s is 1.0, the symbol rate R_s for FSK2, FSK4 and FSK8 is 12.5×10^3 symbols per second, and R_s is 6.25×10^3 symbols per second for FSK16. The number of simulations for each of the testing modulation types under a given SNR is $N_{simu} = 500$.

At first, the number of symbols contained in a data set is set as $N_{symbols} = 300$, and the correct classification rate P_c and false alarm rate P_{FA} for each modulation type are shown in Figure 5.2 and Figure 5.3, respectively. Then the number of symbols in a data set is increased to $N_{symbols} = 500$, and the results are shown in Figure 5.4 and Figure 5.5.

It can be observed that the enhanced FFTC performs well for SNR≥0 dB if the received data contains 300 symbols. When the number of symbols in a data set is increased to 500, the lowest SNR for a reasonably good performance is further decreased to –3 dB. Keep in mind that a correct classification means not only M has been correctly recognized but also the frequency deviation estimation error is less than the FFT

frequency resolution. That is, the enhanced FFTC is also able to provide a good estimate of the unknown frequency deviation.

The enhanced FFTC has also been tested with MFSK data collected from real-world communication channels, which are available on [135]. For FSK2, FSK4 and FSK8 data on [135], the symbol rate varies from 13.3 to 1200 symbols per second, the frequency deviation varies from 27 to 1200 Hz, the frequency deviation ratio varies from 0.666 to 11.33, and the number of samples in each data set ranges from 2.385×10^4 to 4.82×10^5. The numbers of available data sets for FSK2, FSK4 and FSK8 are 80, 12 and 18, respectively. The test results are shown in Table 5.4. The overall correct classification rate is about 89.1%.

Table 5.4 Classification Results of MFSK Data Available on [135]

Classification results / True type	Times as FSK2	Times as FSK4	Times as FSK8	Times as FSK16	Times as FSK32
FSK2	76	1	2	0	1
FSK4	3	8	1	0	0
FSK8	1	1	14	1	1

It is noted that the proposed algorithm's performance drops when applied to the MFSK data on [135]. The major cause is that some MFSK systems work in burst mode. In the tested MFSK signals, fifty five of the eighty FSK2 signals, eight of the twelve FSK4 signals and seven of the eighteen FSK8 signals are of burst mode. In most signal classifiers including the proposed classifiers in this chapter, it is assumed that the signal of interest (SOI) presents in the whole observation interval. However, the MFSK data of

burst mode on [135] do not satisfy the above assumption. Instead, it is found that some portions of the data are signal plus noise, and the other portions are pure noise. Then the performance degradation is not surprising. The rejection of the pure noise portion is beyond the subjects of this dissertation and thus will not be discussed.

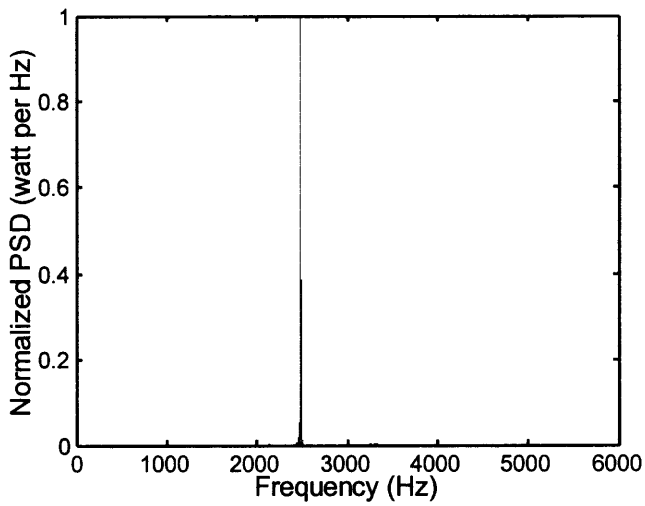

Figure 5.6 Normalized PSD of An FSK2 Signal.

The second cause is that the powers of different modulated frequencies of some MFSK data on [135] are unbalanced. An example is shown in Figure 5.1. In fact, the Adaptive-threshold Rule is able to handle such moderate unbalances in the powers of the modulated frequencies. When the unbalance is much severer, the Adaptive-threshold Rule will fail, leading to misclassifications. As an example of extremely severe unbalance in powers, the estimated PSD of an FSK2 data on [135] is shown in Figure 5.6, where the two modulated frequencies should be 2500 Hz and 3300 Hz. It is evident that the power at 3300 Hz is much less than that at 2500 Hz. Therefore, the Adaptive-threshold Rule would automatically adjust the threshold μ_{TH} to a very small value. However, a very small

threshold μ_{TH} is very likely to take the PSD spikes, which are either owing to the noise or owing to the estimation error, as the candidates of the modulated frequencies. Then a misclassification may happen.

Finally, the numbers of MFSK data sets available on [135] are still too small. With such a few available sets of data, the proposed algorithm cannot be thoroughly evaluated. If more data sets are available, the correct classification rates as well as the false alarm rates should converge to that of the simulated data. For instance, the number of the available FSK2 data sets on [135] is 80, and the successful rate for this type alone is 95% as shown in Table 5.4.

Remarks: In general, the value of M of an MFSK signal is an integer power of two. Therefore, the estimated value of M is rounded to its nearest integer power of two in both the original FFTC and the enhanced FFTC.

In principal, the computational burden of the enhanced FFTC is in the same order of that of the original FFTC. It should be noted that, however, the number of addition operations may not be ignored if the number of RCs is large. The proposed algorithms are also able to work with complex-valued MFSK data. However, the computational burden will be increased.

Finally, it should be noted that it is difficult to conduct a fair performance comparison between the proposed algorithms and the other existing MFSK classification schemes. This is because most of the existing schemes are not able to work under the working conditions assumed in Section 5.2. Moreover, for some published algorithms, the detailed design parameters have not been given out. Therefore, no test has been

performed on other MFSK classification schemes. In fact, the introduction in Section 5.1 can be taken as a general performance analysis and comparison.

5.6 Conclusions

Based on the observation that the modulated frequencies of an MFSK signal correspond to equally spaced impulses in the PSD, this chapter first developed an FFT based algorithm for classifying MFSK signals. Then based on some practical considerations, the FFT based classifier is further enhanced. These two classifiers only require that the received MFSK signal be sampled at a proper sampling rate so that the aliasing in frequency domain can be avoided. Therefore, they are practical in blind environments.

Both classifiers have been tested with the simulated data generated by software generator, and the results have demonstrated their validities. Moreover, both classifiers have been shown to be able to provide very good estimation of the frequency deviation.

The enhanced classifier has also been tested with some MFSK data collected from real-world communication systems. The results show that it has achieved reasonably good test results. However, it is noted that the performance with data from real-world communication channels is worse than that with the simulated data. The causes of performance degradation have been analyzed.

To conclude, the proposed algorithms have greatly promoted the classification of MFSK signals towards practical and blind environments.

CHAPTER 6

AUTOMATIC MODULATION CLASSIFICATION OF JOINT ANALOG AND DIGITAL COMMUNICATION SIGNALS

6.1 Introduction

Due to the current trend of using digital communications instead of analog communications, many recent AMR studies are focused on the classification of digital communication signals only. On the other hand, analog communication techniques are still employed in some communications systems. That is, a communication signal captured by an AMR system may be an analog communication signal or a digital communication signal, but unknown in advance. When an analog (digital) communication signal is fed to an AMR algorithm that is designed for recognizing digital (analog) communication signals only, this signal will be eventually classified as a digital (analog) communication signal of a certain modulation type. Then misclassifications cannot be avoided. This means AMR algorithms, which are able to handle both analog and digital communication signals, are desired in blind environments.

Some published AMR algorithms (e.g., [12], [38], [41], and [87]-[102]) have been focused on the classification of joint analog and digital modulations. As discussed in Subsection 1.2.3 and Chapter 2, however, these algorithms are restricted in practice. For instance, many of these algorithms rely on training to determine the nominal values of their used key features and/or the algorithm parameters (see e.g., [87]-[91]). When the AMR problem is totally blind (i.e., the set of the potential modulation formats is unknown in advance), however, the training data are not available. Then such schemes may fail. A second drawback with these algorithms is that most of them can only work

under relatively high SNR conditions (e.g., SNR≥10 dB or higher). The SNR condition of a real-world communication channel may be worse, and thus AMR algorithms able to work under lower SNR are desired.

Based on the exploration of the cyclostationarities of communication signals, a technique is developed to automatically classify joint analog and digital communication signals in this chapter. Section 6.2 formulates the problem and establishes the working conditions. Section 6.3 explores the cyclostationarities of communication signals under some selected cyclic moments. Section 6.4 presents the schemes for detecting the cycle frequencies of the selected cyclic moments and classifying the modulation types accordingly. Section 6.5 proposes five additional features for modulation classification. Section 6.6 presents the proposed classifier based on the selected cyclic moments and the features proposed in Section 6.5. The performance evaluation results are reported in Section 6.7. A brief conclusion is drawn in Section 6.8.

6.2 Problem Statement and Assumptions

The received signal $y(t)$ can be mathematically expressed as

$$y(t) = x(t) + w(t) \tag{6.1}$$

where $x(t)$ represents the analytic signal of the transmitted communication signal, and $w(t)$ is the additive complex noise.

For analog modulation types, the signal $x(t)$ can be expressed [107] as

AM:
$$x(t) = A\left(1 + K_a s(t)\right)e^{j2\pi f_c t} \tag{6.2}$$

DSB:
$$x(t) = As(t)e^{j2\pi f_c t} \tag{6.3}$$

LSB: $$x(t) = A\left(s(t) - j\tilde{s}(t)\right)e^{j2\pi f_c t} \tag{6.4}$$

USB: $$x(t) = A\left(s(t) + j\tilde{s}(t)\right)e^{j2\pi f_c t} \tag{6.5}$$

FM: $$x(t) = Ae^{j2\pi f_c t + j2\pi f_\Delta \int_{-\infty}^{t} s(v)dv} \tag{6.6}$$

where A is a positive factor used to control the signal power, f_c is the carrier frequency, $s(t)$ represents the real-valued information-bearing signal that satisfies $-1 \le s(t) \le 1$, $\tilde{s}(t)$ stands for the Hilbert transform of $s(t)$, f_Δ is the frequency deviation of FM signal, K_a is the modulation depth (also referred to as *modulation index*) of AM signal, and $0 < K_a \le 1$. It should be noted that (6.6) represents both narrowband FM (NBFM) and wideband FM (WBFM).

For linearly modulated digital communication signals, $x(t)$ can be expressed in a common form [108] as

$$x(t) = A\sum_l s_l g(t - lT)e^{j2\pi f_c t} \tag{6.7}$$

where A is also used to control the signal power, $g(t)$ stands for the pulse shaping function, f_c is the carrier frequency, T is the symbol period and its reciprocal is the symbol rate R_s, and s_l is the $l-th$ transmitted symbol. For different modulation types, s_l will respectively take the following discrete values:

MASK: $$s_l \in \{I_m = m-1:\ m = 1, 2, \cdots, M\} \tag{6.8}$$

MPAM: $$s_l \in \{I_m = 2m-1-M:\ m = 1, 2, \cdots, M\} \tag{6.9}$$

MPSK: $$s_l \in \left\{I_m = e^{j\frac{2\pi(m-1)}{M}}:\ m = 1, 2, \cdots, M\right\} \tag{6.10}$$

QAM: $$s_l \in \left\{ I_m = I_{I,m} + jI_{Q,m} : \ m = 1, 2, \cdots, M \right\} \tag{6.11}$$

where M is the number of distinct symbols in the symbol constellation (i.e., the alphabet size), and $I_{I,m}$ and $I_{Q,m}$ are respectively the in-phase component and the quadrature component of the $m-th$ symbol in the QAM constellation.

For an MFSK signal, $x(t)$ can be expressed [85] as

$$x(t) = A\sum_l e^{j2\pi(f_c+f_l)t} p(t-lT) \tag{6.12}$$

where A, T and f_c have the same meanings as those in (6.7), $p(t)$ is the standard unit pulse of duration T, and f_l is the modulating frequency within the $l-th$ symbol duration. f_l will take the following M discrete values:

$$f^{(m)} = \frac{2m-1-M}{2} f_d, \quad m = 1, 2, \cdots, M \tag{6.13}$$

where f_d is the frequency deviation between two immediately neighboring modulated frequencies.

The proposed classifier can also classify some single-h continuous-phase modulation (CPM) signals. A single-h M-ary CPM signal can be mathematically expressed [108] as

$$x(t) = Ae^{j2\pi f_c t + j2\pi h \int_{-\infty}^{t} \sum_l s_l g(v-lT) dv} \tag{6.14}$$

where s_l takes discrete values as defined in (6.9), h is the modulation index, $g(t)$ is a finite-length pulse nonzero only for $0 \le t \le L_{cpm}T$, and $g(t)$ makes

$$q(t) \overset{\Delta}{=} \int_0^t g(v) dv \tag{6.15}$$

equal to $\frac{1}{2}$ for $t \geq L_{cpm}T$. If $g(t) = 0$ for $t > T$, the CPM is called *full response CPM*; otherwise, it is called *partial response CPM*. A parameter, f_d, is defined as $f_d \overset{\Delta}{=} \frac{h}{T} = hR_s$. For full-response binary CPM with $g(t) = \frac{1}{2T}$, the value of f_d would be the peak-to-peak deviation of instantaneous frequencies. Owing to this, the parameter f_d for CPM is also referred to as *frequency deviation* in the reset, even though it might not be the true peak-to-peak frequency deviation for $g(t)$ of other forms.

Without loss of generality, the following conditions are assumed in the rest of this chapter: (1) $x(t)$ and $w(t)$ are independent of each other; (2) $w(t)$ is complex white Gaussian noise with zero mean; (3) for analog modulations, the information-bearing signal $s(t)$ is ergodic and wide sense stationary (WSS), and it is zero-mean with unknown PDF; (4) for digital modulations, the transmitted symbols $\{s_l\}$ compose a set of i.i.d. discrete random variables, the elements of which are uniformly distributed on the symbol constellation of the concrete modulation type; (5) the symbols of a QAM signal are zero-mean and circularly distributed, i.e., $E[s_l] = 0$ and $E\left[(s_l)^2\right] = 0$, where $E[\bullet]$ stands for the expectation operation; (6) for digital modulations (not including MFSK), the unknown pulse shaping function $g(t)$ may be or may not be the standard unit pulse of duration T, but its bandwidth will be greater than one half of the symbol rate; (7) the unknown frequency deviation ratio D, which is defined as $D \overset{\Delta}{=} f_d / R_s$, is greater than or equal to 0.5 for MFSK; (8) the classifier does not have priori knowledge about the possible values or range of A, K_a, f_Δ, M, R_s, f_d, f_c and the QAM symbol

constellations; (9) when the received signal is CPM, the modulation index h will be either an integer or one half of an odd integer, which is unknown in advance.

The last assumption restricts the proposed classifier to a limited portion of the set of CPM signals. Nevertheless, it has included the following frequently used CPM types: minimum shift keyed (MSK) signals, Gaussian MSK (GMSK) signals, and some other continuous-phase FSK (CPFSK) signals (which are also known as L-REC CPM signals).

It is also assumed that a rough frequency range of the received signal has been obtained by preprocessing. Then the received signal is sampled at a rate higher than four times of its upper frequency bound. However, the sampling may be neither synchronized nor coherent. That is, the sampling may start at any instant, and the sampling rate, f_s, may be neither an integer multiple of the symbol rate R_s nor that of the carrier frequency f_c. For an MFSK signal, the sampling rate may be not integer multiples of the modulated frequencies.

The initial carrier phase is assumed being deterministic but unknown. Since the proposed classifier is based on the detection of the pattern of the cyclostationarity of the received signal as well as other features that are derived from the received signal's PSD, the fixed initial carrier phase is not relevant. Thus it is assumed being zero in the above signal models without loss of generality.

The objective of the proposed classifier is to first discriminate between analog modulations and digital modulations. For a signal classified as analog modulation, it is required to further recognize its concrete modulation type. For a signal classified as digital modulation, the classifier is required to classify its modulation type into one of some nonoverlapping sets of modulation types. Furthermore, if the input signal is a

linearly modulated digital communication signal, the classifier should have its symbol rate estimated. For MFSK and CPM, the number of modulation levels, M, and the frequency deviation f_d should also be estimated.

The proposed algorithm will work with a sample sequence of the input signal to carry out the modulation classification. The input data can be represented by $y(n) \overset{\Delta}{=} y(nT_s), n = 0,1,\cdots N-1$, where N is the number of available data samples, and T_s is the sampling period that is the reciprocal of the sampling rate f_s.

6.3 Cyclostationarities of Communication Signals

Cyclic statistics are useful tools for characterizing and analyzing signals with periodically time-varying characteristics. For a real-valued discrete-time input $\{y(n)\}$, the *kth-order time-varying moment*, $m_{ky}(n;\boldsymbol{\tau})$, is defined as

$$m_{ky}(n;\boldsymbol{\tau}) \overset{\Delta}{=} E\left[f_{ky}(n;\boldsymbol{\tau})\right] \tag{6.16}$$

$$f_{ky}(n;\boldsymbol{\tau}) \overset{\Delta}{=} y(n)\,y(n+\tau_1)\cdots y(n+\tau_{k-1}) \tag{6.17}$$

where $\boldsymbol{\tau}$ is a vector whose entries are the lags of $m_{ky}(n;\boldsymbol{\tau})$, i.e., $\boldsymbol{\tau} = [\tau_0,\cdots,\tau_{k-1}]$, and τ_0 is fixed as $\tau_0 = 0$. If $m_{ky}(n;\boldsymbol{\tau})$ is a periodic or almost periodic function of n, the process $\{y(n)\}$ is called *kth-order cyclostationary* and $m_{ky}(n;\boldsymbol{\tau})$ accepts a Fourier series (FS) decomposition [136], [137] as

$$m_{ky}(n;\boldsymbol{\tau}) = \sum_{\alpha\in\Omega_{m,k}} M_{ky}^{\alpha}(\boldsymbol{\tau})e^{j2\pi\alpha n} \tag{6.18}$$

$$M_{ky}^{\alpha}(\boldsymbol{\tau}) \overset{\Delta}{=} \lim_{N\to\infty}\frac{1}{N}\sum_{n=0}^{N-1} m_{ky}(n;\boldsymbol{\tau})e^{-j2\pi\alpha n} = \lim_{N\to\infty}\frac{1}{N}\sum_{n=0}^{N-1} E\left[f_{ky}(n;\boldsymbol{\tau})\right]e^{-j2\pi\alpha n} \tag{6.19}$$

where the FS coefficient, $M_{ky}^{\alpha}(\boldsymbol{\tau})$, is called the *kth-order cyclic moment* of $\{y(n)\}$ at frequency α for lags $\boldsymbol{\tau}=[\tau_0,\tau_1,\cdots,\tau_{k-1}]$. The values of α for which $M_{ky}^{\alpha}(\boldsymbol{\tau})\neq 0$ are called *cycle frequencies of moments*, which are assumed denumerable in number. $\Omega_{m,k}$ in (6.18) denotes the set of the cycle frequencies of the cyclic moment $M_{ky}^{\alpha}(\boldsymbol{\tau})$. It is evident that $M_{ky}^{\alpha}(\boldsymbol{\tau})$ represents the complex strength of a sine wave (with frequency being α) contained in $m_{ky}(n;\boldsymbol{\tau})$. However, $M_{ky}^{\alpha}(\boldsymbol{\tau})$ with for $\alpha=0$ represents the strength of the DC component of $m_{ky}(n;\boldsymbol{\tau})$. Therefore, the zero frequency (i.e., $\alpha=0$) will not be considered as a cycle frequency in the reset of this dissertation.

By following the moment-cumulant formula, the *time-varying kth-order cyclic cumulant*, $c_{ky}(n;\underline{\tau})$, can be expressed as [138]

$$c_{ky}(n;\boldsymbol{\tau})=\sum_{p=1}^{k}\sum_{\substack{J_1\cup\cdots\cup J_p=J\\ J_1\cap\cdots\cap J_p=\varnothing}}\left[(-1)^{p-1}(p-1)!\prod_{i=1}^{p}m_{v_iy}\left(n;\boldsymbol{\tau}_{J_i}\right)\right] \tag{6.20}$$

where $\varnothing$ represents a null set, and J represents the set of index indicators of the entries in the vector $\boldsymbol{\tau}=[\tau_0,\tau_1,\cdots,\tau_{k-1}]$, i.e., $J=\{0,1,\cdots,k-1\}$. For a value of p in the two-folded summations of (6.20), the indicator set J is partitioned into p distinct subsets $\{J_i:$ $J_i\subseteq J$, $i=1,2,\cdots,p$ $\}$. In each partition, the order of the time-varying moment $m_{v_iy}\left(n;\boldsymbol{\tau}_{J_i}\right)$ equals to the number (denoted by v_i) of indicators in the indicator set J_i, and J_i denotes the lag indices of the vector $\boldsymbol{\tau}_{J_i}$. For example, if the set J_i is $J_i=\{1,3\}$, then $m_{v_iy}\left(n;\boldsymbol{\tau}_{J_i}\right)$ will be $m_{v_iy}\left(n;\boldsymbol{\tau}_{J_i}\right)=E\left[y(n+\tau_1)y(n+\tau_3)\right]$, $\boldsymbol{\tau}_{I_i}$ will be $\boldsymbol{\tau}_{J_i}=\{\tau_1,\tau_3\}$, and v_i will be two. It should be noted that, for a given value of p, there may be multiple

different ways to partition the set J. The inner summation of (6.20) extends over all possible partitions for a give value of p. As an example, the case of $k=3$ is employed to explain the partition procedure as follows. For $p=1$, the only partition is $J_1 = J = \{0,1,2\}$; for $p=2$, there are three ways to partition the set J, i.e., $\{J_1=\{0\},\ J_2=\{1,2\}\}$, $\{J_1=\{1\},\ J_2=\{0,2\}\}$ and $\{J_1=\{2\},\ J_2=\{0,1\}\}$; for $p=3$, the only partition is $\{J_1=0,\ J_2=1,\ J_3=2\}$. Then (6.20) for $k=3$ will be evaluated as

$$\begin{aligned} c_{3y}(n;\boldsymbol{\tau}) &= E\left[y(n)y(n+\tau_1)y(n+\tau_2)\right] \\ &\quad - E\left[y(n)\right]E\left[y(n+\tau_1)y(n+\tau_2)\right] - E\left[y(n+\tau_1)\right]E\left[y(n)y(n+\tau_2)\right] \\ &\quad - E\left[y(n+\tau_2)\right]E\left[y(n)y(n+\tau_1)\right] + 2E\left[y(n)\right]E\left[y(n+\tau_1)\right]E\left[y(n+\tau_2)\right] \end{aligned} \tag{6.21}$$

It follows that the *kth-order cyclic cumulant*, $C_{ky}^{\alpha}(\boldsymbol{\tau})$, which is the FS coefficient of $c_{kx}(n;\boldsymbol{\tau})$, is given by [138]

$$C_{ky}^{\alpha}(\boldsymbol{\tau}) = \sum_{p=1}^{k} \sum_{\substack{J_1\cup\cdots\cup J_p=J \\ J_1\cap\cdots\cap J_p=\varnothing}} (-1)^{p-1}(p-1)! \sum_{\alpha_1,\cdots,\alpha_p} \prod_{i=1}^{p} M_{v_i,y}^{\alpha_i}\left(\boldsymbol{\tau}_{J_i}\right) \times \eta\left(\alpha-\alpha_1-\cdots-\alpha_p\right) \tag{6.22}$$

where $\eta(\alpha)$ is the Kronecker combo (train) function that is nonzero and unity only when $\alpha = 0$ (mod 2). The values of α for which $C_{ky}^{\alpha}(\boldsymbol{\tau}) \neq 0$ are called *cycle frequencies of cumulants*. It should be noted that the set of cycle frequencies for $C_{ky}^{\alpha}(\boldsymbol{\tau})$ may be different from that for $M_{ky}^{\alpha}(\boldsymbol{\tau})$.

For a complex-valued input $\{y(n)\}$, the function $f_{ky}(n;\boldsymbol{\tau})$ may or may not use the conjugate version of $y(n+\tau_i)$ for $i=0,1,\cdots,k-1$. This is formally expressed as

$$f_{ky}(n;\boldsymbol{\tau}) \overset{\Delta}{=} y^{\{*\}}(n)\,y^{\{*\}}(n+\tau_1)\cdots y^{\{*\}}(n+\tau_{k-1}) \tag{6.23}$$

where the superscript {*} stands for an optional complex conjugate operation. Then for a fixed lag vector $\boldsymbol{\tau}$, the kth-order cyclic moment as well as kth-order cyclic cumulant can be defined in 2^k different ways.

Owing to the existence of carrier frequency and/or the periodic transitions of symbols, a communication signal may exhibit cyclostationarity, whereas the order of cyclostationarity and the cycle frequencies are dependent on the selection of $f_{ky}(n;\boldsymbol{\tau})$ and the concrete modulation type. For the complex-valued sample sequence $\{y(n)\}$ of a communication signal, it is well-known that the choice of $f_{ky}(n;\boldsymbol{\tau})$ without conjugation is related to the carrier frequency and that the choice of $f_{ky}(n;\boldsymbol{\tau})$ with $k/2$ conjugations (k even) is related to the symbol rate (e.g., [117], [123] and [139)]). Communication signals can be classified based on the detection of their patterns of cyclostationarities.

In classifying communication signals based on their cyclostationarities, the very first step is to choose a proper set of cyclic statistics. It is well-known that higher-order ($k \geq 3$) cyclic cumulants have some important properties that second-order cyclic cumulants or cyclic moments do not have. For example, higher-order cyclic cumulants are insensitive to Gaussian noises. However, the computational complexity increases and the output SNR decreases with increasing order k [139]. In general, higher-order statistics require larger data record [140]. Therefore, it is always desirable to use the smallest possible value of k [139]. On the other hand, it will be seen later that cyclic statistics of order $k \leq 2$ suffice to complete the task described in Section 6.2. Based on the above considerations, the proposed classifier is designed to employ the first-order

cyclic moment M_{1y}^{α}, the unconjugate second-order cyclic moment $M_{2,0y}^{\alpha}$ and the conjugate second-order cyclic moment $M_{2,1y}^{\alpha}$, which are defined, respectively, as

$$M_{1y}^{\alpha} \stackrel{\Delta}{=} \lim_{N\to\infty} \frac{1}{N} \sum_{n=0}^{N-1} E\left[y(n)\right] e^{-j2\pi\alpha n} \tag{6.24}$$

$$M_{2,0y}^{\alpha} \stackrel{\Delta}{=} \lim_{N\to\infty} \frac{1}{N} \sum_{n=0}^{N-1} E\left[y^2(n)\right] e^{-j2\pi\alpha n} \tag{6.25}$$

$$M_{2,1y}^{\alpha} \stackrel{\Delta}{=} \lim_{N\to\infty} \frac{1}{N} \sum_{n=0}^{N-1} E\left[y^*(n)y(n)\right] e^{-j2\pi\alpha n} \tag{6.26}$$

where the corresponding time-varying moments are $m_{1y}(n;\boldsymbol{\tau}=0) \stackrel{\Delta}{=} E\left[y(n)\right]$, $m_{2,0y}(n;\boldsymbol{\tau}=0) \stackrel{\Delta}{=} E\left[y^2(n)\right]$ and $m_{2,1y}(n;\boldsymbol{\tau}=0) \stackrel{\Delta}{=} E\left[\left|y(n)\right|^2\right]$, respectively.

Before continue, some conditions implied in Section 6.2 are explicitly presented in the following and they will be used in derivation without further notification: $E\left[w(t)\right]=0$, $E\left[w(t+v)w^*(t)\right]=\sigma_w^2\delta(v)$, $E\left[w(t+v)w(t)\right]=0$ for any value of v, $E\left[\left|w(t)\right|^4\right]=2\sigma_w^4$, $E\left[x^{(*)}(t+v)w^{(*)}(t)\right]=0$ for any value of v, $E\left[s(t)\right]=0$, where σ_w^2 is the variance of $w(t)$, and $\delta(\bullet)$ stands for the Dirac delta. Also, the autocorrelation function of $s(t)$, defined as $r_{ss}(v) \stackrel{\Delta}{=} E\left[s(t+v)s(t)\right]$, is an even function of v since $s(t)$ is real-valued. Further, the i.i.d. assumption on $\{s_l\}$ will be taken into account implicitly. The mean value and variance of s_l are denoted by $\bar{m}_s$ and σ_s^2, respectively.

It should be noted that the cycle frequency α defined above is a normalized frequency (normalized w.r.t. the sampling rate f_s). In the following, the analysis of the cyclostationarity of a signal is based on the continuous-time signal $y(t)$, rather than on its

discrete-time version, i.e., $y(n)$. Then the notation n in the time-varying moments and cyclic moments will be replaced with the notation t. The analysis based on $y(t)$ should be equivalent to that based on $y(n)$ as long as the sampling rate f_s is sufficiently high. However, the cycle frequencies derived based on $y(t)$ are non-normalized. If the latter is denoted by f, then its corresponding normalized version, α, will be $\alpha = f / f_s$. Nevertheless, one can easily identify the two versions in a concrete environment. Therefore, the same term *cycle frequency* will be used to alternatively represent both versions in the reset. Moreover, for the simplicity of presentation, the set of cycle frequencies for M_{1y}^{α}, $M_{2,0y}^{\alpha}$ and $M_{2,1y}^{\alpha}$ are denoted by Ω_1, Ω_{20} and Ω_{21}, respectively.

For an AM signal, it is straightforward to show

$$m_{1y}(t;\boldsymbol{\tau}=0) = E\left[y(t)\right] = E\left[A\left(1+K_a s(t)\right)e^{j2\pi f_c t} + w(t)\right] = Ae^{j2\pi f_c t} \tag{6.27}$$

$$m_{2,0y}(t;\boldsymbol{\tau}=0) = E\left[y^2(t)\right] = A^2\left(1+K_a^2 r_{ss}(0)\right)e^{j4\pi f_c t} \tag{6.28}$$

$$m_{2,1y}(t;\boldsymbol{\tau}=0) = E\left[\left|y(t)\right|^2\right] = A^2\left(1+K_a^2 r_{ss}(0)\right)+\sigma_w^2 \tag{6.29}$$

where the only nonzero FS coefficient of $m_{1y}(t;\boldsymbol{\tau}=0)$ is equal to A which is the cyclic moment corresponding to the cycle frequency f_c, the only nonzero FS coefficient of $m_{2,0y}(t;\boldsymbol{\tau}=0)$ is $A^2\left(1+K_a^2 r_{ss}(0)\right)$ which is the cyclic moment corresponding to the cycle frequency $2f_c$, and the only nonzero FS coefficient of $m_{2,1y}(t;\boldsymbol{\tau}=0)$ is $A^2\left(1+K_a^2 r_{ss}(0)\right)$ whose corresponding frequency is zero. As aforementioned, the zero frequency is not considered as a cycle frequency. Therefore, $\Omega_1 = \{f_c\}$, $\Omega_{20} = \{2f_c\}$ and $\Omega_{21} = \varnothing$. The

sets of cycle frequencies for other modulation types are determined in the same manner and will not explained in the reset.

For a DSB signal, the time-varying moments will be

$$m_{1y}(t;\tau=0)=E\left[y(t)\right]=E\left[As(t)e^{j2\pi f_c t}+w(t)\right]=0 \tag{6.30}$$

$$m_{2,0y}(t;\tau=0)=A^2 r_{ss}(0)e^{j4\pi f_c t} \tag{6.31}$$

$$m_{2,1y}(t;\tau=0)=A^2 r_{ss}(0)+\sigma_w^2 \tag{6.32}$$

Then the sets of cycle frequencies will be $\Omega_1=\varnothing$, $\Omega_{20}=\{2f_c\}$ and $\Omega_{21}=\varnothing$.

In order to analyze the cyclostationarity of a SSB signal, it is necessary to evaluate $E\left[\tilde{s}(t)\right]$, $E\left[s(t)\tilde{s}(t)\right]$ and $E\left[\tilde{s}^2(t)\right]$. They are derived as

$$E\left[\tilde{s}(t)\right]=E\left[\int_{-\infty}^{\infty}\frac{s(t-v)}{\pi v}dv\right]=\int_{-\infty}^{\infty}\frac{E\left[s(t-v)\right]}{\pi v}dv=0 \tag{6.33}$$

$$E\left[s(t)\tilde{s}(t)\right]=E\left[\int_{-\infty}^{\infty}\frac{s(t)s(t-v)}{\pi v}dv\right]=\int_{-\infty}^{\infty}\frac{r_{ss}(v)}{\pi v}dv=0 \tag{6.34}$$

$$\begin{aligned}E\left[\tilde{s}^2(t)\right]&=E\left[\int_{-\infty}^{\infty}\int_{-\infty}^{\infty}\frac{s(t-v_1)s(t-v_2)}{\pi v_1\pi v_2}dv_1 d_{v_2}\right]=\int_{-\infty}^{\infty}\int_{-\infty}^{\infty}\frac{r_{ss}(v_2-v_1)}{\pi v_1\pi v_2}dv_1 d_{v_2}\\&=\int_{-\infty}^{\infty}\frac{1}{\pi v_2}\left\{\int_{-\infty}^{\infty}\frac{r_{ss}(v_2-v_1)}{\pi v_1}dv_1\right\}d_{v_2}=\int_{-\infty}^{\infty}\frac{1}{\pi v_2}\tilde{r}_{ss}(v_2)d_{v_2}\\&=-\int_{-\infty}^{\infty}\frac{1}{\pi(0-v_2)}\tilde{r}_{ss}(v_2)d_{v_2}=-\tilde{\tilde{r}}_{ss}(v)|_{v=0}=r_{ss}(v)|_{v=0}=r_{ss}(0)\end{aligned} \tag{6.35}$$

where the last step of (6.34) is owing to the fact that $r_{ss}(v)$ is even and thus $\frac{r_{ss}(v)}{\pi v}$ is odd function of v. In (6.35), $\tilde{\tilde{r}}_{ss}(v)$ represents the Hilbert transform of $\tilde{r}_{ss}(v)$, and the well-know property of Hilbert transform, i.e., $\tilde{\tilde{r}}_{ss}(v)=-r_{ss}(v)$, has been applied in derivation. Armed with the above results, the time-varying moments of an SSB signal will be

$$m_{1y}(t;\boldsymbol{\tau}=0)=E\left[y(t)\right]=E\left[A\left(s(t)\mp j\tilde{s}(t)\right)e^{j2\pi f_c t}+w(t)\right]=0 \tag{6.36}$$

$$m_{2,0y}(t;\boldsymbol{\tau}=0)=A^2\left\{E\left[s^2(t)\right]-E\left[\tilde{s}^2(t)\right]\mp j2E\left[s(t)\tilde{s}(t)\right]\right\}e^{j4\pi f_c t}=0 \tag{6.37}$$

$$m_{2,1y}(t;\boldsymbol{\tau}=0)=A^2\left\{E\left[s^2(t)\right]+E\left[\tilde{s}^2(t)\right]\right\}+\sigma_w^2=2A^2r_{ss}(0)+\sigma_w^2 \tag{6.38}$$

where the minus sign and addition sign of the operator $\mp$ are for LSB and USB, respectively. Therefore, $\Omega_1=\varnothing$, $\Omega_{20}=\varnothing$ and $\Omega_{21}=\varnothing$ for both LSB and USB.

For an FM signal, the conjugate second-order time-varying moment will be

$$m_{2,1y}(t;\boldsymbol{\tau}=0)=E\left[\left|y(t)\right|^2\right]=E\left[\left|Ae^{j2\pi f_c t+j2\pi f_\Delta\int_{-\infty}^{t}s(v)dv}+w(t)\right|^2\right]=A^2+\sigma_w^2 \tag{6.39}$$

Therefore, the set of cycle frequencies for FM will be $\Omega_{21}=\varnothing$.

The analysis of $m_{1y}(t;\boldsymbol{\tau}=0)$ and $m_{2,0y}(t;\boldsymbol{\tau}=0)$ of an FM signal would be difficult due to lack of the knowledge of the PDF of the information-bearing signal $s(t)$. In Section 6.2, $s(t)$ is assumed being ergodic. Here the modulated signal $x(t)$ for FM is further assumed being ergodic, and thus $y(t)$ is also ergodic. Then an FM signal can be analyzed either based on the above-introduced ensemble-average framework where the input signal is treated as a stochastic process, or based on the time-average framework where the input signal is viewed as a sample path of the stochastic process. As stated in [139], the results from one framework are generally true in the other (i.e., with probability equal to one) if the process is ergodic. This chapter is mainly based on the ensemble-average frame work since it provides some useful abstractions in analysis and derivations. On the other hand, the time-average framework is conceptually and mathematically closer to the practice of signal processing. The latter is used to establish

a connection between the kth-order cyclic moment $m_{ky}(t;\boldsymbol{\tau})$ and the spectrum of $f_{ky}(t;\boldsymbol{\tau})$ in the following. The kth-order time-varying moment $m_{ky}(t;\boldsymbol{\tau})$ in the time-average framework is defined as [139]

$$m_{ky}(t;\boldsymbol{\tau}) \stackrel{\Delta}{=} \hat{E}^{\{\alpha\}}\left\{f_{ky}(t;\boldsymbol{\tau})\right\} \tag{6.40}$$

where

$$\hat{E}^{\{\alpha\}}\left[z(t)\right] \stackrel{\Delta}{=} \sum_{\alpha}\left\langle z(u)e^{-j2\pi\alpha u}\right\rangle e^{j2\pi\alpha t} \tag{6.41}$$

is the multiple sine-wave extraction operation and

$$\left\langle q(t)\right\rangle \stackrel{\Delta}{=} \lim_{\Gamma\to\infty}\frac{1}{\Gamma}\int_{-\Gamma/2}^{\Gamma/2} q(u)du \tag{6.42}$$

is the usual time-averaging operation. The sum of (6.41) is over all values of α (which are assumed denumerable in number) that result in nonzero terms. The cyclic moment $M_{ky}^{\alpha}(\boldsymbol{\tau})$ is defined as

$$M_{ky}^{\alpha}(\boldsymbol{\tau}) \stackrel{\Delta}{=} \left\langle f_{ky}(t;\boldsymbol{\tau})e^{-j2\pi\alpha t}\right\rangle \tag{6.43}$$

Then $f_{ky}(t;\boldsymbol{\tau})$ can be represented as

$$f_{ky}(t;\boldsymbol{\tau}) = m_{ky}(t;\boldsymbol{\tau}) + f_{ky,res}(t;\boldsymbol{\tau}) = \sum_{\alpha} M_{ky}^{\alpha}(\boldsymbol{\tau})e^{j2\pi\alpha t} + f_{ky,res}(t;\boldsymbol{\tau}) \tag{6.44}$$

where $\left\langle f_{ky,res}(t;\boldsymbol{\tau})e^{-j2\pi\alpha t}\right\rangle = 0$ for any real-valued α, and the sum is over the denumerable set of real-valued α for which $M_{ky}^{\alpha}(\boldsymbol{\tau}) \neq 0$. Again, $\alpha = 0$ is not considered as a cycle frequency in the context of this dissertation even though $M_{ky}^{\alpha}(\boldsymbol{\tau})|_{\alpha=0}$ might be nonzero.

From (6.40) through (6.44), it is evident that $m_{ky}(t;\boldsymbol{\tau})$ contains and only contains all the additive sine-wave components of $f_{ky}(t;\boldsymbol{\tau})$, where $M_{ky}^{\alpha}(\boldsymbol{\tau})$ is the complex strength of a additive sine-wave with frequency α. In fact, $M_{ky}^{\alpha}(\boldsymbol{\tau})$ is the Fourier transform (FT) of $f_{ky}(t;\boldsymbol{\tau})$ at frequency α. This establishes a connection between the cyclic moment $M_{ky}^{\alpha}(\boldsymbol{\tau})$ and the FT of $f_{ky}(t;\boldsymbol{\tau})$. That is, the cycle frequencies of $M_{ky}^{\alpha}(\boldsymbol{\tau})$ are equal to the nonzero frequencies where the FT of $f_{ky}(t;\boldsymbol{\tau})$ contain spectral impulses (i.e., Dirac delta functions). In another word, a nonzero frequency will be a cycle frequency if it corresponds to a spectral impulse (i.e., a Dirac delta) of the FT of $f_{ky}(t;\boldsymbol{\tau})$. Furthermore, the signal $y(t)$ can be claimed not being *kth*-order cyclostationary (in the sense of $M_{ky}^{\alpha}(\boldsymbol{\tau})$ and its associated $f_{ky}(t;\boldsymbol{\tau})$) if no such nonzero frequency exists.

For a noiseless narrowband FM (NBFM) signal $x(t)$ in the form of (6.6), its FT can be approximated [107] by

$$X(f) \approx A\delta(f-f_c) + jAS(f-f_c) \tag{6.45}$$

where $S(f)$ is the FT of the information-bearing signal $s(t)$, and the result is derived based on the assumption $\left|2\pi f_{\Delta}\int_{-\infty}^{t} s(v)\,dv\right| \ll 1$ radian. In the study of this dissertation, the cases of tone-modulation are not considered. Then it can be assumed that $S(f)$ does not contain spectral impulses without loss of generality. Furthermore, since the noise $w(t)$ is assumed white, it will not contribute spectral impulses to the FT of $y(t)$. Then with the above-derived connection between the cycle frequencies and the FT of $f_{ky}(t;\boldsymbol{\tau})$, it can

be concluded that $m_{1y}(t;\boldsymbol{\tau}=0)=\hat{E}^{\{\alpha\}}\{y(t)\}$ will have and only have one additive sine wave with frequency being f_c (i.e., M_{1y}^{α} has one cycle frequency at f_c) if the parameter f_Δ is very small. When the value of f_Δ is higher such that the condition $\left|2\pi K_f \int_{-\infty}^{t} s(v)dv\right| \ll 1$ does not hold, however, the approximation of (6.45) will be weaker or even invalid. Instead, it is more proper to analyze by using the model of wideband FM (WBFM). As shown later, M_{1y}^{α} does not have cycle frequency for WBFM. Then the set of cycle frequencies of M_{1y}^{α} for NBFM can be expressed as $\Omega_1=\{f_c^{(\pm)}\}$, where the superscript $(\pm)$ means the cycle frequency may or may not exist. The unconjugate second-order time-varying moment can be derived as $m_{2,0y}(t;\boldsymbol{\tau})\overset{\Delta}{=}\hat{E}^{\{\alpha\}}\{y^2(t)\}=\hat{E}^{\{\alpha\}}\left\{A^2 e^{j4\pi f_c t+j4\pi f_\Delta \int_{-\infty}^{t} s(v)dv}\right\}$, where the signal in the braces is simply an FM signal with carrier frequency $2f_c$ and frequency deviation $2f_\Delta$. Therefore, the above analysis can be applied. That is, Ω_{20} will be $\Omega_{20}=\{(2f)^{(\pm)}\}$. In designing the proposed classifier, however, it is assumed that the condition $\left|4\pi f_\Delta \int_{-\infty}^{t} s(v)dv\right| \ll 1$ does not hold. That is, the set of cycle frequencies of $M_{2,0y}^{\alpha}$ for NBFM can be expressed as $\Omega_{20}=\varnothing$, rather than $\Omega_{20}=\{(2f)^{(\pm)}\}$. This is found to be proper through simulations. In summary, the sets of cycle frequencies for NBFM will be $\Omega_1=\{f_c^{\pm}\}$, $\Omega_{20}=\varnothing$ and $\Omega_{21}=\varnothing$.

Now go back to the ensemble-average framework. According to the definition of cycle frequencies and cyclic moments, if an analytic signal $y(t)$ is first-order cyclostationary in the sense of M_{1y}^{α}, then it can be written as

$$y(t)=E\left[y(t)\right]+y_{res}(t)=\sum_{q=1}^{Q}M_{1y}^{f_q}e^{j2\pi f_q t}+M_{1y}^{0}+y_{res}(t) \tag{6.46}$$

where $y_{res}(t)$ is a random signal with zero-mean (i.e., $E\left[y_{res}(t)\right]=0$), M_{1y}^{0} represents the complex strength of the DC component of $E\left[y(t)\right]$ and it might be zero, Q denotes the number of distinct cycle frequencies, f_q is the $q-th$ cycle frequency of M_{1y}^{α}, the value of M_{1y}^{α} at the cycle frequency f_q is represented by $M_{1y}^{f_q}$, and $M_{1y}^{f_q}\neq 0$ for $q=1,2,\cdots,Q$. For the signal $y(t)$ as expressed in (6.46), its autocorrelation function, defined as $r_{yy}(t;v)\overset{\Delta}{=}E\left[y(t+v)y^{*}(t)\right]$, can be evaluated as

$$\begin{aligned} r_{yy}(t;v)=&\sum_{q=1}^{Q}\left|M_{1y}^{f_q}\right|^2 e^{j2\pi f_q v}+2\sum_{q=1}^{Q}\left(M_{1y}^{0}\right)^{*}\mathrm{Re}\left(M_{1y}^{f_q}e^{j2\pi f_q\left(t+\frac{v}{2}\right)}\right)e^{j\pi f_q v}\\ &+\left|M_{1y}^{0}\right|^2+\sum_{q=1}^{Q}\sum_{\substack{p=1\\p\neq q}}^{Q}M_{1y}^{f_q}\times\left(M_{1y}^{f_p}\right)^{*}e^{j2\pi\left(f_q-f_p\right)t+j2\pi f_q v}+r_{y_{res}y_{res}}(t;v) \end{aligned} \tag{6.47}$$

where $r_{y_{res}y_{res}}(t;v)\overset{\Delta}{=}E\left[y_{res}(t+v)y_{res}^{*}(t)\right]$ is the ACF of $y_{res}(t)$, and the operator $\mathrm{Re}(\bullet)$ serves to take the real part of its complex operand. When $Q=1$, $M_{1y}^{0}=0$, and $y_{res}(t)$ is WSS , i.e., $r_{y_{res}y_{res}}(t;v)=r_{y_{res}y_{res}}(v)$, the ACF $r_{yy}(t;v)$ will be

$$r_{yy}(t;v)=\left|M_{1y}^{f_1}\right|^2 e^{j2\pi f_1 v}+r_{y_{res}y_{res}}(v) \tag{6.48}$$

Then the PSD of $y(t)$ will be

$$S_y(f) = \left|M_{1y}^{f_1}\right|^2 \delta(f - f_1) + S_{y_{res}}(f) \tag{6.49}$$

where $S_{y_{res}}(f)$ is the PSD of $y_{res}(t)$, i.e., the FT of $r_{y_{res}y_{res}}(v)$. When the above conditions do not hold, however, $r_{yy}(t;v)$ is generally a function of t. Nevertheless, one can evaluate the average PSD of $y(t)$ by first evaluating the average ACF $\bar{r}_{yy}(v)$ as

$$\bar{r}_{yy}(v) \stackrel{\Delta}{=} \langle r_{yy}(t;v) \rangle = \sum_{q=1}^{Q} \left|M_{1y}^{f_q}\right|^2 e^{j2\pi f_q v} + \left|M_{1y}^{0}\right|^2 + \bar{r}_{y_{res}y_{res}}(v) \tag{6.50}$$

where $\bar{r}_{y_{res}y_{res}}(v) \stackrel{\Delta}{=} \langle r_{y_{res}y_{res}}(t;v) \rangle$, and it will equal to $r_{y_{res}y_{res}}(v)$ if $y_{res}(t)$ is WSS. Then the average PSD of $y(t)$, denoted by $\bar{S}_y(f)$, will be

$$\bar{S}_y(f) = \sum_{q=1}^{Q} \left|M_{1y}^{f_q}\right|^2 \delta(f - f_q) + \bar{S}_{y_{res}}(f) + \left|M_{1y}^{0}\right|^2 \delta(f) \tag{6.51}$$

where $\bar{S}_{y_{res}}(f)$ is the average PSD of $y_{res}(t)$, i.e., the FT of $\bar{r}_{y_{res}y_{res}}(v)$. From all the above, it can be concluded that a cycle frequency of the first-order cyclic moment M_{1y}^{α} of the signal $y(t)$ will contribute a spectral impulse (i.e., Dirac delta in frequency domain) to the PSD (or average PSD) of $y(t)$ at that frequency location. In another word, one can claim that $y(t)$ is not first-order cyclostationary if its PSD does not have spectral impulse at any nonzero frequency. It should be noted that, however, the signal $y(t)$ is not guaranteed to be first-order cyclostationary if its PSD contains spectral impulses at nonzero frequencies. For example, a signal $y(t) = \xi(t)e^{j2\pi f_c t}$ is not first-order cyclostationary if $\xi(t)$ is a zero-mean random signal. It is easy to show that the PSD of

$y(t)$ will be $S_y(f)=\sigma_\xi^2\delta(f-f_c)$ if $\xi(t)$ is white with variance σ_ξ^2. That is, the PSD of $y(t)$ has a spectral impulse at nonzero frequency f_c, but it is not first-order cyclostationary in the sense of M_{1y}^α.

Based on the above result, the cycle frequencies of M_{1y}^α and $M_{2,0y}^\alpha$ for WBFM can be analyzed as follows. For at WBFM signal $y(t)$ as modeled by (6.1) and (6.6), its PSD can be derived as

$$S_y(f)=\begin{cases} S_{\mathrm{Re}(x)}(f)+\sigma_w^2 & , \text{ for } f\geq 0 \\ 0 & , \text{ for } f<0 \end{cases} \tag{6.52}$$

where $S_{\mathrm{Re}(x)}(f)$ is the PSD of the signal $\mathrm{Re}(x(t))$, and it can be expressed [107] as

$$S_{\mathrm{Re}(x)}(f)=\frac{A^2}{2f_\Delta}\times\left(p_s\left(\frac{f-f_c}{f_\Delta}\right)+p_s\left(\frac{f+f_c}{f_\Delta}\right)\right) \tag{6.53}$$

and $p_s(s)$ is the PDF of the information-bearing signal $s(t)$. The signal $s(t)$ is assumed zero-mean in the study of this dissertation. Also, the tone-modulation will not be taken into account for WBFM. It is noted that the signal $s(t)$ is assumed being a pulse-train in some examples of [107] — such WBFM signals are actually MFSK and thus will not be covered in the context of FM. Then it is reasonable to assume the PDF $p_s(s)$ of the random variable $s(t)$ is smooth, i.e., not containing impulse for any value of $s(t)$. It follows that the PSD of $y(t)$ does not contain spectral impulse, and thus $y(t)$ is not first-order cyclostationary, i.e., $\Omega_1=\varnothing$ for WBFM. The second-order cyclic moment $M_{2,0y}^\alpha$ is

actually the first-order cyclic moment of the signal $z(t) \overset{\Delta}{=} (y(t))^2$. The ACF of $z(t)$, denoted by $r_{zz}(t;v)$, can be evaluated as

$$\begin{aligned} r_{zz}(t;v) &= E\left[z(t+v)z^*(t)\right] = E\left[y^2(t+v)y^{2*}(t)\right] \\ &= E\left[x^2(t+v)x^{2*}(t)\right] + E\left[w^2(t+v)w^{2*}(t)\right] \\ &\quad + 4E\left[x(t+v)x^*(t)\right] \times E\left[w(t+v)w^*(t)\right] \\ &= r_{x_2x_2}(t;v) + 2\left(\sigma_w^2\right)^2 \delta(v) + 4r_{xx}(t;v)\sigma_w^2\delta(v) \end{aligned} \tag{6.54}$$

where $r_{x_2x_2}(t;v)$ is the ACF of the signal $x_2(t) \overset{\Delta}{=} x^2(t)$. For a noiseless FM signal $x(t)$ as defined in (6.6), the signal $x_2(t)$ is also a noiseless FM signal with amplitude A^2, information-bearing signal $s(t)$, frequency deviation $2f_\Delta$ and carrier frequency $2f_c$. Also based on the analysis of [107], the PSD $S_{\mathrm{Re}(x_2)}(f)$ of the signal $\mathrm{Re}(x_2(t))$ can be evaluated as

$$S_{\mathrm{Re}(x)}(f) = \frac{A^4}{4f_\Delta} \times \left(p_s\left(\frac{f-2f_c}{2f_\Delta}\right) + p_s\left(\frac{f+2f_c}{2f_\Delta}\right)\right) \tag{6.55}$$

Moreover, $r_{xx}(t;v)$ is equal to A^2 for the delay $v=0$ since an FM signal has constant envelope. Then the PSD of $z(t)$ will be

$$S_z(f) = S_{x_2}(f) + 2\left(\sigma_w^2\right)^2 + 4A^2\sigma_w^2 S_y(f) = \begin{cases} S_{\mathrm{Re}(x_2)}(f) + \sigma_w^2 & \text{, for } f \geq 0 \\ 0 & \text{, for } f < 0 \end{cases} \tag{6.56}$$

where $S_{x_2}(f)$ and $S_{\mathrm{Re}(x_2)}(f)$ are the PSDs of $x_2(t)$ and $\mathrm{Re}(x_2(t))$, respectively. Then similar to the analysis on the signal $y(t)$, it can be concluded that $z(t)$ is not first-order

cyclostationary. Equivalently, $M_{2,0y}^{\alpha}$ does not have cycle frequency, i.e., $\Omega_{20} = \varnothing$. In summary, the cycle frequency sets for WBFM are $\Omega_1 = \varnothing$, $\Omega_{20} = \varnothing$ and $\Omega_{21} = \varnothing$.

For linearly modulated digital communication signals, the time-varying moment $m_{1y}(t;\boldsymbol{\tau}=0)$ will have the following general form

$$m_{1y}(t;\boldsymbol{\tau}=0) = E\left[A\sum_l s_l g(t-lT)e^{j2\pi f_c t} + w(t)\right] = A\bar{m}_s \sum_l g(t-lT)e^{j2\pi f_c t} \quad (6.57)$$

For an MPAM, MPSK or QAM signal, the mean value of symbols is $\bar{m}_s = 0$, resulting in $\Omega_1 = \varnothing$. For an MASK signal, the symbols' mean value is $\bar{m}_s = (1+M)/2$. Then $m_{1y}(t;\boldsymbol{\tau}=0)$ for MASK can be rewritten as

$$m_{1y}(t;\boldsymbol{\tau}=0) = \frac{A(1+M)}{2}\sum_l g(t-lT)e^{j2\pi f_c t} = \frac{A(1+M)}{2T}\sum_l G\left(\frac{l}{T}\right)e^{j2\pi(f_c+l/T)t} \quad (6.58)$$

where $G(f)$ is the FT of $g(t)$. Then it is straightforward $\Omega_1 = \left\{f_c + \frac{l}{T}: \quad l = \text{integer}\right\}$ for MASK. It should be noted that $g(t)$ is generally band-limited and the envelope of $|G(f)|$ will decrease as $|f|$ increases in practical communication systems. That is, $\left|G\left(\frac{l}{T}\right)\right|$ with $l \neq 0$ would be weaker than $|G(0)|$. In fact, if $g(t)$ is the standard unit pulse of duration T, a raised-cosine function or a square-root raised-cosine function, the value of $\left|G\left(\frac{l}{T}\right)\right|$ will be zero for a nonzero integer l. That is, for an MASK signal, the existence of cycle frequency at f_c is almost independent of $g(t)$ if $|G(0)|$ is nonzero (this condition is true in most practical communications systems). On the other hand, the existence of the other cycle frequencies as well as the strengths of the cyclic moment at

those frequencies are highly dependent on the pulse-shaping function $g(t)$. Therefore, the set Ω_1 for MASK is rewritten as $\Omega_1 = \left\{ f_c, \left(f_c + \frac{l}{T} \right)^{(-)} \text{ for } l = \text{nonzero integer} \right\}$, where the superscript $(-)$ denotes the corresponding cycle frequency's dependency on the pulse-shaping function.

For linearly modulated digital communication signals, $m_{2,0y}(t;\tau=0)$ will be

$$\begin{aligned} m_{2,0y}(t;\tau=0) &= E\left[\left(A\sum_l s_l g(t-lT) e^{j2\pi f_c t} + w(t) \right)^2\right] \\ &= A^2 e^{j4\pi f_c t} \left\{ \sum_l \left(E\left[s_l^2\right] - \bar{m}_s^2 \right) g^2(t-lT) + \bar{m}_s^2 \sum_l \sum_k g(t-lT) g(t-kT) \right\} \\ &= \frac{A^2}{T} \sum_l \left\{ \left(E\left[s_l^2\right] - \bar{m}_s^2 \right) \times G_{20}^{(0)}\left(\frac{l}{T}\right) + \bar{m}_s^2 \sum_k G_{20}^{(k)}\left(\frac{l}{T}\right) \right\} \times e^{j2\pi\left(2f_c + \frac{l}{T}\right)t} \end{aligned} \tag{6.59}$$

where $G_{20}^{(k)}(f)$ is the FT of $g(t) \times g(t-kT)$, and $G_{20}^{(k)}(f) = G(f) \otimes \left(G(f) e^{-j2\pi fkT} \right)$ with the operator $\otimes$ standing for the convolution operation. For an MPSK signal with $M \geq 4$ or a QAM signal, both $E\left[s_l^2\right]$ and $\bar{m}_s$ would be zeros, resulting in $m_{2,0y}(t;\tau=0) = 0$ which in turn leads to $\Omega_{20} = \varnothing$. On the other hand, the time-varying moment $m_{2,0y}(t;\tau=0)$ for MASK will be

$$m_{2,0y}(t;\tau=0) = \frac{A^2}{T} \sum_l \left\{ \frac{M^2-1}{12} G_{20}^{(0)}\left(\frac{l}{T}\right) + \frac{(M+1)^2}{4} \sum_k G_{20}^{(k)}\left(\frac{l}{T}\right) \right\} e^{j2\pi t\left(2f_c + \frac{l}{T}\right)} \tag{6.60}$$

and that for MPAM will be

$$m_{2,0y}(t;\tau=0) = \frac{A^2\left(M^2-1\right)}{3T} \sum_l G_{20}^{(0)}\left(\frac{l}{T}\right) e^{j2\pi t\left(2f_c + \frac{l}{T}\right)} \tag{6.61}$$

Then the set Ω_{20} for both MASK and MPAM will be $\Omega_{20} = \left\{ 2f_c + \frac{l}{T} : \ l = \text{integer} \right\}$.

Owing to the above-discussed characteristics of $G(f)$ and the special forms of $G_{20}^{(k)}(f)$, the existence of a cycle frequency $2f_c + \frac{l}{T}$ with nonzero integer l as well as the magnitude of the cyclic moment at this frequency will also be highly dependent on the pulse-shaping function $g(t)$. For example, if $g(t)$ is band-limited and its bandwidth is less than or equal to $\frac{1}{T}$, the cycle frequencies $2f_c + \frac{l}{T}$ with $|l| \geq 2$ will vanish since $G_{20}^{(k)}\left(\frac{l}{T}\right) = 0$ for $|l| \geq 2$. For this reason, the set Ω_{20} for MASK and MPAM can be expressed as $\Omega_{20} = \left\{ f_c, \ \left(f_c + \frac{l}{T} \right)^{(-)} \text{ for } l = \text{nonzero integer} \right\}$. It should be noted that PSK2 is equivalent to PAM2. Therefore, the above results for MPAM are also applicable to PSK2.

Similarly, the time-varying moment $m_{2,1y}(t;\boldsymbol{\tau} = 0)$ for a linearly modulated digital communication signal can be derived as

$$\begin{aligned} m_{2,1y}(t;\boldsymbol{\tau} = 0) &= E\left[\left| A \sum_l s_l g(t - lT) e^{j2\pi f_c t} + w(t) \right|^2 \right] \\ &= \frac{A^2}{T} \sum_l \left\{ \sigma_s^2 \times G_{21}^{(0)}\left(\frac{l}{T}\right) + \bar{m}_s^2 \sum_k G_{21}^{(k)}\left(\frac{l}{T}\right) \right\} \times e^{j2\pi \frac{l}{T} t} + \sigma_w^2 \end{aligned} \tag{6.62}$$

where $G_{21}^{(k)}(f)$ is the FT of $g(t) \times g^*(t - kT)$, and $G_{21}^{(k)}(f) = G(f) \otimes \left(G^*(-f) e^{-j2\pi fkT} \right)$. In (6.62), the symbols' mean value $\bar{m}_s$ may be zero (for MPAM, MPSK and QAM), but the symbol variance σ_s^2 will never be zero for linear digital modulations. Then the set

Ω_{21} for these modulations will be $\Omega_{21} = \left\{ \frac{l}{T}, \text{ for } l = \text{nonzero integer} \right\}$. If $g(t)$ is band-limited and its bandwidth is less than or equal to $\frac{1}{T}$, then the cycle frequencies $f_c + \frac{l}{T}$ with $|l| \geq 2$ will vanish since $G_{21}^{(k)}\left(\frac{l}{T}\right) = 0$ for $|l| \geq 2$. On the other hand, owing to the sixth assumption in Section 6.2, the symbol rate (i.e., $\frac{1}{T}$) will definitely be a cycle frequency of $M_{2,1y}^{\alpha}$. Furthermore, the magnitude of $M_{2,1y}^{\alpha}$ for the cycle frequency $\frac{1}{T}$ is generally larger than that for a cycle frequency $\frac{l}{T}$ with $l > 1$ if the latter is a cycle frequency — this can be observed from (6.62). Therefore, Ω_{21} can be expressed by using the above-defined notation as $\Omega_{21} = \left\{ \frac{1}{T}, \left(\frac{l}{T}\right)^{(-)} \text{ for integer } l > 1 \right\}$.

For an MFSK signal, the time-varying moment $m_{1y}(t;\boldsymbol{\tau} = 0)$ is

$$\begin{aligned} m_{1y}(t;\boldsymbol{\tau} = 0) &= E\left[A\sum_l p(t - lT) e^{j2\pi(f_c + f_l)t} + w(t) \right] \\ &= A\sum_l p(t - lT) E\left[e^{j2\pi(f_c + f_l)t} \right] = \frac{A}{M}\sum_{m=1}^{M} e^{j2\pi\left(f_c + \frac{2m-1-M}{2} f_d\right)t} \end{aligned} \tag{6.63}$$

where the identity $\sum_l p(t - lT) = 1$, which is owing to the fact that $p(t)$ is the standard unit pulse of duration T, has been used in derivation. The result of (6.63) means $\Omega_1 = \left\{ f_c + \frac{2m-1-M}{2} f_d, \text{ for } m = 1, \cdots, M \right\}$. That is, the cycle frequencies for M_{1y}^{α} are simply the modulated frequencies of the MFSK signal. Similarly, $m_{2,0y}(t;\boldsymbol{\tau} = 0)$ is derived as

$$m_{20y}(t;\tau=0)=E\left[\left(A\sum_l p(t-lT)e^{j2\pi(f_c+f_l)t}+w(t)\right)^2\right]$$
$$=A^2\sum_l p(t-lT)E\left[e^{j2\pi(2f_c+2f_l)t}\right]=\frac{A^2}{M}\sum_{m=1}^{M}e^{j2\pi\left(2\left(f_c+\frac{2m-1-M}{2}f_d\right)\right)t} \tag{6.64}$$

where the transform from the square of the summations w.r.t. index l to the summations of squares is owing to the fact that $p(t)$ is the standard unit pulse of duration T, and the special form of $p(t)$ also leads to $p^2(t-lT)=p(t-lT)$ for any value of l. Equation (6.64) means that the cycle frequencies for $M_{2,0y}^{\alpha}$ are twice of the modulated frequencies, i.e., $\Omega_{20}=\{2f_c+(2m-1-M)f_d,\text{ for } m=1,\cdots,M\}$.

Both CPM and MFSK have constant envelope. It is straightforward to show $m_{2,1y}(t;\tau=0)=A^2+\sigma_w^2$, which in turn means $\Omega_{21}=\varnothing$ for CPM and MFSK signals. It should be noted that the channel distortion and the signal filtering operation in the preprocessing may make the CPM or MFSK signal lose the property of constant-envelope and exhibit a certain amplitude modulation. The result is that the FT of $m_{2,0y}(t;\tau=0)$ sometimes does have a spectral impulse for frequency equal to the symbol rate. Then the signal will be determined as having a cycle frequency at symbol rate for $M_{2,1y}^{\alpha}$. This has been counted for in designing the proposed classifier as shown later.

Now consider an M-ary CPM with the pulse shaping function $g(t)$ spans over LT seconds in time. The time-varying moments of the received signal $y(t)$ will be

$$m_{1y}(t;\tau=0)=E[y(t)]=E[x(t)]=E\left[Ae^{j2\pi f_c t+j2\pi h\int_{-\infty}^{t}\sum_l s_l g(v-lT)dv}\right] \tag{6.65}$$

$$m_{2,0y}(t;\tau=0)=E\left[y^2(t)\right]=E\left[x^2(t)\right]=E\left[A^2e^{j4\pi f_c t+j4\pi h\int_{-\infty}^{t}\sum_l s_l g(v-lT)dv}\right] \tag{6.66}$$

It follows that, for an input CPM signal with parameters $\{M,\ L,\ g(t),\ A,\ f_c,\ h\}$, the second-order time-varying moment $m_{2,0y}(t;\tau=0)$ is simply the first-order time-varying moment of another CPM signal with parameters $\{M,\ L,\ g(t),\ A^2, 2f_c,\ 2h\}$. Therefore, the following discussions are mainly focused on $m_{1y}(t;\tau=0)$ and M_{1y}^{α}.

For $t\in\left[kT,(k+1)T\right]$, the transmitted CPM signal $x(t)$ can be rewritten as

$$x(t)=A\exp\left(j2\pi f_c t+j\pi h\sum_{n=-\infty}^{k-L}s_n+j\sum_{n=k-L+1}^{k}s_n q(t-nT)\right) \tag{6.67}$$

where $q(t)$ is defined in (6.15). Since the symbols $\{s_n\}$ are assumed to be i.i.d., the expectation value of $x(t)$ can be derived as

$$\begin{aligned}
E\left[x(t)\right]&=Ae^{j2\pi f_c t}\prod_{n=-\infty}^{k-L}E\left[e^{j\pi h s_n}\right]\prod_{n=k-L+1}^{k}E\left[e^{js_n q(t-nT)}\right]\\
&=Ae^{j2\pi f_c t}\prod_{n=-\infty}^{k-L}\left[\frac{1}{M}\sum_{m=1}^{M}e^{j\pi h(2m-1-M)}\right]\prod_{n=k-L+1}^{k}\left[\frac{1}{M}\sum_{m=1}^{M}e^{j(2m-1-M)q(t-nT)}\right]\\
&=Ae^{j2\pi f_c t}\prod_{n=-\infty}^{k-L}\left[\frac{2}{M}\sum_{m=1}^{M/2}\cos\left(\pi h(2m-1-M)\right)\right]\prod_{n=k-L+1}^{k}\left[\frac{1}{M}\sum_{m=1}^{M}e^{j(2m-1-M)q(t-nT)}\right]
\end{aligned} \tag{6.68}$$

and

$$\frac{2}{M}\sum_{m=1}^{M/2}\cos\left(\pi h(2m-1-M)\right)=\begin{cases}0, & \text{for } h=0.5\times(2v+1)\\ 1, & \text{for } h=2v\\ -1, & \text{for } h=2v+1\end{cases} \tag{6.69}$$

where M is assumed to be an odd integer, and v is a positive integer. Therefore, if h is one half of an odd integer, the cyclic moment M_{1y}^{α} does not have cycle frequency. If

h is an integer, the time-varying moment $m_{1y}(t;\tau=0)$ can be rewritten based on (6.68) and (6.69) as

$$m_{1y}(t;\tau=0)=\begin{cases} Ae^{j2\pi f_c t}\sum_k z(t-kT), & h \text{ even} \\ Ae^{j2\pi f_c t}c_\infty \sum_k (-1)^k z(t-kT), & h \text{ odd} \end{cases} \tag{6.70}$$

$$z(t)\overset{\Delta}{=}\frac{2}{M}\prod_{l=1}^{L}\left[\sum_{m=1}^{M/2}\cos\left((2m-1-M)q(t-(l-L)T)\right)\right]\mathrm{rect}\left(\frac{t-T/2}{T}\right) \tag{6.71}$$

$$\mathrm{rect}(t)\overset{\Delta}{=}\begin{cases} 1, & |t|\le T/2 \\ 0, & \text{otherwise} \end{cases} \tag{6.72}$$

where c_∞ is an undetermined constant that can be assumed to be $+1$ or -1. The result of (6.70) through (6.72) is coincident with that of equation (47) in [141], where the latter is only for binary CPM signals and thus is a special case of (6.70).

If $z(t)$ as defined in (6.71) is not $z(t)\equiv 0$, then $m_{1y}(t;\tau=0)$ for a CPM signal with integer h will be a periodic function of t, and it can be decomposed into FS as

$$m_{1y}(t;\tau=0)=\begin{cases} \frac{A}{T}\sum_k Z\left(\frac{k}{T}\right)e^{j2\pi\left(f_c+\frac{k}{T}\right)t}, & h=\text{even} \\ \frac{Ac_\infty}{T}\sum_{k=\text{odd}} Z\left(\frac{k}{2T}\right)e^{j2\pi\left(f_c+\frac{k}{2T}\right)t}, & h=\text{odd} \end{cases} \tag{6.73}$$

where $Z(f)$ is the FT of $z(t)$. It follows that the cycle frequencies of M_{1y}^{α} are

$$\Omega_1=\begin{cases} \left\{f_c+\frac{k}{T}: k=\text{integer}\right\}, & h=\text{even} \\ \left\{f_c+\frac{k}{2T}: k=\text{odd}\right\}, & h=\text{odd} \end{cases} \tag{6.74}$$

As mentioned above, $m_{2,0y}(t;\tau=0)$ is simply the first-order time-varying moment of a CPM signal with modulation index $2h$ and carrier frequency $2f_c$. Then the cycle frequencies of $M_{2,0y}^{\alpha}$ will be

$$\Omega_{20}=\begin{cases}\left\{2f_c+\dfrac{k}{T}: k=\text{integer}\right\}, & h=\text{integer}\\ \left\{2f_c+\dfrac{k}{2T}: k=\text{odd}\right\}, & h=0.5\times\text{odd}\end{cases} \tag{6.75}$$

It should be noted that the results of (6.74) and (6.75) are only general results. The values of k, for which the FS coefficients (i.e., the values of the cyclic moment) are nonzero, are dependent on the concrete pulse shaping function $g(t)$ and the value of modulation index h. Equivalently, the numbers and values of the cycle frequencies of M_{1y}^{α} and $M_{2,0y}^{\alpha}$ are dependent on the concrete pulse shaping function $g(t)$ and the values of L and h. As examples, the FS representations of $m_{1y}(t;\tau=0)$ for binary CPM with 1-REC and 2-REC pulse shaping functions are derived based on (6.71) through (6.73), and they are presented as follows:

$$m_{1y}(t;\tau)=\frac{1}{2}e^{j2\pi\left(f_c+\frac{h}{2T}\right)t}+\frac{1}{2}e^{j2\pi\left(f_c-\frac{h}{2T}\right)t},\quad \text{for } L=1,\ M=2,\ h=\text{integer} \tag{6.76}$$

$$m_{1y}(t;\tau)=\frac{\sin\left(\frac{h\pi}{2}\right)}{4j}\left(e^{j2\pi\left(f_c-\frac{h}{2T}\right)t}-e^{j2\pi\left(f_c+\frac{h}{2T}\right)t}\right),\quad \text{for } L=2,\ M=2,\ h=\text{odd} \tag{6.77}$$

$$m_{1y}(t;\tau)=\frac{(-1)^{h/2}}{4}\left(e^{j2\pi\left(f_c+\frac{h}{2T}\right)t}+e^{j2\pi\left(f_c-\frac{h}{2T}\right)t}\right),\quad \text{for } L=2,\ M=2,\ h=\text{even} \tag{6.78}$$

It is straightforward to derive the cycle frequencies from the above results. For the simplicity, they are omitted here.

In designing the proposed classifier, the major concern on CPM signals with $h = 0.5 \times \text{integer}$ is to classify the ones with $h = \text{integer}$ into the same set of modulation types with MFSK signals and to classify the ones with $h = 0.5 \times \text{odd}$ into a distinct set. This can be achieved since either or both of M_{1y}^{α} and $M_{2,0y}^{\alpha}$ will have multiple cycle frequencies for CPM signals with $h = 0.5 \times \text{integer}$ and the patterns of the cycle frequencies of M_{1y}^{α} and $M_{2,0y}^{\alpha}$ are different for $h = \text{integer}$ and $h = 0.5 \times \text{odd}$. In fact, for some CPM signals such as 1-REC CPM and 2-REC CPM signals with $h = 0.5 \times \text{integer}$, the values of M and f_d (where $f_d = \frac{h}{T}$) can also be recognized via M_{1y}^{α} and $M_{2,0y}^{\alpha}$. This can be observed from (6.76) through (6.78). An MSK signal is simply a 1-REC CPM signal with $h = \frac{1}{2}$ [108], thus its values of M and f_d can be determined based on M_{1y}^{α} and $M_{2,0y}^{\alpha}$. Theoretically, it cannot directly apply the above results to GMSK signals since the pulse shaping function $g(t)$ of a GMSK signal has infinite width in time domain. In practice, however, a GMSK signal with pulse $g(t-T)$ is equivalent to a CPM signal with finite-width pulse $g(t-T)\text{rect}\left(\frac{t-T}{2T}\right)$ and $h = \frac{1}{2}$ [141]. Then the above general discussions are also applicable to GMSK signal.

In summary, the cyclic moments M_{1y}^{α} and $M_{2,0y}^{\alpha}$ suffice to achieve the classification goals on CPM signals with $h = 0.5 \times \text{integer}$. It should be noted that, however, the numbers and values of the cycle frequencies of M_{1y}^{α} and $M_{2,0y}^{\alpha}$ may be different for different combinations of $g(t)$, L, M and h. When the pulse $g(t)$ is not

rectangular, the derivation may be very difficult. Nevertheless, in analyzing the cycle frequencies for a specific CPM signal with $h = 0.5 \times \text{integer}$, one can take use of the general results in (6.70) through (6.73).

The cycle frequencies of M_{1y}^{α}, $M_{2,0y}^{\alpha}$ and $M_{2,1y}^{\alpha}$ for the concerned modulation types are summarized in Table 6.1.

Table 6.1 Cycle Frequencies of Communication Signals†

Cyclic Statistics / Modulation types	M_{1x}^{α}	$M_{2,0x}^{\alpha}$	$M_{2,1x}^{\alpha}$
AM	f_c	$2f_c$	N/A
DSB	N/A	$2f_c$	N/A
LSB	N/A	N/A	N/A
USB	N/A	N/A	N/A
NBFM	f_c ‡	N/A	N/A
WBFM	N/A	N/A	N/A
MASK	$f_c + n \times R_s$	$2f_c + n \times R_s$ ¶	$n \times R_s$, $n \neq 0$ †
MPAM, PSK2	N/A	$2f_c + n \times R_s$ ¶	$n \times R_s$, $n \neq 0$ †
MPSK ($M \geq 4$), QAM	N/A	N/A	$n \times R_s$, $n \neq 0$ †
MFSK	$f_c + 0.5 \times (2m-1-M) \times f_d$, $m=1, \ldots, M$	$2f_c + (2m-1-M) \times f_d$, $m=1, \ldots, M$	N/A
CPM: h = integer	Multiple cycle frequencies #	Multiple cycle frequencies #	N/A
CPM: $h = 0.5 \times$ odd	N/A	Multiple cycle frequencies #	N/A

‡ The presence of this cycle frequency depends on the ratio of the peak frequency deviation to the modulating signal's bandwidth. If this ratio is very small and the SNR is high, f_c may be recognized as a cycle frequency of the first-order cyclic moment.

¶ The presence of these cycle frequencies and their strengths of the cyclic moment for $n \neq 0$ are heavily dependent on the pulse-shaping function g(t) and are generally much weaker than that for $n = 0$.

† The presence of the cycle frequencies and their strengths of the cyclic moment for $n \neq 0$ are heavily dependent on the pulse-shaping function g(t) and are generally much weaker than that for $n > 1$.

See the analysis above this table for details.

6.4 Examination of the Presence of Cyclostationarity

As seen in Table 6.1, the concerned modulation types have different patterns of cyclostationarities for the selected cyclic moments. This can be employed to classify a received communication signal. Then it is necessary to estimate these cyclic statistics and then test if they have cycle frequencies or not and how many cycle frequencies they have.

The cyclic moment $M_{ky}^{\alpha}(\boldsymbol{\tau})$ can be estimated by [138]

$$\hat{M}_{ky}^{\alpha}(\boldsymbol{\tau}) = \frac{1}{N}\sum_{n=0}^{N-1} f_{ky}(n;\boldsymbol{\tau})e^{-j2\pi\alpha n} = \frac{1}{N}\sum_{n=0}^{N-1} y(n)y(n+\tau_1)\cdots y(n+\tau_{k-1})e^{-j2\pi\alpha n} \quad (6.79)$$

This has been shown to be a mean-square sense (m.s.s.) consistent estimator [136], i.e.,

$$\lim_{N\to\infty} \hat{M}_{ky}^{\alpha}(\boldsymbol{\tau}) \overset{m.s.s.}{=} M_{ky}^{\alpha}(\boldsymbol{\tau}) \quad (6.80)$$

In addition, $\sqrt{N}\left(\hat{M}_{ky}^{\alpha}(\boldsymbol{\tau}) - M_{ky}^{\alpha}(\boldsymbol{\tau})\right)$ is asymptotically complex normal with covariances given by

$$\lim_{N\to\infty} N\operatorname{cov}\left\{\hat{M}_{ky}^{\alpha}(\boldsymbol{\tau}), \hat{M}_{ky}^{\beta}(\boldsymbol{\rho})\right\} = S_{2f_{\tau,\rho}}(\alpha+\beta;\beta) \quad (6.81)$$

$$\lim_{N\to\infty} N\operatorname{cov}\left\{\hat{M}_{ky}^{\alpha}(\boldsymbol{\tau}), \hat{M}_{ky}^{*\beta}(\boldsymbol{\rho})\right\} = S_{2f_{\tau,\rho}}^{(*)}(\alpha-\beta;-\beta) \quad (6.82)$$

where $S_{2f_{\tau,\rho}}(\alpha;\beta)$ and $S_{2f_{\tau,\rho}}^{(*)}(\alpha;\beta)$ are respectively the unconjugate and conjugate cyclic spectra of $f_{ky}(n;\boldsymbol{\tau})$, and are respectively defined as [138]

$$S_{2f_{\tau,\rho}}(\alpha;\beta) \overset{\Delta}{=} \lim_{N\to\infty}\frac{1}{N}\sum_{n=0}^{N-1}\sum_{\varsigma=-\infty}^{\infty}\operatorname{cov}\left\{f_{ky}(n;\boldsymbol{\tau}), f_{ky}(n+\varsigma;\boldsymbol{\rho})\right\}e^{-j\varsigma\beta}e^{-j\alpha n} \quad (6.83)$$

$$S_{2f_{\tau,\rho}}^{(*)}(\alpha;\beta) \overset{\Delta}{=} \lim_{N\to\infty}\frac{1}{N}\sum_{n=0}^{N-1}\sum_{\varsigma=-\infty}^{\infty}\operatorname{cov}\left\{f_{ky}(n;\boldsymbol{\tau}), f_{ky}^{*}(n+\varsigma;\boldsymbol{\rho})\right\}e^{-j\varsigma\beta}e^{-j\alpha n} \quad (6.84)$$

After the cyclic moments $\{M_{ky}^{\alpha}(\boldsymbol{\tau})\}$ have been estimated by using (6.79), the cyclic cumulants $\{C_{ky}^{\alpha}(\boldsymbol{\tau})\}$ can be estimated by substituting $\hat{M}_{ky}^{\alpha}(\boldsymbol{\tau})$ into (6.22).

Note that $C_{2y}^{\alpha}(\tau)$ is equal to $M_{2y}^{\alpha}(\tau)$ for zero-mean process, then $\hat{C}_{2y}^{\alpha}(\tau)$ is equal to $\hat{M}_{2y}^{\alpha}(\tau)$ and it thus will also have the above asymptotic properties. A technique has been developed in [138] for detecting the presence of cyclostationarity as follows. Let $\tau_1,\cdots,\tau_\Upsilon$ be a fixed set of lags, α be a candidate cycle frequency of $C_{2y}^{\alpha}(\tau)$, and

$$\hat{C}_{2x}=\left[\mathrm{Re}\left(\hat{C}_{2y}^{\alpha}(\tau_1)\right),\cdots\mathrm{Re}\left(\hat{C}_{2y}^{\alpha}(\tau_\Upsilon)\right),\mathrm{Im}\left(\hat{C}_{2y}^{\alpha}(\tau_1)\right),\cdots\mathrm{Im}\left(\hat{C}_{2y}^{\alpha}(\tau_\Upsilon)\right)\right] \tag{6.85}$$

represents a $1\times 2\Upsilon$ row vector of the estimated second-order cyclic cumulants with $\mathrm{Re}(\bullet)$ and $\mathrm{Im}(\bullet)$ representing the real and imaginary parts, respectively. In order to construct the asymptotic covariance matrix of $\hat{C}_{2y}$, two $\Upsilon-by-\Upsilon$ matrices Q_{2c} and Q_{2c}^{*} are constructed with the (m,n)-*th* entries given, respectively, as

$$Q_{2c}(m,n)=S_{2f_{\tau_m,\tau_n}}(2\alpha;\alpha) \tag{6.86}$$

$$Q_{2c}^{*}(m,n)=S_{2f_{\tau_m,\tau_n}}^{(*)}(0;-\alpha) \tag{6.87}$$

where $S_{2f_{\tau_m,\tau_n}}(2\alpha;\alpha)$ and $S_{2f_{\tau_m,\tau_n}}(0;-\alpha)$ are estimated respectively by

$$\hat{S}_{2f_{\tau_m,\tau_n}}(2\alpha;\alpha)=\frac{1}{NL}\sum_{v=-(L-1)/2}^{(L-1)/2}W^{(N)}(v)\times F_{N,\tau_n}\left(\alpha-\frac{2\pi v}{N}\right)\times F_{N,\tau_m}\left(\alpha+\frac{2\pi v}{N}\right) \tag{6.88}$$

$$\hat{S}_{2f_{\tau_m,\tau_n}}^{(*)}(0;-\alpha)=\frac{1}{NL}\sum_{v=-(L-1)/2}^{(L-1)/2}W^{(N)}(v)\times F_{N,\tau_n}^{*}\left(\alpha-\frac{2\pi v}{N}\right)\times F_{N,\tau_m}\left(\alpha+\frac{2\pi v}{N}\right) \tag{6.89}$$

where $F_{N,\tau}(\omega)$ is defined as $F_{N,\tau}(\omega)=\sum_{n=0}^{N-1} f_{2y}(n;\boldsymbol{\tau})e^{-j2\pi\omega n}$ with $\boldsymbol{\tau}=[0,\tau]$, and $W^{(N)}$ is a spectral window length L (odd). Then based on (6.81) and (6.82), the covariance matrix of $\hat{C}_{2y}$ can be computed as

$$\sum_{2c}=\begin{Bmatrix} \mathrm{Re}\left\{\dfrac{Q_{2c}+Q_{2c}^{(*)}}{2}\right\} & \mathrm{Im}\left\{\dfrac{Q_{2c}-Q_{2c}^{(*)}}{2}\right\} \\ \mathrm{Im}\left\{\dfrac{Q_{2c}+Q_{2c}^{(*)}}{2}\right\} & \mathrm{Re}\left\{\dfrac{Q_{2c}^{(*)}-Q_{2c}}{2}\right\} \end{Bmatrix} \tag{6.90}$$

Then the test statistics will be

$$T_{2c}\overset{\Delta}{=}N\hat{C}_{2y}\sum_{2c}^{-1}\hat{C}_{2y}^{'} \tag{6.91}$$

The asymptotic distribution of T_{2c} has been shown to be central chi-square distribution with 2Υ degrees of freedom if the frequency α is not a cycle frequency [138]. Therefore, a threshold can be selected according to chi-square tables and the required false alarm rate. The frequency α is declared as a cycle frequency if T_{2c} exceeds the threshold for at least one set of $\tau_1,\cdots,\tau_\Upsilon$; otherwise, α is determined as not being a cycle frequency for any of $\tau_1,\cdots,\tau_\Upsilon$.

The above scheme can be formally described by Table 6.2. The selected cyclic moments M_{1y}^{α}, $M_{2,0y}^{\alpha}$ and $M_{2,1y}^{\alpha}$ for the proposed classifier are special cases of $M_{ky}^{\alpha}(n;\boldsymbol{\tau})$, thus they can be estimated by replacing $f_{ky}(n;\boldsymbol{\tau})$ in (6.79) with $y(n)$, $y^2(n)$ and $|y(n)|^2$, respectively. Also, $\hat{M}_{1y}^{\alpha}$, $\hat{M}_{2,0y}^{\alpha}$ and $\hat{M}_{2,1y}^{\alpha}$ will be asymptotically normal as described by (6.81) through (6.84). Then a scheme similar to that of Table 6.2 can be used to check whether a given frequency α is a cycle frequency of M_{1y}^{α} (or that of $M_{2,0y}^{\alpha}$ or $M_{2,1y}^{\alpha}$). In determining the presence of cyclostationarity of an input signal, however, the scheme in

Table 6.2 has to exhaustively search over all possible values of α. The computational burden of this doing will be extremely heavy even though only one distinct lag (i.e., $\Upsilon = 1$) is used. In the rest of this section, schemes with dramatically reduced computational complexity are proposed to detect the cycle frequencies (if they do exist) of M_{1y}^{α}, $M_{2,0y}^{\alpha}$ and $M_{2,1y}^{\alpha}$.

Table 6.2 Test of the Presence of Cyclostationarity

Step 1	For a given false alarm rate P_{FA}, lookup the chi-square tables to find the threshold μ that makes the tail probability of chi-square distribution with 2Υ degrees of freedom equal to P_{FA}.
Step 2	Calculate $\hat{C}_{2y}^{\alpha}(\tau_i)$ for $i = 1, 2, \cdots, \Upsilon$ and then form the vector $\hat{C}_{2y} = \left[\mathrm{Re}\left(\hat{C}_{2y}^{\alpha}(\tau_1)\right), \cdots \mathrm{Re}\left(\hat{C}_{2y}^{\alpha}(\tau_\Upsilon)\right), \mathrm{Im}\left(\hat{C}_{2y}^{\alpha}(\tau_1)\right), \cdots \mathrm{Im}\left(\hat{C}_{2y}^{\alpha}(\tau_\Upsilon)\right)\right]$.
Step 3	Fill in the entries of the covariance matrix $\sum_{2c}$ by using (6.86) through (6.90).
Step 4	Compute the value of the test statistics as $T_{2c} \overset{\Delta}{=} N\hat{C}_{2y} \sum_{2c}^{-1} \hat{C}_{2y}^{'}$
Step 5	If $T_{2c} \geq \mu$, declare α as a cycle frequency at least for one of $\tau_1, \cdots, \tau_\Upsilon$; else, decide that α is not a cycle frequency of $C_{2y}^{\alpha}(\tau)$ for any of $\tau_1, \cdots, \tau_\Upsilon$.

6.4.1 Cycle Frequency Detection and Signal Classification Based on M_{1y}^{α}

The discussion on M_{1y}^{α} in Section 6.3 is briefly reviewed as follows. The cyclic moment M_{1y}^{α} has multiple cycle frequencies for MFSK and CPM with integer h, one cycle frequency for AM, and no cycle frequency for DSB, LSB, USB, WBFM, MPAM, MPSK and QAM. It may or may not have cycle frequency for NBFM — if it does have, the only cycle frequency will be f_c. As to MASK, a cycle frequency at f_c will definitely exist,

while frequencies $f_c + lR_s$ with nonzero integer values of l may also be cycle frequencies for M_{1y}^{α}.

According to its definition, the cyclic moment M_{ky}^{α} will be nonzero for α equal to its cycle frequencies, may be nonzero for $\alpha = 0$, and be zero for α equal to any other real values. This means that a cycle frequency of M_{ky}^{α} should at least correspond to a local peak of $\left|\hat{M}_{ky}^{\alpha}\right|$, where $\hat{M}_{ky}^{\alpha}$ is the estimate of M_{ky}^{α}. This further implies that, when searching the cycle frequencies of M_{ky}^{α} by using $\hat{M}_{ky}^{\alpha}$, one only needs to examine those frequencies whose associated values of $\left|\hat{M}_{ky}^{\alpha}\right|$ are local peaks of $\left|\hat{M}_{ky}^{\alpha}\right|$. As a result, the computational burden will be reduced by at least fifty percents. The general discussion here is certainly applicable to M_{1y}^{α}, $M_{2,0y}^{\alpha}$ and $M_{2,1y}^{\alpha}$.

Furthermore, by careful examination of the cyclic moment M_{1y}^{α} derived in Section 6.3 for each concerned modulation type, it can be concluded that the global maximum of $\left|M_{1y}^{\alpha}\right|$ would correspond to a cycle frequency if M_{1y}^{α} does have one or more cycle frequencies — the zero frequency should not be included in the range for searching the global maximum of $\left|M_{1y}^{\alpha}\right|$. This in turn means that, if the global maximum of $\left|\hat{M}_{1y}^{\alpha}\right|$ is not a cycle frequency, one can claim that the input signal does not have cycle frequency for M_{1y}^{α} and thus no further examination is needed. To reduce the computational complexity, the examination of the global maximum of $\left|\hat{M}_{1y}^{\alpha}\right|$ should be done in the very first step. The cyclic moment $M_{2,0y}^{\alpha}$ is found having the same property for the concerned modulation types.

If the global maximum of $\left|\hat{M}_{1y}^{\alpha}\right|$ is determined as corresponding to a cycle frequency, then it is necessary to further examine whether M_{1y}^{α} has more cycle frequencies or not. For the purpose of signal classification, it is expected the classifier will claim the following results about the cycle frequencies of M_{1y}^{α} : multiple cycle frequencies for CPM with integer h and MFSK, only one cycle frequency for AM and MASK, no or only one cycle frequency for NBFM, and no cycle frequency for the other modulations. The result for NBFM is ambiguous here, but this ambiguity will be removed by further classification as shown in Section 6.6. Then the key issue here is the number of cycle frequencies of M_{1y}^{α} for MASK. If M_{1y}^{α} does have cycle frequencies other than f_c (i.e., cycle frequencies $f_c + lR_s$ with integer $l \neq 0$) for an MASK signal and all or some of these extra cycle frequencies have been detected by the classifier, then it is impossible to discriminate between this MASK signal and MFSK signals (or CPM signals with integer h) based on M_{1y}^{α}. Fortunately, if the pulse $g(t)$ is a rectangular pulse of duration T, a raised-cosine function or a square-root raised-cosine function, frequencies $f_c + lR_s$ with $l \neq 0$ will not be the cycle frequencies of M_{1y}^{α}. Furthermore, even if some frequencies $f_c + lR_s$ with $l \neq 0$ are the cycle frequencies of M_{1y}^{α} when an MASK signal employs a pulse-shaping function $g(t)$ of other forms, the magnitudes of the cyclic moment M_{1y}^{α} at such cycle frequencies will be weaker than that at the cycle frequency f_c — this has been discussed in Section 6.3. All these suggest a way to reject possibly extra cycle frequencies of M_{1y}^{α} for MASK. That is, when the global maximum

of $\left|\hat{M}_{1y}^{\alpha}\right|$ is determined as corresponding to a cycle frequency of M_{1y}^{α}, the classifier will not examine all the other frequencies. Instead, only those frequencies whose corresponding magnitudes of $\hat{M}_{1y}^{\alpha}$ are greater than or equal to $\mu_1 \times \left|\hat{M}_{1y}^{\alpha}\right|_{\max}$ will be examined, where μ_1 is a preset positive constant satisfying $0 < \mu_1 < 1$, and $\left|\hat{M}_{1y}^{\alpha}\right|_{\max}$ is the global maximum of $\left|\hat{M}_{1y}^{\alpha}\right|$ — again, the search of $\left|\hat{M}_{1y}^{\alpha}\right|_{\max}$ and cycle frequencies does not include zero frequency. In obtaining all the results reported in Section 6.7, the parameter μ_1 is chosen as 0.5.

The above method implies that a frequency will not be considered as a candidate cycle frequency of M_{1y}^{α} if its corresponding magnitude of $\hat{M}_{1y}^{\alpha}$ is less than $\mu_1 \times \left|\hat{M}_{1y}^{\alpha}\right|_{\max}$. This doing has been shown to be able to effectively reject the possibly extra cycle frequencies of M_{1y}^{α} for MASK. Since the magnitudes of M_{1y}^{α} corresponding to the cycle frequencies are equal to each other for an MFSK signal, the above select-by-threshold method theoretically will not affect the recognition of the cycle frequencies for MFSK. It is found through simulations that the select-by-threshold almost does not influence the detection of the cycle frequencies for CPM signals.

Based on all the above analysis, a scheme as shown in Table 6.3 is formed for detecting the cycle frequencies of M_{1y}^{α} and classifying modulation types accordingly.

In Step-9 of Table 6.3, if the input is determined as having multiple cycle frequencies, the MFSK classification rules as developed in Chapter 5 will be employed to refine the obtained cycle frequencies, including estimating the frequency deviation and

interpolating some undetected cycle frequencies. For the simplicity, the details of these will not be repeated here.

Table 6.3 Cycle Frequency Detection and Signal Classification Based on M_{1y}^{α}

Step 1	For a given false alarm rate P_{FA}, lookup the chi-square tables to find the threshold μ that makes the tail probability of chi-square distribution with two-degree freedom equal to P_{FA}; select the window function $W^{(N)}(\omega)$ with odd length L for estimating $S_{2f_{\tau_m,\tau_n}}(\alpha;\omega)$; set $\mu_1 = 0.5$.
Step 2	Estimate M_{1y}^{α} by using DFT: $\hat{M}_{1y}^{\alpha} = \frac{1}{N}\sum_{n=0}^{N-1} y(n)e^{-j2\pi\alpha n}$.
Step 3	Compute the vector $F_{N,\tau}(\alpha)$: $F_{N,\tau}(\alpha) = \sum_{n=0}^{N-1} y(n)e^{-j2\pi\alpha n} = N \times \hat{M}_{1y}^{\alpha}$, where $\tau = 0$.
Step 4	Find the global maximum of $\lvert\hat{M}_{1y}^{\alpha}\rvert$ and denoted it by $A_{\max}$ — the zero frequency should be excluded in searching $A_{\max}$; denote the DFT frequency corresponding to $A_{\max}$ by $\alpha_{\max}$.
Step 5	Let $\alpha = \alpha_{\max}$, and check if the current value of α is a cycle frequency of M_{1y}^{α}: (a) form the vector $\hat{M}_{1y} = \left[\mathrm{Re}\{\hat{M}_{1y}^{\alpha}\}, \mathrm{Im}\{\hat{M}_{1y}^{\alpha}\}\right]$; (b) compute $\hat{S}_{2f_{\tau_m,\tau_n}}(2\alpha;\alpha)$ and $\hat{S}^{(*)}_{2f_{\tau_n,\tau_m}}(0;-\alpha)$ according to (6.88) and (6.89), where $\tau_1 = \tau_2 = 0$, $m \in \{1,2\}$, and $n \in \{1,2\}$; (c) form the two-by-two covariance matrix $\sum_{2c}$ by using (6.86), (6.87) and (6.90); (d) compute the decision statistics as $T_{1m} \overset{\Delta}{=} N\hat{M}_{1y}\sum_{2c}^{-1}\hat{M}_{1y}^{'}$; (e) if $T_{1m} > \mu$, declare the current value of α is a cycle frequency of M_{1y}^{α}; else, declare it is not a cycle frequency.
Step 6	If $\alpha_{\max}$ is determined as not being a cycle frequency, declare the input belongs to the set {DSB, SSB, NBFM, WBFM, MPAM, MPSK, QAM, CPM with $h \neq$ integer}, and then the scheme stops; else, set variable $\alpha = 0$ and variable $CNT = 0$, then go to next step.
Step 7	Increase the value of α by one unit. If the new value of α is greater than or equal to one half of the sampling rate, go to Step-9; else, go to next step.
Step 8	If $\lvert\hat{M}_{1y}^{\alpha}\rvert < \mu_1 A_{\max}$ or $\lvert\hat{M}_{1y}^{\alpha}\rvert$ is not a local peak, go to Step-7; else, follow the same procedure of Step-5 to check if the current value of α is a cycle frequency of M_{1y}^{α} or not — if it is, increase the variable CNT by one — then go to Step-7.
Step 9	If CNT equals to one, declare the input belongs to the set {AM, MASK, NBFM}; else, declare the input belongs to the set {MFSK, CPM with $h =$ integer} and take CNT as the estimate of M. Then the scheme stops.

As the result of performing the scheme in Table 6.3, the input will be classified into one of the following sets of modulation types: {AM, MASK, NBFM} — those types claimed as only having one cycle frequency, {DSB, LSB, USB, NBFM, WBFM, MPAM, MPSK, QAM, CPM with non-integer h } — those types not having cycle frequency, and {CPM with integer h, MFSK} — those having multiple cycle frequencies. For CPM with integer h and MFSK, the number of the detected cycle frequencies is taken as the estimate of M, and the most frequently occurring frequency difference between neighboring cycle frequencies is taken as the estimate of f_d.

6.4.2 Cycle Frequency Detection and Signal Classification Based on $M_{2,0y}^{\alpha}$

The discussion on $M_{2,0y}^{\alpha}$ in Section 6.3 is briefly reviewed as follows. The cyclic moment $M_{2,0y}^{\alpha}$ has multiple cycle frequencies for MFSK and CPM with $h = 0.5 \times \text{integer}$, one cycle frequency for AM and DSB, and no cycle frequency for LSB, USB, NBFM, WBFM, QAM and MPSK with $M \geq 4$. As to MASK and MPAM (including PSK2), a cycle frequency at $2f_c$ will definitely exist, while frequencies $2f_c + lR_s$ with integer $l \neq 0$ may also be cycle frequencies of $M_{2,0y}^{\alpha}$.

As discussed in Subsection 6.4.1, it is reasonable to claim that $M_{2,0y}^{\alpha}$ does not have cycle frequency if the global maximum of $\left|\hat{M}_{2,0y}^{\alpha}\right|$ is determined as not being a cycle frequency. Furthermore, a cycle frequency should correspond to a local peak in $\left|\hat{M}_{2,0y}^{\alpha}\right|$. Also, in order not to confuse MASK, PSK2 and MPAM with MFSK and CPM with $h = 0.5 \times \text{integer}$, it is expected that for the former only the cycle frequency at $2f_c$ is

detected. This can be achieved by using the select-by-threshold method introduced in Subsection 6.4.1.

Table 6.4 Cycle Frequency Detection and Signal Classification Based on $M_{2,0y}^{\alpha}$

Step 1	For a given false alarm rate P_{FA}, lookup the chi-square tables to find the threshold μ that makes the tail probability of chi-square distribution with two-degree freedom equal to P_{FA}; select the window function $W^{(N)}(\omega)$ with odd length L for estimating $S_{2f_{\tau_m,\tau_n}}(\alpha;\omega)$; set $\mu_2 = 0.5$.
Step 2	Estimate $M_{2,0y}^{\alpha}$ by using DFT: $\hat{M}_{2,0y}^{\alpha} = \frac{1}{N}\sum_{n=0}^{N-1} y^2(n)e^{-j2\pi\alpha n}$.
Step 3	Calculate the vector $F_{N,\tau}(\alpha)$ as $F_{N,\tau}(\alpha) = \sum_{n=0}^{N-1} y^2(n)e^{-j2\pi\alpha n} = N \times \hat{M}_{2,0y}^{\alpha}$, where $\tau = 0$.
Step 4	Find the global maximum of $\lvert\hat{M}_{2,0y}^{\alpha}\rvert$ and denoted it by $A_{\max}$ — the zero frequency should be excluded in searching $A_{\max}$; denote the DFT frequency corresponding to $A_{\max}$ by $\alpha_{\max}$.
Step 5	Let $\alpha = \alpha_{\max}$, and check if the current value of α is a cycle frequency of $M_{2,0y}^{\alpha}$: (a) form the vector $\hat{M}_{2,0y} = \left[\mathrm{Re}\{\hat{M}_{2,0y}^{\alpha}\}, \mathrm{Im}\{\hat{M}_{2,0y}^{\alpha}\}\right]$; (b) compute $\hat{S}_{2f_{\tau_m,\tau_n}}(2\alpha;\alpha)$ and $\hat{S}_{2f_{\tau_n\tau_m}}^{(*)}(0;-\alpha)$ according to (6.88) and (6.89), where $\tau_1 = \tau_2 = 0$, $m \in \{1,2\}$, and $n \in \{1,2\}$; (c) form the two-by-two covariance matrix $\sum_{2c}$ by using (6.86), (6.87) and (6.90); (d) compute the decision statistics as $T_{2c} \overset{\Delta}{=} N\hat{M}_{2,0y}\sum_{2c}^{-1}\hat{M}_{2,0y}^{'}$; (e) if $T_{2c} > \mu$, declare the current value of α is a cycle frequency of $M_{2,0y}^{\alpha}$; else, declare it is not a cycle frequency.
Step 6	If $\alpha_{\max}$ is determined as not being a cycle frequency, declare the input belongs to the set {SSB, FM, QAM, MPSK with $M \geq 4$}, and then the scheme stops; else, set variable $\alpha = 0$ and variable $CNT = 0$, then go to next step.
Step 7	Increase the value of α by one unit. If the new value of α is greater than or equal to one half of the sampling rate, go to Step-9; else, go to next step.
Step 8	If $\lvert\hat{M}_{2,0x}^{\alpha}\rvert < \mu_2 A_{\max}$ or $\lvert\hat{M}_{2,0y}^{\alpha}\rvert$ is not a local peak, go to Step-7; else, follow the same procedure of Step-5 to check if the current value of α is a cycle frequency of $M_{2,0y}^{\alpha}$ or not — if it is, increase the variable CNT by one — then go to Step-7.
Step 9	If CNT equals to one, declare the input belongs to the set { AM, DSB, MASK, MPAM, PSK2}; else, declare the input belongs to the set {MFSK, CPM with $h = 0.5 \times$ integer} and take CNT as the estimate of M. Then the scheme stops.

A scheme, which is very similar to that in Table 6.3, is formed in Table 6.4 for detecting the cycle frequencies of M_{1y}^{α} and classifying modulation types accordingly.

In Step-9 of Table 6.4, if the input is determined as having multiple cycle frequencies, the MFSK classification rules as developed in Chapter 5 will be employed to refine the obtained cycle frequencies, including estimating the frequency deviation and interpolating some undetected cycle frequencies. For the simplicity, the details of these will not be repeated here.

As the result of performing the scheme in Table 6.4, the input will be classified into one of the following sets of modulation types: {AM, DSB, MASK, MPAM, PSK2} — those types claimed as only having one cycle frequency, {LSB, USB, NBFM, WBFM, QAM, MPSK with $M \geq 4$} — those types not having cycle frequency, and {CPM with $h = 0.5 \times \text{integer}$, MFSK} — those having multiple cycle frequencies. For CPM with $h = 0.5 \times \text{integer}$ and MFSK, the number of the detected cycle frequencies is taken as the estimate of *M*, and one half of the most frequently occurring frequency difference between neighboring cycle frequencies is taken as the estimate of f_d.

6.4.3 Cycle Frequency Detection and Signal Classification Based on $M_{2,1y}^{\alpha}$

The cyclic moment $M_{2,1y}^{\alpha}$ is used to separate linearly modulated digital communication signals from the others. On the one hand, linearly modulated digital communication signals have symbol rate and the symbol rate will be a cycle frequency of $M_{2,1y}^{\alpha}$. Depending on the pulse shaping function $g(t)$, $M_{2,1y}^{\alpha}$ may also have cycle frequencies at integer multiples of the symbol rate. On the other hand, analog communication signals do

not have symbol rate and $M_{2,1y}^{\alpha}$ does not have cycle frequency. Therefore, if $M_{2,1y}^{\alpha}$ has been determined as having one cycle frequency, it can be concluded that the input has symbol rate, i.e., the input should be a digital communication signal. However, the results for MFSK and CPM are ambiguous. As analyzed in Section 6.3, the cyclic moment $M_{2,1y}^{\alpha}$ theoretically will not have cycle frequency for MFSK and CPM. Owing to the channel distortion and/or the BPF used in the preprocessing, however, an MFSK or CPM signal may lose the property of constant envelope. The result is that the symbol rate may be detected as a cycle frequency of $M_{2,1y}^{\alpha}$. That is, an MFSK or CPM signal will be classified as either having symbol rate or not having symbol rate. The ambiguity on MFSK and CPM can be removed by detecting the number of cycle frequencies of M_{1y}^{α} and $M_{2,0y}^{\alpha}$.

Owing to the above analysis and considerations, the aim of this subsection is to design a scheme that is able to correctly detect the presence of the symbol rate of the linearly modulated digital communication signals with reduced computational complexity.

As shown in (6.62), $M_{2,1y}^{\alpha}$ with $\alpha = 0$ will be nonzero for linear digital modulations even though $\alpha = 0$ will never be considered as a cycle frequency in this dissertation. Furthermore, the value of $\left|M_{2,1y}^{\alpha}\right|$ for $\alpha = 0$ is generally greater than that for $\alpha = lR_s$ with $l \neq 0$. That is, the value of $\left|M_{2,1y}^{\alpha}\right|$ for $\alpha = R_s$ is generally not the global maximum of $\left|M_{2,1y}^{\alpha}\right|$. Therefore, one cannot claim whether $M_{2,1y}^{\alpha}$ has cycle frequency or not (equivalently, has symbol rate or not) by simply examining the frequency corresponding to the global maximum of $\left|\hat{M}_{2,1y}^{\alpha}\right|$, as in the cases of M_{1y}^{α} and $M_{2,0y}^{\alpha}$.

Nevertheless, there are stills some other properties that can be used to reduce the computational complexity.

Table 6.5 Symbol Rate Detection and Signal Classification Based on $M_{2,1y}^{\alpha}$

Step 0	Estimate the input signal's bandwidth and denote it by $\hat{B}$ — this is done in preprocessing.
Step 1	For a given false alarm rate P_{FA}, lookup the chi-square tables to find the threshold μ that makes the tail probability of chi-square distribution with two-degree freedom equal to P_{FA}; select the window function $W^{(N)}(\omega)$ with odd length L for estimating $S_{2f_{\tau_m,\tau_n}}(\alpha;\omega)$; set $\lambda_1 = 0.5$ and $\lambda_2 = 2.0$.
Step 2	Estimate $M_{2,1y}^{\alpha}$ by using DFT: $\hat{M}_{2,1y}^{\alpha} = \frac{1}{N}\sum_{n=0}^{N-1}\lvert y(n)\rvert^2 e^{-j2\pi\alpha n}$.
Step 3	Calculate the vector $F_{N,\tau}(\alpha)$ as $F_{N,\tau}(\alpha) = \sum_{n=0}^{N-1}\lvert y(n)\rvert^2 e^{-j2\pi\alpha n} = N \times \hat{M}_{2,1y}^{\alpha}$, where $\tau = 0$.
Step 4	Let $\alpha = \min(\lambda_2\hat{B}, f_s/2)$.
Step 5	Decrease α by one DFT frequency unit. If the new value of α is less than $\lambda_1\hat{B}$, declare that symbol rate has not been detected, i.e., the input signal will belong to the set {AM, DSB, SSB, FM, MFSK, CPM}, then the scheme stops; else, go to next step.
Step 6	If $\lvert\hat{M}_{2,1y}^{\alpha}\rvert$ for the current value of α is not a local peak, go to Step-5; else, go to next step.
Step 7	Check if the current value of α is a cycle frequency of $M_{2,1y}^{\alpha}$: (a) form the vector $\hat{M}_{2,1y} = \left[\mathrm{Re}\{\hat{M}_{2,1y}^{\alpha}\}, \mathrm{Im}\{\hat{M}_{2,1y}^{\alpha}\}\right]$; (b) compute $\hat{S}_{2f_{\tau_m,\tau_n}}(2\alpha;\alpha)$ and $\hat{S}^{(*)}_{2f_{\tau_n,\tau_m}}(0;-\alpha)$ according to (6.88) and (6.89), where $\tau_1 = \tau_2 = 0$, $m \in \{1,2\}$, and $n \in \{1,2\}$; (c) form the two-by-two covariance matrix $\sum_{2c}$ by using (6.86), (6.87) and (6.90); (d) compute the decision statistics as $T_{2c} \overset{\Delta}{=} N\hat{M}_{2,1y}\sum_{2c}^{-1}\hat{M}_{2,1y}^{'}$; (e) if $T_{2c} > \mu$, declare the current value of α is a cycle frequency of $M_{2,1y}^{\alpha}$; else, declare it is not a cycle frequency.
Step 8	If the value of α is determined as a cycle frequency, declare the input belongs to the set {MASK, MPAM, MPSK, QAM, MFSK, CPM}, and then the scheme stops; else, repeat from Step-5.

As analyzed in Section 6.3, if the input is a linearly modulated communication signal, the symbol rate will be a cycle frequency of $M_{2,1y}^{\alpha}$ and will at least correspond to a local peak of $\left|\hat{M}_{2,1y}^{\alpha}\right|$. This can be used to reduce the computational complexity by at least fifty percents. Furthermore, it can be observed from (6.62) that the value of $\left|M_{2,1y}^{\alpha}\right|$ for $\alpha = R_s$ will be greater than that for $\alpha = lR_s$ with $l > 1$. This implies that the value of $\left|\hat{M}_{2,1y}^{\alpha}\right|$ for $\alpha = R_s$ is expected to be greater than that for $R_s < \alpha < f_s/2$.Then similar to the case of estimating the symbol rate by using fourth-order cyclic moment in Chapter 4, the symbol rate detection can be done by sequential search.

Since the input $\{y(n)\}$ is assumed being oversampled, the symbol rate search range will be $(0, f_s/2)$, where f_s is the sampling rate. In fact, the search range can be further narrowed based on the estimated frequency range of the received signal. For linearly modulated digital communication signals, the effective bandwidth of the transmitted signal is generally in the range $(R_s, 2R_s)$. Assuming that the effective bandwidth of the input signal has been estimated and denoted by $\hat{B}$ in preprocessing, $\hat{B}$ will be approximately within the range from R_s to $2R_s$ if the SNR is not too low. Then the symbol rate search range can be narrowed to $\left[\lambda_1\hat{B},\ \min\left(\lambda_2\hat{B}, f_s/2\right)\right]$, where λ_1 is a preset positive constant that is less than or equal to 0.5, and λ_2 is a preset positive constant that is greater than one. The narrowed search range also helps in rejecting the possible cycle frequencies whose values are lR_s with integer $l > 1$. In all the experiments reported in Section 6.7, λ_1 is chosen as 0.5, and λ_2 is chosen as 2.0. The estimation of the input

in Section 6.7, λ_1 is chosen as 0.5, and λ_2 is chosen as 2.0. The estimation of the input signal's bandwidth, i.e., the determination of $\hat{B}$, can be carried out by any existing approaches such as [142] and [143]. Since the bandwidth estimation is beyond the subjects of this dissertation, it will not be further discussed.

The above discussions lead to the scheme as shown in Table 6.5. As the result of performing the scheme in Table 6.5, the input will be classified into one of the following sets of modulation types: {AM, DSB, LSB, USB, FM, MFSK, CPM} — those types claimed as not having cycle frequency (i.e., no symbol rate can be found), {MASK, MPAM, MPSK, QAM, MFSK, CPM} — those types with a cycle frequency being detected. For the latter set, the detected cycle frequency is taken as the estimate of the symbol rate.

6.5 Other Features for Signal Classification

In modulation classification, the proposed algorithm will examine the pattern of the cyclostationarity of the input signal via M_{1y}^{α}, $M_{2,0y}^{\alpha}$ and $M_{2,1y}^{\alpha}$. In addition, the proposed classifier also employs five extra features, i.e., $P_{y,norm}$, $P_{y2,norm}$, P_L, P_M and P_R.

In most cases, AM and DSB can be separated from each other based on M_{1y}^{α} since the cycle frequency set of M_{1y}^{α} is $\Omega_1 = \{f_c\}$ for AM and is $\Omega_1 = \varnothing$ for DSB. Occasionally, the scheme in Table 6.3 will claim M_{1y}^{α} has one cycle frequency for an input DSB signal. Then this DSB signal will be incorrectly recognized as AM since the patterns of the cycle frequencies of $M_{2,0y}^{\alpha}$ and $M_{2,1y}^{\alpha}$ are the same for both AM and DSB. The features $P_{y,norm}$ and $P_{y2,norm}$ are designed to handle such cases. In the proposed

That is, these two features will not be used if the discrimination between AM and DSB can be achieved based on the selected cyclic moments.

The feature $P_{y,norm}$ is defined and extracted as follows. At first, the PSD $S_y(f)$ of the input signal $\{y(n)\}$ is estimated by using average periodogram method ([131] and [132]) as

$$\hat{S}_y(f)=\frac{1}{K}\sum_{k=0}^{K-1}\left\{\frac{1}{N_{seg}}\left|\sum_{n=0}^{N_{seg}-1}y(n+kN_{seg})e^{j\frac{2\pi}{N_{seg}}fn}\right|^2\right\},\ \text{for}\ f=0,1,\cdots,N_{seg}-1 \quad (6.92)$$

where K is the number of segments, N_{seg} is the number of samples in each segment, the product of K and N_{seg} is the largest number that is less than N, and N is the total number of available samples. Then the estimated PSD is normalized as

$$\hat{S}_{y,norm}(f)\overset{\Delta}{=}\frac{\hat{S}_{y,norm}(f)}{\max\left(\hat{S}_{y,norm}(f)\right)} \quad (6.93)$$

Finally, the feature $P_{y,norm}$ is defined as

$$P_{y,norm}\overset{\Delta}{=}\sum_{f=0}^{N_{seg}-1}\hat{S}_{y,norm}(f) \quad (6.94)$$

The feature $P_{y2,norm}$ is defined in the same way, except that $y(n+kN_{seg})$ will be replaced with $y^2(n+kN_{seg})$ in (6.92). As shown in Appendix B, the value of $P_{y2,norm}$ will be greater than that of $P_{y,norm}$ if the input is a noiseless AM signal. It is found via simulations that, even when the input AM signal is noisy, this relationship still holds as long as the SNR is not too low. For a received DSB signal, the PSD $S_y(f)$ of $\{y(t)\}$ and the PSD $S_{y2}(f)$ of $\{y^2(t)\}$ can be respectively derived as

not too low. For a received DSB signal, the PSD $S_y(f)$ of $\{y(t)\}$ and the PSD $S_{y2}(f)$ of $\{y^2(t)\}$ can be respectively derived as

$$S_y(f) = A^2 S_s(f - f_c) + \sigma_w^2 \tag{6.95}$$

$$S_{y2}(f) = A^4 (\bar{m}_{s2})^2 \delta(f - 2f_c) + A^4 S_\zeta(f - 2f_c) + 4A^2\sigma_w^2 \bar{m}_{s2} + 2\sigma_w^4 \tag{6.96}$$

where $S_s(f)$ stands for the PSD of $s(t)$, $\bar{m}_{s2} = E\left[s^2(t)\right]$, and $S_\zeta(f)$ stands for the PSD of $\xi(t) \overset{\Delta}{=} s^2(t) - \bar{m}_{s2}$. It is evident that $S_{y2}(f)$ will have a spectral impulse. Here a weak assumption is imposed on the PSD of $s(t)$, i.e., $S_s(f)$ does not contain spectral impulse. Then if $S_y(f)$ and $S_{y2}(f)$ are respectively normalized w.r.t. their own global maximum, the area under the former will be greater than that of the latter. That is, the value of $P_{y,norm}$ will be greater than that of $P_{y2,norm}$ for DSB. Simulation results have shown that the assumption on the PSD of $s(t)$ is appropriate. Then if the modulation type of the input has been narrowed into the set of {AM, DSB}, it can be further recognized by comparing the extracted values of $P_{y,norm}$ and $P_{y2,norm}$ from this input.

For an input signal, the features P_L, P_M and P_R are defined and measured as follows. At first, the PSD of the received signal $\{y(n)\}$ is estimated by using (6.92) and denoted by $\hat{S}_y(f)$. Secondly, the input signal's bandwidth is estimated using any existing method (e.g., [142] and [143]) and denoted by $\hat{B}$. Thirdly, three functions $\Delta_L(f)$, $\Delta_M(f)$ and $\Delta_R(f)$ are established, which are respectively defined as

$$\Delta_L(f) \overset{\Delta}{=} \begin{cases} \frac{f}{\hat{B}}, & \text{for} \quad 0 \le f \le \hat{B} \\ 0, & \text{otherwise} \end{cases} \tag{6.97}$$

$$\Delta_M(f) \overset{\Delta}{=} \begin{cases} \frac{2f}{\hat{B}}, & \text{for } 0 \le f \le \frac{\hat{B}}{2} \\ -\frac{2f}{\hat{B}}+2, & \text{for } \frac{\hat{B}}{2} \le f \le \hat{B} \\ 0, & \text{otherwise} \end{cases} \tag{6.98}$$

$$\Delta_R(f) \overset{\Delta}{=} \begin{cases} -\frac{f}{\hat{B}_L}+1, & \text{for } \quad 0 \le f \le \hat{B} \\ 0, & \text{otherwise} \end{cases} \tag{6.99}$$

Finally, the features are obtained by

$$P_L = \max_{v \in (0, f_s/2)} \left(xcorr\left(\Delta_L(f-v), \hat{S}_y(f) \right) \right) \tag{6.100}$$

$$P_M = \max_{v \in (0, f_s/2)} \left(xcorr\left(\Delta_M(f-v), \hat{S}_y(f) \right) \right) \tag{6.101}$$

$$P_R = \max_{v \in (0, f_s/2)} \left(xcorr\left(\Delta_R(f-v), \hat{S}_y(f) \right) \right) \tag{6.102}$$

where $xcorr\left(a(f-v), b(f)\right)$ stands for the cross-correlation between $a(f)$ and $b(f)$ with delay being v.

The three triangles $\Delta_L(f)$, $\Delta_R(f)$ and $\Delta_M(f)$ are used to mimic the PSDs of LSB signals, USB signals and non-SSB signals (not including MFSK and CPM), respectively. For AM, DSB, FM and linear digital modulations, the PSD of the transmitted signal is symmetric with respect to the carrier frequency, and the shape of the PSD is more like the shape of $\Delta_M(f)$. Therefore, the value of P_M will be greater than that of P_L and P_R for a linearly modulated digital communication signal. For LSB, the PSD of the transmitted signal is not symmetric with respect to the carrier frequency, and its shape is more like that of $\Delta_L(f)$, resulting in that P_L will be the largest one. Similarly, $\Delta_R(f)$ will be the largest for USB. Therefore, the features P_L, P_M and P_R together reflect which class the received signal's PSD is more like.

However, the features P_L, P_M and P_R are not used to mimic the PSDs of MFSK and CPM. On the one hand, MFSK and the concerned CPM types can be recognized by detecting the number of cycle frequencies of M_{1y}^{α} or $M_{2,0y}^{\alpha}$. On the other hand, it cannot be predicted which one will be the largest among P_L, P_M and P_R. This is explained by using binary FSK (i.e., FSK2). For FSK2, its PSD will be symmetric with respect to the carrier frequency. If the frequency deviation ratio (i.e., f_d / R_s) is small, the shape of the PSD will be more like that of $\Delta_M(f)$, and thus P_M will be the largest one. When the frequency deviation ratio is very large, however, the PSD of FSK2 will have a deep valley centered at the carrier frequency. Then the largest one will not be P_M . That is, the classification result based on P_L, P_M and P_R is ambiguous for FSK2. Owing to the above, these three features are not used to recognize MFSK and CPM.

In the proposed algorithm as shown in Section 6.6, the features P_L, P_M and P_R are only used to discriminate among LSB, USB and FM.

The advantage of the above features is that one does not need to select decision thresholds for them. Instead, the decision is made by checking which one is larger (for $P_{y,norm}$ and $P_{y2,norm}$) or largest (for P_L , P_M and P_R). Moreover, unlike [12], the discrimination among LSB, USB and non-SSB does require knowing or estimating the carrier frequency.

6.6 The Proposed Classification Algorithm

By detecting the patterns of the cycle frequencies of the selected cyclic moments M_{1y}^{α}, $M_{2,0y}^{\alpha}$ and $M_{2,1y}^{\alpha}$ as well as applying the features developed in Section 6.5, the modulation type of an input signal can be hierarchically classified as follows.

Discrimination between analog modulations and digital modulations At the very beginning, the modulation type of the input signal may be any one in the set $\Xi = \{\text{AM, DSB, LSB, USB, FM, MASK, MPSK, QAM, MFSK, CPM}\}$. In the set Ξ, the analog communication signals do not have symbol rate, while the digital communication signals do have symbol rate. By detecting the existence of the symbol rate, the modulation type of the input signal can be narrowed down to a smaller set. This is done by detecting the existence of the cycle frequency of $M_{2,1y}^{\alpha}$, i.e., performing the scheme formed in Table 6.5 (see Subsection 6.4.3 for details). As the result, the modulation type of the input signal will be classified into either the subset Ξ_1 = {MASK, MPAM, MPSK, QAM, MFSK, CPM} or the subset Ξ_2 = {AM, DSB, LSB, USB, FM, MFSK, CPM}, where the cause of the ambiguity on MFSK and CPM has been discussed in Section 6.3.

Splitting the modulation-type set Ξ_1 This set includes MASK, MPAM, MPSK, QAM, MFSK and CPM, which are declared having symbol rate. The cyclic moment M_{1y}^{α} is employed to further classify these modulation types into several subsets. This task is carried out by using the scheme described in Table 6.3. As mentioned in Subsection 6.4.1, the scheme in Table 6.3 is able to classify the initial set Ξ into the following subsets: {AM, MASK, NBFM}, {DSB, LSB, USB, NBFM, WBFM, MPAM, MPSK,

QAM, CPM with $h \neq$ integer }, and {CPM with $h =$ integer, MFSK}. Then when the input signal belongs to the set $\Xi_1 = \{\text{MASK, MPAM, MPSK, QAM, MFSK, CPM}\}$, the scheme in Table 6.3 will classify its modulation type into to one of the following subsets: $\Xi_{1,1}$ = {MASK}, $\Xi_{1,2}$ = {MFSK, CPM with $h =$ integer }, $\Xi_{1,3}$ = {MPAM, MPSK, QAM, CPM with $h \neq$ integer }. For a modulation type in the subset $\Xi_{1,2}$, the number of modulation levels (i.e., M) and the frequency deviation f_d will also been estimated. For a modulation type in the subset $\Xi_{1,1}$ or $\Xi_{1,2}$, the symbol rate has been estimated in previous level.

Discrimination among modulation-type set $\Xi_{1,3}$ This subset includes MPAM, MPSK, QAM and CPM with $h = 0.5 \times$ odd integer, where the symbol rate has been detected based on $M^{\alpha}_{2,1y}$. The further discrimination is carried out based on the cyclic moment $M^{\alpha}_{2,0y}$. The scheme of Table 6.4 in Subsection 6.4.2 detects the number of cycle frequencies of $M^{\alpha}_{2,0y}$ and is able to discriminate the modulation-type set Ξ into the following subsets: {AM, DSB, MASK, MPAM, PSK2}, {LSB, USB, NBFM, WBFM, QAM, MPSK with $M \geq 4$ }, {CPM with $h = 0.5 \times$ integer, MFSK}. Then when the modulation type of the input signal belongs to the set $\Xi_{1,3}$ = {MPAM, MPSK, QAM, CPM with $h \neq$ integer }, the scheme will further classify the modulation type into one of the following subsets: $\Xi_{1,3,1}$ = {MPAM, PSK2}, $\Xi_{1,3,2}$ = {QAM, MPSK with $M \geq 4$}, and $\Xi_{1,3,3}$ = {CPM with $h = 0.5 \times$ odd integer }. For a modulation type in the set $\Xi_{1,3,3}$, the values of M and f_d have also been estimated.

With the estimated values of f_d, M and R_s, one can further check if a signal belonging to the set $\Xi_{1,3,3}$ is MSK (including GMSK) or not.

Splitting the modulation-type set Ξ_2 This subset includes AM, DSB, LSB, USB, FM, MFSK and CPM. For CPM and MFSK classified into this set, it is implied the symbol rate has not been detected in the previous classification level. Similar to the discrimination among the subset Ξ_1, the cyclic moment M_{1y}^{α} serves the initial classification of the set Ξ_2. The classification scheme based on M_{1y}^{α} is discussed in Subsection 6.4.1 and its implementation is described in Table 6.3. The scheme is able to classify the initial set Ξ into the following subsets: {AM, MASK, NBFM}, {DSB, LSB, USB, NBFM, WBFM, MPAM, MPSK, QAM, CPM with $h \neq$ integer }, and {CPM with $h =$ integer, MFSK}. When the modulation type of the input signal is limited to the set $\Xi_2 =$ {AM, DSB, LSB, USB, FM, MFSK, CPM}, the scheme of Table 6.3 will classify it into one of the following subsets: {AM, NBFM}, {DSB, LSB, USB, NBFM, WBFM, CPM with $h \neq$ integer }, {CPM with $h =$ integer, MFSK}.

Theoretically, M_{1y}^{α} does not have cycle frequency for DSB and SSB. Occasionally, however, some DSB and SSB signals are determined as having a cycle frequency for M_{1y}^{α}. If this does happen, the input DSB or SSB signal will be classified into the same subset of AM and NBFM. That is, the resultant subsets will be $\Xi_{2,1} =$ {CPM with $h =$ integer, MFSK}, $\Xi_{2,2} =$ {AM, NBFM, DSB, LSB, USB}, and $\Xi_{2,3} =$ {DSB, LSB, USB, NBFM, WBFM, CPM with $h \neq$ integer }. For modulation types in the set $\Xi_{2,1}$, the

number of modulation levels (i.e., M) and the frequency deviation f_d have also been estimated.

Discriminating among the modulation-type set $\Xi_{2,2}$ This subset includes AM, DSB, LSB, USB and NBFM. The classification of modulation types in this subset will be accomplished by using the cyclic moment $M_{2,0y}^{\alpha}$ and the features P_L, P_M, P_R, $P_{y,norm}$ and $P_{y2,norm}$ as follows.

The first step is to classify based on the cyclic moment $M_{2,0y}^{\alpha}$ by using the scheme of Table 6.4 in Subsection 6.4.2, which is able to discriminate the modulation-type set Ξ into the following subsets: {AM, DSB, MASK, MPAM, PSK2}, {LSB, USB, NBFM, WBFM, QAM, MPSK with $M \geq 4$}, {CPM with $h = 0.5 \times \text{integer}$, MFSK}. Then when the modulation type of the input signal belongs to the subset $\Xi_{2,2}$= {AM, DSB, LSB, USB, NBFM}, that scheme will further classify the modulation type into one of the following subsets: $\Xi_{2,2,1}$= {AM, DSB}, $\Xi_{2,2,2}$= {LSB, USB, NBFM}. Since the signals falling into the set $\Xi_{2,2}$ will not have cycle frequency or will only have one cycle frequency for $M_{2,0y}^{\alpha}$, a simplified version of the scheme in Table 6.4 is used here as explained in the following. The modified scheme will only examine the frequency corresponding to the global maximum of $\left|\hat{M}_{2,0y}^{\alpha}\right|$. If this frequency is determined as not being a cycle frequency of $M_{2,0y}^{\alpha}$, the input is claimed to be of a modulation type in the subset $\Xi_{2,2,2}$, and then the modified scheme stops; otherwise, it is claimed to be of a modulation type in the subset $\Xi_{2,2,1}$, and other frequency locations will not be examined.

If the modulation type of the input signal is determined as belonging to the subset $\Xi_{2,2,1}$ = {AM, DSB}, the features $P_{y,norm}$ and $P_{y2,norm}$ as defined in Section 6.5 will be calculated. If the value of $P_{y,norm}$ is greater than that of $P_{y2,norm}$, the input will be classified into the subset $\Xi_{2,2,1,1}$ = {DSB}; otherwise, the input will be classified into the subset $\Xi_{2,2,1,2}$ = {AM}. The relationships between $P_{y,norm}$ and $P_{y2,norm}$ for AM and DSB are analyzed in Section 6.5.

If the modulation type of the input signal is determined as belonging to the subset $\Xi_{2,2,2}$= {LSB, USB, NBFM}, the features P_L, P_M and P_R as defined in Section 6.5 will be calculated. If P_L is the largest among P_L, P_M and P_R, the input will be classified into the set $\Xi_{2,2,2,1}$= {LSB}; if P_R is the largest, the input will be classified into the subset $\Xi_{2,2,2,2}$= {USB}; otherwise, it will be classified into the subset $\Xi_{2,2,2,3}$ = {NBFM}.

That is, at the end of this step, the concrete modulation type of an input signal, which belongs to the modulation-type set $\Xi_{2,2}$, has been recognized.

Discrimination among the modulation-type set $\Xi_{2,3}$ This subset includes DSB, LSB, USB, NBFM, WBFM and CPM with $h \neq$ non-integer. For a CPM signal falls in this set, it means that the symbol has not been detected. Moreover, as assumed in Section 6.2, the modulation index h will be one half of an odd integer if it is not an integer. That is, the modulation index h of a CPM signal falling in the set $\Xi_{2,3}$ will be $h = 0.5 \times \text{odd}$.

Again, the cyclic moment $M_{2,0y}^{\alpha}$ serves as the first tool for classifying among the subset $\Xi_{2,3}$. For a signal belonging to the subset $\Xi_{2,3}$ = {DSB, LSB, USB, NBFM, WBFM, CPM with $h \neq 0.5 \times \text{odd_integer}$ }, the scheme in Table 6.4 will further classify

its modulation type into one of the following subsets: $\Xi_{2,3,1}$ = {DSB}, $\Xi_{2,3,2}$ = {CPM with $h \neq 0.5 \times$ odd_integer }, and $\Xi_{2,3,3}$ = {LSB, USB, NBFM, WBFM}. For a signal classified into to the subset $\Xi_{2,3,2}$, the number of modulation levels (i.e., M) and the frequency deviation f_d are also estimated.

If the modulation type of the input signal is determined as belonging to the subset $\Xi_{2,3,3}$= {LSB, USB, NBFM, WBFM}, the features P_L, P_M and P_R as defined in Section 6.5 will be calculated. If P_L is the largest among P_L, P_M and P_R, the input will be classified into the set $\Xi_{2,3,3,1}$= {LSB}; if P_R is the largest one, the input will be classified into the subset $\Xi_{2,3,3,2}$= {USB}; otherwise, it will be classified into the subset $\Xi_{2,3,3,3}$= {NBFM, WBFM}.

Note that the subset $\Xi_{2,3,3,1}$ is identical to the subset $\Xi_{2,2,2,1}$ and the subset $\Xi_{2,3,3,2}$ is identical to the subset $\Xi_{2,2,2,2}$. That is, LSB (or USB) may be recognized from different decision paths. Also, the subset $\Xi_{2,3,3,3}$ contains the subset $\Xi_{2,2,2,3}$, i.e., NBFM may be recognized from two different decision paths. Similarly, MFSK and CPM are also recognized from two different paths.

Final classification results The decision flow of the proposed classifier is shown in Figure 6.1. At the end of classification, a received signal will be classified into one of the following groups: {AM}, {DSB}, {LSB}, {USB}, {FM}, {MASK: R_s has been estimated}, {MPAM, PSK2: R_s has been estimated}, {QAM, MPSK with $M \geq 4$: R_s has been estimated}, {MFSK, CPM with $h =$ integer: M and f_d have been estimated}, and {CPM with $h = 0.5 \times$ odd_integer: M and f_d have been estimated}. However, it is not

guaranteed that the symbol rate of MFSK and CPM will be detected. The proposed classifier does not intend to discriminate between NBFM and WBFM. Therefore, the modulation-type sets $\Xi_{2,2,2,3}$ (i.e., NBFM) and $\Xi_{2,3,3,3}$ (i.e., NBFM and WBFM) are merged as the set {FM} in the final results.

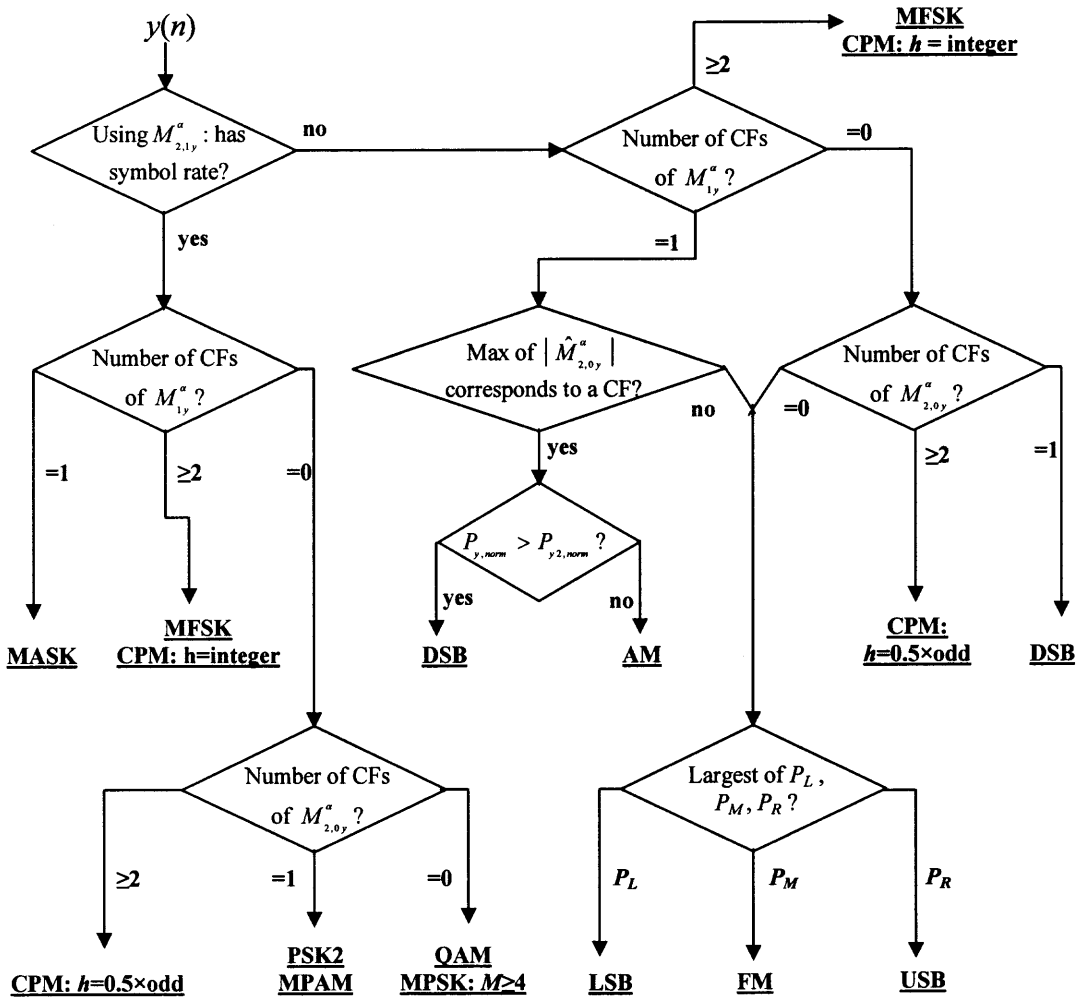

Figure 6.1 Decision Tree of the Proposed Classifier (CF stands for *cycle frequency*).

6.7 Test Results and Discussions

The testing signals used in simulation are generated by hardware and software signal generators with random sequences, many of the testing signals are transmitted through over the air. White Gaussian noise is added to the testing signal for the Monte Carlo simulation.

In the simulations, the proposed classifier has been tested with the twenty seven modulation formats as shown in Table 6.6. The performance is evaluated by the correct classification rate and the false alarm rate, where the meanings of correct classifications are defined in Table 6.7. Since the proposed classifier may project several different modulation formats into a same set of modulation types, the individual correct classification rate is calculated based on the target set of modulation types. For example, the proposed algorithm classifies all MPSK with M≥4 and QAM signals into the same set, i.e., the set of {MPSK with M≥4, QAM}. If the testing modulation formats include PSK4, PSK8 and QAM16, each of the above modulation formats is tested 100 times, and the numbers of correct classifications (according to definitions of Table 6.7) are respectively 95, 91 and 93, the individual correct classification rate for the target set {MPSK with M≥4, QAM} will be evaluated as $(95+91+93)/(100+100+100)=93\%$. After the individual correct classification rates for all target sets have been calculated, the overall correct rate will be evaluated as their arithmetic mean. The individual false alarm rates and the overall false alarm rates are evaluated in a similar way.

Three experiments on the modulation formats as described in Table 6.6 have been carried out. In each experiment, the number of tests for each testing modulation format under a given SNR is 500. The data record size for a testing modulation format in each

experiment is described in Table 6.8. In all simulations, the window function $W^{(N)}(\omega)$ used in Table 6.3 through Table 6.5 is chosen as a Kaiser window with length of 151 (i.e., L=151) and parameter $\beta = 0.5$.

Table 6.6 The Testing Modulation Formats

Modulation Type	Pulse Shaping Function	Parameters
AM	N/A	†
DSB	N/A	†
LSB	N/A	†
USB	N/A	†
NBFM	N/A	$D = 0.5$ † ‡
WBFM	N/A	$D = 5.0$ † ‡
OOK	Rectangular function of duration T	$R_s = 3000$ Hz †
PSK2	Square-root raised cosine function, roll-off factor 0.35	$R_s = 10000$ Hz †
PSK4	Square-root raised cosine function, roll-off factor 0.35	$R_s = 10000$ Hz †
$\frac{\pi}{4}$-DQPSK	Square-root raised cosine function, roll-off factor 0.35	$R_s = 10000$ Hz †
PSK8	Square-root raised cosine function, roll-off factor 0.35	$R_s = 10000$ Hz †
QAM16	Square-root raised cosine function, roll-off factor 0.35	$R_s = 10000$ Hz †
QAM32	Square-root raised cosine function, roll-off factor 0.35	$R_s = 10000$ Hz †
QAM64	Square-root raised cosine function, roll-off factor 0.35	$R_s = 10000$ Hz †
QAM256	Square-root raised cosine function, roll-off factor 0.35	$R_s = 10000$ Hz †
CPM2	Square-root raised cosine function, roll-off factor 0.35	$R_s = 5000$ Hz, $f_d = 7500$ Hz †
CPM4	Square-root raised cosine function, roll-off factor 0.35	$R_s = 10000$ Hz, $f_d = 5000$ Hz †
MSK	Square-root raised cosine function, roll-off factor 0.35	$R_s = 10000$ Hz, $f_d = 5000$ Hz †
GMSK	Gaussian pulse shaping, bandwidth factor 0.30	$R_s = 10000$ Hz, $f_d = 5000$ Hz †
MFSK2	Rectangular function of duration T	$f_d / R_s = 0.6$ ¶
MFSK2	Rectangular function of duration T	$f_d / R_s = 1.0$ ¶
MFSK4	Rectangular function of duration T	$f_d / R_s = 0.6$ ¶
MFSK4	Rectangular function of duration T	$f_d / R_s = 1.0$ ¶
CPM2	Rectangular function of duration T	$f_d / R_s = 0.5$ ¶
CPM2	Rectangular function of duration T	$f_d / R_s = 1.0$ ¶
CPM4	Rectangular function of duration T	$f_d / R_s = 0.5$ ¶
CPM4	Rectangular function of duration T	$f_d / R_s = 1.0$ ¶

† The sampling rate is 4.6387×10^4 Hz, and the carrier frequency is about a quarter of the sampling rate.

‡ D is the ratio of the peak frequency deviation to the modulating signal's bandwidth.

¶ The sampling rate is four times of the estimated bandwidth, and the carrier frequency is uniformly distributed within a small range around one fourth of the sampling rate.

Table 6.7 Definitions of Correct Classifications

Modulation Type	Should be recognized as	Additional conditions
AM	AM	
DSB	DSB	
LSB	LSB	
USB	USB	
NBFM	FM	
WBFM	FM	
MASK	MASK	$\lvert R_s - \hat{R}_s \rvert <$ DFT Resolution
MPAM	MPAM or PSK2	$\lvert R_s - \hat{R}_s \rvert <$ DFT Resolution
PSK2	MPAM or PSK2	$\lvert R_s - \hat{R}_s \rvert <$ DFT Resolution
MPSK: $M \geq 4$	QAM or MPSK with $M \geq 4$	$\lvert R_s - \hat{R}_s \rvert <$ DFT Resolution
QAM	QAM or MPSK with $M \geq 4$	$\lvert R_s - \hat{R}_s \rvert <$ DFT Resolution
MFSK	MFSK or CPM with h = integer	$\hat{M} = M$, $\lvert f_d - \hat{f}_d \rvert <$ DFT Resolution
CPM: h = integer	MFSK or CPM with h = integer	$\hat{M} = M$, $\lvert f_d - \hat{f}_d \rvert <$ DFT Resolution
CPM: $h = 0.5 \times$ odd	CPM with $h = 0.5 \times$ odd	$\hat{M} = M$, $\lvert f_d - \hat{f}_d \rvert <$ DFT Resolution

Table 6.8 Data Record Size in Different Experiments

Experiments / Signal types	Experiment 1 (Case-1)	Experiment 2 (Case-2)	Experiment 3 (Case-3)
Analog Communication Signals	0.3333 seconds	0.50 seconds	0.6667 seconds
Digital Communication Signals	1000 symbols	1500 symbols	2000 symbols

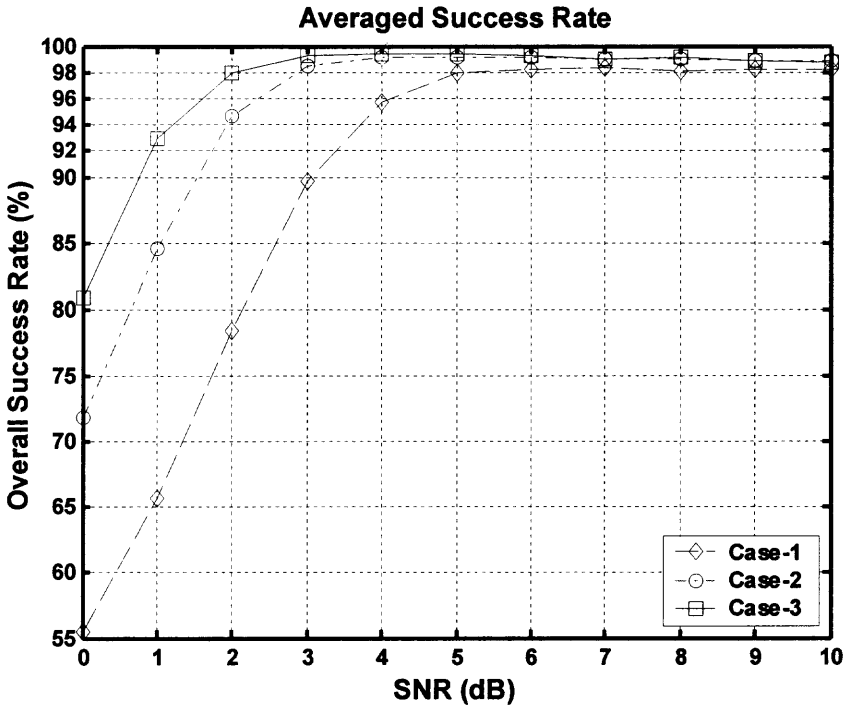

Figure 6.2 The overall correct classification rate vs. SNR.

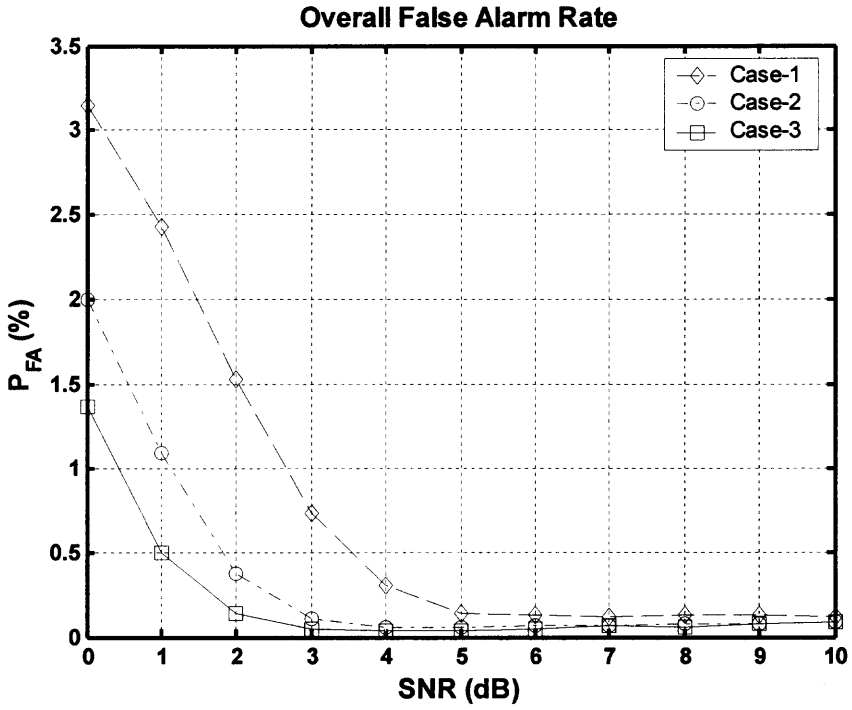

Figure 6.3 The overall false alarm rate vs. SNR.

The overall correct classification rates for these experiments are shown in Figure 6.2, and the overall false alarm rates are shown in Figure 6.3. It is evident that the proposed classifier performs very well. Since the correct rate is evaluated according to the definitions of Table 6.6, the results in Figure 6.2 imply that the symbol rates for linearly modulated digital communication signals as well as the values of M and f_d for CPM and MFSK have also been estimated with high accuracy.

The individual correct classification rate and false alarm rate for each target set of modulation types can be found in [144]. For the simplicity, they are not reported here.

It should be noted that it is very difficult to perform fair performance comparisons with the existing algorithms. For example, as mentioned in Section 6.1, many existing classifiers such as [87]-[91] rely on off-line training to obtain the nominal key feature values. However, the proposed classifier is designed to work in a blind environment, i.e., training data are unavailable. If the existing algorithms such as [87]-[91] are trained with data of some modulation formats but tested with data of other modulation formats (e.g., the modulation type is the same, but the modulation parameters are changed greatly), it is unfair to them. On the other hand, if they are tested with data drawn from modulation formats that are exactly the same of the reference modulation formats, it would be unfair to the proposed classifier. The maximum likelihood (ML) method is often used as a benchmark to evaluate the performance of a classifier. For analog communication signals, however, it is very difficult to apply the ML method since it will be difficult to find a probability distribution function to describe an unknown information-bearing signal. For these reasons, the performance comparison has not been conducted yet. Nevertheless, it

should be able to find a way to fairly compare the performance, and this will be done in the future research.

The computational complexities for signals with different modulation formats are not equal. Some modulation types such as MASK require less computational power, while the others such as AM will need more computation power. Since the proposed classifier only examines a very limited number of different frequency locations when detecting the pattern of the cycle frequencies of the selected cyclic moments, the computational burdens of such examinations are trivial and thus can be ignored. Then the major computational burdens lie in the estimation of the selected cyclic moments and the extraction of the proposed features. Assume the number of available data samples, N, is an integer power of two (this can be achieved by padding zeros if the number of the originally available data samples is not an integer power of two), and the number of segments, Q, in estimating the average PSD of the received signal is also an integer power of two, then the proposed classifier can be implemented by using FFT technique. By calculating the computational burden of each decision path in Figure 5.1 and then averaging over them, the average computational complexity of the proposed classifier has been shown to be in the order of $O\left(\frac{85}{8}N+\frac{55}{4}N\log_2 N-\frac{5}{2}N\log_2 Q+\frac{9}{16}N^2\right)$, where the sampling rate is assumed to be greater than four times of the received signal's bandwidth (this in turn implies the widths of the triangles for calculating the features P_L, P_M and P_R are less than or equal to $N/4$), the values of both N and Q are integer powers of two, the estimation of the selected cyclic moments and the calculation of the average PSD are realized by using FFT technique, and the computational burden is evaluated in the number of real-valued multiplication operations.

6.8 Conclusions

Based on the investigation of the patterns of the cyclostationarities and the spectral properties of communication signals, an algorithm for classification of joint analog and digital modulations has been developed.

In modulation classification, the proposed classifier employs three selected cyclic moments of the input signal as well as five other features that are extracted from the spectra of the input signal and the squared input signal. Based on the exploration of the relationship between the cyclic moments and the Fourier transforms of their generator functions, the computational complexity in testing the presence of cyclostationarity has been dramatically reduced. The other five features are designed in such a way that the classification decision is made by checking which one is larger or largest. Therefore, the task of selecting feature thresholds has been avoided. Further, the ideas employed in the symbol rate estimator proposed in Chapter 4 and the two MFSK classifiers proposed in Chapter 5 have also been adopted in this classifier.

The proposed classifier has been demonstrated to be able to achieve promising performance through simulations with testing data generated by software and hardware generators. The proposed classifier is capable of recognizing the concrete modulation type if the input is an analog communication signal or an exponentially modulated digital communication signal. When the input is a linearly modulated digital communication signal, the proposed algorithm will classify it into one of several nonoverlapping subsets of modulation types. In addition, it provides a very good estimate of the symbol rate if the input is a linearly modulated digital communication signal and a very good estimate of

the frequency deviation if the input is an exponentially modulated digital communication signal.

The proposed classifier does not impose unreasonable constraints on the input signal, except that the modulation index should be an integer or one half of an odd integer if the input is of CPM. Therefore, it is practical in most cases.

CHAPTER 7

SUMMARY AND FUTURE WORKS

In this chapter the contributions made in this dissertation research work are summarized. The future research is discussed.

7.1 Evaluation of Azzouz and Nandi's Approach to AMR

In literature survey, a thorough evaluation on the well-known features proposed by Azzouz and Nandi has been conducted in the beginning stage of this dissertation research in order to examine their performance and capability in automatic modulation recognition (AMR). The computer simulation results have demonstrated that the applications of these features are restricted in practice. The causes leading to the restrictions are discussed. Furthermore, the ways to improve performance and to classify additional modulation formats based on the same set of features are suggested.

7.2 Estimation of Carrier Frequency and Symbol Rate

The estimation of modulation parameters is an integrated part of automatic modulation recognition. On the one hand, the modulation parameters themselves are part of the signature of a communication system, thus the estimated modulation parameters can be used to help the recognition of the input signal. On the other hand, the further demodulation of the input signal generally requires knowing the modulation parameters such as carrier frequency and symbol rate. In AMR applications, the parameter estimation problems are blind in nature, since the concrete modulation type, the pulse-shaping

function (if applicable) and the nominal values of the parameters of the input are unknown in advance. Consequently, many existing approaches are not feasible anymore.

The proposed carrier frequency estimator is based on the phases of the autocorrelation functions of the input. Unlike the well-known cyclic-correlation based ones, the proposed carrier frequency estimator does not require the transmitted symbols being non-circularly distributed. The proposed carrier frequency estimator has been compared with the cyclic moment based ones and is found to be able to provide better overall performance in blind environments.

The popular approach to estimate the symbol rate is to find the peak corresponding to the symbol rate among the conjugate cyclic correlations of the input complex signal. However, the peak corresponding to the symbol rate is generally only a local peak rather than the global maximum of the cyclic correlations, especially when the excess bandwidth is small and the SNR is low. This makes the symbol rate search very difficult. Instead of expecting the symbol rate corresponds to the global maximum of the cyclic moments or assuming the symbol rate range and the excess bandwidth factor are known in advance, the proposed symbol rate estimator employs fourth-order cyclic moments to accommodate signals with zero or very small excess bandwidths and utilizes a bank of filters to adapt to the unknown symbol rate range of the input. By careful investigation of the properties of the peaks corresponding to the symbol rate among the cyclic moments, a scheme has been developed to extract symbol rate candidates from each set of cyclic moments corresponding to each filter. A measurement is designed to evaluate to what extent a candidate would be the true symbol rate. The final estimate of the symbol rate is obtained based on the weighted majority voting, where the weight of a

candidate is its confident measurement. Simulation results have shown that the proposed symbol rate estimator has provided a considerably improved performance compared to that of the popularly used cyclic correlation based one.

In developing both estimators, it is assumed knowing in advance the concrete modulation type, pulse-shaping function or the range of the parameter of interest. Therefore, the two proposed estimators are practical.

7.3 Classification of MFSK

In classification of M-ary frequency shift keying (MFSK) signals, some researchers proposed to employ the maximum likelihood (ML) tests. In blind environments, however, the number of different modulation formats and the possible values of the modulation parameters are not available in advance. Therefore the ML methods are not feasible, and one can only resort to feature based methods. Among the existing feature-based MFSK classification techniques, the reasonable ones may be those that recognize the number of modulation levels, M, by counting the number of distinct modulated frequencies (such as counting the number of hills in the histogram of the zero-crossing intervals). However, it is not trivial for machine to do so. In fact, to the author's best knowledge, the detailed realizations of such techniques cannot be found in the public literature. The two MFSK signal classifiers proposed in this dissertation, which are based on the investigation of the spectral properties of MFSK signals, have been shown to provide reasonably good performance when tested by simulated data and by real data that are collected from the real-world communication channels. In addition to recognizing the value of M, these two classifiers also provide good estimate of the frequency deviation. In these two classifiers,

it is only assumed that a rough estimate of the frequency range of the input is known via preprocessing. Therefore, they are practical in blind environments.

7.4 AMR Involving both Analog and Digital Modulations

In the classification involving both analog and digital modulations, many classifiers rely on training to obtain the nominal feature values for the reference modulation formats. This is certainly impossible in blind environments. Furthermore, many classifiers can only work under high SNR conditions. This also restricts their applications. The proposed algorithm for classification of joint analog and digital modulations, which is based on the detection of the presence of cyclostationarity of different orders and the examination of some other features, has been demonstrated to be able to achieve promising performance through simulations with testing data generated by software and hardware generators. Based on the exploration of the relationship between the cyclic moments and the Fourier transforms of their generator functions, the computational complexity in testing the presence of cyclostationarity has been dramatically reduced. In addition to the detection of the cyclostationary pattern of the input signal, the proposed classifier employs five features in classification. The proposed features are designed in such a way that the decision is made by checking which one is larger or largest. Therefore, the task of selecting feature thresholds has been avoided. Further, the ideas employed in the proposed symbol rate estimator and the two MFSK classifiers have also been adopted in this classifier. The proposed classifier is capable of recognizing the concrete modulation type if the input is an analog communication signal or an exponentially modulated digital communication signal. When the input is a linearly modulated digital communication

signal, the proposed algorithm will classify it into one of several subsets of modulation types. In addition, it provides a very good estimate of the symbol rate if the input is a linearly modulated digital communication signal and a very good estimate of the frequency deviation if the input is an exponentially modulated digital communication signal. The proposed classifier does not impose unreasonable constraints on the input signal, except that the modulation index should be an integer or one half of an odd integer if the input is of CPM. Therefore, it is practical in most cases.

7.5 Future Research

As mentioned above, the proposed classifier for classification of joint analog and digital modulations can only handle a limited portion of CPM signals. Moreover, it only separates the linear digital modulations into several nonoverlapping subsets, but does not recognize the concrete modulation type. Further, multiple-carrier modulations such as orthogonal frequency division multiplexing (OFDM) have not been considered in this dissertation. It is noted that some work has been done in these areas. When no priori knowledge of the possible modulation formats is available, however, most of the existing algorithms will not feasible. To make the AMR more practical, these should be studied in the future research.

APPENDIX A

DERIVATION OF THE POWER SPECTRAL DENSITY OF AN MFSK SIGNAL

This appendix derives the power spectral density (PSD) of the equivalent lowpass signal of an MFSK signal.

The equivalent lowpass signal $x_{lp}(t)$ of an MFSK signal $x(t)$ as defined in (5.2) can be mathematically expressed as

$$x_{lp}(t) = \sqrt{\frac{2E_s}{T}} \sum_n e^{j2\pi f_n t} p(t - nT) \tag{A.1}$$

where $p(t)$ as defined in (5.3) is the standard unit pulse of duration T, and the modulating frequencies $\{f_n\}$ are i.i.d. and uniformly distributed on the discrete values $\{f^{(m)}\}$ as defined in (5.4).

The autocorrelation function of $x_{lp}(t)$ is

$$\begin{aligned} r_{x_{lp}x_{lp}}(t;\tau) &\stackrel{\Delta}{=} E\left[x_{lp}(t+\tau)x_{lp}^*(t)\right] \\ &= E\left[\frac{2E_s}{T}\sum_n\sum_k e^{j2\pi f_n(t+\tau)} p(t+\tau-nT) e^{-j2\pi f_k t} p^*(t-kT)\right] \end{aligned} \tag{A.2}$$

where the two-folded summations can be split into two terms: $n = k$ and $n \neq k$. That is

$$\begin{aligned} r_{x_{lp}x_{lp}}(t;\tau) &= E\left[\frac{2E_s}{T}\sum_n e^{j2\pi f_n(t+\tau)} p(t+\tau-nT) e^{-j2\pi f_n t} p^*(t-nT)\right] \\ &\quad + E\left[\frac{2E_s}{T}\sum_n\sum_{k\neq n} e^{j2\pi f_n(t+\tau)} p(t+\tau-nT) e^{-j2\pi f_k t} p^*(t-kT)\right] \end{aligned} \tag{A.3}$$

Denote the first term and the second term on the right-hand side (RHS) of (A.3) by RHS_1 and RHS_2, respectively. They can be evaluated as

$$
\begin{aligned}
RHS_1 &= E\left[\frac{2E_s}{T}\sum_n e^{j2\pi f_n\tau} p(t+\tau-nT)\,p^*(t-nT)\right] \\
&= \frac{2E_s}{T}\sum_n E\left[e^{j2\pi f_n\tau}\right] p(t+\tau-nT)\,p^*(t-nT) \\
&= \frac{2E_s}{MT}\sum_{m=1}^{M} e^{j2\pi f^{(m)}\tau}\sum_n p(t+\tau-nT)\,p^*(t-nT)
\end{aligned}
\tag{A.4}
$$

and

$$
\begin{aligned}
RHS_2 &= \frac{2E_s}{T}\sum_n\sum_{k\neq n} E\left[e^{j2\pi f_n(t+\tau)}\right]E\left[e^{-j2\pi f_k t}\right] p(t+\tau-nT)\,p^*(t-kT) \\
&= \frac{2E_s}{TM^2}\sum_n\sum_{k\neq n} p(t+\tau-nT)\,p^*(t-kT)\sum_{m=1}^{M} e^{j2\pi f^{(m)}(t+\tau)}\sum_{l=1}^{M} e^{-j2\pi f^{(l)}t} \\
&= \frac{2E_s}{TM^2}\sum_n\sum_{k} p(t+\tau-nT)\,p^*(t-kT)\sum_{m=1}^{M} e^{j2\pi f^{(m)}(t+\tau)}\sum_{l=1}^{M} e^{-j2\pi f^{(l)}t} \\
&\quad -\frac{2E_s}{TM^2}\sum_n p(t+\tau-nT)\,p^*(t-nT)\sum_{m=1}^{M} e^{j2\pi f^{(m)}(t+\tau)}\sum_{l=1}^{M} e^{-j2\pi f^{(l)}t}
\end{aligned}
\tag{A.5}
$$

Since $p(t)$ satisfies (5.3), it can be concluded that only one term in the summations $\sum_n\sum_k p(t+\tau-nT)\,p^*(t-kT)$ can be nonzero for any given values of t and τ, and this nonzero value is equal to one. Then (A.5) can be further rewritten as

$$
\begin{aligned}
RHS_2 &= \frac{2E_s}{TM^2}\sum_{m=1}^{M} e^{j2\pi f^{(m)}(t+\tau)}\sum_{l=1}^{M} e^{-j2\pi f^{(l)}t} \\
&\quad -\frac{2E_s}{TM^2}\sum_n p(t+\tau-nT)\,p^*(t-nT)\sum_{m=1}^{M} e^{j2\pi f^{(m)}(t+\tau)}\sum_{l=1}^{M} e^{-j2\pi f^{(l)}t}
\end{aligned}
\tag{A.6}
$$

Based on (A.4) and (A.6), the autocorrelation function $r_{x_{lp}x_{lp}}(t;\tau)$ can be expressed as

$$
r_{x_{lp}x_{lp}}(t;\tau) = A_{x_{lp}x_{lp}}(t;\tau) + B_{x_{lp}x_{lp}}(t;\tau) + C_{x_{lp}x_{lp}}(t;\tau) \tag{A.7}
$$

where

$$
A_{x_{lp}x_{lp}}(t;\tau) \overset{\Delta}{=} \frac{2E_s}{TM^2}\sum_{m=1}^{M} e^{j2\pi f^{(m)}\tau}\sum_{l=1}^{M} e^{j2\pi f^{(l)}(m-l)t} \tag{A.8}
$$

$$B_{x_{lp}x_{lp}}(t;\tau)\overset{\Delta}{=}-\frac{2E_s}{TM^2}\sum_{m=1}^{M}\sum_{l=1}^{M}\sum_{n}e^{j2\pi\left(f^{(m)}-f^{(l)}\right)nT}p_m(t+\tau-nT)\,p_l^*(t-nT) \tag{A.9}$$

$$C_{x_{lp}x_{lp}}(t;\tau)\overset{\Delta}{=}\frac{2E_s}{MT}\sum_{m=1}^{M}e^{j2\pi f^{(m)}\tau}\sum_{n}p(t+\tau-nT)\,p^*(t-nT) \tag{A.10}$$

$$p_m(t)\overset{\Delta}{=}p(t)e^{j2\pi f^{(m)}t} \tag{A.11}$$

It is evident that the autocorrelation function $r_{x_{lp}x_{lp}}(t;\tau)$ is time-varying. The average autocorrelation function of $x_{lp}(t)$ is

$$\bar{r}_{x_{lp}x_{lp}}(\tau)\overset{\Delta}{=}\lim_{\Gamma\to\infty}\frac{1}{\Gamma}\int_{-\frac{\Gamma}{2}}^{\frac{\Gamma}{2}}r_{x_{lp}x_{lp}}(t;\tau)\,dt=\bar{A}_{x_{lp}x_{lp}}(\tau)+\bar{B}_{x_{lp}x_{lp}}(\tau)+\bar{C}_{x_{lp}x_{lp}}(\tau) \tag{A.12}$$

where

$$\bar{A}_{x_{lp}x_{lp}}(\tau)\overset{\Delta}{=}\lim_{\Gamma\to\infty}\frac{1}{\Gamma}\int_{-\frac{\Gamma}{2}}^{\frac{\Gamma}{2}}A_{x_{lp}x_{lp}}(t;\tau)\,dt \tag{A.13}$$

$$\bar{B}_{x_{lp}x_{lp}}(\tau)\overset{\Delta}{=}\lim_{\Gamma\to\infty}\frac{1}{\Gamma}\int_{-\frac{\Gamma}{2}}^{\frac{\Gamma}{2}}B_{x_{lp}x_{lp}}(t;\tau)\,dt \tag{A.14}$$

$$\bar{C}_{x_{lp}x_{lp}}(\tau)\overset{\Delta}{=}\lim_{\Gamma\to\infty}\frac{1}{\Gamma}\int_{-\frac{\Gamma}{2}}^{\frac{\Gamma}{2}}C_{x_{lp}x_{lp}}(t;\tau)\,dt \tag{A.15}$$

By using the well-known relationship $\int_{-\infty}^{\infty}e^{j2\pi ft}dt=\delta(f)$, $\bar{A}_{x_{lp}x_{lp}}(\tau)$ can be further evaluated as

$$\bar{A}_{x_{lp}x_{lp}}(\tau)=\frac{2E_s}{TM^2}\sum_{m=1}^{M}\sum_{l=1}^{M}e^{j2\pi f^{(m)}\tau}\delta(m-l)=\frac{2E_s}{TM^2}\sum_{m=1}^{M}e^{j2\pi f^{(m)}\tau} \tag{A.16}$$

$B_{x_{lp}x_{lp}}(t;\tau)$ is a periodic function of t with period being T, thus $\bar{B}_{x_{lp}x_{lp}}(\tau)$ can be obtained by averaging $B_{x_{lp}x_{lp}}(t;\tau)$ over one period as

$$\bar{B}_{x_{lp}x_{lp}}(\tau)=\frac{-2E_s}{T^2M^2}\sum_{m=1}^{M}\sum_{l=1}^{M}\sum_{n}\int_0^T e^{j2\pi\left(f^{(m)}-f^{(l)}\right)nT}p_m(t+\tau-nT)\,p_l^*(t-nT)\,dt \tag{A.17}$$

Now let $v = t - nT$ and substitute it into (A.17), $\bar{B}_{x_{lp}x_{lp}}(\tau)$ will become

$$\begin{aligned}\bar{B}_{x_{lp}x_{lp}}(\tau) &= \frac{-2E_s}{T^2M^2}\sum_{m=1}^{M}\sum_{l=1}^{M}\sum_{n}\int_{-nT}^{-(n-1)T} e^{j2\pi\left(f^{(m)}-f^{(l)}\right)nT} p_m(v+\tau)\,p_l^*(v)\,dv \\ &= \frac{-2E_s}{T^2M^2}\sum_{m=1}^{M}\sum_{l=1}^{M}\int_{-\infty}^{\infty}\lambda(v)\,p_m(v+\tau)\,p_l^*(v)\,dv\end{aligned} \tag{A.18}$$

where $\lambda(v)$ is defined as

$$\lambda(v) \overset{\Delta}{=} e^{j2\pi\left(f^{(m)}-f^{(l)}\right)nT} \quad \text{for} \quad -nT \le v < -(n-1)T \tag{A.19}$$

It should be noted that the nonzero region of $p_l(v)$ is (0, T), and the value of $\lambda(v)$ is one in this region since the value of n is zero for $0 \le v < T$. Thus, (A.18) can be rewritten as

$$\begin{aligned}\bar{B}_{x_{lp}x_{lp}}(\tau) &= \frac{-2E_s}{T^2M^2}\sum_{m=1}^{M}\sum_{l=1}^{M}\sum_{n}\int_{0}^{T} p_m(v+\tau)\,p_l^*(v)\,dv \\ &= \frac{-2E_s}{T^2M^2}\sum_{m=1}^{M}\sum_{l=1}^{M}\int_{-\infty}^{\infty} p_m(v+\tau)\,p_l^*(v)\,dv \\ &= \frac{-2E_s}{T^2M^2}\sum_{m=1}^{M}\sum_{l=1}^{M} p_m(\tau)\otimes p_l^*(-\tau)\end{aligned} \tag{A.20}$$

where the notation $\otimes$ stands for the convolution operation.

$C_{x_{lp}x_{lp}}(t;\tau)$ is also a periodic function of t. Thus $\bar{C}_{x_{lp}x_{lp}}(\tau)$ can be obtained in a similar way as

$$\begin{aligned}\bar{C}_{x_{lp}x_{lp}}(\tau) &= \frac{2E_s}{MT^2}\sum_{m=1}^{M} e^{j2\pi f^{(m)}\tau}\sum_{n}\int_{0}^{T} p(t+\tau-nT)\,p^*(t-nT)\,dt \\ &= \frac{2E_s}{MT^2}\sum_{m=1}^{M} e^{j2\pi f^{(m)}\tau}\int_{-\infty}^{\infty} p(t+\tau)\,p^*(t)\,dt \\ &= \frac{2E_s}{MT^2}\sum_{m=1}^{M} e^{j2\pi f^{(m)}\tau}\,p(\tau)\otimes p^*(-\tau)\end{aligned} \tag{A.21}$$

The Fourier transforms of $p(t)$ and $p_m(t)$ are respectively

$$P(f) \overset{\Delta}{=} F\left[p(t)\right] = T\frac{\sin(\pi fT)}{\pi fT}e^{-j2\pi fT} = T\text{sinc}(fT)e^{-j2\pi fT} \tag{A.22}$$

$$P_m(f) \overset{\Delta}{=} F\left[p_m(t)\right] = \int_{-\infty}^{\infty} p_m(t)\,dt = T\text{sinc}\left(fT - f^{(m)}T\right)e^{-j\pi\left(fT - f^{(m)}T\right)} \tag{A.23}$$

where $F[\bullet]$ stands for the Fourier transform of the operand.

According to Wiener-Kinchine Theorem, the PSD $S_{x_{lp}}(f)$ of the equivalent lowpass signal $x_{lp}(t)$ is the Fourier transform of $\bar{r}_{x_{lp}x_{lp}}(\tau)$. That is,

$$S_{x_{lp}}(f) = F\left[\bar{r}_{x_{lp}x_{lp}}(\tau)\right] = F\left[\bar{A}_{x_{lp}x_{lp}}(\tau)\right] + F\left[\bar{B}_{x_{lp}x_{lp}}(\tau)\right] + F\left[\bar{C}_{x_{lp}x_{lp}}(\tau)\right] \tag{A.24}$$

where

$$F\left[\bar{A}_{x_{lp}x_{lp}}(\tau)\right] = \frac{2E_s}{TM^2}\sum_{m=1}^{M}\delta\left(f - f^{(m)}\right) \tag{A.25}$$

$$\begin{aligned} F\left[\bar{B}_{x_{lp}x_{lp}}(\tau)\right] &= \frac{-2E_s}{T^2M^2}\sum_{m=1}^{M}\sum_{l=1}^{M}P_m(f)P_l^*(f) = -\frac{2E_s}{M^2}\sum_{m=1}^{M}\text{sinc}^2\left(fT - f^{(m)}T\right) \\ &-\frac{4E_s}{M^2}\sum_{m=1}^{M-}\sum_{l>m}^{M}\text{sinc}\left(fT - f^{(m)}T\right)\text{sinc}\left(fT - f^{(l)}T\right)\cos\left(\pi T\left(f^{(m)} - f^{(l)}\right)\right) \end{aligned} \tag{A.26}$$

$$F\left[\bar{C}_{x_{lp}x_{lp}}(\tau)\right] = \frac{2E_s}{T^2M}\sum_{m=1}^{M}\left|P\left(f - f^{(m)}\right)\right|^2 = \frac{2E_s}{M}\sum_{m=1}^{M}\text{sinc}^2\left(T\left(f - f^{(m)}\right)\right) \tag{A.27}$$

Then the PSD of the equivalent lowpass signal of an MFSK signal will be

$$\begin{aligned} S_{x_{lp}}(f) = \frac{2E_s}{M^2T}\Bigg\{&\sum_{m=1}^{M}\delta\left(f - f^{(m)}\right) + (M-1)T\sum_{m=1}^{M}\text{sinc}^2\left(Tf - Tf^{(m)}\right) \\ &-2T\sum_{m=1}^{M-1}\sum_{l>m}^{M}\text{sinc}\left(Tf - Tf^{(m)}\right)\text{sinc}\left(Tf - Tf^{(l)}\right)\cos\left(\pi T\left(f^{(m)} - f^{(l)}\right)\right)\Bigg\} \end{aligned} \tag{A.28}$$

It should be noted that the FSK2 signal's PSD derived in [107] is a special case of (A.28).

APPENDIX B

THE RELATIONSHIP BETWEEN THE NORMALIZED PSD OF AN AM SIGNAL AND THAT OF ITS SQUARED SIGNAL

This appendix serves to derive the relationship between the feature $P_{x,norm}$ and the feature $P_{x2,norm}$ for a noiseless AM signal, where both features are defined in Section 6.5.

According to (6.2), the samples of a noiseless AM signal can be expressed as

$$x(n) = z(n)e^{j2\pi T_s f_c n + j\theta_c}, \text{ for } n = 0,1,\cdots,N-1 \tag{B.1}$$

where $s(n) \overset{\Delta}{=} s(nT_s)$, θ_c stands for the unknown initial carrier phase that is deterministic, T_s is the sampling period that is the reciprocal of the sampling rate f_s, $z(n) \overset{\Delta}{=} A(1+K_a s(n))$, and $z(n)$ is real-valued and is nonnegative for any n.

The estimated PSD $\hat{S}_x(k)$ of $x(n)$ can be derived as

$$\begin{aligned}
\hat{S}_x(k) &= \frac{1}{N}\left|\sum_{n=0}^{N-1} x(n)e^{-j\frac{2\pi}{N}kn}\right|^2 = \frac{1}{N}\left|\sum_{n=0}^{N-1} z(n)e^{-j\frac{2\pi}{N}kn + j(2\pi f_c n T_s + \theta_c)}\right|^2 \\
&= \frac{1}{N}\sum_{n=0}^{N-1} z^2(n) + \frac{2}{N}\sum_{n=0}^{N-2}\sum_{m>n}^{N-1} z(n)z(m)\cos\left(2\pi\left(\frac{k}{N} - \frac{f_c}{f_s}\right)\times(m-n)\right) \\
&\le \frac{1}{N}\sum_{n=0}^{N-1} z^2(n) + \frac{2}{N}\sum_{n=0}^{N-2}\sum_{m>n}^{N-1} z(n)z(m) = \hat{S}_x(k)|_{k=NT_s f_c} = \frac{1}{N}\left(\sum_{n=0}^{N-1} z(n)\right)^2
\end{aligned} \tag{B.2}$$

where the facts of $0 \le \left|\cos\left(2\pi\left(\frac{k}{N} - \frac{f_c}{f_s}\right)\times(m-n)\right)\right| \le 1$ and $z(n) \ge 0$ have been applied in derivation. Equation (B.2) points out that the global maximum of $\hat{S}_x(k)$ will be exactly equal to $\frac{1}{N}\left(\sum_{n=0}^{N-1} z(n)\right)^2$ if $NT_s f_c$ is an integer. In general, it cannot be guaranteed

$NT_s f_c$ will be an integer. When the number of available samples, i.e., N, is sufficiently large, however, the DFT resolution will be sufficiently high such that the fractional part of $NT_s f_c$ will be sufficiently small. Then it is reasonable to take $\frac{1}{N}\left(\sum_{n=0}^{N-1} z(n)\right)^2$ as the global maximum of $\hat{S}_x(k)$. Thus the normalized PSD $\hat{S}_{x,norm}(k)$ of $x(n)$ will be

$$\hat{S}_{x,norm}(k) = \frac{\hat{S}_x(k)}{\frac{1}{N}\left(\sum_{n=0}^{N-1} z(n)\right)^2} = \frac{\frac{1}{N}\left|\sum_{n=0}^{N-1} z(n) e^{-j\frac{2\pi}{N}kn + j(2\pi f_c n T_s + \theta_c)}\right|^2}{\frac{1}{N}\left(\sum_{n=0}^{N-1} z(n)\right)^2} \tag{B.3}$$

and the feature $\hat{P}_{x,norm}$ will be evaluated as

$$\hat{P}_{x,norm} = \sum_{k=0}^{N-1} \hat{S}_{x,norm}(k) = \frac{\sum_{k=0}^{N-1} \hat{S}_x(k)}{\frac{1}{N}\left(\sum_{n=0}^{N-1} z(n)\right)^2} \tag{B.4}$$

By applying Parseval's Theorem, equation (B.4) can be further rewritten as

$$\hat{P}_{x,norm} = \frac{\sum_{n=0}^{N-1} |x(n)|^2}{\frac{1}{N}\left(\sum_{n=0}^{N-1} z(n)\right)^2} = \frac{\sum_{n=0}^{N-1} |z(n)|^2}{\frac{1}{N}\left(\sum_{n=0}^{N-1} z(n)\right)^2} = \frac{\sum_{n=0}^{N-1} z^2(n)}{\frac{1}{N}\left(\sum_{n=0}^{N-1} z(n)\right)^2} \tag{B.5}$$

where the last step is owing to the fact that $z(n)$ is nonnegative real value.

Similarly, the feature $P_{x2,norm}$, which corresponds to the normalized PSD of $x^2(n)$, can be derived as

$$\hat{P}_{x2,norm} = \sum_{n=0}^{N-1} z^4(n) \Big/ \left(\frac{1}{N}\left(\sum_{n=0}^{N-1} z^2(n)\right)^2\right) \tag{B.6}$$

Then the difference between $\hat{P}_{x2,norm}$ and $\hat{P}_{x,norm}$ can be written as

$$\hat{P}_{x2,norm} - \hat{P}_{x,norm} = \frac{\sum_{m=0}^{N-1} z^4(m)\left(\sum_{n=0}^{N-1} z(n)\right)^2 - \left(\sum_{m=0}^{N-1} z^2(m)\right)^3}{\frac{1}{N}\left(\sum_{m=0}^{N-1} z^2(m)\right)^2\left(\sum_{n=0}^{N-1} z(n)\right)^2} \tag{B.7}$$

Since the data $\{x(n)\}$ represent an AM signal captured by an AMR system, then some of them should be nonzero. Then some of $\{z(n)\}$ should be nonzero. Moreover, $z(n) \geq 0$ for any n. Therefore, the denominator on the RHS of (B.7) should be positive. That is, in order to determine the relationship between $P_{x,norm}$ and $P_{x2,norm}$, one only needs to check the sign of the numerator on the RHS of (B.7). The numerator at the RHS of (B.7) can be rewritten as

$$\begin{aligned}
\mathbb{N} &\overset{\Delta}{=} \sum_{m=0}^{N-1} z^4(m)\left(\sum_{n=0}^{N-1} z(n)\right)^2 - \left(\sum_{m=0}^{N-1} z^2(m)\right)^3 \\
&= \sum_{k=0}^{N-1}\sum_{m=0}^{N-1}\sum_{n=0}^{N-1} z^2(k)z(m)z(n)\left(z^2(k) - z(m)z(n)\right) \\
&= \sum_{\substack{k=0 \\ m=k}}^{N-1}\sum_{\substack{n=0 \\ n\neq k}}^{N-1}\left(\mathbb{Z}(k,m,n) + \mathbb{Z}(k,n,m) + \mathbb{Z}(n,m,k)\right) + \sum_{\substack{k=0 \\ k\neq n}}^{N-1}\sum_{\substack{m=0 \\ m\neq k}}^{N-1}\sum_{\substack{n=0 \\ n\neq m}}^{N-1}\mathbb{Z}(k,m,n)
\end{aligned} \tag{B.8}$$

where the function $\mathbb{Z}(k,m,n)$ is defined as

$$\mathbb{Z}(k,m,n) \overset{\Delta}{=} z^2(k)z(m)z(n)\left(z^2(k) - z(m)z(n)\right) \tag{B.9}$$

The first term on the RHS of (B.8) can be evaluated as

$$\begin{aligned}
&\sum_{\substack{k=0 \\ m=k}}^{N-1}\sum_{\substack{n=0 \\ n\neq k}}^{N-1}\left(\mathbb{Z}(k,m,n) + \mathbb{Z}(k,n,m) + \mathbb{Z}(n,m,k)\right) \\
&= \sum_{k=0}^{N-1}\sum_{\substack{n=0 \\ n\neq k}}^{N-1}\left\{z^2(k)z(n)\left[2z(k) + z(n)\right] \times \left[z(n) - z(k)\right]^2\right\} \geq 0
\end{aligned} \tag{B.10}$$

When the AM signal does convey information, there should exist at least one pair of n and k for which $z(k)$ is not equal to $z(n)$ if $k \neq n$. Then the result of (B.10) should be greater than zero.

The second term on the RHS of (B.8) does not exist if N is less than three. For $N \geq 3$, that term can be reorganized as

$$\begin{aligned}\sum_{\substack{k=0\\k\neq n}}^{N-1}\sum_{\substack{m=0\\m\neq k}}^{N-1}\sum_{\substack{n=0\\n\neq m}}^{N-1}\mathbb{Z}(k,m,n) &= \sum_{k=0}^{N-1}\sum_{m>k}^{N-1}\sum_{n>m}^{N-1}\mathbb{Z}(k,m,n)+\sum_{k=0}^{N-1}\sum_{m>k}^{N-1}\sum_{n>m}^{N-1}\mathbb{Z}(k,n,m)\\ &\quad+\sum_{k=0}^{N-1}\sum_{m>k}^{N-1}\sum_{n>m}^{N-1}\mathbb{Z}(m,n,k)+\sum_{k=0}^{N-1}\sum_{m>k}^{N-1}\sum_{n>m}^{N-1}\mathbb{Z}(m,k,n)\\ &\quad+\sum_{k=0}^{N-1}\sum_{m>k}^{N-1}\sum_{n>m}^{N-1}\mathbb{Z}(n,m,k)+\sum_{k=0}^{N-1}\sum_{m>k}^{N-1}\sum_{n>m}^{N-1}\mathbb{Z}(n,k,m)\\ &= \sum_{k=0}^{N-1}\sum_{m>k}^{N-1}\sum_{n>m}^{N-1}z(k)z(m)z(n)\times H(k,m,n)\end{aligned} \tag{B.11}$$

where the function $H(k,m,n)$ is defined as

$$H(k,m,n) \stackrel{\Delta}{=} z^3(k)+z^3(m)+z^3(n)-3z(k)z(m)z(n) \tag{B.12}$$

In the following, $H(k,m,n)$ will be shown to be nonnegative for any combination of k, m and n. It is noted that the function $H(k,m,n)$ is symmetric with respect to $z(k)$, $z(m)$ and $z(n)$. Moreover, $z(k)$, $z(m)$ and $z(n)$ are all nonnegative. Thus one can assume $z(m) \geq z(n) \geq z(k) \geq 0$ without loss of generality. The function $H(k,m,n)$ can be rewritten as

$$\begin{aligned}H(k,m,n) &= z^3(k)+z^3(m)+z^3(n)-3z(k)z(m)z(n)\\ &= \left(z(m)-z(k)\right)^3+\left(z(n)-z(k)\right)^3\\ &\quad+3z(k)\times\left(\left(z(n)-z(m)\right)^2+\left(z(m)-z(k)\right)\times\left(z(n)-z(k)\right)\right)\geq 0\end{aligned} \tag{B.13}$$

That is, the last term on the RHS of (B.8) is greater than or equal to zero. In general, this term is greater than zero if the information-bearing signal $s(n)$ is not constant.

Combining the above results, it can be concluded that the value of $\hat{P}_{x2,norm}$ is greater than that of $\hat{P}_{x,norm}$ for a noiseless AM signal.

REFERENCES

1. C. S. Weaver, C. A. Cole, R. B. Krumland, and M. L. Miller, "The automatic classification of modulation types by pattern recognition," *Technical Report No. 1829-2*, Stanford Electronics laboratories, Stanford University, Stanford, CA, April, 1969.

2. Y. T. Chan, L. G. Gadbois, and P. Yansouni, "Identification of the modulation type of a signal," —, pp. 838-841, 1985.

3. P. M. Fabrizi, L. B. Lopes, and G. B. Lockhart, "Receiver recognition of analogue modulation types," *Proceedings of the 1986 International Conference on Radio Receiver and Associated Systems*, Bangor, Wales, pp. 135-140, 1986.

4. P. A. J. Nagy, "Analysis of a method for classification of analogue modulated radio signals," *Proceedings of the 1994 European Association for Signal Processing VII Conference*, Edinburgh, Scotland, pp. 1015-1018, Sept. 1994.

5. S. D. Jovanovic, M. I. Doroslovacki, and M. V. Dragosevic, "Recognition of low modulation index AM signals in additive Gaussian noise," *Proceedings of the 1994 European Association for Signal Processing V Conference*, Edinburgh, Scotland, pp. 1923-1926, 1994.

6. Y. O. Al-Jalili, "Identification algorithm of upper sideband and lower sideband SSB signals," *Signal Processing*, Vol. 42, No. 2, pp. 207-213, March 1995.

7. A. K. Nandi and E. E. Azzouz, "Automatic analogue modulation recognition," *Signal Processing*, Vol. 46, No. 2, pp. 211-222, Oct. 1995.

8. I. Druckmann, E. I. Plotkin, and M. N. S. Swamy, "Automatic modulation type recognition," *Proceedings of the 1998 IEEE Canadian Conference on Electrical and Computer Engineering*, Vol. 1, pp. 65-68, May 1998.

9. B. Seaman and R. M. Braun, "Using cyclostationarity in the modulation classification of analogue signals," *Proceedings of the 1998 South African Symposium on Communications and Signal Processing*, pp. 261-266, Sept. 1998.

10. J. R. Waller and G. D. Brushe, "A method for differentiating between frequency and phase modulated signals," *Proceedings of Conference on Information, Decision and Control*, pp. 489-494, Feb. 1999.

11. S. Taira and E. Murakami, "Automatic classification of analogue modulation signals by statistical parameters," *Proceedings of the 1999 Military Communications Conference*, Vol. 1, pp. 202-207, Nov. 1999.

12. E. E. Azzouz and A. K. Nandi, *Automatic modulation recognition of communication signals*, Netherlands: Kluwer Academic Publishers, 1996.

13. H. Guldemır and A. Sengur, "Comparison of clustering algorithms for analog modulation classification," *Expert Systems with Applications*, Vol. 30, pp. 642-649, 2006.

14. J. C. Bezdek, *Fuzzy mathematics in pattern classification*, PhD thesis, Applied Mathematics Center, Cornell University Ithaca, 1973.

15. A. K. Jain and R. C. Dubes, *Algorithms for clustering data*, Prentice-Hall, Englewood Cliffs, NJ, 1988.

16. R. R. Yager and D. P. Filev, "Generation of fuzzy rules by mountain clustering," *IEEE Transactions on Systems, Man and Cybernetics*, Vol. 24, pp. 209-219, 1994.

17. S. L. Chiu, "Fuzzy model identification based on cluster estimation," *Journal of Intelligent and Fuzzy Systems*, Vol. 2, No. 3, pp. 267-278, Sept. 1994.

18. W. Su and J. Kosinski, "Comparison and modification of automated communication modulation recognition methods," *Proceedings of the 2002 Military Communications Conference*, 2002.

19. W. Su and J. Kosinski, "Comparison and simulation of digital modulation recognition algorithms," *Proceedings of the 2003 International Symposium on Advanced Radio Technologies*, pp. 81-87, March 2003.

20. W. Su and J. Kosinski, "A survey of digital modulation recognition methods," *Proceedings of the 2003 Global Signal Processing Conferences* (GSPx), Dallas, TX, April 2003.

21. F. F. Liedtke, "Computer simulation of an automatic classification procedure for digitally modulated communication signals with unknown parameters," *Signal Processing*, Vol. 6, No. 4, pp. 311-323, Aug. 1984.

22. R. J. Mammore, R. J. Rothaker, and C. I. Podilchuk, "Estimation of carrier frequency, modulation type and bit rate of an unknown modulated signal," *Proceedings of the 1987 IEEE International Conference on Communications*, Vol. 2, pp. 1006-1012, June 1987.

23. P. C. Sapiano, J. D. Martin, and R. J. Holbeche, "Classification of PSK signals using the DFT of phase histogram," *Proceedings of the 1995 International Conference on Acoustics, Speech, and Signal Processing*, Vol. 3, pp. 1868-1871, May 1995.

24. M. P. DeSimio and G. E. Prescott, "Adaptive generation of decision functions for classification of digitally modulated signals," *Proceedings of the 988 IEEE National Aerospace and Electronics Conference*, Vol. 3, pp. 1010-1014, May 1988.

25. J. Reichert, "Automatic classification of communication signals using higher order statistics," *Proceedings of the 1992 IEEE International Conference on Acoustics, Speech, and Signal Processing*, Vol. 5, pp. 221-224, March 1992.

26. S. -Z Hsue and S. S. Soliman, "Automatic modulation recognition of digitally modulated signals," *Proceedings of the 1989 IEEE Military Communications Conferenc*e, Vol. 3, pp. 645-649, Oct. 1989.

27. S. -Z. Hsue and S. S. Soliman, "Automatic modulation classification using zero crossing," *IEE Proceedings for Radar and Signal Processing*, Vol. 137, No. 6, pp. 459-464, Dec. 1990.

28. D. Grimaldi, S. Rapuano, and G. Truglia, "An automatic digital modulation classifier for measurement on telecommunication networks," *Proceedings of the 2002 IEEE Instrumentation and Measurement Technology Conference*, pp. 957-962, May 2002.

29. W. Akmouche, "Detection of multicarrier modulations using 4th-order cumulants," *Proceedings of the 1999 IEEE Military Communications Conference*, Vol. 1, pp. 432-436, Nov. 1999.

30. N. Benvenuto and W. R. Daumor, "Classification of voiceband data signals," *Proceedings of the 1990 IEEE International Conference on Communications*, Vol. 3, pp. 1010-1013, April 1990.

31. J. S. Sewall and B. F. Cockburn, "Signal classification in digital telephone networks," *Proceedings of the 1995 Canadian Conference on Electrical and Computer Engineering*, Vol. 2, pp. 957-961, Sept. 1995.

32. S. S. Soliman and S.-Z. Hsue, "Signal classification using statistical moments," *IEEE Transactions on Communications*, Vol. 40, No. 5, pp. 908-916, May 1992.

33. Y. Yang and S. S. Soliman, "An improved moment-based algorithm for signal classification," *Signal Processing*, Vol. 43, No. 3, pp. 231-244, May 1995

34. K. Assaleh, K. Farrell, and R. J. Mammone, "A new method of modulation classification for digitally modulated signals," *Proceedings of the 1992 IEEE Military Communications Conference*, Vol. 12, pp. 712-716, Oct. 1992.

35. C. M. Spooner, "Classification of co-channel communication signals using cyclic cumulants," *Proceedings of the Twenty-Ninth Asilomar Conference on Signals, Systems and Computers*, Vol. 1, pp. 531-536, Nov. 1995.

36. P. Marchand, C. L. Martret, and J.-L. Lacoume, "Classification of linear modulations by a combination of different orders cyclic cumulants," *Proceedings of the IEEE Signal Processing Workshop on Higher-Order Statistics*, pp. 47-51, July 1997.

37. P. Marchand, J.-L. Lacoume, and C. L. Martret, "Multiple hypothesis modulation classification based on cyclic cumulants of different orders," *Proceedings of the 1998 IEEE International Conference on Acoustics, Speech, and Signal Processing*, Vol. 4, pp. 2157-2160, May 1998.

38. C. Dubuc, D. Boudreau, F. Patenaude, and R. Inkol, "An automatic modulation recognition algorithm for spectrum monitoring applications," *Proceedings of the 1999 IEEE International Conference on Communications*, Vol. 1, pp. 570-574, June 1999.

39. V. Ramakomar, D. Habibi, and A. Bouzerdoum, "Automatic recognition of digitally modulated communications signals," *Proceedings of the Fifth International Symposium on Signal Processing and Its Applications*, Vol. 2, pp. 753-756, Aug. 1999.

40. G. Arulampalam, V. Ramakonar, A. Bouzerdoum, and D. Habibi, "Classification of digital modulation schemes using neural networks," *Proceedings of the Fifth International Symposium on Signal Processing and Its Applications*, Vol. 2, pp. 649-652, Aug. 1999.

41. D. Boudreau, et al., "A fast automatic modulation recognition algorithm and its implementation in a spectrum monitoring application," *Proceedings of the 2000 IEEE Military Communications Conference*, Vol. 2, pp. 732-736, Oct. 2000.

42. Y. Zhao, G. Ren, X. Wang, Z. Wu, and X. Gu, "Automatic digital modulation recognition using artificial neural networks," *Proceedings of the 2003 International Conference on Neural Networks and Signal Processing*, Vol. 1, pp. 257-260, Dec. 2003.

43. A. Swami and B. Sadler, "Modulation classification via hierarchical agglomerative cluster analysis," *Proceedings of 1997 First IEEE Signal Processing Workshop on the Signal Processing Advances in Wireless Communications*, pp. 141-144, April 1997.

44. A. Swami and B. M. Sadler, "Hierarchical digital modulation classification using cumulants," *IEEE Transactions on Communications*, Vol. 48, No. 3, pp. 416-429, March 2000.

45. A. Swami, S. Barbarossa, and B. M. Sadler, "Blind source separation and signal classification," *Conference Record of the Thirty-Fourth Asilomar Conference on Signals, Systems and Computers*, Vol. 2, pp. 1187-1191, Oct. 2000.

46. G. Han, J. Li and C. Chen, "A robust MDPSK modulation classifier based on cumulants," *Proceedings of the Seventeenth International Conference on Advanced Information Networking and Applications*, pp. 265-268, March 2003.

47. W. Dai, Y. Wang, and J. Wang, "Joint power estimation and modulation classification using second- and higher statistics," *Proceedings of the 2002 IEEE Wireless Communications and Networking Conference*, Vol. 1, pp. 155-158, March 2002.

48. A.-V. Rosti and V. Koivunen, "Classification of MFSK modulated signals using the mean of complex envelope" *Proceedings of the 2000 European Signal Processing Conference*, Vol. 1, pp. 581-584, 2000.

49. K. C. Ho, W. Prokopiw, and Y. T. Chan, "Modulation identification by the wavelet transform," *Proceedings of the 1995 IEEE Military Communications Conference*, Vol. 2, pp. 886-890, Nov. 1995.

50. K. C. Ho, W. Prokopiw, and Y. T. Chan, "Modulation identification of digital signals by the wavelet transform," *IEE Proceedings for Radar, Sonar and Navigation*, Vol. 147, No. 4, pp. 169-176, Aug. 2000.

51. L. Hong and K. C. Ho, "Identification of digital modulation types using the wavelet transform," *Proceedings of 1999 IEEE Military Communications Conference*, Vol. 1, pp. 427-431, Oct. 1999.

52. S. Cho, C. H. Lee, J. Chun, and D. Ahn, "Classification of digital modulations using the LPC," *Proceedings of the IEEE 2000 National Aerospace and Electronics Conference*, pp. 774-778, Oct. 2000.

53. B. F. Cockburn and R. Hang, "A novel voiceband QAM constellation discrimination technique," *Proceedings of the 1997 IEEE Canadian Conference on Electrical and Computer Engineering*, Vol. 1, pp. 205-210, May 1997.

54. X. Huo and D. Donoho, "A simple and robust modulation classification method via counting," *Proceedings of the 1998 IEEE International Conference on Acoustics, Speech, and Signal Processing*, Vol. 6, pp. 3289-3292, May 1998.

55. T. A. Drumright and Z. Ding, "A new algorithm for QAM signal classification in AWGN channels," *Proceedings of the 2002 IEEE International Symposium on Circuits and Systems*, Vol. 1, pp. 849-852, May 2002.

56. K. Farrell and R. J. Mammone, "Modulation classification using a neural tree network," *Proceedings of the 1993 IEEE Military Communications Conference*, pp. 1028-1032, Oct. 1993.

57. G. Hatzichristos and M. P. Fargues, "A hierarchical approach to the classification of digital modulation types in multipath environments," *Proceedings of the Thirty-Fifth Asilomar Conference on Signals, Systems and Computers*, Vol. 2, pp. 1494-1498, Nov. 2001.

58. M. L. D. Wong and A. K. Nandi, "Automatic digital modulation recognition using spectral and statistical features with multi-layer perceptrons," *Proceedings of the Sixth International, Symposium on Signal Processing and its Applications*, Vol. 2, pp. 390-393, Aug. 2001.

59. J. Venalainen, L. Terho, and V. Koivunen, "Modulation classification in fading multipath channel," *Proceedings of the Thirty-Sixth Asilomar Conference on Signals, Systems and Computers*, Vol. 2, pp. 1890-1894, Nov. 2002.

60. W. Wei and J. M. Mendel, "A fuzzy logic method for modulation classification in nonideal environments," *IEEE Transactions on Fuzzy Systems*, Vol. 7, No. 3, pp. 333-344, June 1999.

61. J. Lopatka and M. Pedzisz, "Automatic modulation classification using statistical moments and a fuzzy classifier," *Proceedings of the Fifth International Conference on Signal Processing*, Vol. 3, pp. 1500-1506, Aug. 2000.

62. K. Kim and A. Polydoros, "Digital modulation classification: the BPSK versus QPSK case," *Proceedings of the 1998 IEEE Military Communications Conference*, Vol. 2, pp. 431-436, Oct. 1988.

63. A. Polydoros and K. Kim, "On the detection and classification of quadrature digital modulations in broad-band noise," *IEEE Transactions on Communications*, Vol. 38, No. 8, pp. 1199-1211, Aug. 1990.

64. L. Hong and K. C. Ho, "BPSK and QPSK modulation classification with unknown signal level," *Proceedings of the 2000 IEEE Military Communications Conference*, Vol. 2, pp. 976-980, Oct. 2000.

65. L. Hong and K. C. Ho, "Classification of BPSK and QPSK signals with unknown signal level using the Bayes technique," *Proceedings of the 2003 International Symposium on Circuits and Systems*, Vol. 4, pp. IV.1-IV.4, May 2003.

66. L. Hong and K. C. Ho, "Modulation classification of BPSK and QPSK signals using a two element antenna array receiver," *Proceedings of the 2001 IEEE Military Communications Conference*, Vol. 1, pp. 118-122, Oct. 2001.

67. L. Hong and K. C. Ho, "An antenna array likelihood modulation classifier for BPSK and QPSK signals," *Proceedings of the 2002 IEEE Military Communications Conference*, Vol. 1, pp. 647-651, Oct. 2002.

68. Y. Yang and S. S. Soliman, "Optimum classifier for *M*-ary PSK signals," *Proceedings of 1991 IEEE International Conference on Communications*, Vol. 3, pp. 1693-1697, June 1991.

69. Y. Yang and S. S. Soliman, "A suboptimal algorithm for modulation classification," *IEEE Transactions on Aerospace and Electronic Systems*, Vol. 33, No. 1, pp. 38-45, Jan. 1997.

70. Y. Yang and C.-H. Liu, "An asymptotic optimal algorithm for modulation classification," *IEEE Communications Letters*, Vol. 2, No. 5, pp. 117-119, May 1998.

71. C.-Y. Huang and A. Polydoros, "Likelihood methods for MPSK modulation classification," *IEEE Transactions on Communications*, Vol. 43, No. 2/3/4, pp. 1493-1504, Feb./March/April 1995.

72. P. C. Sapiano and J. D. Martin, "Maximum likelihood PSK classifier," *Proceedings of the 1996 IEEE Military Communications Conference*, Vol. 3, pp. 1010-1014, Oct. 1996.

73. C. Y. Hwang and A. Polydoros, "Advanced methods for digital quadrature and offset modulation classification," *Proceedings of the 1991 IEEE Military Communications Conference*, Vol. 2, pp. 841-845, Nov. 1991.

74. C. S. Long, K. M. Chugg, and A. Polydoros, "Further results in likelihood classification of QAM signals," *Proceedings of the 1994 IEEE Military Communications Conference*, Vol. 1, pp. 57-61, Oct. 1994.

75. K. M. Chugg, C.-S. Long, and A. Polydoros, "Combined likelihood power estimation and multiple hypothesis modulation classification," *Proceedings of the Twenty-Ninth Asilomar Conference on Signals, Systems and Computers*, Vol. 2, pp. 1137-1141, Nov. 1995.

76. N. Benvenuto and T. W. Goeddel, "Classification of voiceband data signals using the constellation magnitude," *IEEE Transactions on Communications*, Vol. 43, No. 11, pp. 2759-2770, Nov. 1995.

77. N. E. Lay and A. Polydoros, "Modulation classification of signals in unknown ISI environments," *Proceedings of the 1995 IEEE Military Communications Conference*, Vol. 1, pp. 170-174, Nov. 1995.

78. R. Raheli, A. Polydoros, and C.-K. Tzou, "Per-survivor processing: a general approach to MLSE in uncertain environments," *IEEE Transactions on Communications*, Vol. 43, No. 2/3/4, pp. 354-364, Feb./March/April 1995.

79. W. Wei, *Classification of digital modulations using constellation analysis*, PhD. Thesis, Department of Electrical Engineering, University of Southern California, California, May 1998.

80. W. Wei and J. M. Mendel, "Maximum-likelihood classification for digital amplitude-phase modulations," *IEEE Transactions on Communications*, Vol. 48, No. 2, pp. 189-193, Feb. 2000.

81. J. A. Sills, "Maximum-likelihood modulation classification for PSK/QAM," *Proceedings of the 1999 IEEE Military Communications Conference*, Vol. 1, pp. 217-220, Nov. 1999.

82. S. Taira, "Automatic classification of QAM signals in fading channel," *Proceedings of the Fifty-First IEEE Vehicular Technology Conference*, Vol. 3, pp. 1717-1721, May 2000.

83. B. F. Beidas and C. L. Weber, "Higher-order correlation-based approach to modulation classification of digitally frequency-modulated signals," *IEEE Journal on Selected Areas in Communications*, Vol. 13, No. 1, pp. 89-101, Jan. 1995.

84. B. F. Beidas and C. L. Weber, "Modulation classification of MFSK signals using the higher-order correlation domain," *Proceedings of the 1995 IEEE Military Communications Conference*, Vol. 1, pp. 186-191, Nov. 1995.

85. B. F. Beidas and C. L. Weber, "Higher-order correlation based classification of asynchronous MFSK signals," *Proceedings of the 1996 IEEE Military Communications Conference*, Vol. 3, pp. 1003-1009, Oct. 1996.

86. B. F. Beidas and C. L. Weber, "Asynchronous classification of MFSK signals using the higher order correlation domain," *IEEE Transactions on Communications*, Vol. 46, No. 4, pp. 480-493, April 1998.

87. F. Jondral, " Automatic classification of high frequency signals," *Signal Processing*, Vol. 9, No. 3, pp. 177-190, Oct. 1985.

88. E. R. Adams, P. C. J. Hill, and C. N. Kempson, "A statistical approach to modulation recognition for communications signal monitoring and surveillance," *Proceedings of the 1988 International Conference on Digital Processing of Signals in Communications*, pp. 31-37, Sept. 1988.

89. L. V. Domínguez, J. M. Borrallo, and J. P. García, "A general approach to the automatic classification of radio communication signals," *Signal Processing*, Vol. 22, No. 3, pp. 239-250, 1991.

90. T. G. Callaghan, J. L. Pery, and J. K. Tjho, "Sampling and algorithms aid modulation recognition," *Microwaves RF*, Vol. 24, No. 9, pp. 117-119 and 121, Sept. 1985.

91. J. E. Hipp, "Modulation classification based on statistical moments," *Proceedings of the 1986 IEEE Military Communications Conference*, pp. 20.2.1-20.2.6, Oct. 1986

92. J. Aisbett, "Automatic modulation recognition using time domain parameters," *Signal Processing*, Vol. 13, No. 3, pp. 323-328, Oct. 1987.

93. Z. B. Krsmanovic, N. K. Remenski, and P. M. Petrovic, "Automatic classification of HF radio signals," *Proceedings of the 1989 Global Communications Conference*, pp. 33-36, 1989.

94. P. M. Petrovic, Z. B. Krsmanovic and N. K. Remenski, "An automatic VHF signal classifier," *Proceedings of Mediterranean Electrotechnical Conference*, pp. 385-387, April 1989.

95. P. M. Petrović, Z. B. Krsmanović, and N. K. Remenski, "Automatic HF signal classification," *Proceedings of the Fourth International Conference on HF Radio Systems and Techniques*, pp. 210-214, April 1988.

96. S. B. McMillan, B. P. Flanagan, and T. K. Doong, "Determination of the modulation type of communication signals," *Proceedings of the 1990 International Conference on Acoustics, Speech, and Signal Processing*, Vol. 3, pp. 1683-1686, April 1990.

97. A. Martin, "A signal analysis and classification strategy for implementation in an EW communication receiver," *Proceedings of the Fifth International Conference on Radio Receiver and Associated Systems*, pp. 222-226, 1990.

98. E. E. Azzouz and A. K. Nandi, "Procedure for automatic recognition of analogue and digital modulations," *Communications, IEE Proceedings-*, Vol. 143, No. 5, pp. 259-266, Oct. 1996.

99. A. K. Nandi and E. E. Azzouz, "Algorithms for Automatic Modulation Recognition of Communication Signals," *IEEE Transactions on Communications*, Vol. 46, No. 4, pp. 431-436, April 1998.

100. N. Kim, N. Kehtarnavaz, S. Brown, and T. Mckinney, "Hierarchical classification of modulation signals," *Proceedings of the Fifth Biannual World Automation Congress*, Vol. 14, pp. 243-248, June 2002.

101. O. A. Dobrel, A. Abdi, Y. Bar-Ness, and W. Su, "The classification of joint analog and digital modulations," *Proceedings of the 2005 IEEE Military Communications Conference*, pp. 1-6, Oct. 2005.

102. J. Kitchen, "A periodogram-based matching technique for modulation recognition," *Proceedings of the Sixth Australian Communication Theory Workshop*, pp. 49-55, Feb. 2005.

103. S. C. Kremer and J. Shiels, "A testbed for automatic modulation recognition using artificial neural networks," *Proceedings of the 1997 Canadian Conference on Electrical and Computer Engineering*, pp. 67-70, May 1997.

104. J. Kreuzberger, "Detection of speech modulated SSB and AM signals in the HF-band," *Proceedings of the 1999 IEEE Military Communications Conference*, pp. 208-211, 1999.

105. M. Lu, X. Xiao, and L. Li, "Cyclic spectral features based modulation recognition," *Proceedings of the 1996 International Conference on Communication Technology*, Vol. 2, pp. 792-795, May 1996.

106. Z. Zhao and J. Shang, "A new method for modulation types recognition based on the time frequency representations," *Proceedings of the 2002 Sixth International Conference on Signal Processing*, Vol. 1, pp. 208-211, Aug. 2002.

107. A. B. Carlson, Communication systems — An introduction to signals and noise in electrical communication, Third Edition, McGraw-Hill, Inc., New York, 1986.

108. J. G. Proakis, *Digital communications*, Third Edition, McGraw-Hill, Inc., New York, 1995.

109. M. I. Skolnik, *Introduction to radar systems*, Second Edition, McGraw-Hill, Inc., New York, 1980.

110. S. Kay, "A fast and accurate single frequency estimator," *IEEE Transactions on Signal Processing*, Vol. 37, No. 12, pp. 1987-1990, Dec. 1989.

111. B. Volcker and P. Handel, "Frequency estimation from proper sets of correlations," *IEEE Transactions on Signal Processing*, Vol. 50, No. 4, pp. 791-802, April 2002.

112. W.-Y. Kuo and M. P. Fitz, "Frequency offset compensation of pilot symbol assisted modulation in frequency flat fading," *IEEE Transactions on Communications,* Vol. 45, No. 11, pp. 1412-1426, Nov. 1997.

113. M. Morelli and U. Mengali, "Carrier-frequency estimation for transmissions over selective channels," *IEEE Transactions on Communications*, Vol. 48, No. 9, pp. 1580-1589, Sept. 2000.

114. E. Serpedin, A. Chevreuit, G. B. Giannakis, and P. Loubaton, "Blind channel and carrier frequency offset estimation using periodic modulation precoders," *IEEE Transactions on Signal Processing*, Vol. 48, No. 8, pp. 2389-2405, Aug. 2000.

115. F. Gini and G. B. Giannakis, "Frequency offset and symbol timing recovery in flat-fading channels: a cyclostationary approach," *IEEE Transactions on Communications*, Vol. 46, pp. 400-411, Mar. 1998.

116. M. Ghogho, A. Swami, and T. Durrani, "On blind carrier recovery in time-selective fading channels," *Proceedings of the Thirty-Third Asilomar Conference on Signals, Systems and Computers*, Vol. 1, pp. 243-247, 1999.

117. P. Ciblat, P. Loubaton, E. Serpedin, and G. B. Giannakis, "Performance analysis of blind carrier frequency offset estimators for noncircular transmissions through frequency-selective channels," *IEEE Transactions on Signal Processing*, Vol. 50, No. 1, pp. 130-140, Jan. 2002.

118. G. B. Giannakis and G. Zhou, "Harmonics in multiplicative and additive noise: parameter estimation using cyclic statistics," *IEEE Transactions on Signal Processing*, Vol. 41, No. 9, pp. 2217-2221, Sept. 1995.

119. M. Ghogho, A. Swami, and A. Nandi, "Non-linear least squares estimation for harmonics in multiplicative and additive noise," *Proceedings of Ninth IEEE Signal Processing Workshop on Statistical Signal and Array Processing*, pp. 407-410, Sept. 1988.

120. G. Zhou and G. B. Giannakis, "Harmonics in multiplicative and additive noise: performance analysis of cyclic estimators," *IEEE Transactions on Signal Processing*, Vol. 43, No. 6, pp. 1445-1460, June 1995.

121. D. Kim, M. J. Narasimha, and D. C. Cox, "An improved single frequency estimator," *IEEE Signal Processing Letters*, Vol. 3, No. 7, pp. 212-214, July 1996.

122. Y. T. Chan, J. W. Plews, and K. C. Ho, "Symbol rate estimation by the wavelet transform," *Proceedings of the 1997 IEEE International Symposium on Circuits and Systems,* Vol. 1, pp. 177-180, June 1997.

123. P. Ciblat, P. Loubaton, E. Serpedin, and G. B. Giannakis, "Asymptotic analysis of blind cyclic correlation-based symbol-rate estimators," *IEEE Transactions on Information Theory*, Vol. 48, No. 7, pp. 1992-1934, July 2002.

124. D. E. Reed and M. A. Wickert, "Symbol-rate detection by a power-series-nonlinear envelope detector receiver," *Proceedings of the 1988 International Conference on Computer Communication*, pp. 179-183, March 1988.

125. L. Mazet and P. Loubaton, "Cyclic correlation based symbol rate estimation," *Proceedings of the Thirty-Third Asilomar Conference on Signals, Systems, and Computers*, Vol. 2, pp. 1008-1012, Oct. 1999.

126. M. Kueckenwaitz, F. Quint, and J. Reichert, "A robust baud rate estimator for noncooperative demodulation," *Proceedings of the 2000 IEEE Military Communications Conference*, Vol. 2, pp. 971-975, Oct. 2000.

127. S. Houcke, A. Chevreuil, and P. Loubaton, "Blind equalization — case of an unknown symbol period," *IEEE Transactions on Signal Processing*, Vol. 51, No. 3, pp. 781-793, March 2003.

128. D. E. Reed, "Comparison of symbol-rate detector and radiometer intercept receiver performances in a nonstationary environment," *Proceedings of the 1989 IEEE Military Communications Conference*, Vol. 2, pp. 359-363, Oct. 1989.

129. C. Corduneanu, *Almost Periodic Functions*, New York: Interscience (Wiley), 1968.

130. D. E. Reed and M. A. Wickert, "Minimization of detection of symbol-rate spectral lines by delay and multiply receivers," *IEEE Transactions on Communications*, Vol. 36 , No. 1, pp. 118-120, Jan. 1988.

131. P. D. Welch, "The use of fast Fourier transform for the estimation of power spectra: a method based on time averaging over short, modified periodograms," *IEEE Transactions on Audio Electroacoustics*, Vol. 15, No. 2, pp. 70-73, June 1967.

132. S. M. Kay, *Modern Spectral Estimation: Theory and Application*, Englewood Cliffs, NJ: Prentice Hall, 1988.

133. Z. Yu, Y. Q. Shi, and W. Su, "M-ary frequency shift keying signal classification based-on discrete Fourier transform," *Proceedings of the 2003 IEEE Military Communications Conference*, Vol. 2, pp. 1167-1173, Oct. 2003.

134. E. E. Azzouz and A. K. Nandi, "New techniques for the baud duration estimation," *Proceedings of the 1996 European Signal processing Conference*, pp. 639-642, 1996

135. FSK and MFSK communication data under the topics of FSK-systems and MFSK-systems in the Digital Modes Section. [Online]. Available: http://rover.vistecprivat.de/~signals/DIG_intro.htm

136. A. V. Dandawate, *Exploring cyclostationarity and higher-order statistics in signal processing*, Ph.D. Dissertation, University of Virginia, Charlottesville, VA, May 1993.

137. A. V. Dandawate and G. B. Giannakis, "Nonparametric polyspectral estimators for *k*th-order (almost) cyclostationary processes," *IEEE Transactions on Information Theory*, Vol. 40, No. 1, pp. 67-84, Jan. 1994.

138. A. V. Dandawate and G. B. Giannakis, "Statistical tests for presence of cyclostationarity," *IEEE Transactions on Signal processing*, Vol. 42, No. 9, Sept. 1994.

139. W. A. Gardner and C. M. Spooner, "The cumulant theory of cyclostationary time-series, Part I: foundation," *IEEE Transactions on Signal Processing*, Vol. 42, No. 12, pp. 3287-3408, Dec. 1994.

140. X. D. Zhnag, *Analysis of time-series — methods of higher-order statistics*, First Edition, Publishing House of Tsinghua University, Beijing, China, 1996.

141. A. Napolitano and C. M. Spooner, "Cyclic Spectral Analysis of Continuous-Phase Modulated Signals," *IEEE Transactions on Signal Processing*, Vol. 49, No. 1, pp. 30-44, Jan. 2001.

142. S. Qian and D. Chen, *Joint Time-Frequency Analysis - Methods and Applications*, Prentice Hall, 1996, ISBN 0-13-254384-2

143. M. H. Hayes, *Statistical Digital Signal Processing and Modeling*, John Wiley & Sons, 1996, ISBN 0-47159431-8.

144. Z. Yu, "A technique to classify analog and digital communication signals," *Technical Report*, E.C.E. Dept., NJIT, Newark, NJ, 2006.